Hydrogen Enhanced Combustion

by

Steven Mitchell Pearce

A thesis presented for the degree of
Doctor of Philosophy
in
Mechanical Engineering
at the
University of Canterbury,
Christchurch, New Zealand.

July 7^{th} 2000

INEERING
BRARY

A CONVERTED SPIRIT.

Genius of Alcohol. "And to think that I was once regarded as an impediment to locomotion!"

- 7 MAY 2001

Abstract

Current four stroke engine research objectives focus on increasing part load thermal efficiency while reducing exhaust emissions. Methods currently employed to achieve this are homogeneous charge lean burn technology, stratified charge lean burn technology and the use of alternative fuels. Of all possible alternative fuels hydrogen is viewed by many as being, ultimately, the fuel of the future. Methanol is regarded as being a likely transitional fuel between the current petroleum transport fuels and hydrogen. Hydrogen is known to be effective in extending the operating lean limit of an engine when used in small amounts in conjunction with conventional fuels.

This thesis presents the results of an investigation into the use of hydrogen as a supplementary fuel in a methanol fuelled Ricardo E6 engine. Three methods of introducing supplementary hydrogen into the engine were investigated: Untimed manifold injection, early direct injection and injection through a modified spark-plug.

Suitable injection systems were designed and tested on the Ricardo E6 engine. An engine management system, data acquisition system and post processing software were developed to enable data to be acquired and analyzed. The direct injection systems were the subject of schlieren visualization investigations of injected gas distribution to improve performance and elucidate engine related phenomena. Results detailing the effects of hydrogen supplementation on the engine performance, combustion and exhaust gas emissions are presented and discussed.

The early direct injection of hydrogen through a dedicated cylinder head tapping proved to be the least effective method of introducing supplementary hydrogen in the Ricardo E6 engine. The position of the injector diametrically opposite the spark-plug coupled with low levels of bulk mixture motion in the cylinder resulted in the formation of an inversely stratified charge (lean near spark-plug) even when injection commenced very early in the compression stroke. The inversely stratified charge resulted in a given level of hydrogen supplementation not being as effective as was the case in the other two fuelling systems.

The homogeneous air/fuel mixture formed by the untimed manifold injection of hydrogen was found to have a beneficial effect on both the combustion and emissions of the engine especially in lean air/fuel mixtures. Introducing supplementary hydrogen into the inlet manifold of the engine was however found to reduce the volumetric efficiency of the engine, reducing the level of output power produced by the engine.

Injecting hydrogen through a modified spark-plug was found to be the most effective way of introducing supplementary hydrogen. The improved performance of the modified spark-plug system over the other two systems was found to be due to the presence of a localized hydrogen/air mixture at the spark-plug electrodes at the time of ignition. Extension of the lean limit past that possible with methanol alone was demonstrated whilst maintaining both a high thermal efficiency and low indicated specific unburned hydrocarbon emissions.

Direct injection of supplementary hydrogen into the combustion chamber, either with the aim of forming a homogeneous charge, or forming a richer air/fuel mixture in the vicinity of the spark-plug without the use of a pre-chamber, has not been reported previously in the published literature. The investigation of both of these fuelling methods is presented in this thesis and constitutes an original contribution to the field of engine research.

Acknowledgements

There are many people who need to be thanked.

Dr Roger Green for initially proposing the project. Dr Ian Huntsman for expressing a willingness to take on the role of academic supervisor after the departure of Dr Roger Green. Dr Neil Glasson for agreeing to provide technical supervision in addition to his busy industry workload and family life.

I am also greatly indebted to fellow combustion group postgraduate Ramon Brown for his guidance and companionship through what has been a long and oftentimes frustrating research project. His in-depth knowledge of combustion, practical abilities and willingness to offer constructive criticism has proven invaluable many a time.

The technical staff especially Ron Tinker, thermodynamic laboratory manager, workshop staff especially Ken Brown, electronics technicians especially Julian Philips and computing personal especially Paul Southward. I would also like to thank the expert input of Andrew Cree in all areas of the work.

Over the years I have had many flatmates but I would especially like to thank Kevin Duignan, Tony Dodds and Georgie Studholme for their understanding, patience and encouragement especially when the going was tough.

My family, especially my parents, have always supported me in my endeavors and I thank them for their support, financial and emotional over the last 6 years.

Last but certainly not least I would like to express my deepest and most heartfelt appreciation and love to my wife Caroline for her support, love and understanding over the last 5 years. I look forward with anticipation and excitement to continuing our wonderful life together.

Contents

List of Figures

List of Tables

Glossary

SYMBOLS

$\triangle\theta$	Mass Fraction Burned Duration
η	Efficiency
γ	Ratio of specific heats, c_p/c_v
λ	Relative air fuel ratio
n	Polytropic exponent
	Moles
p	Absolute cylinder pressure
P	Power
$\mathbf{Q}_{HV}$	Fuel heating value
$\tilde{R}$	Universal Gas Constant
$\mathbf{r}_c$	Compression ratio
V	Cylinder volume

SUBSCRIPTS

app	Apparent
b	Combustion Duration
c	Compression
d	Flame Development Duration
e	Expansion
g	Gross
H2	Hydrogen
i	Gross indicated
	Ignition Delay Duration
m	Mechanical
MeOH	Methanol
n	Net
o	Overall Combustion Duration
	Stagnation value

SUBSCRIPTS
(continued)

p	Products
r	Reactants
th	Thermal

SUPERSCRIPTS

o	Degrees

ABBREVIATIONS

ABDC	After Bottom Dead Center
BMEP	Brake Mean Effective Pressure
bsfc	brake specific fuel consumption
bsHC	Brake Specific HC
bsNO$_x$	Brake Specific NO$_x$
CA	degrees Crank Angle
CCV	Cycle by Cycle Variation
CCVC	Compound Vortex Controlled Combustion
CJC	Cold Junction Compensation
COV	Coefficient Of Variation
DC	Direct Current
DISC	Direct Injection Stratified Charge
DMA	Direct Memory Access
EEOC	Estimated End Of Combustion
EGR	Exhaust Gas Recirculation
FID	Flame Ionization Detector
fifo	first in first out
GDI	Gasoline Direct Injection
HAJI	Hydrogen Assisted Jet Ignition
HEF	Hydrogen Energy Fraction
Hz	Hertz
IMEP	Indicated Mean Effective Pressure
IR	Infrared
is	indicated specific
isfc	indicated specific fuel consumption
IVC	inlet valve closure
kHz	kilo hertz
km	kilometers

ABBREVIATIONS
(continued)

LCV	Lower Calorific Value
LFTB	Liquid Fuels Trust Board
MB	MegaByte
mbar	milli bar
mfb	mass fraction burned
MHz	Mega Hertz
NDIR	Nondispersive Infrared
PJC	Pulsed Jets Combustion
ppr	pulses per revolution
RAM	Random Access Memory
rps	revolutions per second
SI	Spark Ignition
SLPM	Standard Litres Per Minute
SOS	Slotted Optical Switch
TDC	Top Dead Center
UHC	Unburnt HydroCarbons

Chapter 1

Introduction

This chapter introduces firstly the concept of hydrogen as the energy carrier of the future then secondly the envisaged role of methanol as the transitional fuel between our current petroleum based transportation fuels and a possible *hydrogen economy*[1]. The concept of methanol being an effective hydrogen storage medium is introduced and the current state of the requisite technology outlined. Methanol production and the extent of previous research involving methanol as a fuel in New Zealand is reviewed. The goals of improved part load efficiency, reduced exhaust emissions and reduced cyclic variability in automotive four stroke engines are identified and the research goals of the thesis defined. Finally the structure of the thesis is presented.

1.1 Hydrogen as an Energy Carrier

It is widely believed that hydrogen will ultimately be the renewable energy vector of the future [DeLuchi 1989][2] , [Jamal and Wysznski 1994] , [Scott 1994]. The reasons for this are threefold:

1. Hydrogen is environmentally friendly. When burnt in air the only potential pollutants are oxides of nitrogen (NO_x) and hydrogen peroxide (H_2O_2). When utilized in a fuel cell, the only by-product is water.

2. Hydrogen can be produced from water and any primary energy source (ie hydrogen can be manufactured from renewable energy sources such as solar, wind, hydro-electric, ocean currents/waves). Hydrogen is potentially a sustainable form of energy.

3. Hydrogen can be used to store and transport energy. Hydrogen is thus well suited for use with many of the renewable energy sources whose availability is often hard to match with demand.

[1] The term *Hydrogen Economy* is a phrase adopted to describe a future where hydrogen is the accepted means of storing and transporting energy

[2] Name and year entries denote references, details of which may be found at the end of the thesis starting on page 251

The storage and reticulation of hydrogen for use in stationary applications such as homes and industry is technically feasible with the use of gas pipelines and high pressure gas storage tanks. For mobile applications however, space and/or weight constraints are providing challenges for engineers to overcome.

Hydrogen, with it's low ignition energy and extreme lean limit of flammability, when utilized in an internal combustion engine via the inlet manifold (known as external mixture formation) can result in pre-ignition and possible backfire into the inlet manifold when using richer air/fuel mixtures [Das 1990]. One possible method of overcoming this undesirable effect is by injecting hydrogen directly into the combustion chamber during the compression stroke [Homan *et al.* 1983].

The technology required to utilize hydrogen to power automobiles via either the internal combustion engine or hydrogen fuel cells has been successfully demonstrated by most of the major car manufacturers such as BMW, Daimler Benz, Ford, General Motors and Toyota [Nowell 1999].

Before the use of hydrogen as an energy vector in the automotive sector becomes widespread, however, significant advances need to be made on a number of fronts [Peschka and Escher 1993] , [Lipman and DeLucchi 1996]. Firstly, hydrogen is a costly alternative compared with conventional petroleum fuels. In order for the use of hydrogen to become a commercial reality it must become an economic alternative via either a reduction in the manufacturing costs and/or recognition of it's environmental benefits through taxes and levies applied by central government. Secondly, as virtually all the world's current production of hydrogen is from natural gas, hydrogen at present is a non-renewable form of energy. Thirdly, there is no significant infrastructure in place for the distribution, storage and dispensing of hydrogen either in gaseous or cryogenic liquid form. Fourthly, current on-board hydrogen storage techniques (via a compressed gas, a cryogenic liquid or a metal hydride) are currently either heavier and/or bulkier than conventional petroleum methods.

Thus an automotive system capable of storing an equivalent amount of hydrogen energy on-board with a similar weight and volume to that of conventional petroleum based fuels is desirable if hydrogen is to become a viable automotive fuel.

Such a system has yet to be satisfactorily developed. In the intervening transition period hydrogen could be generated by an on-board hydrogen generator from liquid fuels such as alcohols. Suitable storage technology when available would replace the on-board hydrogen generator [Houseman and Voecks 1980].

1.2 Methanol as a Transitional Fuel

Methanol is widely regarded, out of all the other possible alternatives, as the most likely transitional fuel between our current petroleum based transportation fuels and the use of hydrogen as a transportation energy vector [Nichols 1994]. The reasons for this are: [Bernhardt 1977] , [Houseman and Voecks 1980] , [Sinor 1996].

1. Methanol is a liquid at ambient temperature. It can therefore be stored and distributed in the conventional manner through the present liquid fuel infrastructure.
2. Methanol can be manufactured from renewable resources (although currently virtually all methanol is produced from non-renewable natural gas).
3. Methanol has a high octane number (c.f. gasoline) and offers the potential for improved thermal efficiencies using purpose designed engines.
4. Methanol exhibits good flammability under lean mixture operation and hence improved engine efficiencies and emissions (c.f. gasoline).
5. Lower boil off rates (c.f. gasoline).
6. Methanol is biodegradeable.
7. Methanol can be considered to be a chemical hydrogen storage medium (see page 4).

The use of methanol as an automotive fuel creates an opportunity to operate engines at higher power outputs (c.f. gasoline) due to the use of higher compression ratios to take advantage of the higher octane number and increased evaporative cooling of the charge. The higher power output can be used to create higher torque from the same displacement (performance enhancement) or can be used to create the same torque using a smaller displacement (therefore lighter) engine (with resulting vehicle fuel efficiency enhancement) [Huff and Hodgson 1993]. The use of higher compression ratios, along with methanol's improved lean burn characteristics, provides the potential to improve the thermal efficiency of the engine, and in the case of lean burn operation, reduce engine emissions also [Bernhardt 1977] , [Huff and Hodgson 1993].

1.3 The Use of Hydrogen as a Supplementary Fuel

The superior combustion and emissions characteristics of hydrogen have been recognized for many years [Lipman and DeLucchi 1996]. In addition to a strong research effort focused on the development of dedicated hydrogen fuelled engines, there has been an equally large effort focused on research into ways to use hydrogen to improve the performance of conventionally fuelled engines [Pettersson and Sjostrom 1991a] , [Jamal and

Wysznski 1994]. Much of the earlier research was conducted with gasoline as the primary fuel as at that point in time there were not the same fears about the supply of gasoline running out and alternative fuels were not being examined with the same vigor as they are today. Later, after the oil shocks of the seventies, and with growing concerns about the long term supply prospects of petroleum based fuels, methanol began to be used as the primary fuel in hydrogen enhanced combustion research.

The earliest interest in the use of hydrogen to enhance combustion focused on hydrogen's ability to extend the lean limit of combustion in an engine, thereby creating the opportunity to operate at air/fuel ratios significantly leaner than that of conventionally fuelled gasoline engines [Houseman and Hoehn 1974]. It was found that only small quantities of hydrogen were required to dramatically increase the resultant mixture's flame speed allowing a corresponding extension of the engine's lean limit of combustion. It is this extension of the lean limit of combustion that provides the basis for improvements in part load fuel economy (bsfc) and engine emissions, especially those of NO_x. The high flame speed of hydrogen, and it's wide flammability limits, also allow an engine to be operated over a wide range of air/fuel ratios without requiring inlet air throttling reducing the volumetric efficiency and pumping losses further enhancing part load fuel economy [Houseman and Voecks 1980] , [Sjostrom *et al.* 1981] , [Jamal and Wysznski 1994].

In order to use hydrogen for combustion enhancement there must be a supply of hydrogen available at the engine. The storage of two different fuels on-board a vehicle is not desirable for two reasons: Firstly, physically this would require two separate sets of storage, fuel lines and fuel metering arrangements. Secondly, it would require, on the part of the driver of the vehicle, two separate fuelling operations. The likely adverse consumer reaction to this would spell the end of such a system before it became a commercial reality.

There are two possible solutions to this problem. The first is to reduce the amount of hydrogen required to be stored to an amount that will allow an extended time between refuelling (eg 10 000 km) with an acceptably small storage device (eg < 20 L) as proposed by Lumsden [1995] is his work on the HAJI system (see page 24). The second possibility is to refuel and store only one fuel and form the second fuel from the first on-board the vehicle.

1.4 Methanol as a Hydrogen Storage Medium

Methanol can be considered to be a chemical hydrogen storage medium. Methanol has a hydrogen to carbon ratio of 4:1 compared with 1.77:1 for gasoline. When viewed in this manner, methanol is in fact the most efficient hydrogen carrier currently available. In such a system, hydrogen is stored as a constituent element in liquid methanol which is

distributed, stored and dispensed in a conventional manner [Houseman and Voecks 1980] , [Sjostrom *et al.* 1981] , [Seifritz 1989] , [Hirota *et al.* 1991] , [Jones and Wyszynski 1993b] , [Jamal and Wysznski 1994] , [Nowell 1999].

Methanol offers the following advantages as a chemical hydrogen storage medium.

1. Contains no carbon-carbon bonds which are hard to break and result in undesirable byproducts.
2. Has a very high hydrogen to carbon ratio giving it a high energy density (1.8 times higher than cryogenic liquid H_2).
3. Is a liquid at ambient conditions allowing ease of handling.

Utilizing methanol as a hydrogen storage medium requires a method of releasing the hydrogen molecules from the parent methanol molecule on-board the vehicle.

1.5 Production of Hydrogen from Methanol

Techniques and equipment for reforming liquid methanol into a hydrogen rich gas for automotive use have been investigated for a number of years [Sjostrom *et al.* 1981] , [Konig *et al.* 1985] , [Jones and Wyszynski 1990] , [Pettersson and Sjostrom 1991b] , [Jones and Wyszynski 1993a] , [Jones and Wyszynski 1993b] , [Wyszynski and Wagner 1995] , [Cohn *et al.* 1996].

The early use for the reformed gas was in internal combustion engines as outlined on page 3. However the development of the hydrogen fuel cell in the eighties by NASA for use in it's space exploration program provided a glimpse at the possible automotive power source of the future. Hydrogen fuel cells have the ability to convert the chemical energy of the fuel source into useful work with a higher efficiency than is conventionally attainable by the internal combustion engine. Internal combustion engines typically have a thermal efficiency of approximately 19% compared to the approximately 38% that is possible from a hydrogen fuel cell [Nowell 1999]. The problems of hydrogen storage on-board a vehicle, discussed on page 1, however, are still present and for this reason the focus of methanol reforming shifted from providing a hydrogen rich gas to power internal combustion engines to powering hydrogen fuel cells. Many of the major car manufacturers (Daimler-Benz/Ford, Toyota, General Motors, Volkswagen) are directly involved with hydrogen fuel cell vehicle development programs utilizing methanol as the fuel. Steam reforming has been adopted as the preferred method to produce hydrogen from methanol [Nowell 1999].

Thus the technology to manufacture the required hydrogen rich gas on-board a vehicle is well established and has reached the pre-production/demonstration stage for use in conjunction with methanol fuel cell vehicles.

1.6 Methanol Production in New Zealand

New Zealand is fortunate to have at its disposal significant energy resources (condensate, natural gas, coal, peat and forest biomass). In response to the large increase in international oil prices following the 1973 Arab-Israeli war (the so called *energy crisis*), the government of the time passed the Liquid Fuels Trust Act in 1978 and formed the Liquid Fuels Trust Board (LFTB). The LFTB was charged with the overall aim of reducing the use of imported fuels for transport fuels in New Zealand. It was funded by a 0.1 cent per liter levy on motor spirits and automotive diesel [Cole *et al.* 1986] , [Ministry of Commerce 1990].

The LFTB was instrumental in the decision being made to build two methanol production plants, Motonui and Waitara, in Taranaki to utilize New Zealand's largest natural gas resources, the Maui and Kapuni fields. The Motonui plant was originally built to convert natural gas to gasoline with crude methanol being an intermediate step in the process. The later addition of two distillation units gave the flexibility of being able to manufacture either 720 000 tonnes of gasoline or 1.8 million tonnes of chemical grade methanol per year. The Waitara plant is a stand alone methanol production facility with a capacity of 530 000 tonnes per year of chemical grade methanol. The two plants are linked by a pipeline to enable crude methanol from Motonui to be distilled at Waitara.

New Zealand therefore has the capability in place to manufacture up to 2.33 million tonnes (45.9 PJ) of methanol per year. In 1992, New Zealand's transportation fleet consumed 131.0 PJ of energy [CAE 1996]. Thus without any further investment in plant, there is the potential to supply ≈35% of our transport energy requirements with methanol[3]. New Zealand is therefore well placed to utilize methanol in it's transportation fleet.

1.7 Background to this Investigation

Internal combustion engine research is focused primarily on engines utilizing the two major combustion ignition systems in use, spark ignition and compression ignition. Due to the very different natures of each of these systems, the focus of this work will be limited

[3] This figure does not take into account the possible gains in efficiency possible with the use of methanol as a fuel

to spark ignition engines only.

Current research into four stroke internal combustion engines for automotive applications is taking place on several fronts [Heywood 1991] , [Heywood 1997].

1. Improving part load engine efficiency. Although 4 stroke engines are at their most efficient at full load, automotive 4 stroke engines are only operated there for a small proportion of their operating cycle.

2. Reducing exhaust emissions in response to a worldwide increase in awareness of the harmful effects that automobile emissions are having on both the environment and the health of humans, especially in the more densely populated urban areas.

3. Utilizing alternative fuels that are able to be manufactured from renewable resources thus taking the pressure off non-renewable petroleum feedstocks.

4. Reducing cyclic variability thus leading simultaneously to extension of the lean limit of combustion, possible increases in compression ratio, and more optimized spark timings which all lead to improved efficiency and maximum power with reduced emissions.

The partial addition of hydrogen to conventionally fuelled engines has been observed by previous researchers to have led to improvements in all the areas listed above [Houseman and Hoehn 1974] , [MacDonald 1976] , [Finegold 1978] , [Rauckis and McLean 1979] , [Jamal and Wyszynski 1994] , [Apostolescu and Chirac 1996]. In addition methanol / hydrogen mixtures have very wide flammability limits. This enables power regulation to be achieved by varying mixture strength rather that by throttling the mixture. This leads to further efficiency gains at the part load condition by improving volumetric efficiencies through the elimination of pumping losses due to throttling.

Full advantage cannot be taken of the improvements in efficiency and exhaust gas emissions that can theoretically be obtained in a lean burn homogeneous charge engine due to practical constraints such as poor ignitability, slow burning, misfire and increased cyclic variation. These effects are a consequence of operating an engine with very lean mixtures and result in poorer fuel economy and higher exhaust emissions.

The concept of stratified combustion has been proposed as a way of taking full advantage of the potential benefits of lean burn technology not able to be realized by conventional homogeneous charge lean burn combustion systems. As the name implies, the stratified charge engine operates by burning a stratified charge which varies from being most commonly stoichiometric or rich of stoichiometric near the ignition source to lean in the rest of the combustion chamber. Thus when the spark is fired, the more easily

to ignite richer mixture is ignited instead of the lean mixture which would be either hard or impossible to ignite on its own. The improved ignitability and faster propagation of the rich burning flame kernel into the lean portion of the charge both help to increase the combustion rate of the charge as a whole reducing cyclic variations. The increased rate of combustion also helps reduce the tendency of lean burn engines to produce high levels of CO and UHC due to insufficient time for post flame front oxidization reactions to occur. NO_x emissions are still lower than a conventional engine as the combustion occurs in either a locally fuel rich or fuel lean environment, both conditions that do not favor the formation of NO_x. Combustion of the leaner mixture, (with subsequent lower flame temperatures), near the combustion chamber walls, results in low heat transfer and therefore high thermal efficiencies as is also the case in homogeneous charge lean burn engines.

There are two main methods by which a stratified charge can be created in an engine. The first involves the fuel being injected directly into the combustion chamber and relying on the induced inlet air swirl to form a rich air/fuel mixture at the spark plug at the time of ignition. These open chamber designs require the fuel injection timing to be varied with speed and load [Hasalett *et al.* 1976]. The second involves the use of a pre-chamber which is connected to the main chamber by either a single [Date *et al.* 1974] or multiple passages [Yagi *et al.* 1980] , [Lawrence 1999]. These divided chamber designs are mechanically more complex often requiring additional fuel mixing and induction systems and are consequently more expensive to manufacture.

Previous work in the Department of Mechanical Engineering at the University of Canterbury has focused on investigating charge stratification using a low pressure direct injection of gaseous fuel through a specially modified spark-plug. Work has been conducted both on a constant volume combustion chamber and a Ricardo E6 test engine.

Damiano [1993] investigated the stratification of a quiescent methane/oxygen mixture in a constant volume combustion chamber with premixed methane/oxygen. Robinson [1995] studied the formation of nitrogen oxides in homogeneous and heterogeneous mixtures of hydrogen and air. Roache [1998] also investigated the formation of NO in homogeneous and heterogeneous mixtures of hydrogen and air. Roache also investigated the effect of hydrogen enrichment on methane/air mixtures in both homogeneous and heterogeneous (stratified) charges. All three investigators found that charge stratification resulted in the equipment lean limit of flammability being extended. In addition Roache [1998] found that charge stratification of hydrogen could be used to achieve similar increases in combustion rate while using up to 10 times less hydrogen as in the homogeneous charge case. Charge stratification was also found to reduce the formation of NO in hydrogen/air mixtures over that which is formed by an equivalent homogeneous mixture.

Zavier [1991] investigated the effects of stratifying pre-mixed charges of methane and gasoline with methane from a modified spark-plug arrangement in a Ricardo E6 test engine. The equipment lean limit of combustion was able to be extended however UHC emissions were higher. This was thought to be due to the injected methane gas being burnt near it's rich flammability limit and/or increased quenching of the combustion in the larger dead volume of the arrangement. Calvert [1994] also worked with a Ricardo E6 engine using methane as the fuel. Calvert however utilized a pre-chamber design to try to control the flow field in the vicinity of the spark plug. Again the equipment lean limit of combustion was able to be extended. UHC levels were also reduced compared to those of Zavier due to reduced quench volumes and better control over the air/fuel mixture at the point of ignition. UHC levels were still greater than those obtained with baseline engine operation with methane, believed to be due to the increased crevice volumes over the baseline engine configuration.

It is therefore anticipated that the stratification of a methanol fuelled engine with hydrogen should result in increased rates of combustion, and reduced NO_x emissions, when compared to a similar homogeneous mixture of methanol and hydrogen of equivalent overall air/fuel ratio.

1.8 Research Objectives

The objectives of this research were threefold:

- to develop an engine data acquisition and post-processing system capable of providing accurate cylinder pressure, IMEP values, and mass fraction burned combustion data, and
- develop a hydrogen injection system capable of direct hydrogen injection with fine control of the injection quantities, and
- by means of engine testing investigate different methods of supplying supplementary hydrogen to the engine. By evaluation of the resulting combustion characteristics, emissions and performance identify the preferred system for introducing supplementary hydrogen

1.9 Outline of Thesis

This thesis presents the results of an investigation carried out into the effect that hydrogen has in enhancing the combustion of methanol in a four stroke research engine. This work was carried out in the Department of Mechanical Engineering at the University of

Canterbury.

This chapter introduces first the concept of hydrogen as the energy carrier of the future, then the envisaged role of methanol as the transitional fuel between our current petroleum based automotive system and a "hydrogen economy". The concept of methanol being an effective hydrogen storage medium is introduced and the current state of the requisite technology outlined. Methanol production, and the extent of previous research involving methanol as a fuel in New Zealand, is reviewed. The goals of improved part load efficiency, reduced exhaust emissions, and reduced cyclic variability in automotive four stroke engines are identified and the research goals of the thesis defined.

Chapter 2 reviews research that has been conducted into the use of hydrogen supplementation to enhance the performance of internal combustion engines.

Chapter 3 presents the development details of the three proposed hydrogen injection systems. The selection of the chosen hydrogen injector is discussed along with the associated mounting arrangements that are required. Results of preliminary injector open flow testing to determine the relationship between supply pressure, injector current and flow rate are presented. Results of dynamic injector testing are also presented.

Chapter 4 introduces schlieren optical methods and their principle of operation before describing the apparatus used and the test procedure. The performance of both the direct and puff injection injector configurations described in Chapter 3 are further improved through the use of schlieren photography to visualize the resulting injected gas distribution.

Chapter 5 details the development of an engine data acquisition system incorporating an optical rotary encoder. The hardware required to ensure the correct phasing between the acquired engine pressure data and crank-angle position is described. Details of the software written to acquire and post process the engine combustion data are then outlined. The novel method employed to accurately determine the location of the rotary encoder index pulse is presented before an analysis of the performance of the data acquisition system as a whole.

Chapter 6 describes the test apparatus which was used for the duration of the engine testing. Modifications made to the standard Ricardo E6 engine are presented. The development of the engine management system is described. The fuel injection and supply systems are then outlined and the test cell safety system and instrumentation is described.

Chapter 7 builds upon the description of the experimental apparatus described in Chapter 6. Details of fuel preparation, engine testing philosophy and spark timings used are presented. A description of the exhaust emission testing equipment and procedures used therewith follows. The procedures developed for the calibration of the piezo-electric pressure transducer, electronic data acquisition, and engine operation and testing are then presented.

Chapter 8 presents the results and discussion of the investigation into the simplest of the three methods being investigated, hydrogen supplementation via untimed manifold injection. First the engine configuration and the relevant operating parameters are discussed, then the effects on the fluid properties are looked at before the effects on the combustion characteristics, engine performance and emissions are presented.

In Chapter 9 the results of an investigation into the early direct injection of hydrogen into the combustion chamber will be presented. Preliminary investigations into early direct injection, early direct injection timing and lean air/fuel mixtures are discussed. A schlieren investigation looking at the injected hydrogen distribution of both the early direct injector and the modified spark-plug injector is outlined. A set of engine test results comparing the three methods of supplying supplementary hydrogen to an engine including the effects on the combustion characteristics, engine performance and emissions are presented and discussed. The results of an investigation into the effects of injection duration on the performance of the modified spark-plug injector is then presented.

Chapter 10 outlines the optimum method of fuelling an engine on supplementary hydrogen via early direct injection through a modified spark-plug injector as determined in the Chapter 9. The results of a series of tests comparing the baseline engine operation with the optimum fuelling system is then presented. A possible vehicular engine fuelling regime is then discussed.

In Chapter 11 the key achievements of the thesis are summarized. Conclusions are drawn on the performance of each of the hydrogen injection systems employed. The optimal hydrogen supplementation system for the Ricardo E6 engine is presented along with a suggested fuel management scenario for the engine. Recommendations for further work that could be undertaken as a result of this research project are then presented.

Chapter 2

Hydrogen Enhanced Combustion Research

This chapter reviews research that has been conducted into the use of hydrogen supplementation to enhance the performance of internal combustion engines.

2.1 Introduction

The earliest interest in hydrogen enhanced combustion focused on hydrogen's ability to extend the lean limit of combustion in an engine beyond that which can be utilized in a conventionally fuelled automotive gasoline engine [Houseman and Hoehn 1974] , [MacDonald 1976] , [Finegold 1978] , [Jordan 1979] , [Rauckis and McLean 1979] , [Brinkman and Stebar 1985] , [Jamal and Wysznski 1994] , [Apostolescu and Chirac 1996]. In these investigations the supplementary hydrogen was introduced to the engine via untimed manifold injection. Hydrogen enrichment was also investigated for use with gasoline fuelled aircraft to reduce fuel consumption and reduce exhaust pollution [Menard *et al.* 1976]. It was found that only small quantities of hydrogen were required to dramatically increase the resultant air/fuel mixture's flame speed allowing a corresponding extension of the engine's lean limit of combustion. It is this extension of the lean limit of combustion that provided the basis for improvements in fuel economy and engine emissions that were of primary interest.

2.2 Engine Cold Starting

Another area involving the use of hydrogen in supplementing the operation of an engine is in overcoming the inherently poor cold start characteristics of methanol fuelled engines. Methanol is a single component fuel with a single boiling point at 65 ^{o}C. Gasoline on the other hand contains several components that have a range of boiling points from 27 to 225 ^{o}C. With a gasoline fuelled engine, cold starting is achieved by over-fuelling (i.e. using the choke) in order to provide enough of the vaporized component to start the engine. With methanol as the fuel this technique is not applicable thus cold starting a methanol engine is a major problem. Hydrogen is gaseous at all operating conditions hence the cold engine could be started using hydrogen. This would cause no problems with pre-ignition

because, initially at least, the engine is cold so there are no hot surfaces on which hydrogen could ignite. When using a liquid fuel, a major source of exhaust emissions is due to cold-start enrichment of the air/fuel mixture. This source would be eliminated using hydrogen to cold start the engine. The use of hydrogen in the cold starting of engines is not the focus of this piece of research and will not be addressed further. Additional information can be found by referring to Pettersson and Sjostrom [1991a] , Pettersson and Sjostrom [1991b] and Maxwell *et al.* [1993].

2.3 Hythane

One of the most abundant gaseous alternative fuels that is currently available is natural gas (comprised predominantly of methane). The use of methane as a fuel in internal combustion engines does however have some inherent problems. Methane-air mixtures suffer from low flame propagation rates which become increasingly slower as the air/fuel ratio of the mixture moves leaner of the stoichiometric air/fuel ratio [Unich *et al.* 1993]. Thus the lean burn combustion strategies that are commonly employed in conventionally fuelled engines in order to achieve higher thermal efficiencies and reduced emissions (increased turbulence and/or stratified charge combustion) are unable to be employed to the same extent in natural gas fuelled engines. A technique that is commonly used to increase the rate of flame propagation in methane/air fuel mixtures is to increase the level of turbulence in the combustion chamber with improved intake manifold and combustion chamber design. There are however penalties associated with the use of excessive turbulence such as higher heat transfer, higher peak cylinder temperatures and therefore higher NO_x [Karim *et al.* 1996]. Another approach to the problem is to add a quantity of hydrogen to the methane. The resulting fuel mixture has a much faster burning rate than methane alone. Another advantageous property of hydrogen is that it has very wide limits of flammability which, combined with it's high flame speed, offer the potential of operating the engine leaner than is possible with methane alone.

A commonly used mixture of methane and hydrogen is known as Hythane[1]. Hythane comprises of methane with the addition of 15-20% hydrogen by volume. The addition of hydrogen occurs before the storage of the fuel mixture and therefore a homogeneous gas mixture is formed. Benefits obtained through the use of Hythane reported in the literature include decreased brake specific unburned hydrocarbons (bsUHC), CO and CO_2 emissions as well as increased brake thermal efficiencies. The emissions of brake specific NO_x are higher than those obtained when burning methane at the same spark timing. This increase has been attributed to the increased residence time of the combustion gases at higher temperatures due to the increase combustion rate of Hythane [Wallace and Cat-

[1] Hythane is a registered trademark of Hydrogen Consultants Inc. Mixtures of natural gas and hydrogen have become known as Hythane and are commonly referred to as such in the literature.

telan 1994].

Hythane is widely regarded as the means by which the widespread use of methane will gain acceptance especially given the stringent requirements on both engine efficiency and pollutants. This thesis does not focus on the the role of hydrogen in enhancing the combustion of methane via Hythane but additional information can be found by referring to Swain *et al.* [1993] , Hoekstra *et al.* [1994] , Raman *et al.* [1994] , Hoekstra *et al.* [1995] , Karim *et al.* [1996] and Sierens and Rosseel [2000].

2.4 Dedicated Fuelling via Manifold Injection of Hydrogen

The most simple method (technically) to introduce hydrogen to an engine, and the one which has attracted the most research interest, is that of untimed manifold injection.

As the name suggests, untimed manifold injection involves the continuous addition, to the inlet manifold of an engine, of gaseous hydrogen. The hardware requirements are therefore correspondingly very simple - the hydrogen supply requires only an adjustable throttling valve in it to vary the flow rate of hydrogen before it is plumbed into the inlet manifold.

While untimed manifold injection provides a technically simple means of fuelling a dedicated hydrogen vehicle, this method does have some serious problems associated with it especially with near stoichiometric mixtures [Watson and Milkins 1978].

1. Low volumetric efficiency (resulting in reduced engine power c.f. gasoline)
2. Pre-ignition and back-firing into the inlet manifold
3. Knocking combustion

These problems can be largely overcome by injecting the hydrogen directly into the combustion chamber after the inlet valve has shut (see page 23).

2.5 Supplementary Fuelling via Manifold Injection of Hydrogen

The untimed manifold injection of hydrogen, due largely to it's technical simplicity, has also been widely used when investigating the supplementation of conventional liquid fuels with hydrogen. The potential problems outlined in the previous section are, with the exception of reduced volumetric efficiency, generally not encountered with untimed manifold hydrogen supplementation due to the typically low levels of supplementation

used.

When applying supplementary fuelling to an engine, the hydrogen is induced into the cylinder with the inlet air along with vaporized liquid fuel forming a homogeneous charge in the cylinder.

2.5.1 Combustion Rate

It has been observed by several researchers that hydrogen addition increases the rate of combustion in an engine.

Rauckis and McLean [1979] investigated the effects of hydrogen addition on the combustion of indolene as part of their research into the processes controlling ignition and flame propagation in lean mixtures. Hydrogen was used as a supplementary fuel because the addition of small amounts would have a large effect on the laminar flame speed and ignition delay period. It was thought that small amounts of hydrogen would have relatively little effect on the flow processes and turbulence structure in the cylinder. They attempted to correlate their experimental results to the following phenomenological description of flame propagation in a homogeneous, fully vaporized charge, supporting evidence having been provided by Tabaczynski *et al.* [1977] amongst others.

> *... the spark discharge is followed by a delay period (not a homogeneous autoignition delay) during which the flame kernel develops and grows until it's size is of the order of the local turbulent integral length scale and during which the burning rate is largely governed by laminar flame speed limitations. The delay period is followed by a turbulent burning period during which the flame speed is accelerated due to the effect of turbulence, and during which increases are observed in both the flame speed and the ratio of flame speed to the local laminar flame speed. The turbulent burning rate is strongly influenced by the local turbulent intensity during this period.*

In addition they proposed that the addition of hydrogen would accelerate the early stages of combustion due to the rapid chain branching oxidation characteristic of hydrogen which is known to be faster than the partially degenerate chain reactions that are characteristic of hydrocarbon oxidation. It was found that the combustion duration of all three nominated phases of combustion (0-2% mfb, 2-10% mfb and 10-90% mfb durations[2]) were reduced with the most significant effect being on the 0-2% mfb duration.

[2]The preceding terms refer to various phases of the combustion process as determined by a mass fraction burned analysis performed on the combustion pressure data. Details of the mass fraction burned analysis is presented on page 79

Rauckis and McLean [1979] concluded that the combustion process consists of an ignition delay period dominated by chemical dynamic effects and a main combustion period which is dominated by turbulent transportation phenomenon.

Decreasing combustion durations in gasoline fuelled engines at a given air/fuel ratio with increasing hydrogen supplementation have also been reported by Jordan [1979].

Schafer [1981] in his investigation into hydrogen supplementation of a methanol fuelled engine also found that all phases of combustion duration were reduced at a given air/fuel ratio as the level of hydrogen supplementation was increased. Schafer failed to offer any explanation for his observations.

Annand [1983] compared several models for the ignition delay period in a spark ignited homogeneous charge engine using propane and iso-octane as the fuels of interest. He concluded that the "eddy burning" model of ignition delay proposed by Tabaczynski *et al.* [1980], which takes into account the laminar flame speed of the mixture, gave quite good correlations with observed ignition delay periods.

Sher and Hacohen [1989] conducted an investigation into the effects of hydrogen enrichment on both the ignition delay and the combustion duration of a gasoline fuelled SI engine. Experimental results from Rauckis and McLean [1979] as well as their own were correlated with an earlier "eddy burning" descriptive model of flame propagation by Tabaczynski *et al.* [1977]. There was good correlation of combustion duration with the eddy burning model but the model underestimated the pronounced effect that hydrogen supplementation had on reducing the ignition delay duration. As the eddy burning model takes into account laminar flame speed effects, Sher and Hacohen concluded that:

> *... the time required to establish a self-sustaining combustion wave is strongly dependent not only on the hydrodynamic processes, but also on the rapid dissociation of the hydrogen molecules into highly active radicals (in particular in the spark neighborhood). The chemistry in this region undoubtedly enhances the ignition process, but does not affect the laminar burning velocity of the unburned charge as measured under steady-state conditions. The effect of added hydrogen would therefore be to accelerate the very early stages of the ignition process by rapid chain branching oxidation which greatly stimulates the otherwise slow thermal ignition process.*

Interestingly in an earlier investigation by Sher and Hacohen [Sher and Hacohen 1987] in which a model was developed to simulate the four-stroke cycle of an SI engine fuelled

with hydrogen enriched gasoline, the model predicted overall combustion durations to decrease with increasing hydrogen supplementation and as the overall air/fuel ratio became richer. The plots of combustion duration however differed from all other plots presented in that they did not include experimental values for comparison with the predicted results. In addition the effect of hydrogen supplementation on the ignition delay duration was not mentioned at any point in the paper.

Apostolescu and Chirac [1996] in their investigation into the combustion of hydrogen enriched gasoline plotted the results of Sher and Hacohen [1989] along with their own and came to the same conclusions as Sher and Hacohen that hydrogen supplementation had a pronounced effect on the early stages of flame development. They also tried to correlate the combustion durations with the laminar burning velocity using the eddy turbulent entrainment model of turbulent combustion in a pre-mixed spark ignition engine reported by Hires *et al.* [1978]. The correlation with the experimental results was found to be poor which again highlights the inadequacy of the eddy turbulent entrainment model when applied to situations where hydrogen is used as a supplementary fuel.

Thomas *et al.* [1993] have proposed a different mechanism for the observed increase in the rate of combustion with hydrogen supplementation. In their investigation into the early phase of flame development of hexane, they used high speed electronically derived images of the chemi-luminescent light resulting from combustion to derive information on early flame kernel behavior. Hydrogen supplementation was used to vary the combustion dynamics of the flame kernel behavior. They concluded that the hydrogen flame front, with it's high flame speed and wide combustion limits, would have quickly travelled across the combustion chamber and seeded hydrocarbon combustion in more than one place resulting in the observed reduction in cyclic variations. This conclusion was reached from chemi-luminescent images of the combustion process however it was noted that the chemi-luminescent frequency of hydrogen is outside the range of the camera used so the actual hydrogen flame was not observed, only the resultant hexane combustion.

Rauckis and McLean [1979] also observed that the effects of hydrogen addition on the combustion duration were also more pronounced in lean mixtures due to the acceleration of the normally slower thermal ignition reactions in lean charges. Schafer [1981] also demonstrated that the effects of hydrogen addition were more pronounced in leaner mixtures. Sher and Hacohen [1989] however disputed this finding claiming that their study showed no evidence of this.

2.5.2 Cyclic Variability

Variations in combustion, cycle-to-cycle, are always present in both spark-ignition and compression ignition engines. The effects of increased cyclic variability on the performance of an engine range from increased emissions, reduced efficiency and power and, in the case of an automotive engine, a deterioration in vehicle drivability. A summary of the effects of cycle-by-cycle variations (CCV) in combustion can be seen in Figure 2.1.

The causes of cyclic variability can be divided into chemical and physical factors [Young 1981].

Chemical factors affecting cyclic variability are:

1. Air/fuel ratio. Minimum cyclic variations are known to occur at slightly rich air/fuel ratios and increase as the air/fuel ratio becomes richer or leaner.
2. Dilution. Increased dilution of the air/fuel mixture increases cyclic variability.
3. Flame speed. Fuels with higher flame speeds give lower levels of cyclic variability.

Physical factors affecting cyclic variability are:

1. Pressure variations. Increasing cyclic pressure variations lead to increased combustion variability. Minimum cyclic variability is known to occur near MBT spark timing.
2. Mixture motion. Increasing mixture motion is thought to increase combustion variability.
3. Combustion chamber geometry. Geometries which result in faster combustion also result in reduced cyclic variability.
4. Engine speed. Increases in engine speed increase cyclic variability possibly due to increases in mixture motion variability.

For the same average value of IMEP, higher COV_{IMEP} have been shown to increase NO_x production compared with lower level of COV_{IMEP} [Atkinson *et al.* 1995]. The increase in NO_x production from the faster burning cycles more than offsets the reductions in NO_x production from the slower burning cycles.

Hydrogen supplementation has also been widely recognized as having the effect of reducing the CCV of combustion in engines. Rauckis and McLean [1979] have shown that the addition of hydrogen has a large effect on the CCV of lean mixtures but at

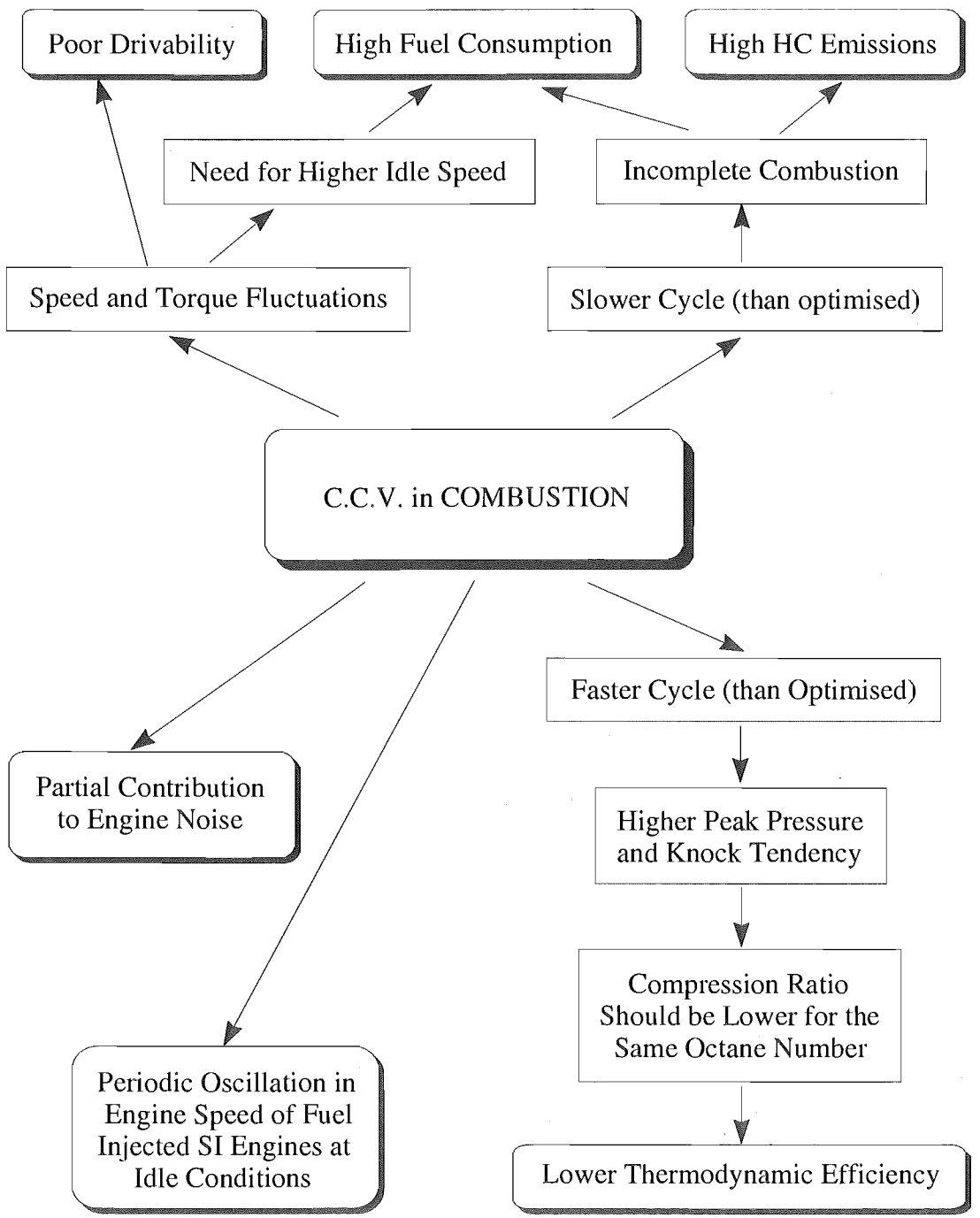

Figure 2.1 Effect of Cycle-by-Cycle Variations in Combustion on Engine Performance (after: Ozdor *et al.* 1996)

near stoichiometric conditions the effects are negligible. They concluded that CCV must involve both chemical and physical phenomena with chemical phenomena dominating in lean mixtures and physical phenomena dominating in near stoichiometric conditions. Apostolescu and Chirac [1996] also reported reduced CCV with increasing levels of hydrogen supplementation. They found that the influence of hydrogen supplementation on CCV can be correlated with it's influence on the flame initiation stage.

The subject of cyclic variability in combustion is an important one and there has been a large quantity of research carried out on it. There have been several excellent review papers published on the subject and they may be referred to for a more in-depth treatment of the topic e.g. [Young 1981] , [Germane *et al.* 1983] , [Ozdor *et al.* 1994].

2.5.3 Brake Power

The introduction of hydrogen to the inlet manifold of an engine causes the power output of the engine to be reduced. This is because an increasingly large proportion of the inlet manifold is occupied by hydrogen displacing inlet air and having a corresponding detrimental effect of the volumetric efficiency of the engine hence reducing power output [Sher and Hacohen 1987].

2.5.4 Thermal Efficiency

Rauckis and McLean [1979] noted that the observed improvements in thermal efficiency for very lean mixtures can be attributed to reduced combustion durations resulting from hydrogen addition. Apostolescu and Chirac [1996] also observed improved thermal efficiencies with increasing hydrogen supplementation. They attributed this to the air/fuel mixture being more diluted with air resulting in the polytropic index (n_c) of compression being closer to that of air ($n_c = 1.4$) as well as reduced time based heat transfer effects due to the shortening of the combustion duration. Swain *et al.* [1993] found that thermal efficiency was improved in a natural gas engine supplemented with hydrogen particularly at lean relative air/fuel ratios (λ) where the decreased combustion durations result in reduced heat transfer to the coolant water. Schafer in his investigation found that the addition of hydrogen at brake mean effective pressures (BMEP) less than 5 bar resulted in an improved effective efficiency. However at BMEP's over 5 bar the effect of added hydrogen had a negative effect on the effective efficiency. The reasons given for the improvement at part loads is that at part load the engine is able to be operated without throttle when supplemented with hydrogen and the lean air/fuel mixtures are thermodynamically more favorable.

2.5.5 Exhaust Gas Emissions

Apostolescu and Chirac [1996] observed increases in the specific NO_x emissions with hydrogen supplementation at a particular value of λ. This increase was thought to result from the faster burning mixtures and resultant higher peak temperatures due to hydrogen addition. Increasing $bsNO_x$ with hydrogen supplementation has been reported by Swain *et al.* [1993] in a natural gas engine for lean mixtures. Interestingly their results showed that for rich mixtures, $bsNO_x$ was slightly less with hydrogen supplementation but certainly the effect of hydrogen supplementation on $bsNO_x$ is slight for richer mixtures and quite pronounced for lean mixtures. Schafer also reported increased NO emissions, compared to straight methanol operation, in leaner mixtures when supplemented with increasingly large levels of hydrogen.

Apostolescu and Chirac [1996] found the engine specific hydrocarbon emissions were reduced at a particular value of λ by the addition of hydrogen. They attributed this to the associated reduction of cycle-by-cycle variability reducing and/or eliminating the effect of incomplete combustion, rather than a reduction in flame quenching in the piston top-land crevice due to the increased laminar flame speed of the mixture. Swain *et al.* [1993], using a natural gas fuelled engine, reported reduced bsHC readings with hydrogen supplementation. The effect is negligible in richer mixtures but quite pronounced in leaner mixtures. Schafer [1981] reports that the level of HC emissions was reduced at all air/fuel ratios with the addition of hydrogen but the effect was most pronounced in lean air/fuel ratios where the additional hydrogen was able to maintain combustion in regions where un-supplemented methanol/air mixtures can not. It was also shown that when using the same hydrogen flow rate, there is a considerable reduction in HC emissions when methanol is the fuel compared to when gasoline is used.

CO emissions have been generally shown to be unaffected by the addition of hydrogen. As would be expected the CO emission levels are high with rich air/fuel ratios and as the mixture is progressively leaned out they reduce to a negligible level due to the excess air that is available to complete oxidation to CO_2. As the engine approaches it's lean limit of combustion, CO emission levels increase gradually due to the increased quench layer thickness and the partial oxidation of unburned fuel in the exhaust stroke. Thus when supplementing an engine with hydrogen, the engine will usually be operated in a lean air/fuel regime to take advantage of the wider flammability limits of hydrogen and the CO emissions would be correspondingly very low [MacDonald 1976] , [Schafer 1981].

2.6 Direct Injection of Hydrogen

Introducing hydrogen to an engine via injection directly into either the combustion chamber (internal mixture formation) or a combustion pre-chamber is technically more difficult to implement than the untimed manifold injection of hydrogen. Despite the difficulties involved, this method does offer the potential to not only overcome the volumetric efficiency penalty of the untimed manifold injection method but also to enable the formation of a stratified charge.

The technical requirements for such a system are a high pressure supply of hydrogen, an injector capable of being accurately controlled and of being able to withstand the back-pressure against it due to combustion, and a control system capable of controlling both the timing and the duration of the hydrogen injection. Due in part to the technical complexity of direct injection supplementation of hydrogen, there has been relatively little work carried out in this area compared with manifold injection, especially when the injected hydrogen is used as a supplementary fuel. The majority of direct hydrogen injection work has been carried out on dedicated hydrogen fuelled engines.

2.6.1 Dedicated Hydrogen Fuelled Engines

The two most commonly implemented methods of fuelling an engine on 100% hydrogen via internal mixture formation are low pressure injection immediately after the closure of the inlet valve and high pressure injection late in the compression stroke.

Internal mixture formation via low pressure injection eliminates the problems encountered with manifold injection of low volumetric efficiency and backfiring [Suzuki *et al.* 1980]. Pre-ignition and knocking combustion may however still occur [MacCarley and Van Vorst 1980]. Control of air/fuel ratio (and hence power) can be achieved by variation of either injection pressure or injection duration (or a combination of both). Variation of injection duration is preferable as reducing the injection pressure will adversely affect the mixing of hydrogen with the induced air in the cylinder [Pichainarong *et al.* 1990].

Internal mixture formation via high pressure injection late in the compression stroke also overcomes the volumetric efficiency and backfire problems associated with manifold injection. High pressure injection has the added advantage over low pressure injection that pre-ignition is eliminated and knocking combustion may be controlled [Homan *et al.* 1983] , [Furuhama *et al.* 1991]. Knocking combustion is controlled by injecting hydrogen towards the source of ignition over a period of time including the time when ignition actually occurs [Homan *et al.* 1983]. This results in the combustion of a hetero-

geneous charge which burns with a reduced rate of pressure rise compared to that of an equivalent homogeneous charge thereby eliminating the knocking combustion. The major disadvantage of the high pressure late injection of hydrogen is a possible reduction in thermal efficiency due to inadequate mixing of the air/fuel mixture [Pichainarong *et al.* 1990].

While the dedicated fuelling of engines on hydrogen is not the focus of this thesis, a great deal of work has been completed in this area. Of note is the work carried out at the at the Musashi Institute of Technology in Japan, principally by Shoichi Furuhama [Saga and Furuhama 1976] , [Furuhama *et al.* 1978] , [Furuhama 1979] , [Furuhama and Kobayashi 1982] , [Furuhama and Kobayashi 1982a] , [Takiguchi *et al.* 1987] , [Pichainarong *et al.* 1990] , [Furuhama *et al.* 1991] , [Koyanagi *et al.* 1993]. Of the major automobile manufacturers, Daimler-Benz AG have also undertaken long running research into fuelling engines utilizing direct hydrogen injection [Binder and Withalm 1980] , [Withalm and Gelse 1986] , [Jorach and Prescher 1994].

2.6.2 Supplementary Fuelling via Direct Injection of Hydrogen

To the best of the author's knowledge, the only use of supplementary hydrogen that is being directly injected into the combustion chamber of an engine is that associated with the hydrogen assisted jet ignition (HAJI) concept.

The HAJI concept [Watson 1995] was initially proposed by Professor Watson at the University of Melbourne and has since been the topic of ongoing development by graduate students Kyaw , Lumsden and Lawrence as well as post doctoral fellow Glasson.

The HAJI system development follows on from work by Gussak who proposed the "LAG" process whereby a "torch" of active species is ejected from a pre-chamber into the main chamber to initiate combustion at many sites within the charge thereby effectively accelerating the combustion rate in the main chamber air/fuel mixture [Gussak 1975] , [Gussak 1976]. Honda, in the 1970's, produced the CCVC stratified charge engine which featured a pre-chamber. Difficulty was experienced in obtaining optimum jet momentum over a wide range of operating conditions. There were also substantial heat losses associated with the pre-chamber design. Oppenheim and his co-workers Maxson *et al.* [1991] have proposed the use of pulsed jet combustion (PJC) for the combustion of very lean mixtures. The size of the pre-chamber used is much smaller than the pre-chambers used in previous pre-chamber design engines for example the Honda CCVC engine.

The HAJI system takes advantage of the order of magnitude faster flame kernel growth that is exhibited by hydrogen mixtures as compared to conventional hydrocarbon fuels [Kyaw and Watson 1993]. A jet with enhanced momentum is achieved from

only a small proportion of the total charge energy which includes active radicals and intermediate species of combustiou which combined, assist in initiating combustion in mixtures that are significantly leaner than the lean flammability limit that can be attained with conventional ignition systems.

The HAJI system consists of a small pre-chamber approximately 1.5% of the clearance volume of the engine. An injector is used to supply hydrogen to the pre-chamber by an injector where it mixes with air and some main chamber fuel. At present the amount of hydrogen used is 5% of the total fuel energy. Once ignited by a miniature spark-plug, jets of burning air/fuel mixture and active species are issued into the main combustion chamber [Lawrence 1999]. The HAJI system allows stable combustion of lean main combustion chamber mixtures that have characteristically slow rates of flame propagation and leads to improved thermal efficiency and reduced NO_x emissions.

The development of the HAJI system has taken place both on a test engine and in a four cylinder engine [Glasson *et al.* 1996]. The HAJI system has been demonstrated to reduce combustion variability and extend the lean limit of an engine considerably. This allows un-throttled engine operation over a wide range of power outputs. An corresponding increase in part load efficiency over that which can be obtained without the use of the HAJI system is also apparent.

One area of concern with the HAJI system is the increased level of unburnt hydrocarbon emissions that have been observed to occur. This area has been the subject of recent research which has concluded that the increased UHC emissions as a result of increased levels of wall quenching [Lawrence 1999].

2.7 Summary

To date the vast majority of investigations into the use of hydrogen supplementation in spark ignition engines has concentrated on untimed manifold injection. As far as the author is aware, the only reported use of the direct injection of supplementary hydrogen has been in conjunction with the use of a pre-chamber. The aim of this, the HAJI system, is to inject into the main combustion chamber multiple jets of burning air/fuel mixture and/or active species. There has been no known work on the proposed area of direct injection of supplementary hydrogen into the combustion chamber, either with the aim of forming a homogeneous charge, or forming a richer air/fuel mixture in the vicinity of the spark-plug.

Chapter 3

Development of Hydrogen Injection Systems

In this chapter the development details of the three proposed hydrogen injection systems are presented. The selection of the hydrogen injector used is discussed along with the associated mounting arrangements that are required. Results of preliminary injector open flow testing to determine the relationship between supply pressure, injector current and flow rate are presented along with the results of dynamic injector testing.

3.1 Selection of Hydrogen Injector

3.1.1 Existing work in the Department

The selection of a hydrogen injector that is suitable for in-cylinder injection of hydrogen was critical for the success of this piece of research.

Commercially available Bosch gasoline manifold electronic fuel injectors have been used previously in the department as gaseous direct injection fuel injectors in constant volume combustion bomb research by Damiano [1993] , Robinson [1995] and Roache [1998], and in stratified charge investigations in a Ricardo E6 engine by Zavier [1991] and Calvert [1994]. These injectors worked well but did leak from the seat with higher gas supply pressures. The injectors used in the engine work were used in conjunction with hypodermic connecting tubes and non-return valves. This enabled them to withstand the high downstream combustion pressures and temperatures which would otherwise preclude their use as direct injection injectors.

Earlier work in this department involving the use of direct hydrogen injection in an engine had been carried out by Glasson [1992]. Glasson designed and built a sonic hydrogen injector that was capable of fuelling an Ricardo E6 engine on hydrogen as the sole fuel at air/fuel ratios from rich ($\lambda = 0.9$) to very lean ($\lambda = 3.0$). The advantage of a sonic injector is that the flow rate of hydrogen injected is independent of the pressure downstream of the injector nozzle. Thus the mass flow rate of such an injector is dependent only on the hydrogen supply pressure and the injection duration. The sealing of

the injector seat against hydrogen leakage using an elastomeric seat proved problematic however with the seating arrangement lasting around 1/2 an hour typically.

Brown [2001] modified Glasson's injector for his investigation of late high pressure hydrogen direct injection fuelling of a Wankel Rotary engine. He attempted to overcome the injector seat sealing problems by using a metal to metal seating arrangement as opposed to Glasson's elastomeric seat. This solution resulted in a small amount of leakage which was tolerable but significantly better durability. It also allowed the effective lift of the injector pintle to be varied to allow the injector to be set up for differing flow rate ranges.

It became apparent when the range of hydrogen fuelling rates required for this project (from 0 to 50% HEF) was compared to the known performance characteristics of the Glasson injector that it would not be suitable. In addition Brown was still using the Glasson injector for his research. A suitable injector therefore had to be obtained for the current work.

3.1.2 Compressible Flow Theory

The advantage of operating an injector as a sonic injector is that the flow rate of hydrogen is not dependent on the pressure of the gas in the combustion chamber but dependent only on the injection supply pressure and duration. From Massey [1989] for compressible flow.

$$\dot{m} = A_c \sqrt{\frac{\gamma}{R}\left(\frac{2}{\gamma+1}\right)^{\frac{\gamma+1}{\gamma-1}}} \frac{p_0}{\sqrt{T_0}} \tag{3.1}$$

$$for \quad \frac{p_c}{p_0} < \left(\frac{2}{\gamma+1}\right)^{\frac{\gamma}{\gamma-1}}$$

where γ = ratio of specific heats
R = gas constant (4126.2 J/kmol.K for hydrogen)
A = area of nozzle (m^2)
p = absolute pressure (Pa)
T = absolute temperature (K)
$_c$ = value at minimum contraction of nozzle
$_0$ = stagnation value

From Equation 3.1 it can be noted that when $\left(\frac{p_c}{p_0}\right) < 0.53$ for hydrogen, the velocity at the minimum area of the contraction is equal to the speed of sound and the flow is

termed to be choked or sonic. At this condition the mass flow rate of hydrogen is the maximum possible and is independent of conditions downstream of the nozzle. Under this condition the mass flow rate of hydrogen into the combustion chamber is dependent only on the hydrogen supply pressure and temperature and the injection duration.

The maximum pressure downstream of the injector during the injection process can be estimated from the maximum pressure due to isentropic compression of the intake air/fuel charge.

$$p_2 = p_1 \left(\frac{V_1}{V_2}\right)^{\gamma} \tag{3.2}$$

For a compression ratio of 10:1 and assuming that the pressure at the start of the compression stroke (p_1) is atmospheric pressure (1.01325 bar), the pressure at the end of the compression stroke (p_2) is:

$$\begin{aligned} p_2 &= 1.01325(10)^{1.4} \\ &= 25.45\ bar \end{aligned} \tag{3.3}$$

The minimum pressure required for sonic flow is then found by substituting the maximum combustion chamber pressure (p_2) into the limiting pressure ratio from equation 3.1 and rearranging to give:

$$\begin{aligned} p_o &= \frac{25.45}{0.53} \\ &= 48.0\ bar \end{aligned} \tag{3.4}$$

In order to be able to inject hydrogen at any point in the compression stroke, the minimum hydrogen supply pressure must therefore be greater than 48.0 bar to achieve sonic flow. Therefore any injector used must operate with a supply pressure of greater than 48 bar and be able to seat properly, not allowing hydrogen to leak when the injector is not actuated.

3.1.3 Mitsubishi Gasoline Direct Injection (GDI) Injector

Mitsubishi were the first company to put into production an engine that employed a solenoid actuated direct injection gasoline injector to facilitate the operation of an engine with either a homogeneous or heterogeneous charge as required. The gasoline was injected directly into the combustion chamber allowing precise control of charge stratification [Kume *et al.* 1996] , [Iwamoto *et al.* 1997].

Two Mitsubishi GDI injectors[1] were obtained from Mitsubishi Motors New Zealand Limited for evaluation as potential direct injection hydrogen injectors for this research. Adapting a Mitsubishi GDI injector for use as a hydrogen injector has the following benefits.

1. The technology is proven. Being a production piece of equipment it is durable and reliable and will eliminate the problems encountered by Glasson and Brown of constantly having to rebuild and adjust the injector to achieve reliable performance.

2. The GDI injector is designed to operate with a fuel pressure of 5 MPa (50 bar) as opposed to a conventional manifold fuel injector which operates with a fuel pressure of 0.2 MPa (2 bar). Thus it is hoped that the injector will have significantly better sealing than a conventional injector and be able to operate with much higher gas supply pressures with little or no leakage.

3. Being solenoid actuated, control of the injection duration and pressure should enable the injector to be used to provide a localized *puff* of hydrogen as well as the larger quantities required for higher rates of supplementation of the main methanol charge.

The disadvantage of using a commercial injector however is that if the desired flow rate of hydrogen cannot be achieved by varying either the supply pressure or the injection duration, there is nothing that can be done to remedy the situation. Another area of concern was the possibility of wear occurring when using a gas in the injector due to the absence of gasoline which would serve to lubricate the seating surfaces[2].

3.2 Preliminary Injector Flow Testing

The Mitsubishi GDI injector was supplied with very little technical data about either its flow or electrical characteristics. In order to determine the basic flow and electrical characteristics of the injector, some preliminary flow testing was carried out.

3.2.1 Open Flow Characteristics

The Mitsubishi GDI injector was first tested with the injector held open in the actuated position. The aim of this was to determine the injector's effective throat area from compressible flow theory to allow computation of mass flow rates for a given condition. As the injector was supplied with very little technical data, there was no way of knowing

[1] Part Number JCMD341969

[2] These concerns proved unfounded as no problems were experienced with leakage from the injector over the duration of the project

Gauge Pressure (psi)	Absolute Pressure (kPa)	Hydrogen (kg/sec)	Calculated Throat Area (mm^2)
100	789.5	4.75E-05	0.096
200	1479.0	1.22E-04	0.132
300	2168.4	1.87E-04	0.138
400	2857.9	2.50E-04	0.140
500	3547.4	3.25E-04	0.147
600	4236.9	4.00E-04	0.151
700	4926.4	4.64E-04	0.151
800	5615.8	5.35E-04	0.153
900	6305.3	5.82E-04	0.148

Table 3.1 Flow Rates and Calculated Throat Areas

what the maximum current was that could be applied to the injector without causing permanent damage.

A series of tests were run and at each supply pressure details of the flow rate and the current required to open and hold the injector open were recorded.

The injector was connected to a high pressure hydrogen supply via a pressure regulator to allow the supply pressure to be varied from 0 to 63 bar. The end of the injector was connected to a large diameter pipe and vented safely outside to the atmosphere. The volumetric flow rate of gas at differing supply pressures was measured using a Hastings 0 - 500 SLPM N_2 thermal mass flow meter. Details of the calculation used to convert the flow of hydrogen as read from the display unit in SLPM N_2 to a mass flow rate can be found in Appendix E.2 on page 239.

The results of open flow testing are summarized in Table 3.1 and plotted in Figure 3.1. It can be seen that the effective critical throat area of the injector was calculated to be ≈ 0.15 mm^2.

At each supply pressure, the current being supplied to the injector was gradually increased until the injector opened (opening current). The gas flow rate was recorded and then the current supplied was reduced until the injector closed (closing current). The values obtained are plotted in Figure 3.2.

The current required to open the injector increases as the gas supply pressure increases. The injector opens inwards so the solenoid is having to actuate against an increasingly large force that is being applied by the gas pressure. The current required

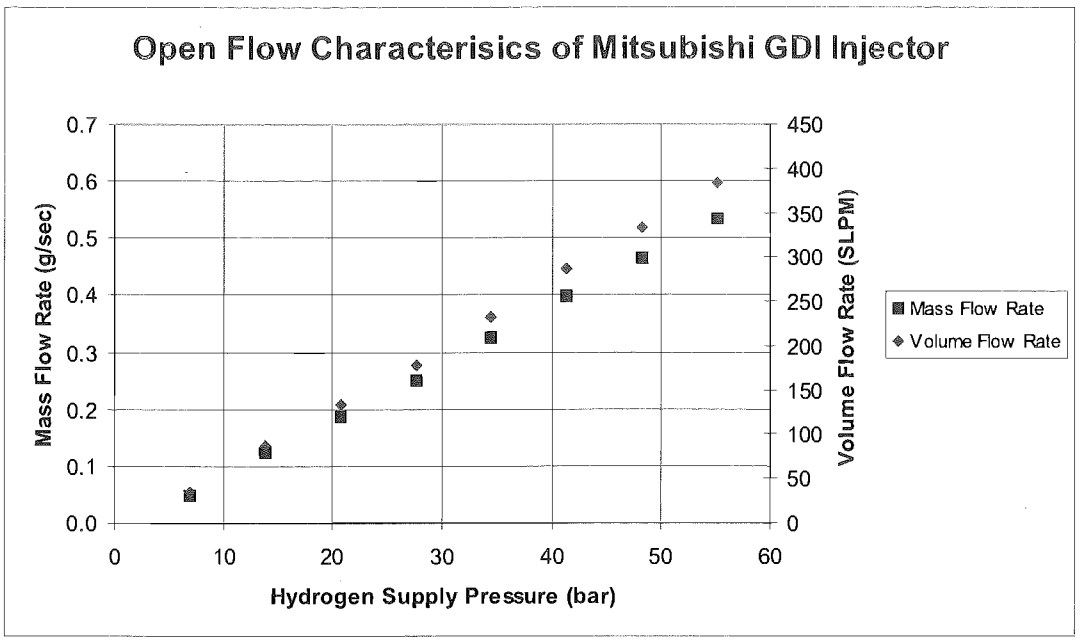

Figure 3.1 Hydrogen Mass Flow verses Supply Pressure

to hold the injector open against the supply gas pressure is less than that required to open it for a combination of two reasons. Firstly there is less area for the gas pressure to act upon when the injector is open hence less force to resist. Secondly when the injector is open, the pressure differential between upstream and downstream is not as great as when the injector is closed, again reducing the force required to keep the injector open. The current required to hold the injector open against the gas supply pressure also increases with increasing supply gas pressure.

It was decided that the hydrogen supply pressure that would be used through out the early direct injection testing would be 55 bar[3,4] for the following reasons:

1. The minimum hydrogen supply pressure required to achieve sonic flow of hydrogen is 48 bar (see page 28). A pressure of 55 bar allows a margin of error in the calculation of this pressure.

2. In order to achieve higher values of hydrogen energy fraction during supplementation, it will be necessary to inject quite high mass flow rates of hydrogen. As the flow through the injector is sonic, the only two ways of increasing the amount of

[3]Note: A full cylinder of hydrogen has a pressure of approximately 150 bar (2175 psi). Thus when the pressure has dropped to 55 bar the cylinder is effectively "empty".

[4]When the engine management system was installed in the test cell and the hydrogen injectors tested, it was discovered that the maximum supply pressure that could be used was 48.2 bar (700 psi). This was due to a limited selection of values for the current limiting resistors in the injector driver. As this value is similar to the minimum value calculated from compressible flow theory and injection at TDC is unlikely, 48.2 bar was used during engine testing

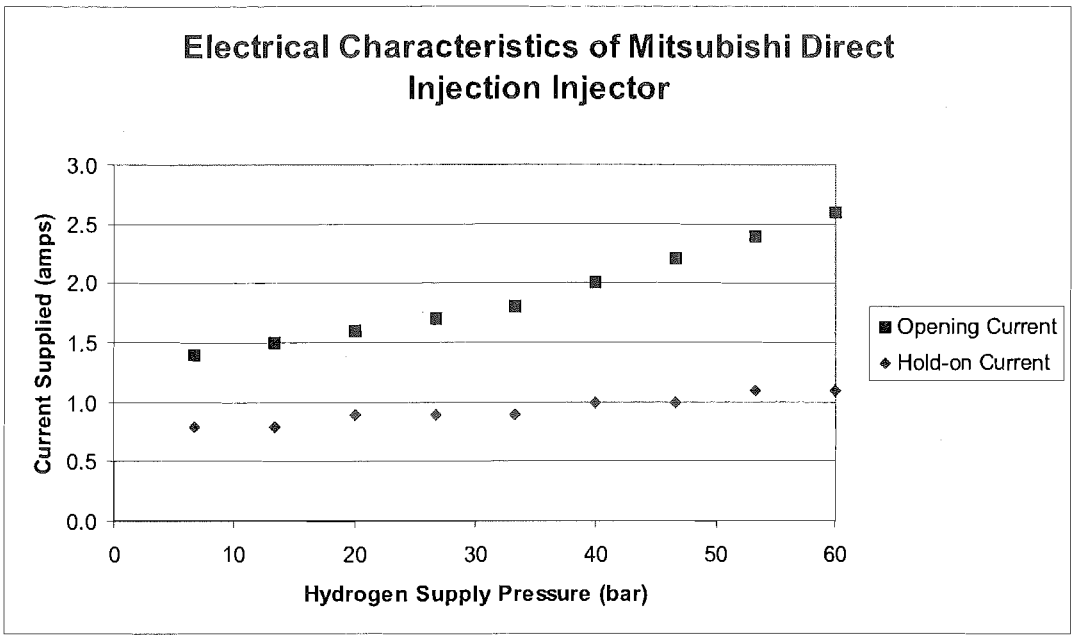

Figure 3.2 Injector Electrical Characteristics verses Supply Pressure

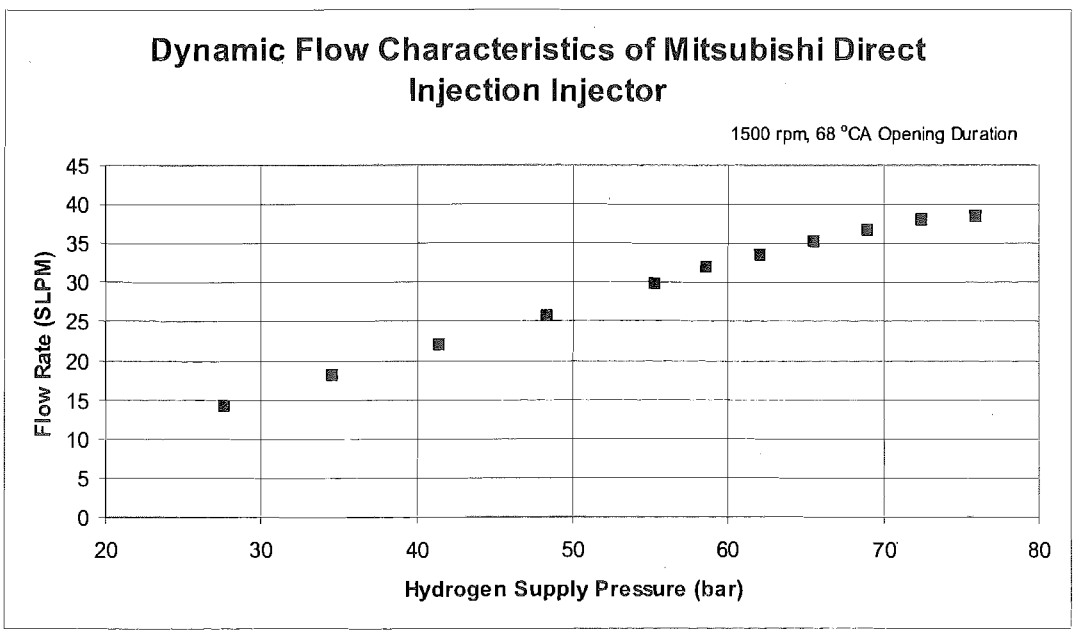

Figure 3.3 Dynamic Injector Flow Characteristics verses Supply Pressure

hydrogen injected is to increase the injection duration or to increase the hydrogen supply pressure. In order to achieve homogeneous mixture formation, the hydrogen is required to be injected in the shortest possible interval after the inlet valve has shut thus requiring the highest hydrogen supply pressure possible to achieve the high substitution levels.

3. The higher the supply pressure the greater the current required to actuate the injector. It was felt the the current required to actuate the injector against a supply pressure of 55 bar (2.4 A) was quite high and using a higher value may result in permanent damage to the solenoid[5].

3.2.2 Engine Actuated Flow Characteristics

Having determined the open flow characteristics of the Mitsubishi GDI injector and calculated it's critical area (see Table 3.1), a test was performed to determine what extent hydrogen of substitution would be practically attainable on the Ricardo E6 engine.

Glasson [1992] had found in the course of his research when fuelling the Ricardo E6 engine solely on hydrogen that if the injection of hydrogen occurred after 284 ^{o}ATDC, NO_x emissions increased due to stratified charge combustion resulting from there being insufficient time for an homogeneous mixture to occur. Thus for the purposes of this test the hydrogen injector was actuated at 216 ^{o}ATDC (inlet valve closes at 216 ^{o}ATDC) and closed at 284 ^{o}ATDC i.e. an injection period of 68 ^{o}CA. The flow rate of hydrogen was measured using a Hastings 0 - 100 SLPM N_2 mass flow meter. The engine speed was 1500 rpm.

It can be seen from Figure 3.3 that for a hydrogen supply pressure of 55 bar, the maximum flow rate of hydrogen that could be expected during actual engine testing is 30 SLPM.

Using a spreadsheet developed to calculate the required flow rates of methanol and hydrogen for a given overall air/fuel ratio and hydrogen energy fraction (HEF), it was found using a hydrogen flow rate of 30 SLPM, the maximum HEF that could be expected during engine testing for λ=1.0 is 20% HEF.

[5] At a later point in the work one of the injectors was accidentally destroyed by allowing it to draw too much current. This injector was taken to pieces to allow the internal configuration to be studied. The intact section of the windings of the solenoid were connected to a power supply and a 3 A current applied continuously for a period of 2 hours with no detectable heating observed in the windings. A 6 A current was then applied continuously for a period of 2 hours with only slight warming being detected in the windings. It was concluded that the current limit of 2.4 A that had been designed into the injection circuit was suitable

Although the degree of hydrogen substitution for the λ=1.0 case is not high, up to 50% HEF substitution will be attainable for leaner air/fuel mixtures. On the basis of the preliminary injector flow testing, it was decided that the Mitsubishi GDI injector would be suitable for the purposes of this investigation.

3.3 Injection Systems

The three systems for introducing supplementary hydrogen into the Ricardo test engine are as follows.

1. Untimed Manifold Injection. Technically the simplest, the aim is to form a homogeneous air/fuel mixture.
2. Early Direct Injection. The aim of this method is to form a homogeneous mixture as in the untimed manifold case but overcome the associated volumetric efficiency penalty.
3. Modified Spark-plug Injection. The aim of this method is to be able to form a localized hydrogen rich air/fuel mixture in the vicinity of the spark-plug.

3.3.1 Untimed Manifold Injection Configuration

The initial attraction in dual fuelling an engine with methanol and hydrogen was the possibility of using the advantageous characteristics of each fuel to overcome the disadvantageous characteristics of the other. Fuelling of a spark ignited engine with hydrogen via external mixture formation is limited by knocking and pre-ignition that can potentially result in flash-back into the inlet manifold resulting in back-fire. Methanol has a high latent heat of vaporization which results in poor fuel vaporization leading to poor cold start characteristics, poor combustion and increased cylinder wear (see pages 13 and 89). A fuelling system that allowed methanol to be injected into the cylinder before the hydrogen was injected could potentially be of benefit to the combustion of both fuels. The initial injection of methanol could cool the cylinder walls and charge before the later injection of hydrogen thereby potentially avoiding the characteristic pre-ignition and knocking combustion of hydrogen. Hydrogen, being a gas and having wide flammability limits, offers the potential of overcoming methanol's poor cold start characteristics.

An inlet manifold that accommodated a hydrogen injector was therefore required. It was decided to remove the existing horizontal throttle plate on the inlet manifold of the engine and replace it with a custom made manifold section. A vertical throttle plate was positioned after the inlet air heating element but before the methanol injector.

Requirements of the custom manifold were as follows:

1. To have the same overall dimensions as the horizontal throttle plate that it is replacing.
2. Incorporate a Mitsubishi GDI injector.
3. Provide attachments to enable a hydrogen supply system to be plumbed to the injector.
4. Prevent the leakage of hydrogen.
5. Take advantage of hydrogen's high buoyancy to promote it's mixing with the incoming air/fuel mixture.

A suitable manifold was designed and manufactured (see Figure A.1). The hydrogen is introduced to the inlet air from the lower portion of the manifold to take advantage of the extremely buoyant nature of hydrogen to enhance the mixing. The layout of the Ricardo E6 head, inlet manifold, methanol injector, vertical throttle plate, air heater and viscous air flow meter is shown in Figure 3.4.

Preliminary testing revealed that there would be no advantage in supplementing hydrogen to the engine manifold in a timed manner. The concept behind timed manifold injection of methanol and hydrogen is that the methanol is injected first, cooling the combustion chamber surfaces. The hydrogen is injected slightly later entering a combustion chamber with cooler surfaces. Thus the well documented problem of pre-ignition of manifold injected hydrogen on hot-surfaces in the combustion chamber is potentially overcome. With the current hydrogen injector and fuel supply system it was impossible to supply sufficient hydrogen in a timed fashion to operate the engine in the region where operation is limited by knock and pre-ignition. From a vehicle concept point of view, if the on-board hydrogen generator (as described on page 5) is less than 100% efficient (energy in divided by energy out), any methanol being diverted to the generator represents an efficiency loss [MacDonald 1976]. Large levels of substitution would therefore not be desirable under these circumstances. The addition of small quantities of hydrogen at lean air/fuel ratios was also observed to have a greater effect than at richer air/fuel ratios. Given the findings of the preliminary engine testing, it was decided to focus the investigation on the effects that small quantities of hydrogen have on the combustion of methanol.

It was decided to supply the hydrogen in a continuous untimed fashion to the inlet manifold. This method is technically the easiest way of adding hydrogen to the inlet air while still forming a homogeneous air/fuel charge with the inlet air and methanol. The hydrogen supply was initially plumbed to the underneath of the inlet manifold in the same position as the original hydrogen injector to take advantage of hydrogen's buoyancy to aid in the formation of a homogeneous mixture. The flow rate of hydrogen was

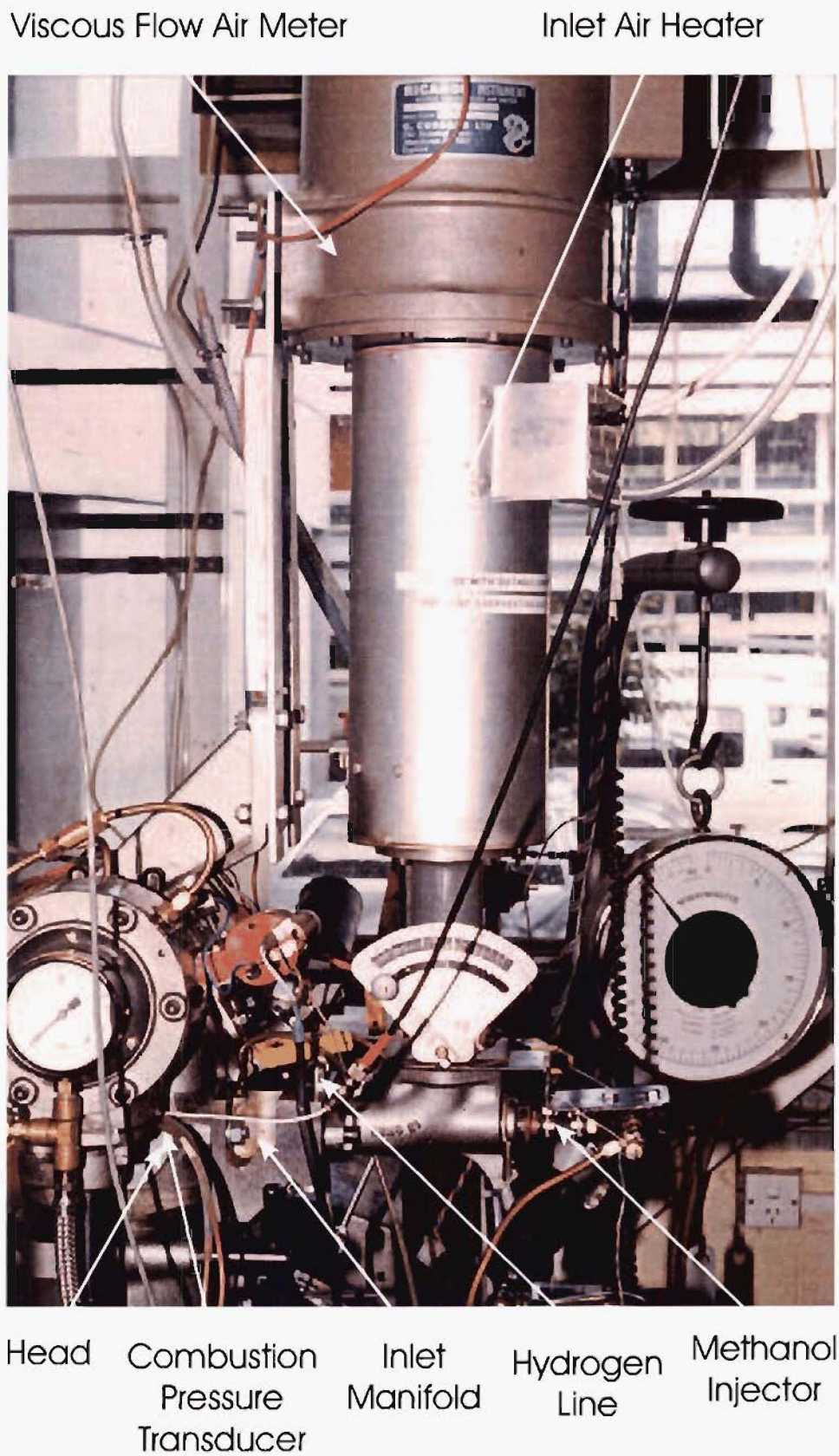

Figure 3.4 Inlet Manifold Arrangement for Untimed Manifold Injection

controlled via regulation of the supply pressure and/or the use of a metering valve in the supply line. This arrangement proved to be problematic as at higher methanol flow rates and with a relatively low level of inlet air heating ($\approx$ 364 W - see page 89), methanol was found to condense on the walls of the inlet manifold and run down into the hydrogen supply line. This has the effect of blocking the flow of hydrogen until sufficient pressure built up releasing a large "bubble" of hydrogen into the inlet air/fuel mixture, resulting in a brief period of engine knock and an associated fluctuation in the output torque of the engine. This was overcome by plumbing the hydrogen supply into the top of the inlet manifold.

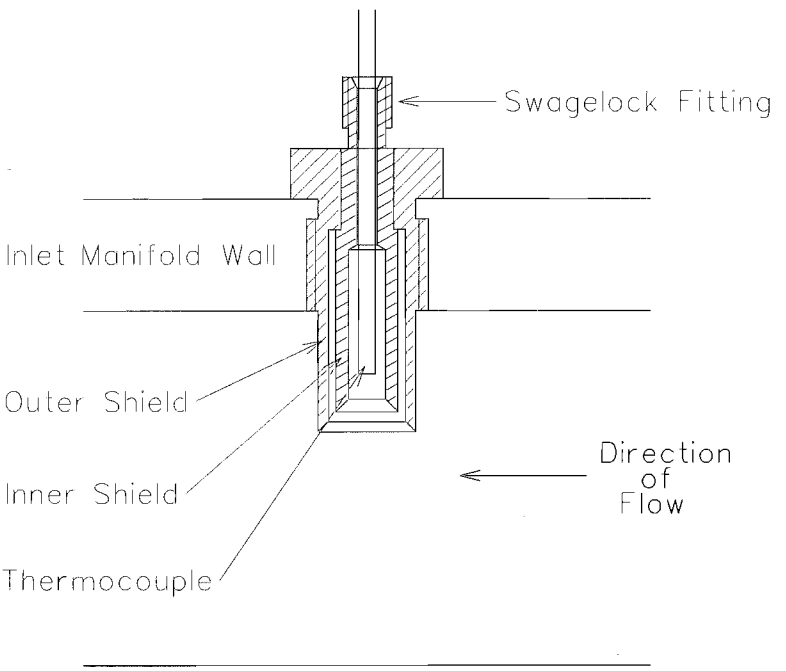

Figure 3.5 Thermocouple in Inlet Manifold

A later decision to monitor the air/fuel mixture resulted in a temperature probe being designed (see Figure 3.5 for a schematic and Figure A.3 for the workshop drawings). Measuring the temperature of a partially evaporated mixture of fuel and air is not a trivial exercise. Inaccuracies occur if liquid impinges on the thermocouple junction and subsequently evaporates as the junction is cooled due by the latent heat of vaporization of the fuel. Using methanol as the fuel compounds the problem as the latent heat of vaporization is approximately 3 times greater than that of gasoline. The thermocouple was thus designed with an outer shield. Any liquid fuel impinging on the outer shield can evaporate and the thermocouple probe is shielded as far as radiation is concerned from the cool outer shield by an inner shield (see Figure 3.5). The thermocouple itself was passed though a 1/8 inch Swagelock fitting with nylon ferrules to prevent conduction from the inlet manifold itself causing any inaccuracies in the temperature measured.

The thermocouple was manufactured by feeding a length of thermocouple wire through a capillary tube. The two wires were carefully melted together using a spark discharge to form a thermocouple junction. While ensuring that neither of the two wires touched the side of the capillary tube, RTV was used to provide a non-conducting barrier between the thermocouple wire and the capillary walls as well as ensuring the inlet manifold is sealed from the atmosphere.

3.3.2 Early Direct Injection Injector Configuration

The design of the configuration that was to support the Mitsubishi GDI injector in it's early direct injection configuration was subject to a number of constraints:

1. Design must incorporate a Mitsubishi GDI injector.
2. Complete injector assembly must fit into the spare spark plug hole in the Ricardo head which is machined for a long reach spark plug[6].
3. The end of the Mitsubishi injector must be as close to the combustion chamber as possible to minimize dead volume in the arrangement.
4. Must provide suitable fittings to allow it to be plumbed to a high pressure hydrogen supply.
5. Prevent the leakage of hydrogen.
6. Allow access for electrical connections to the injector.
7. Assembly must be able to easily be fitted to the engine.

The final design consisted of four separate sections, an endcap, a spacer, the bottom end and a nozzle. The endcap, spacer and bottom end were held together with 4 cap screws that ran the length of the assembly. The layout of the configuration can be seen in Figure 3.6 and all of the manufacturing drawings can be found in Appendix A on page 219.

The endcap was designed to fit on the upstream side of the injector (see Figure 3.6). This endcap fulfilled two functions. Firstly it provided a connection to the high pressure hydrogen supply via a Swagelock fitting. Secondly it sealed against the body of the Mitsubishi GDI injector via a counterbore and an O-ring.

The function of the spacer is to provide support between the endcap and the bottom end as well as keeping the assembly concentric. Its length was adjusted to allow the

[6]This allows the spark plug to remain in the same position relative to the valves etc. for all three fuelling systems

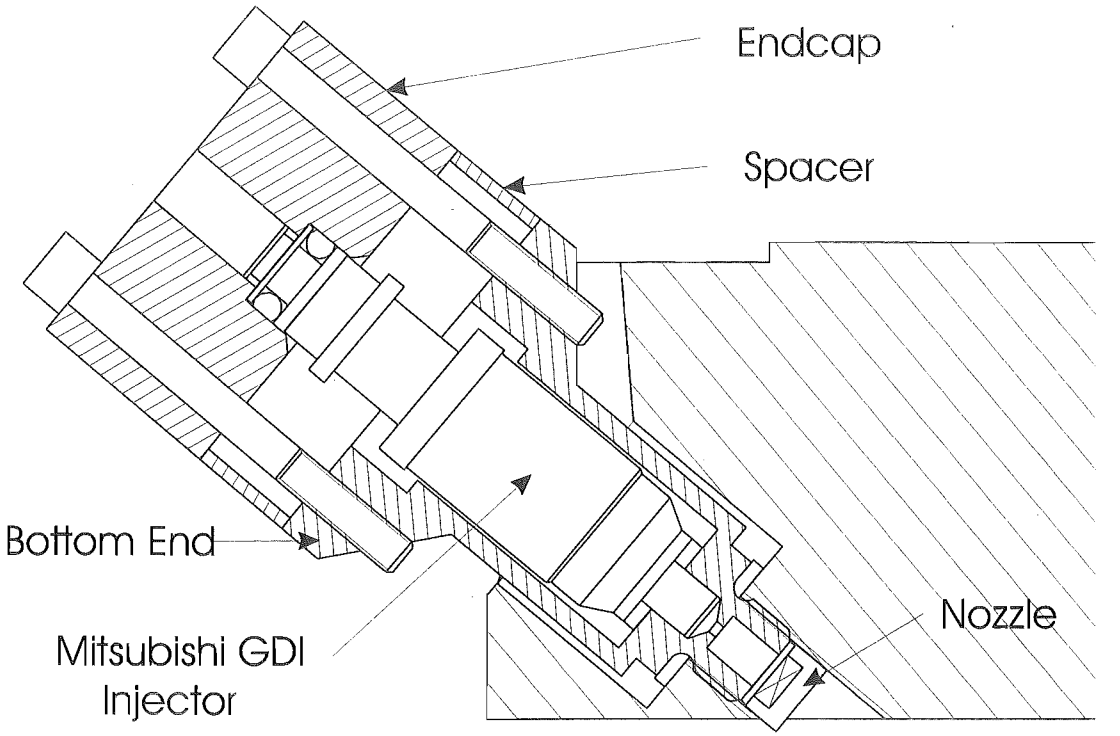

Figure 3.6 Direct Injection Injector Configuration

required amount of compression between the endcap and the bottom end when the cap screws were tightened.

The bottom end was carefully designed to meet the design criteria listed previously. The injector has an outer spark plug thread that allows it to screw into the spare spark plug hole. Sealing of the combustion gases is provided for both on the inside and the outside of the bottom end by copper gaskets. The inside of the bottom end is sized to accommodate a Mitsubishi GDI injector and position it as close as possible to the combustion chamber. The end of the bottom end also has a internally cut thread to allow injection nozzles of various configurations to be attached. The nozzle is held in place with Loctite and a grub screw which is positioned perpendicular to the axis of the nozzle.

The resultant direct injection injector assembly is a compact arrangement that met all the design requirements and proved during the course of the research to function in a satisfactory manner.

3.3.3 Modified Spark-plug Injection Injector Configuration

The modified spark plug arrangement, used to provide an injection of hydrogen to form a localized rich mixture around the spark-plug electrode, is based upon arrangements that have been previously developed within this department for constant volume com-

bustion bomb research by Damiano [1993] , Robinson [1995] and Roache [1998], and in stratified charge investigations in a Ricardo E6 engine by Zavier [1991] and Calvert [1994].

The modified spark plug arrangement must satisfy a number of constraints:

1. The maximum diameter of the arrangement must be such that it can fit into the spark plug hole in the Ricardo E6 engine.
2. The modification must leave the spark-plug with enough thread to safely hold it in the head of the engine under operating conditions.
3. The arrangement must make provision for the spark-plug to be fitted to the engine ie access for a spark-plug socket.
4. The arrangement must incorporate a Mitsubishi GDI injector.
5. The arrangement must provide a flow path for hydrogen into the area around the central ceramic electrode.
6. The arrangement should have a minimum of dead volume.

The spark plug hole that will be used throughout this research program is configured to take a short reach spark plug. The adaption collar was designed to be used with a long reach spark plug so that the length of thread remaining after the adaption collar was fitted to the spark plug would be the same as that on a short reach spark plug. An endcap and spacer were also used as in the early direct injection arrangement.

The difficulty then arose that the ceramic central electrode of the spark-plug to be used was quite short causing there to be a non-direct radial flow path from the center of the adaption ring into the area around the central electrode. The three connecting holes therefore had to be drilled at an angle of $\approx$45 degrees in order for the drill to not contact the ceramic electrode and break. It was later determined in the course of the schlieren photography investigation that these holes were in fact not providing a good supply of hydrogen to the electrode and modifications had to be made (see page 53).

The layout of the modified spark-plug injector configuration is shown in Figure 3.7.

The major drawback of the modified spark-plug injection arrangement is the amount of dead volume between the spark-plug and the injector. During engine operation both fresh air/fuel mixture and partially burnt combustion gases could flow into this volume and be prevented from being properly oxidized by the flame. This will result in this configuration potentially having higher unburnt hydrocarbon emissions than the direct

injection fuelling system which has a lower dead volume associated with it.

The dead volume of the modified spark plug arrangement was measured and found to be 1.167 cm^3 compared with 0.1 cm^3 for the direct injection injection configuration.

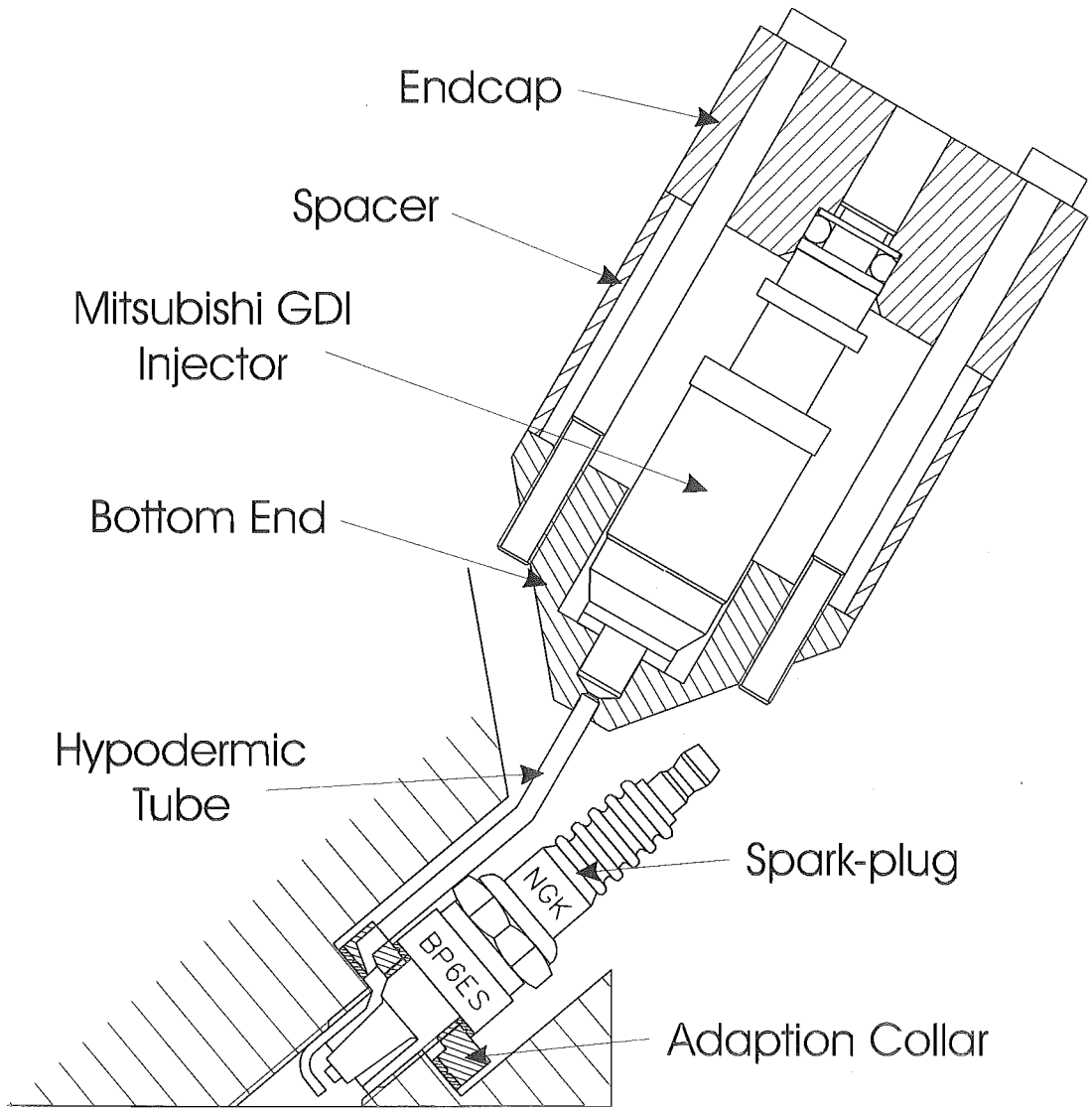

Figure 3.7 Modified Spark-plug Injector Configuration

Master Gasket Sealant was used on all copper gaskets to provide extra sealing capability. As a final check of the collars sealing, the modified spark plug arrangement was fitted to a constant volume combustion bomb and a high pressure supply of nitrogen attached. The nitrogen supply pressure was gradually increased to 85 bar. The gas connection as well as the adaption collar were tested for leaks using "snoop"[7] and found to be leak free.

[7] A liquid that when applied to a joint leaking gas causes bubbles to be formed.

Chapter 4

Schlieren Photography Visualization Investigation

This chapter introduces schlieren methods and their principle of operation before describing the apparatus used and the test procedure. The performance of both the direct and modified spark-plug injection injector configurations described in Chapter 3 are further improved through the use of schlieren photographs to visualize the resultant flow fields.

4.1 Introduction

Situations commonly arise in science and engineering that involve the use of fluids that are colorless and transparent. Observing the interaction of these fluids with objects, their mixing with other similar fluids and the effects of heat on the fluid motion by conventional visual or photographic means is therefore very difficult or impossible.

Most of the situations of interest however involve changes in the density (and therefore the refractive index) of the fluid(s) due to compression (in the case of compressible flow) or temperature (in the case of convection).

Schlieren methods are optical methods of observing and photographing this type of phenomena which take advantage of the effect that changes in the refractive index have on the transmission of light. The best known method is that developed by Toepler [Holder and North 1963] , [Massey 1989] and it is this method that will be used throughout this work.

Schlieren methods have been used to observe and photograph the flow field associated with the injection of hydrogen from both the early direct injection injector and the modified spark-plug injection injector.

4.2 Apparatus

Schlieren photography has been used previously in the Department of Mechanical Engineering by Zavier [1991] , Robinson [1995] , Brown [2001] and in investigations overseas by Heywood and Vilchis [1984] , Koyanagi *et al.* [1993] and Kume *et al.* [1996] amongst others to visualize the injection of one gas into another. The relevant background theory relating to schlieren methods can be obtained from Holder and North [1963] and Robinson [1995]. Actual dimensions of the experimental setup used can be obtained from Brown [2001].

4.2.1 Changes Made to Timing Apparatus

Previous researchers used a remote control box to vary the delay between the firing of the injector and the firing of the strobe light. During the course of early setup experiments this box was found to produce inconsistent injection timings. In order to overcome this problem, a small program was written in C^{++} called LIGHT.C to control the start and duration of hydrogen injection via a UPP board designed and manufactured by electronic technicians in the Department of Mechanical Engineering. As had been the case previously when the injector is triggered, the strobe remote triggering device's leads are shorted leading to the strobe being fired after a variable delay of between 0.0 and 999 ms. The layout of the triggering circuit is shown in Figure 4.1. An injector voltage of 48 volts was used so a rapid rate of current rise would occur ensuring a quick injector opening response. In order to ensure that the maximum current applied to the injector was not greater than 2.4 amps (see page 30), a current limiting resistor of value 20 Ω was added to the circuit.

4.2.2 Physical Arrangement of Test Bomb

The constant volume bomb that was used for the schlieren photography investigation has been manufactured and used in several earlier investigations by Zavier [1991] , Damiano [1993] and Brown [2001]. The inside of the bomb is cylindrical with a diameter of 76.2 mm, the same as the bore of the Ricardo E6.

The end of the early direct injection injector was positioned to line up with the edge of the two glass windows so that the injected hydrogen plume could be recorded as it left the nozzle. Similarly the modified spark plug injector was positioned so that the end of the spark plug thread lines up with the two glass windows with only the side electrode visible in the field of view. Due to the size of the glass windows in the existing schlieren bomb, only a small area in front of the injectors is able to be viewed and photographed using the schlieren setup. The layout of the bomb and relevant dimensions are given in Figure 4.5.

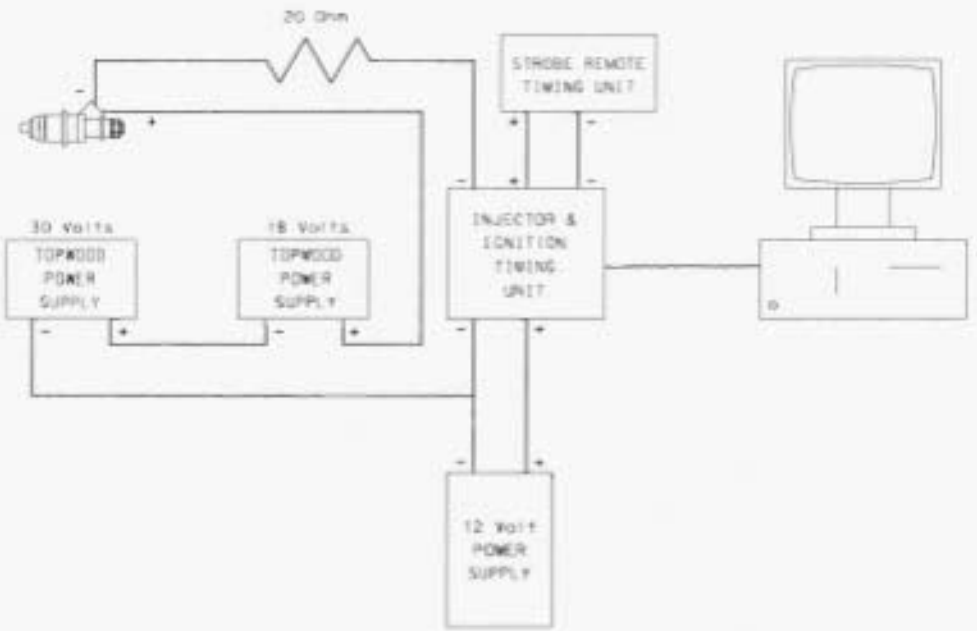

Figure 4.1 Schlieren Apparatus Triggering Circuit

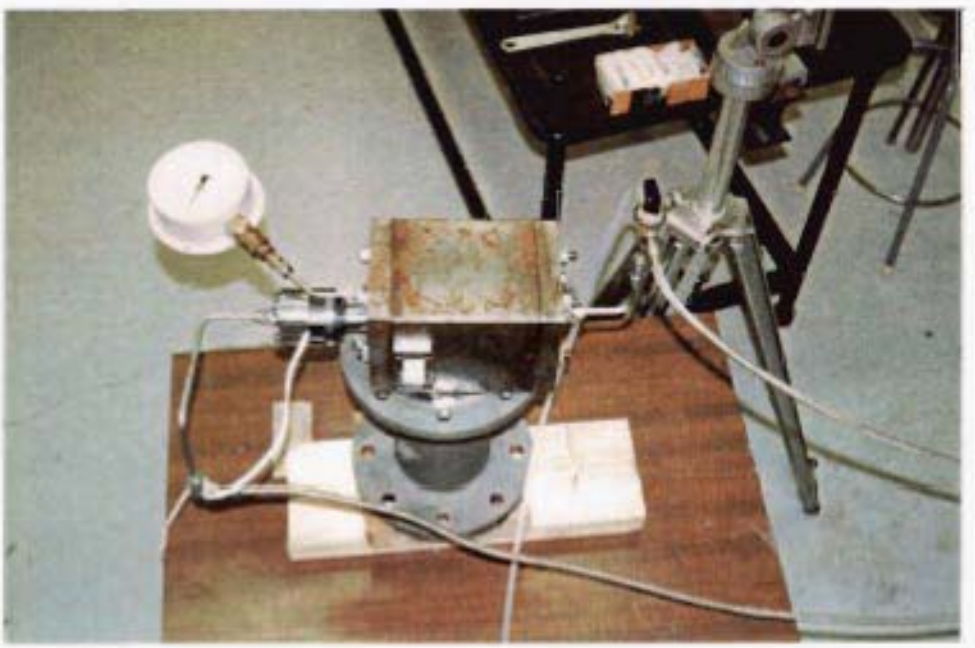

Figure 4.2 Oblique View of Schlieren Bomb

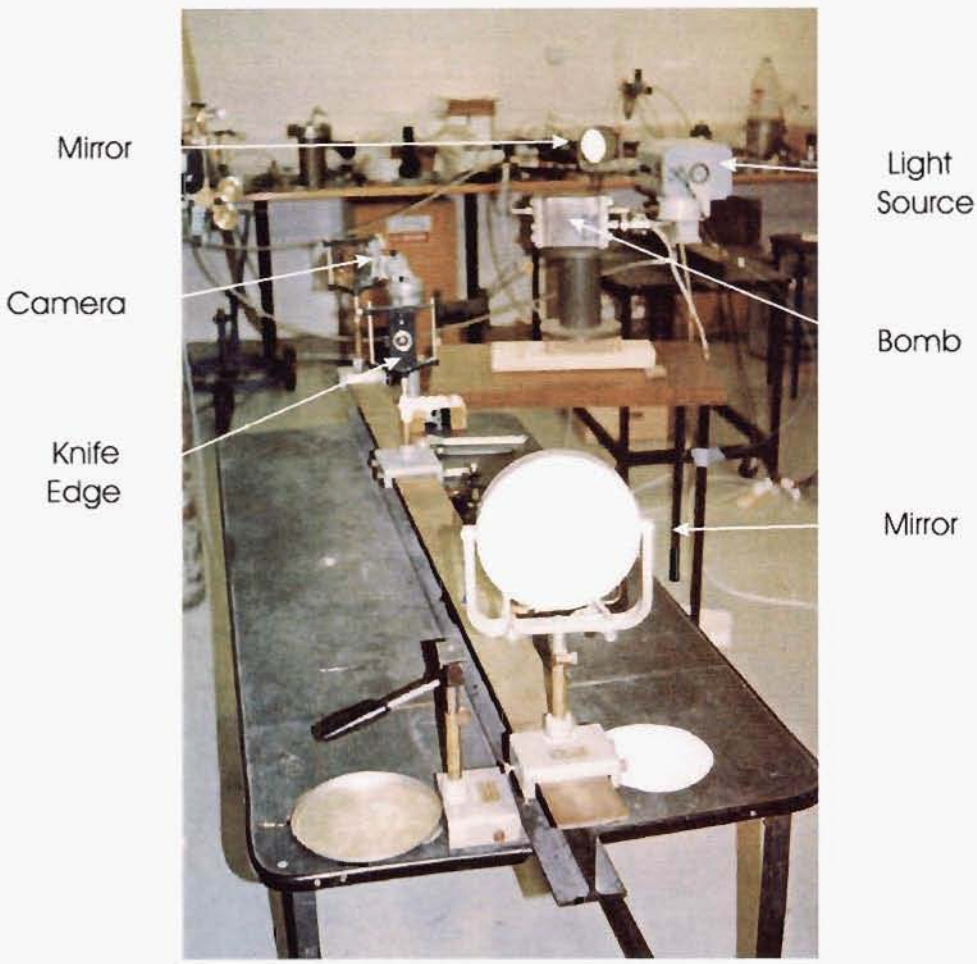

Figure 4.3 Schlieren Apparatus Layout

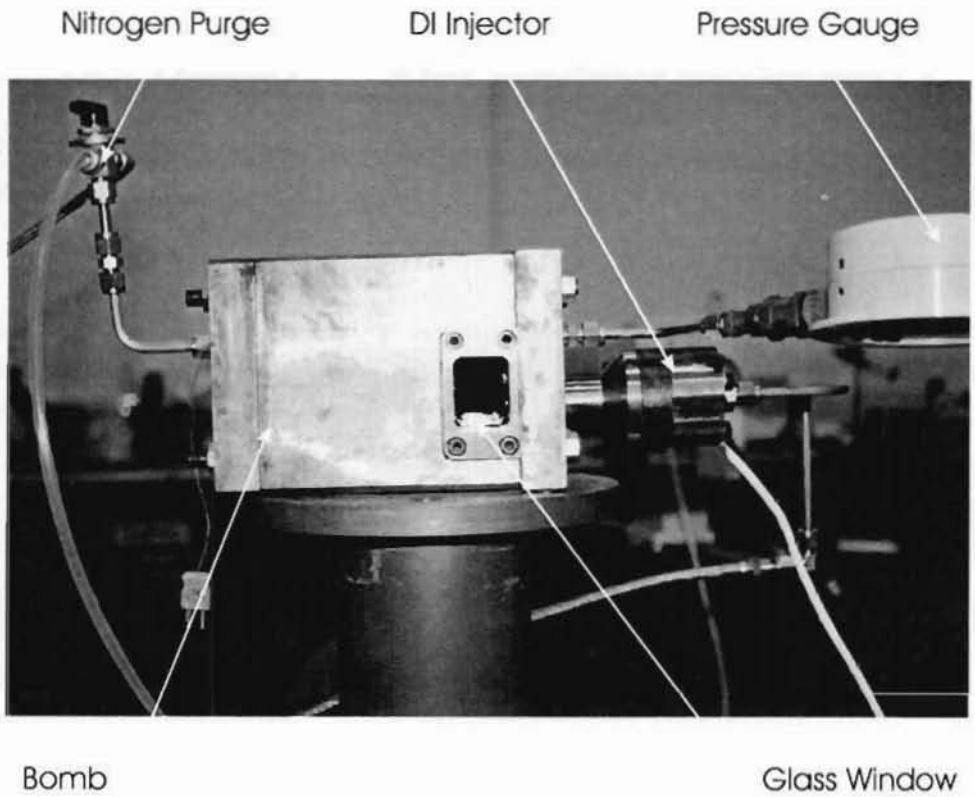

Figure 4.4 Side View of Schlieren Bomb

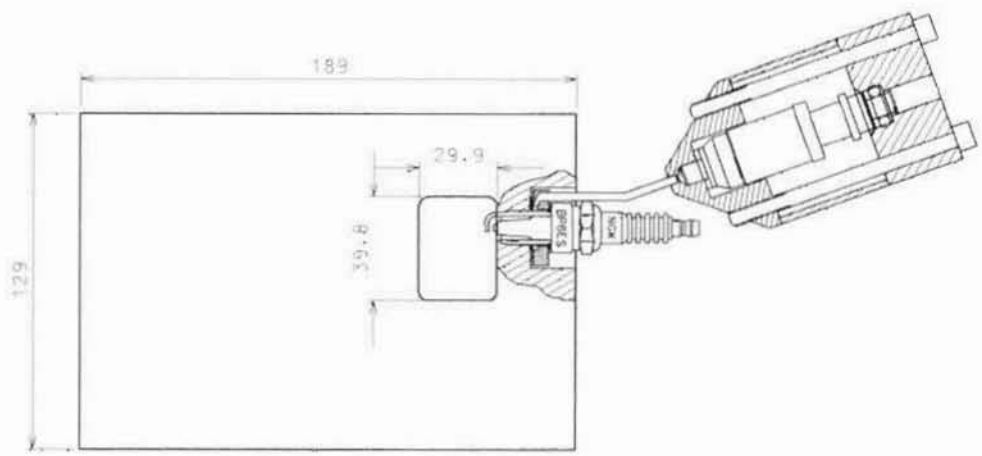

Figure 4.5 Bomb Arrangement with Modified Spark Plug Injector

4.3 Testing Procedure

In order to convey the procedure that is followed when taking a series of schlieren photographs, first the procedure will be described verbally before the exact steps are given.

The aim of the schlieren photography investigation is to obtain a series of photographs which show the flow field resulting from a particular hydrogen injection system under a given set of conditions over a series of known time intervals.

The program LIGHT.C is run on the computer which prompts the operator for the required hydrogen injection duration. The required delay between the start of injection and the firing of the argon strobe light is set on the strobe remote timing unit. At this point all the lights in the room including the computer monitor are switched off. Schlieren photography is carried out in a pitch black room by necessity as the camera shutter is open for long periods of time and any stray light will be recorded, degrading the final image. The assistant then opens and holds open the shutter of the camera manually. Once the input to the computer has been accepted, the program simultaneously starts the injection event and grounds the inputs to the remote timing unit. The grounding of the strobe remote timing unit's inputs starts the preset delay period before the strobe is fired. The signal to end the injection event is sent automatically from the computer. Once the strobe has fired the assistant can then release the shutter of the camera and advance the film. The hydrogen injection duration reset on the computer and the new strobe light delay duration is set on the strobe remote timing unit[1].

The accuracy of the injection durations was checked using a digital oscilloscope and the accuracy of the strobe firing delays using a digital oscilloscope in conjunction with a photo diode. Both were found to be as they had been specified to be.

The procedure that was followed is outlined as follows:

1. Set up schlieren apparatus according to instructions in Zavier [1991] , Damiano [1993] , Robinson [1995] and Brown [2001].
2. Set up schlieren apparatus triggering circuit according to Figure 4.1.
3. Fit injector configuration to be tested to the bomb and test for pressure leaks.
4. Purge the injector gas supply line with hydrogen before setting the hydrogen supply pressure.

[1]Note:- The injected hydrogen plume shown in a series of photographs is not the same plume. For each injection event, only one photograph is taken at a specified time after the injection is commenced. However it is assumed that the injection event is reasonably repeatable so this method will give a good representation of the injection event as a whole.

5. Purge the bomb with oxygen free nitrogen[2] before setting the bomb at the required pressure.
6. Run the injection program LIGHT.C and set the injection duration.
7. Set the required delay between the start of injection and the firing of the strobe light on the strobe remote timing unit and reset.
8. Shut off all the lights and have assistant hold open the shutter on the camera.
9. Run computer program
10. After the strobe has fired, close shutter on the camera.
11. Repeat above items as appropriate.

4.4 Early Direct Injection Injector

The aim of the early direct injection of hydrogen is to overcome the expected volumetric efficiency penalty associated with the manifold injection of hydrogen whilst still maintaining a homogeneous air/fuel mixture. Thus it was decided to start the injection of hydrogen at 220 ^{o}ATDC (the inlet valve having closed at 216 ^{o}ATDC). After preliminary injector flow rate testing it was calculated that the longest injection durations were likely to be approximately 65 ^{o}CA. The in-cylinder pressures at 216 ^{o}ATDC and 285 ^{o}ATDC were calculated to be 1 bar and 2.6 bar respectively for a compression ratio of 10:1 (see page 114). 2.0 bar was chosen as a bomb pressure suitable to represent the cylinder pressure at the time of the injection of hydrogen.

4.4.1 Four Hole Nozzle

Initial experimentation was carried out with a nozzle on the injector which had 4 holes of ϕ2.0 mm drilled on an 8 mm PCD at an angle of 45 degrees to the central axis of the injector body. The injection duration used was 10 ms and the supply pressure was 55 bar. Schlieren photographs of the flow field created are shown in Figures 4.6 to 4.13. Unfortunately the threaded hole in the bomb used to mount the injector is offset from the center of the window in the bomb. As a result the hydrogen jets are set to one side of the photograph and the right hand jet is partially obscured by the edge of the window.

[2] used to prevent a combustible mixture being formed

Figure 4.6 2.0 ms after start

Figure 4.7 2.4 ms after start

Figure 4.8 2.8 ms after start

Figure 4.9 3.2 ms after start

Figure 4.10 3.6 ms after start

Figure 4.11 4.0 ms after start

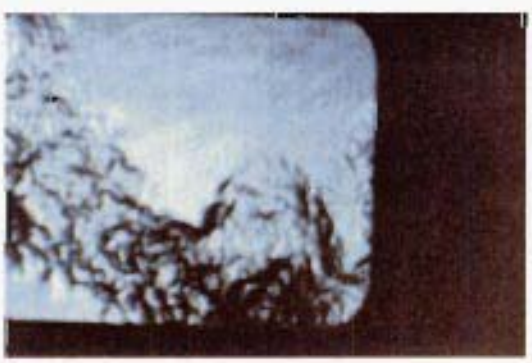

Figure 4.12 4.4 ms after start

Figure 4.13 4.8 ms after start

From the preceding figures the following points are evident:

1. There is a 2 ms delay between when injection is initiated to when the injected plume is first visible entering the combustion chamber.

2. The injected plume appears to be injected at a relatively low velocity as is evidenced by the broad appearance of the individual plumes and their poorly defined irregular edges. The hydrogen is discharged from the critical area of the injector at sonic velocity but due to the dead volume within the nozzle immediately downstream of the critical area, the gas velocity through the nozzle discharge holes is sub-sonic and thus dependent on the cross sectional area of the latter.

3. The plumes are not of equal size indicating that there will be differing degrees of penetration of the hydrogen plumes into the combustion chamber possibly leading to areas of incomplete mixing and a non-homogeneous air/fuel charge. The cause of the unequal jet development is thought to be due to differences in the hole configurations. This would result in differing pressure losses for each jet and hence differing masses of hydrogen injected into the bomb.

4. There is no central hole in the nozzle and it can be seen that the four plumes are leaving a large central area that has no hydrogen being injected into it that again could possibly lead to a non-homogeneous air/fuel charge.

In order to obtain improved injected hydrogen plume distribution and penetration, a second injector nozzle was manufactured with a five hole pattern with smaller diameter holes to promote increased gas velocity.

4.4.2 Five Hole Nozzle

The improved nozzle on the injector has 4 smaller holes of ϕ1.0 mm drilled on an 8 mm PCD at an angle of 45 degrees to the central axis of the injector body. The aim of the smaller hole diameters was to increase the velocity and hence the penetration of the hydrogen jets into the bomb. In addition to these holes, a fifth hole was drilled in the center of the nozzle along the axis of the injector. This central jet was created to overcome the observed poor spatial distribution of injected hydrogen along the axis of the injector.

The injection duration used was 10 ms and the supply pressure was 55 bar, the same as was used previously in the four hole nozzle testing. Schlieren photographs of the flow field created are shown in Figures 4.14 to 4.21.

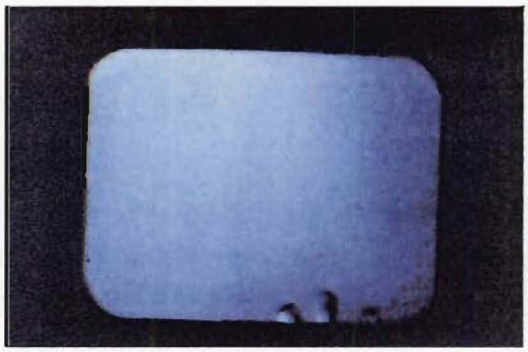

Figure 4.14 2.0 ms after start

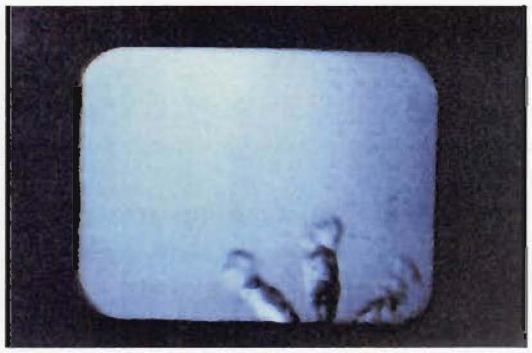

Figure 4.15 2.4 ms after start

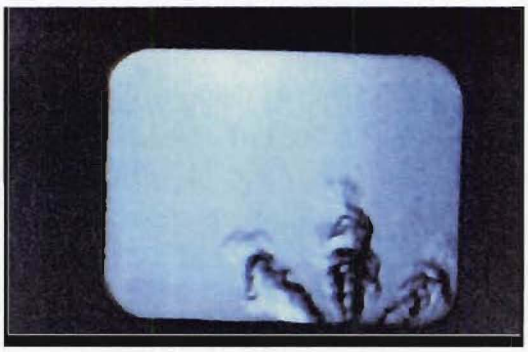

Figure 4.16 2.8 ms after start

Figure 4.17 3.2 ms after start

Figure 4.18 3.6 ms after start

Figure 4.19 4.0 ms after start

Figure 4.20 4.4 ms after start

Figure 4.21 4.8 ms after start

From the preceding figures the following points are evident:

1. The delay between when injection is initiated to when the injected plume is first visible entering the combustion chamber appears to have been reduced from ≈2.0 ms with the 4 hole nozzle to ≈1.8 ms for the 5 hole nozzle. The practical effect of this delay is that in an engine operating at 1500 rpm, no hydrogen will actually enter the combustion chamber until ≈16.2 ^{o}CA after injection is initiated.

2. The injected plume appears to be injected at a high velocity as all the plumes have very regular defined shapes and well defined edges.

3. The plumes are equal in size indicating that there will be equal penetration of the hydrogen plumes into the combustion chamber reducing the possibly of incomplete mixing and a non-homogeneous air/fuel charge.

4. The hydrogen plume from the central hole in the nozzle can be clearly seen in the center of the photograph behind one of the plumes coming "out of the page" at a 45^{o} angle (shown most clearly in Figures 4.17 and 4.18).

It was concluded from the schlieren photographs of the five hole nozzle that it was performing far better than the four hole nozzle and that its performance would be satisfactory for the early direct injection of hydrogen.

4.5 Modified Spark-plug Injector

The aim of stratifying the charge by creating a localized "puff" of hydrogen around the spark-plug is to take advantage of hydrogen's high laminar flame speed and strong flame initiation characteristics. A well developed, regular flame kernel should occur that will then propagate into the main methanol air/fuel mixture producing increased combustion stability and potential for extending the equipment lean limit.

Zavier [1991], during his research into charge stratification, injected puffs of methane around the spark-plug with a modified spark plug arrangement similar to the one being used in the current work. The start of the injection of the puff was varied from 50 to 80 ^{o}BTDC. In the absence of any other guidelines it was decided to base preliminary calculations on these values. The in-cylinder pressures at 280 ^{o}ATDC and 310 ^{o}ATDC were calculated to be 2.4 bar and 5.6 bar respectively for a compression ratio of 10:1. 5.0 bar was chosen as a bomb pressure suitable to represent the cylinder pressure at the time of injection of hydrogen.

Initial testing revealed that a 10 ms duration injected hydrogen puff was not visible around the spark-plug electrodes until approximately 40-50 ms after injection had been

commenced. This delay is not acceptable as it corresponds to a delay of 360 - 450 °CA in an engine running at 1500 rpm! Several possible explanations were considered such as a possible partial blockage of the hypodermic tubing with silver solder, the dead volume of the modified spark-plug arrangement being too great or there not being enough holes in the spark-plug connecting the central electrode cavity with the hydrogen supply ring.

Close inspection revealed that there was no blockage in the hypodermic tubing so some slots were milled in the spark-plug thread to ensure that the flow of gas to the connecting holes was unimpeded (see Figure 4.22).

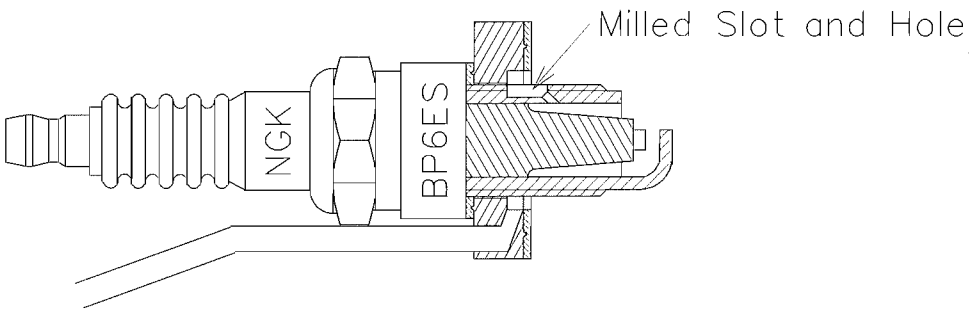

Figure 4.22 Modifications to Spark Plug Arrangement

Subsequent testing of this arrangement revealed a significant difference in the puffs that could be obtained. Using the constant light source and a piece of white card as a screen, it was determined that a supply pressure of 40 bar and a minimum injection duration of 2 ms gave suitably localized mixtures near the spark-plug as far as the naked eye could determine.

The puff initially is very rich depending upon how much air is entrained during the injection process. If little or no air is entrained during injection, the puff may not be able to be ignited immediately. A delay between the injection and ignition would therefore be required to allow time for the injection to occur and a combustible mixture to be formed.

In an actual engine however, in-cylinder charge motion will influence the puff as it leaves the confines of the spark plug body. Zavier [1991] used schlieren photography to visualize the effects of in-cylinder charge motion on the injected puff of methane. Zavier established the velocity field around the spark-plug location for several different engine speeds using hot wire anemometry and replicated it in the constant volume bomb by varying the current applied to a small DC fan located in the base of the bomb. A series of photographs of the injection process were taken at two different engine speeds, 1000 rpm (see Figure 4.23) and 2000 rpm (see Figure 4.24). Both series of photographs show that the injected puff is displaced to one side of the spark-plug by the charge motion

instead of the maintaining the observed symmetrical distribution from injecting into a quiescent mixture. The most likely reason for this displacement is due to swirl induced by the inlet manifold.

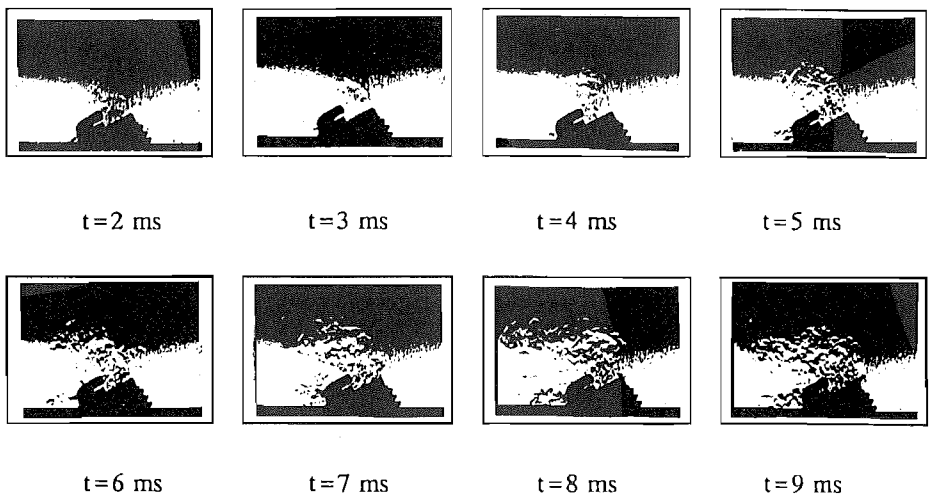

Figure 4.23 Effect of Engine Speed on Puff - 1000 rpm

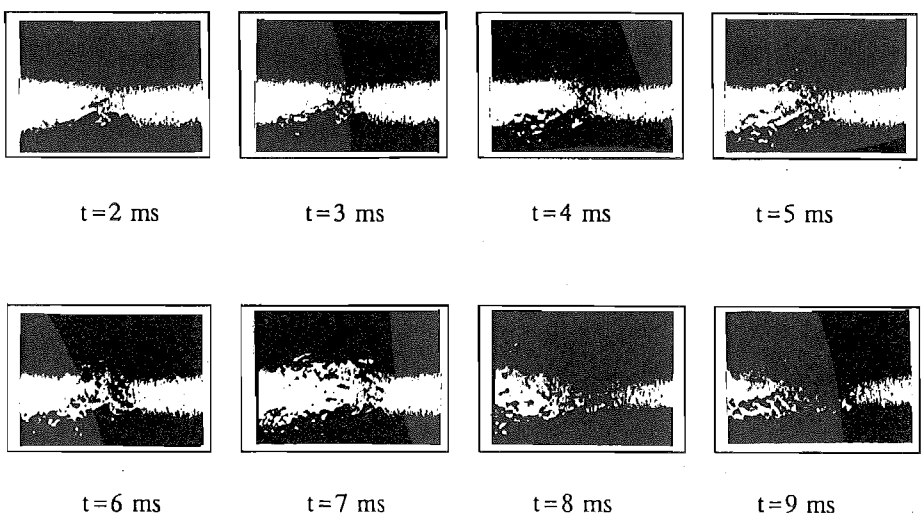

Figure 4.24 Effect of Engine Speed on Puff - 2000 rpm

Schlieren photographs for 2 ms (Figures 4.25 to 4.32), 3 ms (Figures 4.33 to 4.40) and 4 ms (Figures 4.41 to 4.48) injection durations are presented in the forthcoming figures. In all three cases the bomb is pressurized with oxygen free nitrogen at 5 bar.

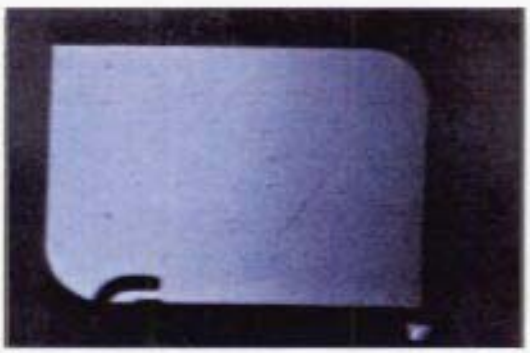

Figure 4.25 $\Delta_{inj} = 2$ ms, 1.0 ms after start

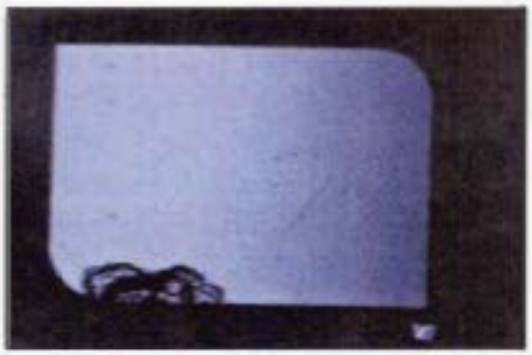

Figure 4.26 $\Delta_{inj} = 2$ ms, 2.0 ms after start

Figure 4.27 $\Delta_{inj} = 2$ ms, 3.0 ms after start

Figure 4.28 $\Delta_{inj} = 2$ ms, 4.0 ms after start

Figure 4.29 $\Delta_{inj} = 2$ ms, 5.0 ms after start

Figure 4.30 $\Delta_{inj} = 2$ ms, 6.0 ms after start

Figure 4.31 $\Delta_{inj} = 2$ ms, 7.0 ms after start

Figure 4.32 $\Delta_{inj} = 2$ ms, 8.0 ms after start

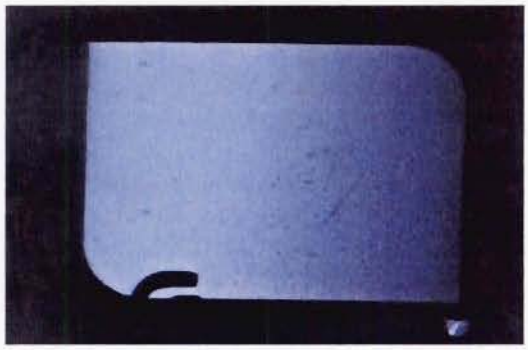

Figure 4.33 $\Delta_{inj} = 3$ ms, 1.0 ms after start

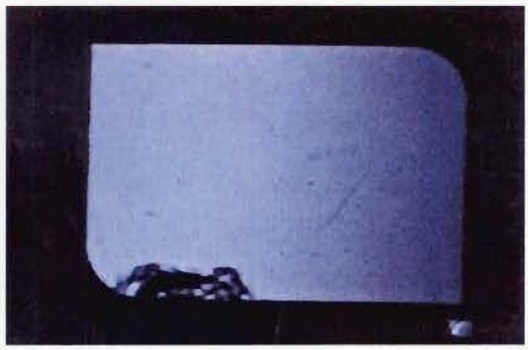

Figure 4.34 $\Delta_{inj} = 3$ ms, 2.0 ms after start

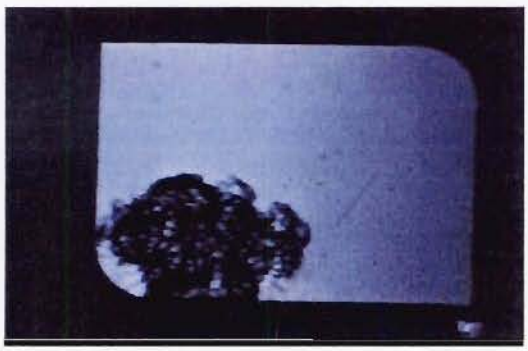

Figure 4.35 $\Delta_{inj} = 3$ ms, 3.0 ms after start

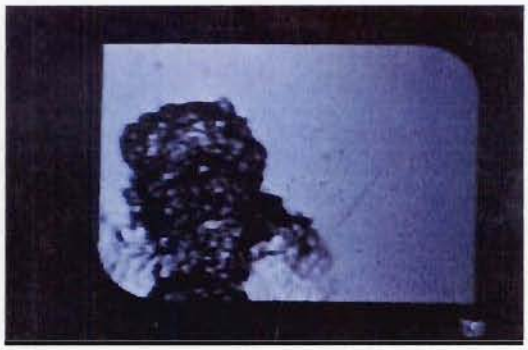

Figure 4.36 $\Delta_{inj} = 3$ ms, 4.0 ms after start

Figure 4.37 $\Delta_{inj} = 3$ ms, 5.0 ms after start

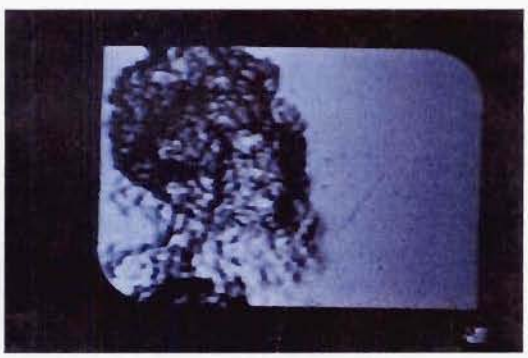

Figure 4.38 $\Delta_{inj} = 3$ ms, 6.0 ms after start

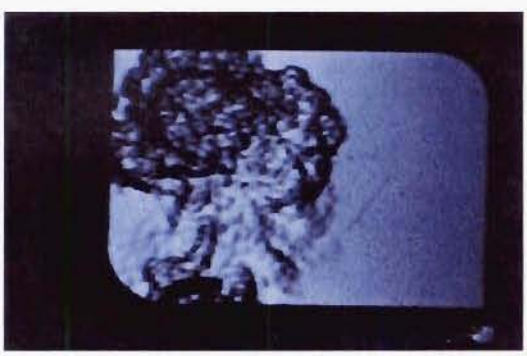

Figure 4.39 $\Delta_{inj} = 3$ ms, 7.0 ms after start

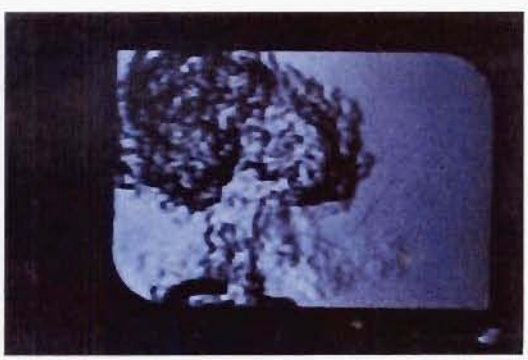

Figure 4.40 $\Delta_{inj} = 3$ ms, 8.0 ms after start

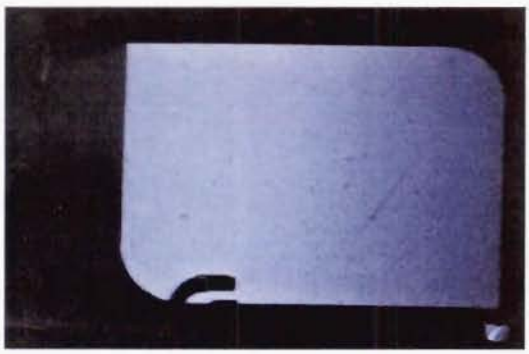

Figure 4.41 $\Delta_{inj} = 4$ ms, 1.0 ms after start

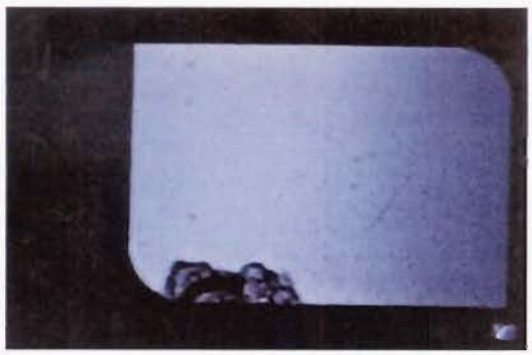

Figure 4.42 $\Delta_{inj} = 4$ ms, 2.0 ms after start

Figure 4.43 $\Delta_{inj} = 4$ ms, 3.0 ms after start

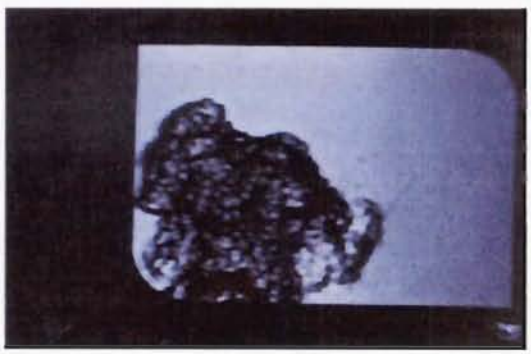

Figure 4.44 $\Delta_{inj} = 4$ ms, 4.0 ms after start

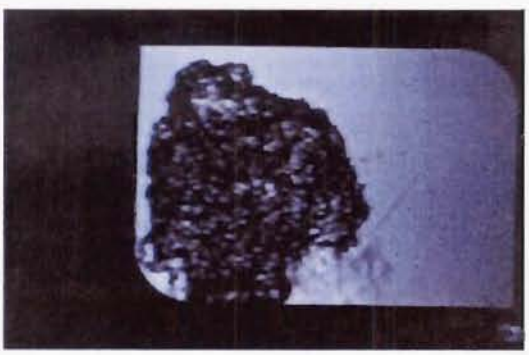

Figure 4.45 $\Delta_{inj} = 4$ ms, 5.0 ms after start

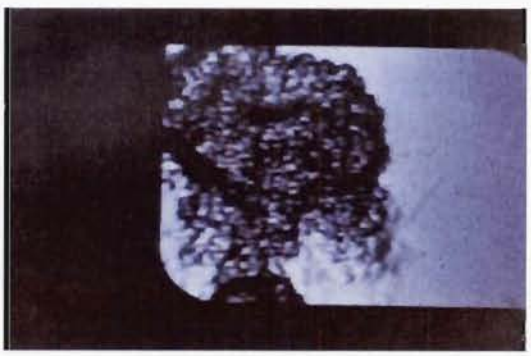

Figure 4.46 $\Delta_{inj} = 4$ ms, 6.0 ms after start

Figure 4.47 $\Delta_{inj} = 4$ ms, 7.0 ms after start

Figure 4.48 $\Delta_{inj} = 4$ ms, 8.0 ms after start

From the preceding figures the following points are evident:

1. The delay between when injection is initiated to when the injected plume is first visible entering the combustion chamber is between 1 and 2 ms. The practical effect of this delay is that in an engine operating at 1500 rpm, no hydrogen will actually enter the combustion chamber until ≈9-18 ^{o}CA after injection is initiated.

2. The injected puff velocity is quite low as evidenced in the width of the puff and the short distance that it penetrates into the combustion chamber (c.f. the 5 hole direct injection nozzle performance in Figures 4.14 to 4.21).

3. The injected puff appears to be quite turbulent in nature.

It was concluded that the modified spark-plug injection arrangement tested was performing in such a manner that it would be possible to successfully use such a system to ignite mixtures in an internal combustion engine.

4.6 Summary

From the schlieren photography investigation, the following conclusions are noted:

- The five hole direct injection nozzle gave the best performance with respect to injection delay, plume velocity, plume distribution and plume penetration.
- At 1500 rpm, no hydrogen will actually enter the combustion chamber until ≈16.2 ^{o}CA after injection is initiated.
- The modified spark-plug injection arrangement, once modifications were carried out, is operating in a satisfactory manner.
- There appears to be a reasonable amount of air entrainment in the puff. This coupled with the effect of charge motion should produce an ignitable mixture at all times[3].

[3]This is in fact what occurred. At no spark timing relative to the injection timing was it impossible to ignite the air/fuel charge

Chapter 5

Data Acquisition and Post-Processing

This chapter details the development of an engine data acquisition system incorporating an optical rotary encoder. The hardware required to ensure the correct phasing between the acquired engine pressure data and crank-angle position is described. Detail of the software written to acquire and post process the engine combustion data are then outlined. The novel method employed to accurately determine the location of the rotary encoder index pulse is presented before an analysis of the performance of the data acquisition system as a whole.

The development of an engine management system based on the output of the rotary encoder is presented in Chapter 6.

5.1 Introduction

In order to have confidence in the results of a detailed thermodynamic analysis of the combustion processes occurring in an internal combustion engine, a great deal of care and attention must first be given to ensuring that the pressure/crank-angle data used in the analysis is accurate.

Early in the planning stages of the research, it was determined that it was necessary to electronically control two fuel injectors independent of each other: One injector for the manifold injection of methanol and one injector for the direct injection of hydrogen. As the timing of the direct injection of hydrogen was critical especially in the case of a the late puff injection of hydrogen around the spark-plug, a control system allowing the injection start and finish crank-angles to be specified would be preferred over a system that relied on time differences relative to a known point in the engine cycle.

The cylinder pressure data acquisition systems that had been previously used on the Ricardo E6 engine were time based [Glasson 1992] , [Calvert 1994]. The data acquisition card sampled cylinder pressure data that incorporated a known point in the engine cycle

at a predetermined internally triggered rate. With the knowledge of the sampling rate and the engine speed, the number of data points in the cycle could be calculated and crank-angles assigned to each data point relative to the known point in the cycle. This method has several disadvantages associated with it:

1. Constant rotational velocity of the crank-shaft is assumed (i.e. no acceleration or deceleration of the crank-shaft due to compression or the combustion of the inlet charge).

2. Due to the information required in order to assign crank-angles, it is computationally more intensive.

3. Due to the need for accurate engine speeds when post-processing, it is unsuitable for providing the basis for any real-time IMEP or COV IMEP calculations/displays.

A more preferable approach from both the computational and accuracy points of view would be to trigger the data acquisition externally from a rotary encoder attached to the crank-shaft. The output from the rotary encoder would also then be used as an input to an engine management system that is able to control injectors based on start/finish crank-angles.

5.2 Rotary Encoder

The most suitable type of rotary encoder for this application is an incremental rotary encoder that provides a train of 0-5 V pulses as it's input shaft is rotated as opposed to an absolute position rotary encoder that gives absolute position as an output voltage. The data acquisition card will use the rising edge of the rotary encoder output pulses to trigger the acquisition of cylinder pressure data. Thus the acquisition becomes crank-angle position based and is not subject to errors caused by fluctuations in crank-shaft speed.

The encoder purchased was a 3600 pulses per revolution (ppr) optical incremental encoder[1]. A 0-5 V differential line driver output was selected as it would be less susceptible to electrical noise from the likes of the ignition system. The encoder has three output channels, 2 giving 3600 ppr and an index channel. One 3600 ppr channel was divided using logic to provide a 1800 ppr channel. The phasing of each of the channels relative to each other are given in Figure 5.1.

From Figure 5.1 the crank-angle that a particular piece of data is acquired at can be calculated from the following relationships.

[1]Part Number Bulletin 845K-SADZ14CTY3

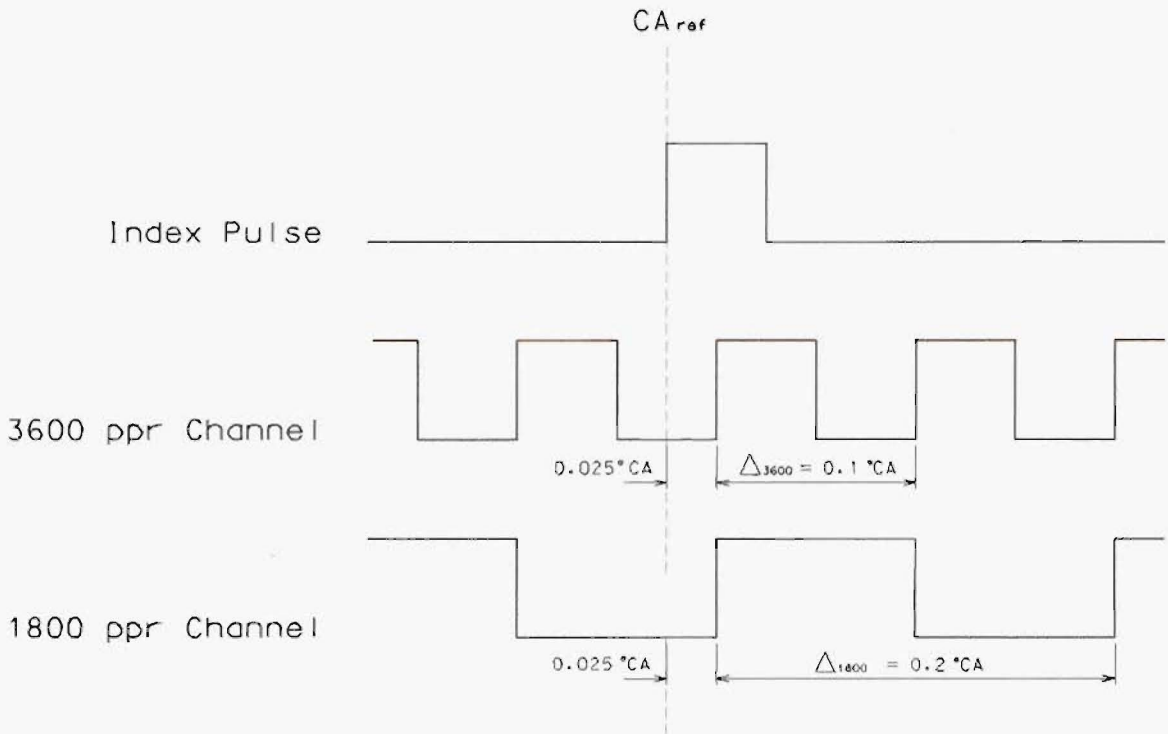

Figure 5.1 Phasing of Channels Used For Data Acquisition

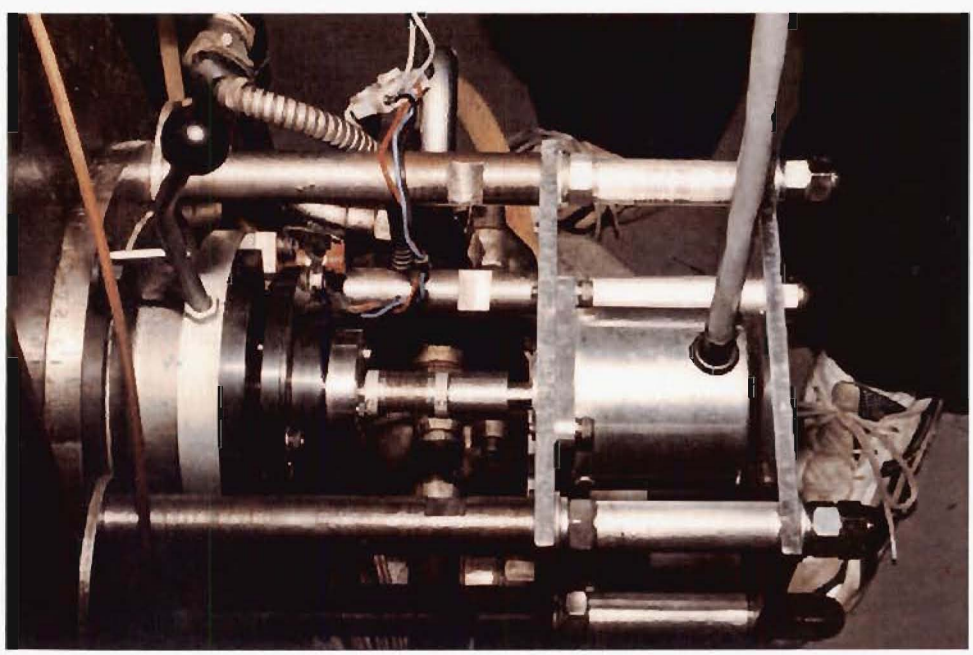

Figure 5.2 Rotary Encoder Mounted on the Crank-shaft

For the i^{th} data set sampled at a resolution of 3600 ppr:

$$CA_i = CA_{ref} + 0.025 + (i-1)(\Delta_{3600}) \tag{5.1}$$

For the i^{th} data set sampled at a resolution of 1800 ppr:

$$CA_i = CA_{ref} + 0.025 + (i-1)(\Delta_{1800}) \tag{5.2}$$

The encoder was initially mounted off the cam-shaft so that there would be an index pulse generated only once every engine cycle[2]. This proved an unsuitable arrangement as the deceleration and acceleration of the cam-shaft due to the opening and shutting of the valves adversely affected the accuracy of the cylinder pressure data assigned crank-angle. In order to overcome this, the encoder was mounted at the end of the crank-shaft and coupled to the crank-shaft with a bellows coupling to account for any mis-alignment of the shafts (see Figure 5.2). In order to mask off one of the two index pulses that now occurred every engine cycle, a slotted optical switch (SOS) was mounted on the cam-shaft (see Figure 5.3). The output of the SOS was connected to the index pulse via some digital logic that resulted in the desired one index pulse per engine cycle.

Two different triggering resolutions were used for the purposes of data acquisition. The first, a 3600 ppr channel, is used for the purposes of accurately locating the index pulse position (see page 72). Data were thus acquired every 0.1 ^oCA.

The second, a 1800 ppr channel, is used for triggering cylinder pressure data acquisition resulting in data being sampled every 0.2 ^oCA.

5.3 Data Acquisition Hardware

5.3.1 Data Acquisition Cards

The data acquisition card that had been previously in the department for engine data acquisition was a Keithly MetraByte DAS-20 [Glasson 1992] , [Calvert 1994]. The DAS-20 system was however being used by Brown [2001] and therefore unavailable. An Advantech PCL-818HG data acquisition card was therefore purchased for the purpose of providing the basis of the engine data acquisition system. In addition to the data acquisition card, a PCLD-889 multiplexing card and a PCLD-8115D wiring terminal board were purchased. The PCLD-889 enables 16 single ended or 8 double ended channels to be multiplexed into one PCL-818HG channel. The PCLD-889 is designed to be used with thermocouple inputs and features integral cold junction compensation (CJC) circuitry.

[2] A four stroke engine cycle is completed every one revolution of the cam-shaft or two revolutions of the crank-shaft

The PCLD-8115D was used to enable ease of connection of inputs to the PCL-818HG.

A schematic of the data acquisition layout is shown in Figure 5.4. Specifications of the individual pieces of hardware may be found in Appendix C on page 233.

Unfortunately the PCL-818HG data acquisition card was not designed to be connected to the PCLD-889 multiplexing board and the PCL-8115D screw terminal accessory board. This was achieved however with some careful rewiring as shown in Figure 5.5. Additional software routines also had to be written to allow the PCL-818HG to scan the required channels on the multiplexing board (see page 72).

5.3.2 Piezo-electric Pressure Transducer

The piezo-electric pressure transducer used for the duration of this work was an AVL 8 QP 500c water cooled type. The water cooling is a feature essential for the thermal protection of the transducer. The transducer was fitted to the head in a custom tapping designed by Glasson [1992] (see page 87).

The output of the pressure transducer was fed to a Cussons charge amplifier to convert the charge to a calibrated voltage (see page 107).

5.3.3 Phasing Board

The accuracy of the proposed data acquisition system is dependent upon knowing accurately the position of the first piece of data acquired relative to the index pulse.

This was first attempted using software. The index channel was sampled using the internal pacer trigger at 100 kHz. When the index pulse was detected, the PCL-818HG was then setup to sample the piezo channel using the external trigger from the rotary encoder and data acquisition commenced. The problem was that the time taken to setup the board for externally triggered data acquisition was unknown and an unknown number of external trigger pulses could pass in the interval before data acquisition begins. This problem would increase with engine speed as the setup time would remain fairly constant but the time before the first external trigger pulse after the index pulse reduces.

In order to overcome the problems of sampling more than one channel and software setup times, it was decided to implement a solution using hardware instead. A daughterboard was designed that was able to be mounted on the PCL-818HG data acquisition board. The requirements of this board were threefold:

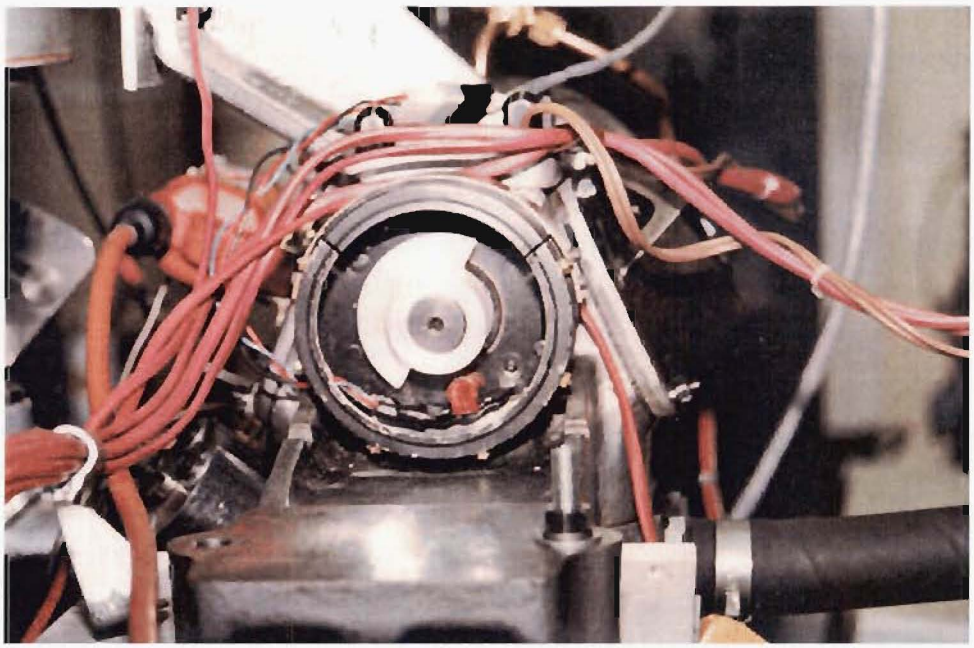

Figure 5.3 Slotted Optical Switch Mounted on the Cam-shaft

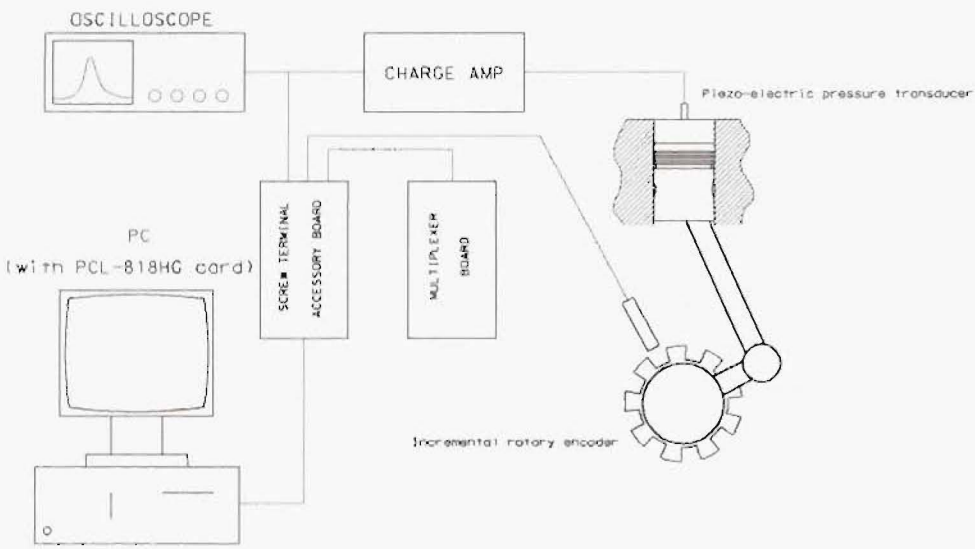

Figure 5.4 Schematic of the Data Acquisition Layout

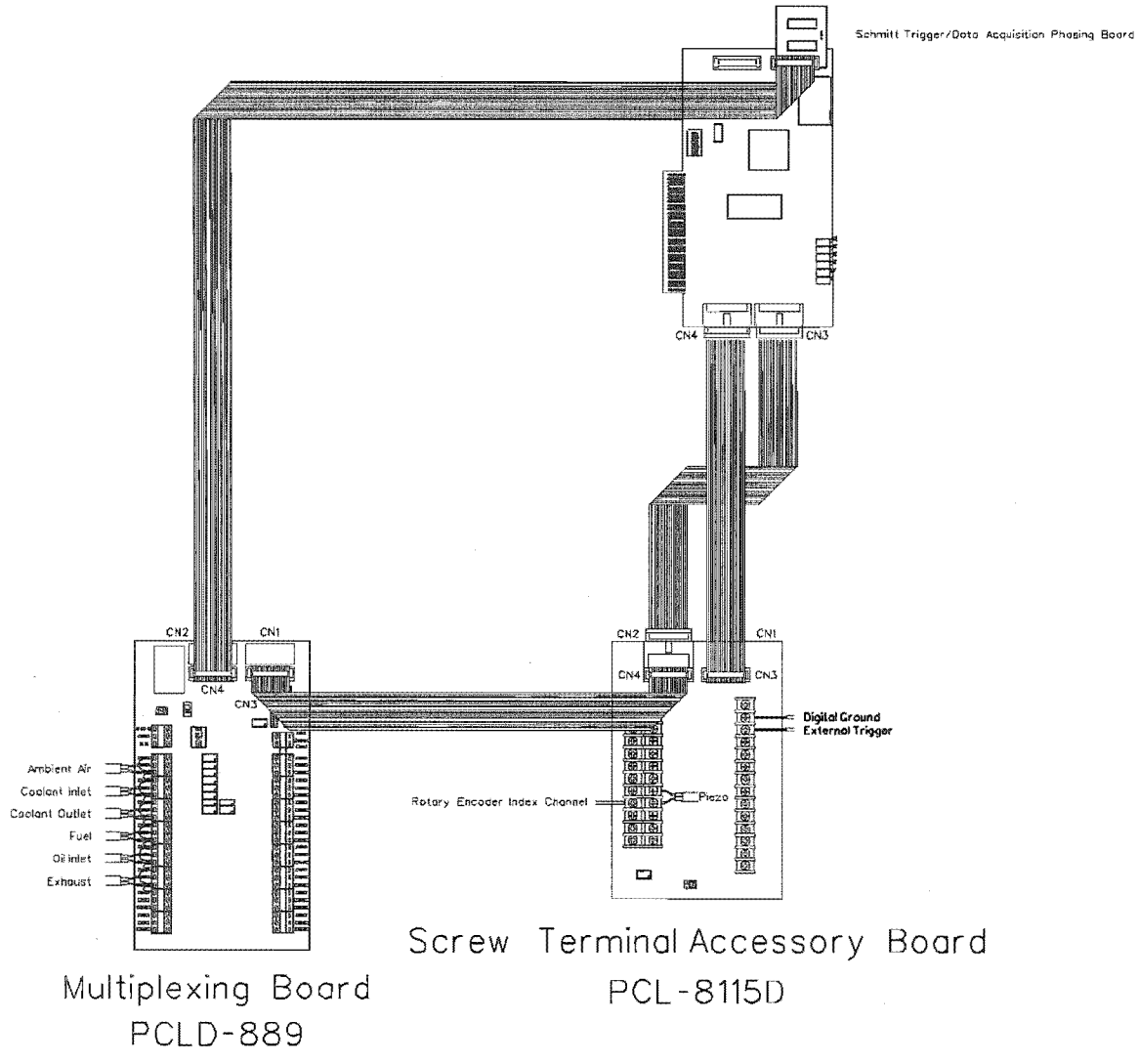

Figure 5.5 Data Acquisition Hardware Wiring Modifications

1. Intercept the external trigger pulses before they reach the data acquisition card itself.
2. Accept the index pulse and a digital output as inputs.
3. Allow the external trigger pulses to reach the data acquisition board once certain conditions have been met.

The daughter board was designed to be *piggybacked* on connector CN1 of the PCL-818HG data acquisition board as this connector carries the required digital output and a 5 V power supply. The digital output DO0 and the index pulse are fed into a D Flip Flop. The index pulse clocks in the digital output (ie the digital output can be high with no effect on the output of the D Flip Flop until an index pulse is received). When the data acquisition software is initialized and ready for use, the digital output DO0 is set high (see page 68). With the digital output high and having received an index pulse, the D Flip Flop pulls one of the inputs of an AND gate high. The other input to the AND gate is the external trigger channel which is now allowed to pass through the AND gate to the data acquisition board acquiring the first piece of data. In this manner it is certain that the first piece of data recorded is at a crank-angle an eighth of an increment (0.025 ^{o}CA) after the rising edge of the index pulse (refer to the diagram of the waveforms in and out of the phasing board in Figure 5.6). The phasing board is shown mounted on the data acquisition board in situ in the computer in Figure 5.7.

5.4 Data Acquisition Software

The requirements of the research called for two very different types of data to be acquired electronically. The first type is the in-cylinder pressure data which must be sampled at a high frequency to accurately capture the events that are occurring at high speeds. The second type of data is the steady state engine temperature data which does not change particularly fast and can be sampled at a low frequency. The approach used for each of the two types differs considerably and each will be described separately. All data acquisition software was written in the C^{++} programming language.

5.4.1 High Frequency Combustion Pressure Measurement

The acquisition of data at high frequencies introduces some technical issues which need to be overcome.

In order to perform a valid statistical analysis on quantities derived from engine pressure data, many consecutive engine cycles are required. The number of cycles that are required in order to achieve the desired accuracy varies according to the extent of the combustion variability [Heywood 1988]. Brunt and Emtage [1996] proposes that a

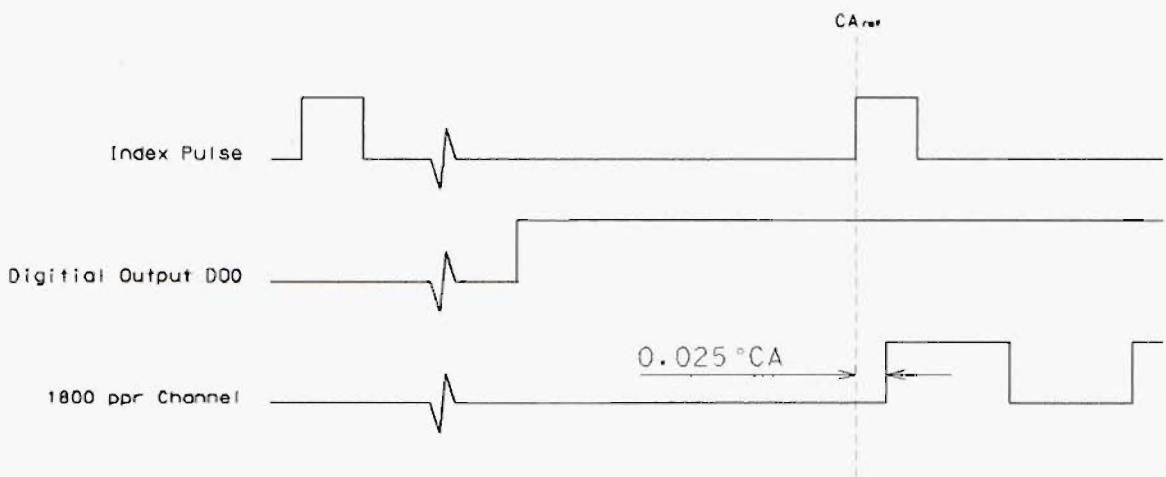

Figure 5.6 Output Waveforms From the Data Acquisition Phasing Board

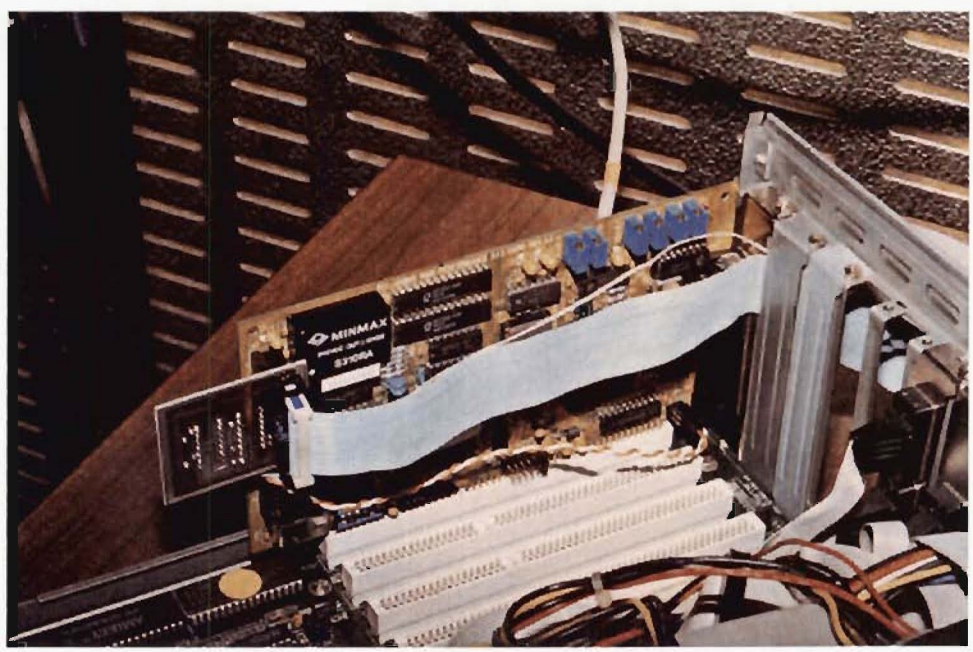

Figure 5.7 Data Acquisition Phasing Board in Situ

minimum of 150 cycles but ideally 300+ cycles are required. For the purposes of the current research project, 350 consecutive engine cycles are acquired and analyzed to ensure accurate statistical results.

Sampling 350 consecutive engine cycles of combustion pressure data at 1800 ppr resolution would result in 1800 (ppr) x 2 (revolutions per cycle) x 350 (engine cycles) = 1.26 million pieces of data! Given the amount of data that was going to be collected and the rate at which the data was going to acquired (1800 ppr x 25 rps = 45 kHz), the speed with which data could be stored was going to be critical. It was decided to create a 6 MB RAM disk out of the 8 MB of random access memory (RAM) that the data acquisition computer had installed. Data could then be transferred directly into memory without the time penalty associated with accessing the computer's hard drive. At the completion of data acquisition, the data file is copied from the RAM drive to the hard drive for storage.

The PCL-818HG card features a fifo buffer which takes data and puts it in a stack. The software merely has to poll the fifo buffer to see if there is any data in it. If there is, it is taken from the fifo and copied to a file in the RAM drive. If while this is occurring any further data is acquired, it is simply written into the fifo where it waits for the fifo to be polled again and to be copied out.

The required hardware has been previously described on page 65. Data acquisition is triggered externally off the rising edges of the 1800 ppr rotary encoder channel thus each channel is sampled every 0.2 ^{o}CA.

The routine used to acquire the high frequency combustion chamber pressure data is called FIFO118. The operation of the data acquisition routine FIFO118 is shown in the flow diagram in Figure 5.8. After acquiring the cylinder pressure data, all steady state engine temperatures were acquired and saved to a file (see page 72).

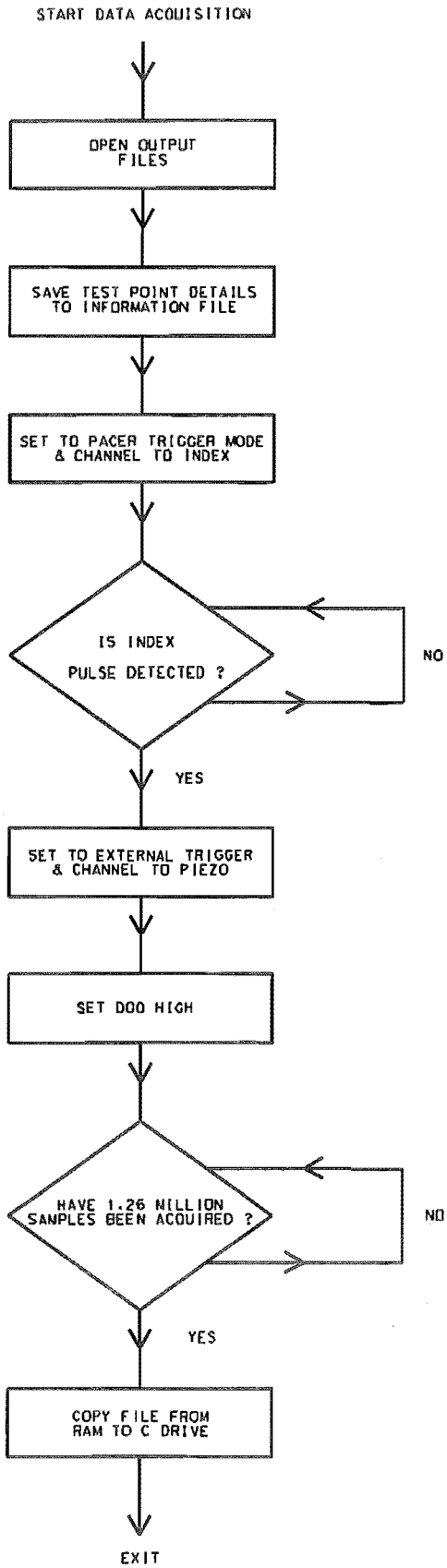

Figure 5.8 Flow Diagram Showing Operation of Data Acquisition Routine FIFO118

5.4.2 Low Frequency Steady State Engine Temperatures

During engine testing, a series of engine steady state operating temperatures were recorded and saved to disk for later use each time cylinder pressure data was acquired. The temperatures of interest were as follows:

- CJC
- Ambient Air
- Coolant Inlet
- Coolant Outlet
- Fuel
- Oil Inlet
- Exhaust

It was stated on page 64 that because the PCLD-889 multiplexer card was not designed to be connected to the PCL-818HG data acquisition board, there are no pre-written software routines to communicate with a multiplexer board. In order to overcome this problem, custom software routines were written to enable a range of multiplexer channels to be scanned and their temperatures read. The multiplexer channel selection is controlled by a series of digital outputs (connector CN2 bit D0 to bit D3). Software was therefore written to send the appropriate digital output, read the channel voltage, convert the voltage to a temperature and print the result both to the screen and a temperature file (*.tmp) if required. The operation of the multiplexer software is shown in the flow diagram in Figure 5.9.

5.5 Determination of Index Pulse Position

The position of the index pulse with respect to the crank-shaft position is critical to ensure the correct assignment of crank-angle to in-cylinder pressure data as well as ensuring the correct phasing of injection events with respect to top dead center (TDC) by the engine management system.

Both the data acquisition system and the engine management system are triggered by the rising edge of the input square wave form from the rotary encoder. The location of the rising edge of the index pulse must therefore be known accurately with respect to crank-angle. Heywood [1988] and Amann [1985] suggest that in order to provide accurate cylinder pressure verses crank-angle data, the phasing must be correct to within 0.2 ^{o}CA.

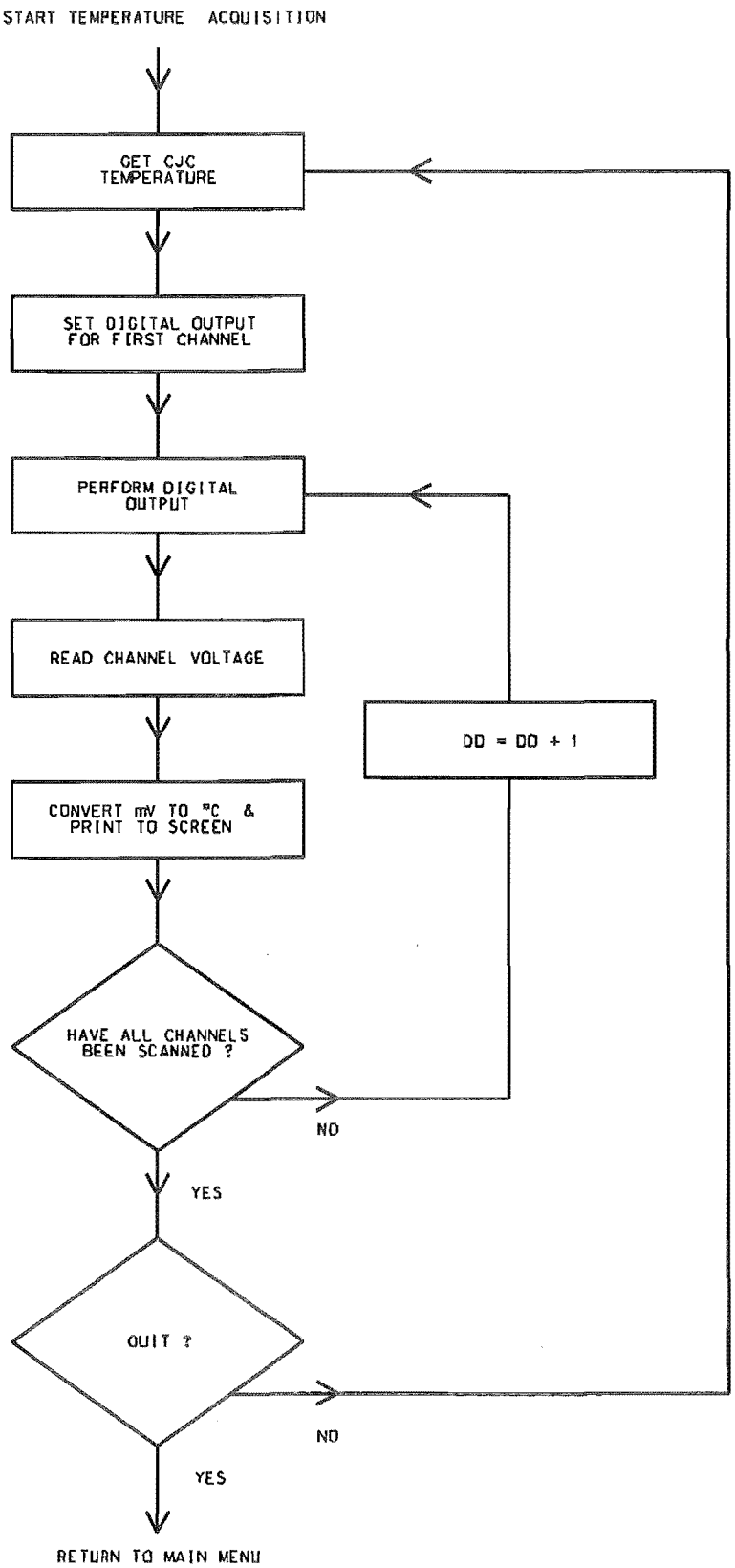

Figure 5.9 Flow Diagram Showing Operation of Multiplexer Software

Accurate phasing of cylinder pressure with crank angle data is critical when performing a thermodynamic combustion analysis. For the purposes of index pulse location, the 3600 ppr resolution is used which triggers the data acquisition every 0.1 ^{o}CA. Thus the position of the leading edge of the index pulse should be able to be found to an accuracy of $\pm$ 0.05 ^{o}CA.

A method is required that relates the data acquired (triggered by the rising edge of the rotary encoder output pulses) to the position of the piston. The traditional method of determining TDC in a reciprocating engine by using a dial gauge to mark the flywheel at TDC [Lancaster *et al.* 1975] is not suitable as it is does not relate crank-angle position to the electronic data that is acquired.

A simple method based on that of the dial gauge was devised and implemented. A simple electric circuit was formed as shown in Figure 5.10. The head is removed and replaced with a spacer to allow access to the piston for the dial gauge. The dial gauge is insulated electrically from the engine block by teflon sheeting. As the piston travels upwards, it makes contact with the dial gauge at around 30 ^{o}CA before TDC while there is still a large amount of piston movement given by small rotations of the crank-shaft. The circuit remains complete as the piston moves past TDC and is broken at the same point after TDC. The calibration setup is shown in Figure 5.11. The data acquisition system is triggered externally by the 3600 ppr channel and is sampling the voltage of the circuit. The resultant output file contains a particular number of +5 V pieces of data corresponding to when the dial gauge was in contact with the piston. Assuming that electrical contact should be broken at the same value of crank-angle before and after TDC, the middle data point represents the piston position at TDC. Post-processing the resultant data file assigns crank-angle data to the voltages according to an initial *guess* as to where the rising edge of the index pulse is. By looking to see the crank-angle that has been assigned to the middle data point, the error in the initial guess at the position of the rising edge of the index pulse is easily calculated and the correct value of the rising edge of the index pulse calculated. The data file can then be re-processed using the corrected value for the rising edge as a check.

During an actual index pulse position calibration, data was acquired from 10 consecutive crankshaft revolutions (and therefore 10 contacts of the dial gauge with the piston). Typically there would be around 1000 data points acquired during the period that the electrical circuit is complete (i.e. at a sampling resolution of 0.1 ^{o}CA this corresponds to a contact duration of approximately 100 ^{o}CA). Typically the variation in the number of data points acquired during each contact period was $\pm$2. The index pulse position was calculated from an average of all 10 crankshaft revolutions. Thus the assumed accuracy of the index pulse calibration method of $\pm$ 0.05 ^{o}CA (see above) is justified. As a check

for an offset gudgen pin the calibration routine was carried out while reversing the direction of the crankshaft revolution. The calculated index pulse position (CA_{ref}) was 540.225 ^{o}CA. The calculated index pulse position was in agreement with that calculated when the crankshaft is rotated in the correct direction indicating a central gudgen pin.

5.6 Cylinder Pressure Data Analysis

5.6.1 Absolute Pressure Referencing

Piezo-electric pressure transducers measure only changes in pressure rather than absolute pressure. In order to determine absolute cylinder pressures, a means of referencing the measured pressure to the absolute pressure is required. One method that is commonly used is to assign the pressure at bottom dead center in the inlet stroke the value of the mean inlet manifold pressure [Lancaster *et al.* 1975] , [Amann 1985] , [Brunt and Pond 1997]. At this point the piston is stationary and the fluid motion through the inlet valve is minimal, thus the pressure drop over the valve is negligible and the assumption that the bulk chamber pressure being the same as the mean manifold pressure is reasonable.

The mean inlet pressure was measured via a tapping in the inlet manifold next to the cylinder head. The pressure tapping was connected to a hand held electronic digital barometer (Airflow digital barometer DB1) which gave a pressure readout in mbar. Prior to engine testing the digital barometer was calibrated against a precision aneroid barometer to ensure an accurate mean inlet manifold pressure.

5.6.2 Indicated Mean Effective Pressure (IMEP)

Indicated mean effective pressure is a very important engine performance variable and one which is used extensively in engine development. Indicated quantities are calculated directly from the p-V diagram of an engine and are used primarily to identify the impact of the compression, combustion and expansion processes on engine performance [Heywood 1988] , [Brunt and Emtage 1996].

The gross indicated mean effective pressure ($IMEP_g$) quantifies the work delivered to the piston by the gases in the cylinder during the compression and expansion strokes of the cycle only. It represents the work available to overcome the pumping work, all other engine losses (friction) and provide useful work at the engine's output shaft. The pumping mean effective pressure ($IMEP_p$) quantifies the work done by the piston on the cylinder gases during the exhaust and induction strokes only. The net indicated mean effective pressure ($IMEP_n$) is therefore the summation of $IMEP_g$ and $IMEP_p$.

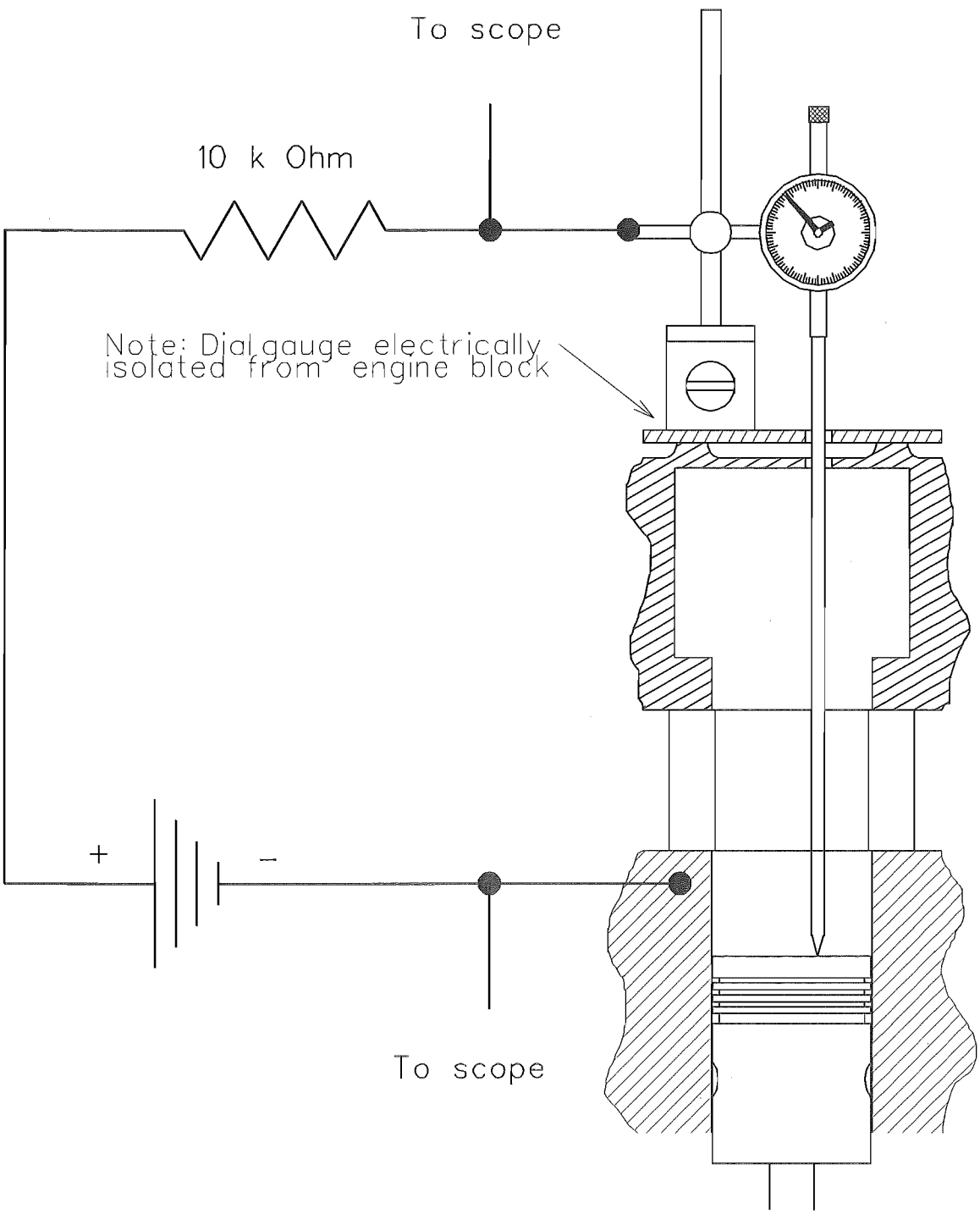

Figure 5.10 Index Pulse Position Circuit

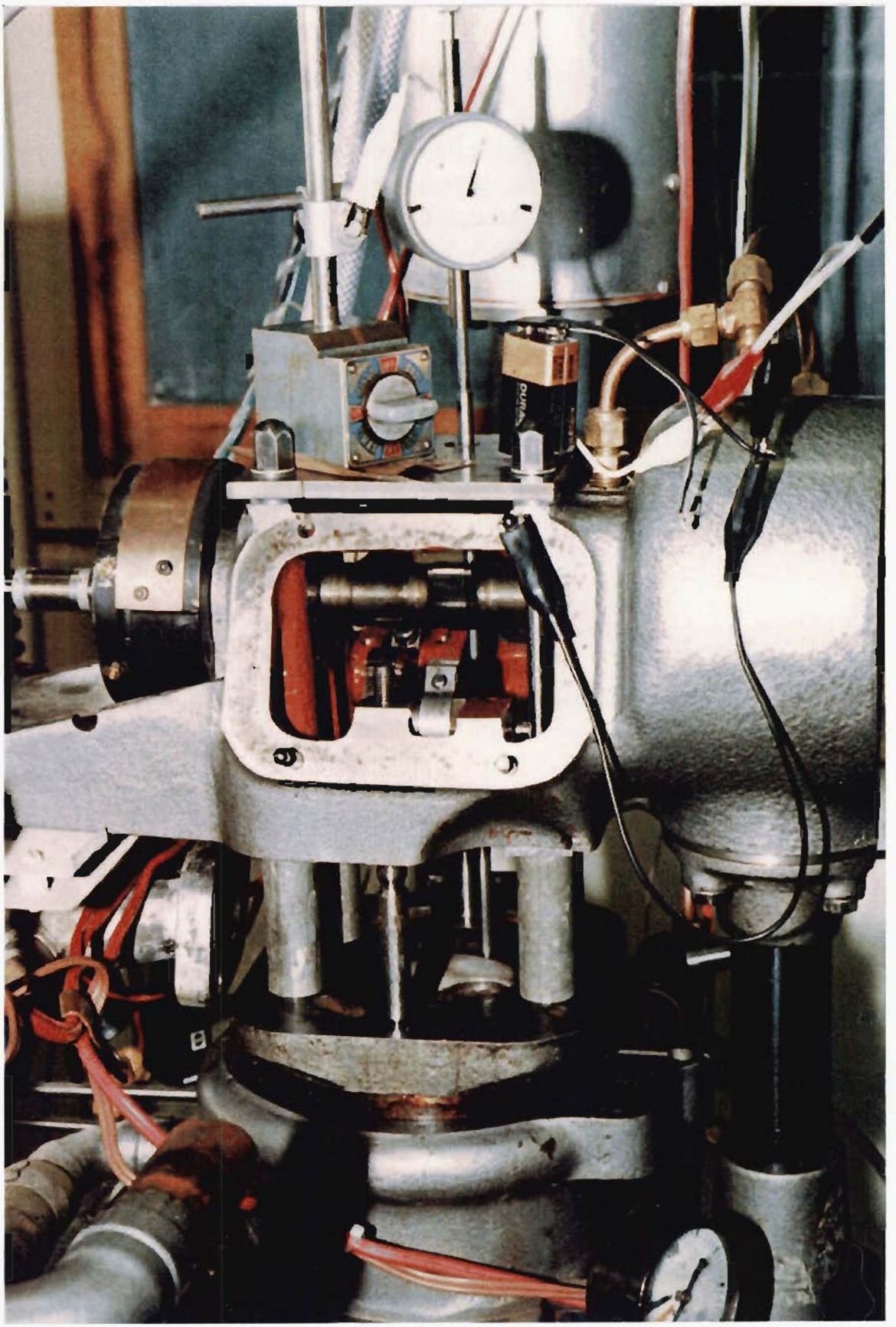

Figure 5.11 Index Pulse Position Calibration

$$IMEP_n = IMEP_g + IMEP_p \tag{5.3}$$

$IMEP_g$ is commonly used to identify the effects the combustion process has on engine performance [Heywood 1988] and for the purposes of this research is considered to be the most appropriate quantity to use. $IMEP_g$ is the measure of thermodynamic work done by the combustion gases on the piston face during the compression and expansion strokes. It is obtained by calculating the integral of p.dV over the compression and expansion strokes divided by the swept volume of the engine.

Brunt and Emtage [1996] conducted an evaluation of five of the different algorithms that can be used to carry out the required integration. With crank-angle resolutions of 1 degree and less, the differences between the quantities calculated by each of the algorithms were negligible. They suggest that the choice of algorithm should therefore be based on computational effort. Their recommended algorithm is as follows:

$$IMEP_g = \frac{\Delta\theta}{V_s} \cdot \Sigma_{i=180}^{i=540} p(i) \cdot \frac{dV(i)}{d\theta} \tag{5.4}$$

At the time of writing the $IMEP_g$ post-processing code however the paper by Brunt and Emtage was not yet available so the following algorithm was used in the work.

$$IMEP_g = \frac{1}{2 \cdot V_s} \Sigma_{i=180}^{i=540} [p(i) + p(i+1)] \cdot [V(i+1) - V(i)] \tag{5.5}$$

At the crank-angle resolution being employed, the two algorithms will yield almost identical results. $IMEP_g$ calculations do not need the measured cylinder pressures to be referenced to an absolute pressure as is required in order to calculate peak cylinder pressures. However the $IMEP_g$ calculation is very sensitive to the phasing of pressure data to crank-angle data.

5.6.3 Indices of Compression and Expansion

For the purposes of performing a mass fraction burned (mfb) analysis on the cylinder pressure/crank-angle data, it is necessary to calculate appropriate values of the indices of compression (n_c) and expansion (n_e) for each individual engine cycle. The indices are calculated by fitting a line of best fit to the appropriate part of the logarithmic p-V diagram for that particular engine cycle.

n_c has to be evaluated after the inlet valve has closed (216 ^{o}ATDC) but before the combustion process begins. Thus n_c is evaluated over the range of crank-angle values from 220 to 320 ^{o}ATDC. This method will yield accurate values of n_c for the manifold injection of hydrogen but will overestimate the value of n_c for the direct injection of hydrogen due to the addition of mass during the compression process (see also page 152).

n_e has to be evaluated after the combustion process has been completed but before the exhaust valve opens. An algorithm can be used to calculate the estimated end of combustion (EEOC) [Brunt and Emtage 1997]. The EEOC is the crank-angle at which the expression:

$$p \cdot V^{1.15} \tag{5.6}$$

reaches a maximum value. n_e is evaluated over a 40 ^{o}CA range of crank-angle values from EEOC + 10 ^{o}CA to EEOC + 50 ^{o}CA.

5.6.4 Mass Fraction Burned Analysis

In order to quantify the effects of hydrogen supplementation on the combustion process itself, a mass fraction burned analysis is performed on the cylinder pressure data.

The results of a mfb analysis show how the combustion process progresses as a function of crank-angle. The mfb analysis allows the effect of combustion on cylinder pressure rise to be separated from changes in cylinder pressure that are due to changes in cylinder volume. The variation of the mass of fuel burnt with crank-angle gives a direct indication of how the combustion has proceeded [Shayler *et al.* 1990]. The rate that the combustion process occurs and it's phasing with respect to crank-angle is a important factor which affects [Brunt and Emtage 1997]:

- power output
- thermal efficiency
- peak cycle pressures (temperatures)
- exhaust emissions

Mass fraction burned profiles are widely used to characterize the different phases of combustion in spark ignition engines [Heywood 1988] , [Rauckis and McLean 1979]. Combustion phases are usually expressed as a duration in ^{o}CA that it takes for the mfb to reach a specified value [Brunt and Emtage 1997]. The definition of the various

combustion phases are arbitrary and made to allow discussion of the results in a manner consistent with previous investigations. The following definitions are most commonly used [Rauckis and McLean 1979]:

- 0-2% mfb Ignition delay duration, $\triangle\theta_i$
- 2-10% mfb Flame development duration, $\triangle\theta_d$
- 10-90% mfb Rapid-burning duration, $\triangle\theta_b$
- 0-90% mfb Overall combustion duration, $\triangle\theta_o$

A mfb analysis can be carried out using two main methods.

The first of these methods is known as a heat release analysis. One of the most important pieces of information available to the combustion researcher is the measured cylinder pressure/volume history. The cylinder pressure is affected by not only the combustion process but also changes in cylinder volume, heat transfer, crevice flows and mass loss. In order to accurately examine the combustion process, the effects of combustion must be separated from these other influences. This is done by applying the First Law of thermodynamics to the cylinder contents while the inlet and exhaust valves are closed. This type of analysis is known as a "heat release analysis" [Chun and Heywood 1987]. Heat release models require the input of an array of operating conditions, unburnt and burnt mixture properties, combustion heat transfer details as well as engine design details [Krieger and Borman 1966] , [Gatowski *et al.* 1984]. These models are however computationally quite intensive and their accuracy dependent on the quality of the information given. Before the model can be used it must be validated against actual engine test data and pressure traces. One of the major advantages of a properly validated first law thermodynamic model however is that is can be used as a predictive tool in engine design and combustion analysis.

The second commonly applied technique for estimating the mfb profile for a particular engine cycle from pressure/volume data and the one used in this work is that developed by Rassweiler and Withrow [Gatowski *et al.* 1984] , [Amann 1985] , [Heywood 1988] , [Shayler *et al.* 1990] , [Brunt and Emtage 1997] , [Ball *et al.* 1998a] , [Ball *et al.* 1998b]. This method assumes that in any crank angle interval the total cylinder pressure change, $\triangle$p comprises of a pressure change due to volume change, $\triangle p_v$ and a pressure change due to combustion, $\triangle p_c$ i.e.:

$$\triangle p = \triangle p_v + \triangle p_c \tag{5.7}$$

where

$$\triangle p_v = p_j - p_i = p_i \left[\left(\frac{V_i}{V_j} \right)^n - 1 \right] \tag{5.8}$$

and

$$\frac{m_{b(i)}}{m_{b(total)}} = \frac{\sum_0^i \triangle p_c}{\sum_0^N \triangle p_c} \tag{5.9}$$

The Rassweiler and Withrow method, despite its inherent simplifications and assumptions, has been shown to give results that are in close agreement with other more complex methods. Due to it's ease of application and good agreement with more complex models, the Rassweiler and Withrow method will continue to be a favored approach to combustion analysis [Shayler *et al.* 1990] , [Brunt and Emtage 1997] , [Ball *et al.* 1998a]. The Rassweiler and Withrow mfb analysis method will be used throughout this work to analyze the acquired engine pressure traces.

5.7 Post-processing Software

A C^{++} program called FOURSTR1 was written to post-process the raw combustion pressure data. The program incorporates all of the calculations mentioned in this chapter. A flow diagram giving the steps that occur as the data are analyzed is shown in Figure 5.12. The post-processing requires more than one pass over the data so the data is read from and written to several intermediate files during the process.

As well as calculating the quantities of interest for each individual engine cycle, basic statistical data for each of the quantities is calculated over the 350 consecutive engine cycles recorded. The statistics calculated were the average and standard deviation of the sample and from these the coefficient of variation (COV). The COV of a quantity is calculated as follows using IMEP as an example [Heywood 1988] , [Ozdor *et al.* 1994]:

$$COV_{IMEP} = \frac{\sigma_{IMEP}}{\overline{IMEP}} \times 100(\%) \tag{5.10}$$

The COV of a quantity is useful as it gives a measure of cycle-by-cycle variability at that particular engine operating condition. The two most commonly reported quantities used to define cycle-by-cycle variability are IMEP and peak cylinder pressure (P_{max}). COV IMEP is preferred to COV P_{max} as COV P_{max} is affected by changes in spark

timing [Ozdor *et al.* 1994].

All pressure derived quantities that are presented, either graphically or quoted in the text, are the average values calculated over 350 consecutive engine cycles.

The following output files are produced:

1. Information File (*.inf). This file contains all relevant information pertaining to the particular test point that the pressure data was acquired at.
2. Pressure Summary File (*.max). This file contains the maximum pressures and rates of pressure rise for each engine cycle as well as the crank-angles that they occur at.
3. Ensemble File (*.pvd). This file contains the ensemble averaged engine cycle.
4. IMEP File (*.mep). This file contains both the IMEP_g and IMEP_n for each engine cycle.
5. Mass Fraction Burned File (*.mfb). This file contains the following values for each engine cycle: n_c, n_e, EEOC, $\triangle\theta_i$, 2% mfb CA, $\triangle\theta_d$, 10% mfb CA, $\triangle\theta_b$, 90% mfb CA, $\triangle\theta_o$.
6. Temperature File (*.tmp). This file contains all the temperatures that were read at the time that the cylinder pressure data was acquired.
7. Summary File (*.sum). This file contains all the key values from the previous files, comma delimited, to be read into a spreadsheet by a purpose written macro.

EXCEL spreadsheet's were used to collate the manually recorded engine data and values calculated from the engine data acquisition and post-processing programs. Engine data was manually entered while the post-processing data was read in from the *.sum files by a purpose written macro. Further calculations were performed on the engine data to determine engine performance parameters (see Sections E.1 to E.12 starting on page 239). All relevant graphs were plotted within EXCEL.

5.8 Analysis of Complete Data Acquisition System

One of the most useful tools in determining whether the data acquisition system as a whole is operating correctly is to analyze the results of motored engine cycles [Lancaster *et al.* 1975] , [Heywood 1988].

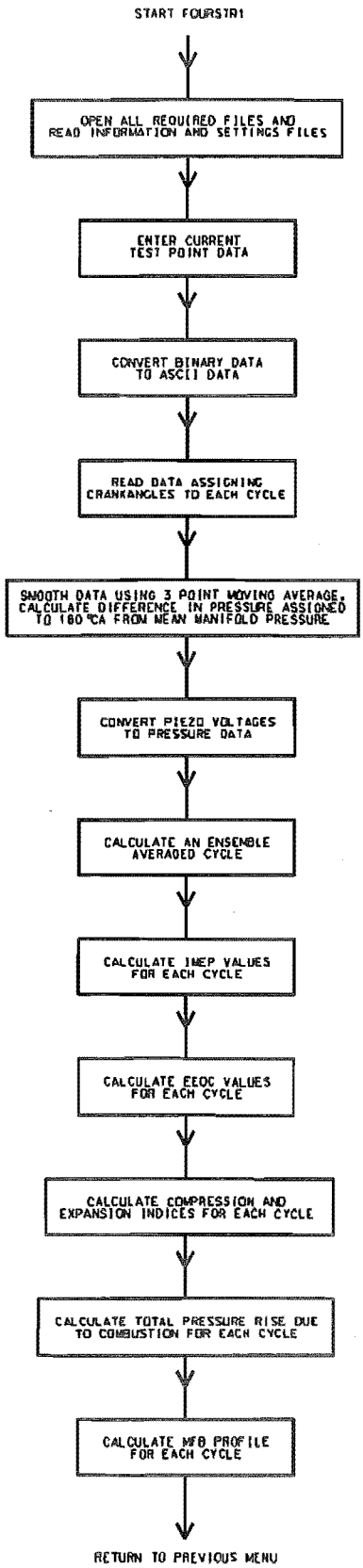

Figure 5.12 Flow Diagram Showing Operation of Post-processing Program FOURSTR1

Motored engine data differs from fired engine data in that it does not have inhomogeneous mixture compositions, high heat transfer rates and other combustion induced effects such as varying polytropic indices [Lancaster *et al.* 1975]. The motored data also exhibits low cyclic variability.

A logarithmic p-V diagram from a motored engine provides a great deal of information about the scaling and phasing of crank-angle/pressure data as well as transducer performance [Lancaster *et al.* 1975] , [Heywood 1988]. Logarithmic plots are used to check the following points [Lancaster *et al.* 1975]:

1. The use of the correct reference pressure when converting the recorded pressure signals to absolute pressures (incorrect assignment indicated by curvature early in the compression stroke).

2. The use of the correct clearance volume (incorrect assignment indicated by curvature late in the compression stroke).

3. The correct phasing of the pressure/crank-angle data (incorrect phasing will result in there being a cross-over of the compression and expansion lines i.e. the expansion pressure will be greater than the compression pressure!).

4. The correct scaling is used (incorrect scaling will result in the slope of the compression line (-n) lying outside the expected range of 1.24 to 1.35).

Figure 5.13 shows a logarithmic p-V diagram from the test engine (CR = 8:1).

Careful observation of Figure 5.13 reveals that the correct reference pressures and clearance volumes were used and the phasing of the pressure/crank-angle data is correct. Further analysis of the original data showed that the slope of the compression line was calculated to be 1.34.

Thus is was concluded that the data acquisition system as a whole is performing acceptably and that the resulting data can be analyzed with confidence.

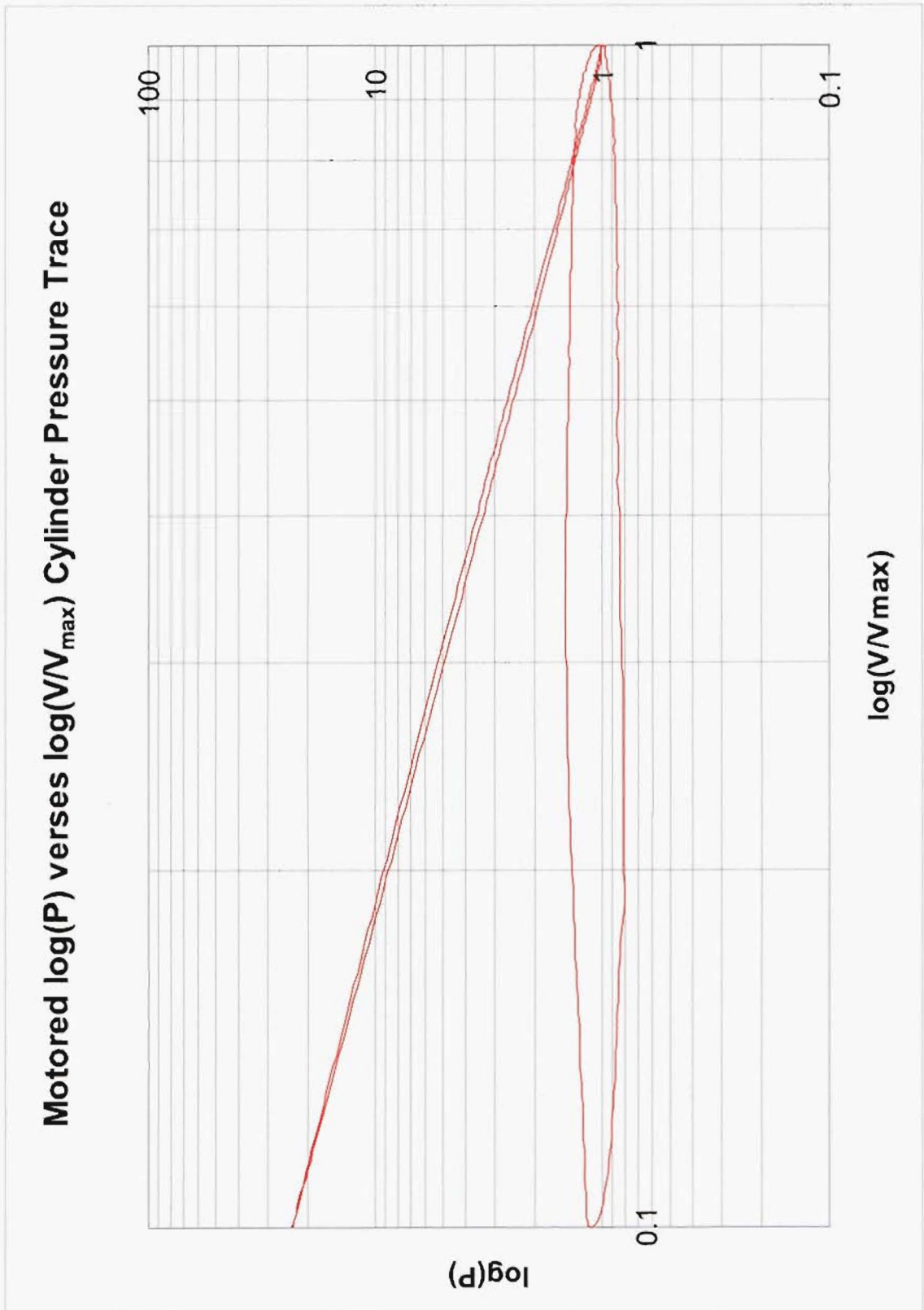

Figure 5.13 Logarithmic Plot of Pressure verses Volume for Motored Engine

Chapter 6

Engine Test Cell Preparation

This chapter describes the test apparatus which was used for the duration of the engine testing. Modifications made to the standard Ricardo E6 engine are presented before the development of the engine management system is described. The fuel injection and supply systems are then outlined before the test cell safety system and instrumentation is described. The engine test procedures can be found in Chapter 7.

6.1 Engine Modifications

The Ricardo E6 engine used in the experimental work differs from that of the standard factory model in the following ways.

6.1.1 Cylinder Head

The original Ricardo E6 cylinder head had been modified previously by Glasson [1992] to incorporate a pressure transducer tapping in addition to the standard two spark plug tappings. The condition of the original head was deteriorating and the prohibitively large cost[1] of a genuine Ricardo cylinder head resulted in an alternative solution being sought. The original cast iron Ricardo E6 cylinder head was replaced by a locally manufactured[2] aluminum cylinder head prior to the commencement of this research project. The replacement head incorporated the following features:

- An integral M10×1 hole to allow for the installation of a combustion pressure transducer
- Valve seat angles changed from 45^o to 30^o due to there being no cast iron valve inserts
- Valves changed to Holden valves
- Original double spring arrangement replaced by single Holden springs

[1] In excess of £3900 - May 1991

[2] Cast and machined by Colin Lyster, 62 Point Rd, Monaco, Nelson

The new alloy cylinder head was manufactured to match the original cylinder head with the addition of a pressure transducer tapping in the same orientation as that used by Glasson.

6.1.2 Cam-shaft Cover

The hydrogen injector part of the modified spark-plug injector configuration that was developed on page 40 is unable to be supported by the thin hypodermic tube which connects the injector to the modified spark plug (see Figure 3.7). Glasson [1992] also used the front spark plug hole to install his hydrogen injector and had concerns about the ability of it's M14 threaded base to adequately support the weight of the injector. He designed and manufactured a replacement cam-shaft cover that incorporated a fixture in a plane parallel to the top of the injector to allow a supporting bracket to be fastened. It was decided to use Glasson's replacement cam-shaft cover to provide a similar supporting bracket for the modified spark-plug injector. The complete injector configuration showing the modified cam-shaft cover, support bracket and injector configuration can be seen in Figure 6.1.

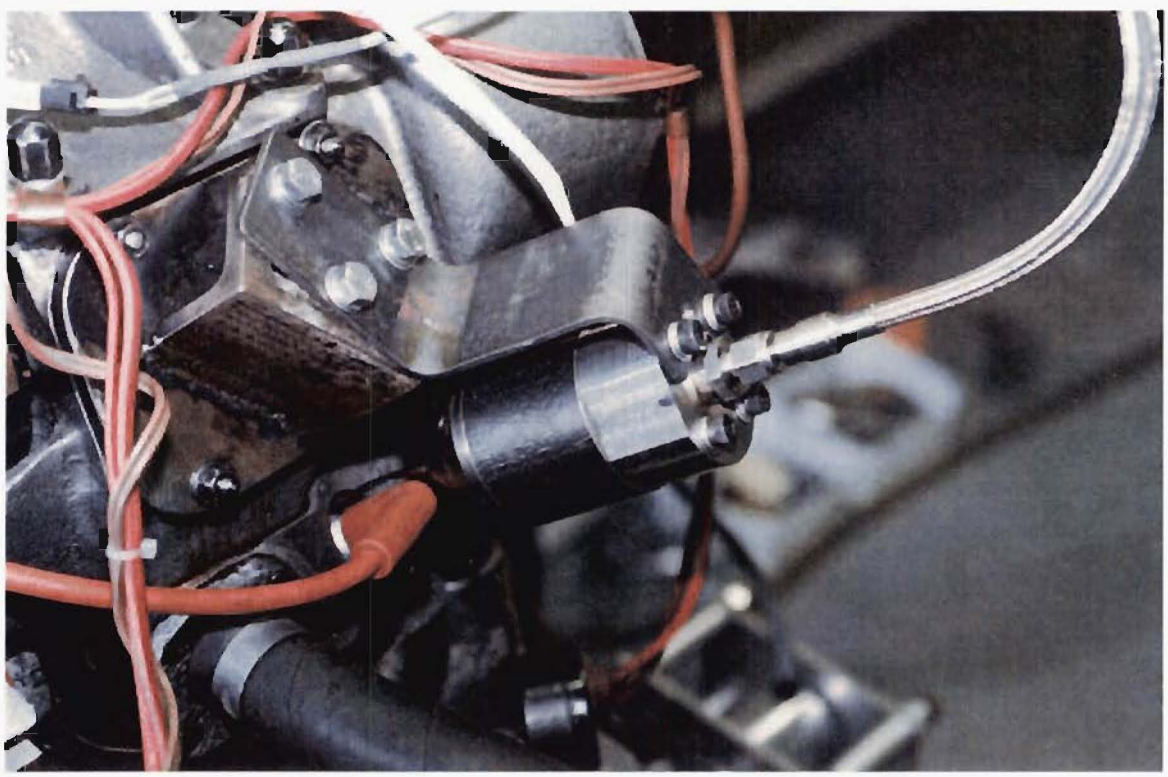

Figure 6.1 Modified Spark-plug Injector Located on the Engine

6.1.3 Crank-case Burst Disk

Glasson [1992] identified the possibility of a combustible mixture being formed in the crank-case of an engine when fuelled on hydrogen due to leakage of gas past the piston rings. Although no reports of such an explosion could be found, Glasson replaced one of the existing crank-case side vents plates with a perspex burst disk and a plate steel surround. The purpose of the burst disk is to control the effects of an explosion by directing the explosive force in a direction that will not result in damage to the engine or harm to anyone in the vicinity of the engine.

6.1.4 Inlet Manifold

The original Ricardo E6 inlet manifold was replaced with a custom designed manifold to allow the manifold injection of hydrogen. The development and manufacture of this manifold has been previously described on page 35.

6.1.5 Inlet Air Heating

One of the major differences between the physical properties of gasoline and methanol is in their respective latent heats of vaporization. Methanol has a latent heat of vaporization $\approx$ 3 times greater than that of gasoline (1100 kJ/kg c.f. 330-400 kJ/kg - see Table B.1 on page 229). This combined with a methanol flow rate of $\approx$ 2.3 times greater than that of gasoline (see page 92) results in the cooling effect of methanol being $\approx$ 7 times greater than that of gasoline. Although the associated increase in evaporative cooling of the inlet charge offers the potential of higher engine output powers (see page 3), excessive inlet charge cooling can lead to some combustion related problems.

Liquid methanol impinging directly onto the cylinder wall has been reported to lead to increased wear of the cylinder lining [Ryan *et al.* 1981] , [Owens *et al.* 1982] , [Ryan *et al.* 1986]. The mechanism proposed for the increased wear is the products of methanol combustion form formic acid which attacks the cast iron cylinder wall forming iron formate. The iron formate is scraped away by the action of the piston rings over time.

The second problem encountered is one of poor mixture formation. Poorly vaporized air/fuel mixtures lead to excessively long ignition delay durations, slower flame speeds, increased wall quenching, increased cyclic variability and increased emissions.

The conventional way to overcome these problems is through heating of the inlet air mixture usually via modified inlet manifolds that incorporate heating using the engine's cooling water. For the purposes of this research, an inlet air heater designed and used previously on a Ricardo engine [Chen 1991] was fitted to the inlet manifold after the

viscous air flow meter (see Figure 3.4).

The control of the inlet air heater was an area that was carefully looked at. A feedback control system based on the temperature of the inlet air mixture as it enters the head of the engine was considered. This control scenario would ideally result in the inlet mixture having a constant preset temperature as it enters the manifold. This method of heating the inlet manifold was however thought to be unsatisfactory as the rated output of the heater would be introduced over a short period of time in response to a drop in inlet manifold temperature. This would lead to an over correction of the temperature. Thus over the 350 consecutive engine cycles that engine data is acquired, the degree of mixture preparation would vary considerably and adversely affect the quality of the combustion data collected. In addition, as the air/fuel ratio of the mixture is varied from rich to lean, the amount of inlet air heating required to maintain the preset mixture temperature will reduce beneficially affecting the volumetric efficiency of the engine. A method of being able to introduce heat to the inlet manifold continuously yet at a constant user defined level up to the rated output of the heater was required. Suitable heater control units[3] were borrowed from the Department of Chemical and Process Engineering (see Figure 6.2).

Figure 6.2 Inlet Air Heater Controller

[3]Temperature Controller INST No 1807 and Average Power Meter INST No 1548

The controller enables the output of the inlet air heater to be set at any level between 0 and 100% in 1% increments. This is achieved by clipping the AC waveform of the input voltage to the heater.

Inlet air heating also reduces the volumetric efficiency of an engine by reducing the density of the induced air. Hydrogen being a gaseous fuel has a low specific density. When introduced into an engine via manifold injection, hydrogen displaces air that would otherwise have been induced and thereby reduces the volumetric efficiency of the engine. In order to separate the effects of inlet air heating on volumetric efficiency from that of hydrogen addition, a constant level of inlet air heating was selected to provide adequate mixture preparation over the experimental operating range[4]. Thus the only variable affecting volumetric efficiency is the amount of hydrogen supplementation.

6.2 Engine Management System

An engine management system (EMS) to control the Ricardo test engine was designed and built within the department in conjunction with the data acquisition system previously described in Chapter 5.

The requirements of the system were to be able to accurately control both the methanol and hydrogen injectors.

The system consists of three main modules, a user interface, a micro-controller and an injector driver board. A constant current drive was used to speed up the opening time of the injectors. The injector outputs are opto-isolated to prevent the possibility of damage to the micro-controller from any failure in the injector drivers. The programmable chip used was a Motorola 68 HC11 E2 and was programmed in assembly language. The software requires accurate knowledge of the index pulse position as all counters are reset when the index pulse is detected. Thus if the rotary encoder is removed from the crank-shaft, the new position of the index pulse will need to be determined (see page 72) and changed in the software. The software can be modified on a host computer and downloaded via a serial link. Input signals from the three rotary encoder channels are received and the two 3600 ppr channels merged into one 7200 ppr channel. Thus the current crank-angle position is known in 0.05 ^{o}CA steps from the index pulse position. The user interface allows the crank-angle at which each injector is opened and closed to

[4]During preliminary engine testing it was found that a setting of 30% on the controller kept the inlet manifold temperature above about 12 °C at $\lambda = 1.0$ and HEF = 0% while keeping the temperature at higher values of λ and HEF from being excessive. This level of inlet air heating corresponds to addition of $\approx$ 364 watts with an input voltage of 240 V)

be set via an LCD display. The crank-angle of interest is set by a pair of directional arrows that increment/decrement values in 0.2 °CA steps. The user interface of the EMS is shown mounted in the Cussons control unit in Figure 6.3 with the oscilloscope and hydrogen mass flow meter display sitting above.

Figure 6.3 Engine Management User Interface (Black Panel)

During the commissioning of the engine management system, a problem was encountered whereby the index pulse was found to trigger intermittently when the engine was running and the spark-plug was firing. This problem was not observed when the engine was only being motored over. It was discovered that noise from the spark discharge was interfering with the engine management system. The solution found was to use a resistive spark-plug which has a built in noise suppression resistor.

6.3 Fuel Injection Systems

6.3.1 Methanol Injector

A major difference between the physical properties of methanol and gasoline lies in their stoichiometric air/fuel ratios (see Table B.2 on page 229). The stoichiometric air/fuel ratio for methanol is 6.4 compared with 14.7 for gasoline. This means that for a given amount of air, the mass flowrate of methanol is 2.3 times greater than that of gasoline.

Given that the respective specific gravities of methanol and gasoline are approximately the same, the volumetric flowrate of methanol is therefore approximately 2.3 times greater than that of gasoline.

The injector used for the manifold injection of both gasoline and methanol was from a Mazda RX7 turbo (part number N326 13 250) that had previously been used by Cree [1992] in his work. Cree selected this particular injector as it has the largest volumetric flow rate (0.5 l/min) of all the injectors that he tested at a fixed supply pressure (2.5 bar).

6.3.2 Hydrogen Injector

The injector configurations used for the direct injection of hydrogen have been previously described in Chapter 3.

6.4 Fuel Supply System

The hydrogen enhanced combustion experiments carried out required the used of two distinctly different fuelling arrangements. The fuel supply system used for each of these is described below.

6.4.1 Methanol Fuel Supply

The fuel supply system used for the methanol was the system originally supplied with the Ricardo E6 for use with gasoline with some modifications.

A constant head supply system was fitted to provide a constant head to a methanol resistant fuel flow meter (see page 97) in accordance with the manufacturers recommendations. Occupational Safety and Health (OSH) regulations required that the 15 liter fuel tank used to hold the methanol be fitted with quick release fittings so it could be stored in the fuel store when not being used. An automotive fuel pump was positioned at the outlet of the tank to pump the fuel up to the constant head tank. The constant head tank has two outlets, one at the bottom leading to the flow meter and an overflow outlet that returns to the fuel tank. The existing gasoline fuel container was left in place to enable methanol to be flushed from the fuel line when required. A three way valve was used to switch between the original fuel system and the new constant head fuel flow meter system. Methanol was supplied to the engine at a pressure of 2.5 bar by the Bosch fuel pump from the original gasoline fuel supply system. The liquid fuel supply system is shown in Figure 6.4.

It was found during experimentation that the methanol fuel flow rate reading was becoming quite erratic at times causing inaccuracy in the fuel flow rate value used to calculate the relative air/fuel ratio. Two causes were identified and steps were taken to minimize their effects.

Firstly the presence of air or fuel vapor in the fuel line was identified as being a cause of concern. The Pierburg methanol flow-meter (see also page 97) operates on a positive displacement principle. Thus any vapor or air in the fuel line will cause apparent variations in the flow-rate due to the compressiblility of the gas. This problem was overcome in part by carefully bleeding the fuel line to ensure no air was trapped within it. In addition, during engine operation, the fuel is heated as it passes through the fuel pump. This heating effect is exasperated as the bulk of the fuel flow is recirculated back through the fuel pump via a pressure relief valve while a smaller quantity flows through to the injector. The recirculation and reheating of the majority of the fuel causes it to heat up forming fuel vapor. To overcome this problem, the fuel supply system incorporates a heat exchanger in the recirculation line. To minimize the possibility of fuel vapor forming during engine testing, it was ensured that the water supply to the fuel heat-exchanger was turning on at full flow. This was noticed to significantly reduce the variability of the fuel flow readings. In addition the vapor trap which is located just above the fuel pump was cleared at regular intervals during the testing procedure.

The second cause identified was the Pierburg flow-meter itself. Although the flow-meter is purported to be methanol resistant, it was found that the flow-meter did suffer from poor lubrication when allowed to sit containing methanol for long periods of time. To overcome this the flow-meter was periodically flushed with castor oil during the testing program. In addition if the flow-meter was to remain unused for a period of time, the system was flushed through with gasoline. For storage for long periods of time, the flow-meter was filled with a light oil as per the manufacturers instructions.

6.4.2 Hydrogen Fuel Supply

The requirements of the three proposed combustion systems under investigation call for two different hydrogen supply systems. The first, a low pressure system, is required to provide low pressure hydrogen for untimed manifold injection. The flow rate of hydrogen is controlled by variation of the supply pressure. The second, a high pressure system, is required to provide high pressure hydrogen to the hydrogen injector for early direct injection system and modified spark-plug system.

In order to comply with OSH regulations, the bulk hydrogen supply is located outside the laboratory buildings in a well ventilated storage building. The hydrogen was piped

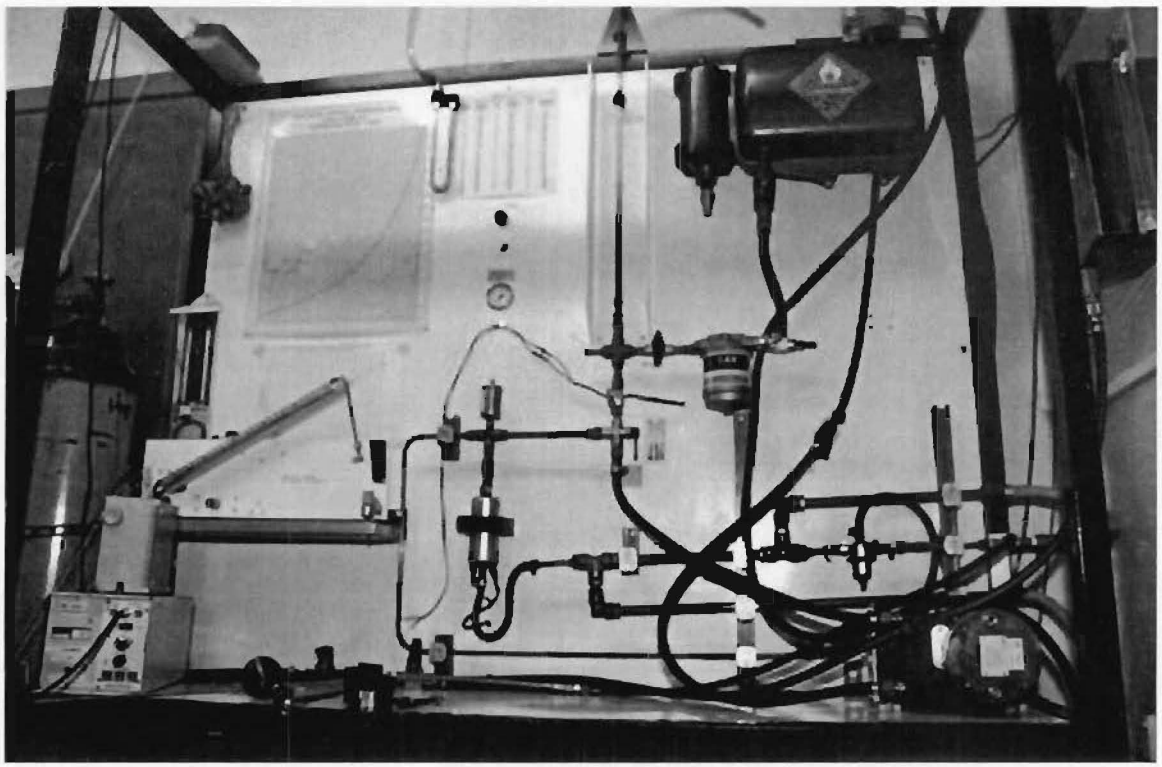

Figure 6.4 Liquid Fuel Supply System

to the test cell in 1/4 inch stainless steel high pressure tubing with Swagelock fittings. The hydrogen used for the research program was purchased in 5.8 m^3 bottles from BOC Gases. In order to increase the time between changing bottles and allow long periods of uninterrupted testing, six bottles of hydrogen were manifolded together. In addition a bottle of oxygen free nitrogen was incorporated into the hydrogen bottle manifold to allow hydrogen to be purged from the supply line right up to the engine.

As the hydrogen line enters the laboratory wing it passes through a normally closed air actuated ball valve (see page 96) before entering the test cell. Once in the test cell, the flow of hydrogen is directed to either a low pressure or high pressure regulator via a three way valve (see Figure 6.5). From the pressure regulators the hydrogen passes through a 60 micron filter to protect the flow-meter and injectors and a Hastings Instruments thermal mass flow meter (see page 97). The hydrogen then proceeds to the inlet manifold or the hydrogen injector. Both the high and low pressure systems have three way valves after the regulator providing a vent to outside the test cell if required to purge the lines.

Loops bent in the stainless steel hydrogen line or high pressure flexible hose were used wherever relative movement of parts was expected especially near the connection of the supply line to the injectors.

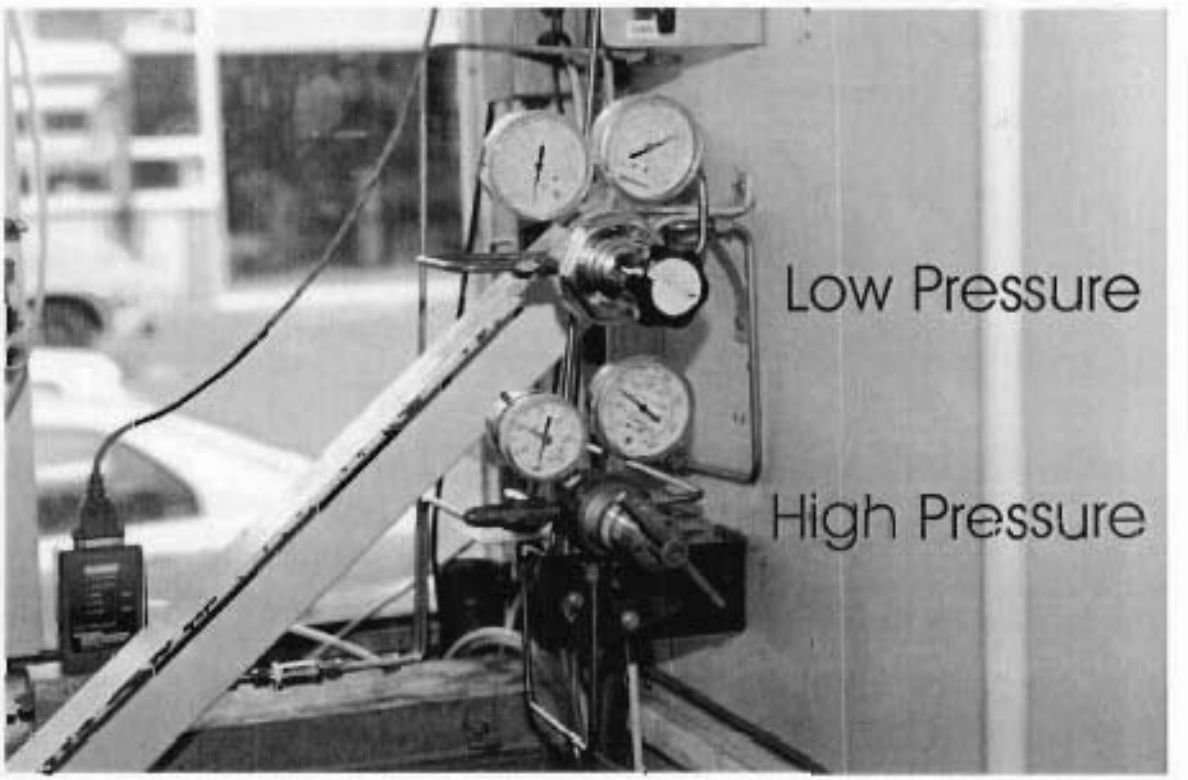

Figure 6.5 High and Low Pressure Hydrogen Regulators

6.5 Safety System

When performing combustion experiments with hydrogen, safety considerations are always of paramount importance. Hydrogen being a colorless, odorless gas is ordinarily impossible to detect if a leak should occur. A gas detection system (Almazda Developments A200M) based on that previously used in the Ricardo E6 test-cell by Glasson [1992] was used. The system utilizes three gas sensitive semiconductor sensors (Figaro TGS 813) calibrated to detect hydrogen levels greater than 20% of the lower explosive limit of hydrogen in air. Two sensors are located in the test cell, one above the engine and one above the pressure regulators where the hydrogen line enters the test cell. The remaining sensor is located in the adjacent engine test cell above the normally closed air actuated ball valve where the hydrogen line enters the laboratory wing. As an added precaution, a hand actuated alarm push switch was fitted to the top of the wiring console beside the original ignition kill switch.

The alarm system can be activated in one of two ways, either one of the sensors triggers or the alarm push switch is activated. When the system is activated, the audible siren sounds and relays are activated to switch on fans in both test cells. The normally closed air actuated ball valve is tripped and the supply of hydrogen to the laboratory wing cut off. As an added safety precaution, if either the laboratory compressed air or

electricity supplies to the gas sensors are cut off, the fans in both test cells are activated and the normally closed air actuated ball valve is closed preventing hydrogen from entering the laboratory wing.

During the course of the research, the safety system was tripped on several occasions and in every case the system operated faultlessly and the potential hazard eliminated by the fans. The cause of the leak could then be traced and repaired.

6.6 Instrumentation

6.6.1 Data Acquisition System

The data acquisition system described previously in Chapter 5 was installed in the testcell.

6.6.2 Methanol Flow Measurement

The measurement of methanol flow rates during engine testing was carried out using a Pierburg methanol resistant high precision flowmeter (PLU 103A). The principle of operation is that of a positive displacement type and gives a frequency output proportional to the volumetric flow rate of the fluid being measured. A display unit was designed and built within the department which converts the frequency output to a volumetric flowrate, incorporating the manufacturers calibration report in the process to ensure greatest accuracy. A liquid crystal screen displays the flow in liters per hour.

6.6.3 Hydrogen Flow Measurement

The measurement of hydrogen flow rates during testing was accomplished using a Hastings Instruments mass flow meter (HFM-201). Signals from the flowmeter unit are sent back to the power supply unit which processes the signal and displays the gas flow in SLPM nitrogen equivalent on a liquid crystal display. The calculation used to convert the flow reading from SLPM nitrogen to kg/sec hydrogen is given in Appendix E.2 on page 239.

6.7 Calibration of Fuel Supply Systems

6.7.1 Pierburg Flow Meter

After installation of the Pierburg high precision flowmeter and display unit in the testcell, a calibration test was carried out. The Mazda fuel injector was removed from the inlet manifold and positioned above a graduated measuring cylinder. The engine was motored

at 1500 rpm with the fuel injector start/finish crank-angles set to give a flow rate of 3.5 litres/hour. The time taken to inject a known quantity of gasoline was then measured. The measured flowrate and the flowrate displayed given by the flowmeter agreed to within 1%. Thus the liquid fuel measurement system was considered to be accurate.

6.7.2 Alcock Viscous Flow Air Meter

During preliminary gasoline engine testing, a calibration check was made on both the air measurement and liquid fuel measurement systems using a Bosch exhaust lambda sensor. The engine was run at 1500 rpm and the fuel flow rate adjusted so that the lambda sensor output voltage was 0.4 V indicating a stoichiometric mixture was being combusted. The recorded fuel flow rate (2.298 litres/hour) and viscous air flow air meter manometer reading (78 mm H_2O) were input into a spreadsheet written to calculate the value of λ that the engine is being run at (LAMBDA GASOLINE.xls) which is based on combustion stoichiometry (see also page 102). The spreadsheet calculated the engine operating point to be in fact $\lambda = 0.98$. Given that the measurement of liquid fuel flow rates were known to be accurate (see previous paragraph), the air flow rate measurement was suspected to be inaccurate.

The inclined manometer of the viscous air flow meter contains a paraffin based liquid of a particular specific gravity. The manometer is set on an angle of 30^o 0" to allow small changes in pressure to be distinguishable. The scale is calibrated to show pressure differentials in mm H_2O. A precision water manometer was borrowed from the Department's aeronautics laboratory to compare with the readings given by the inclined manometer (used in conjunction with the viscous air flow meter). An induced pressure differential of 78 mm H_2O as measured by the inclined manometer corresponded to a pressure differential of 80 mm H_2O as measured by the precision water manometer. Adding 2 mm to the inclined manometer reading used when calculating the value of λ in the previous paragraph resulted in the calculated value of λ to be 1.0, which agrees with the output of the Bosch exhaust lambda sensor.

To adjust the inclined manometer to give correct air flow readings in the future, it was decided to adjust the angle of the inclined manometer rather than try to adjust the specific gravity of the fluid. A pressure differential of 100 mm H_2O (as measured by the precision manometer) was induced. The angle of the inclined manometer was adjusted from 30^o 0" to 29^o 28" so that the inclined manometer also read 100 mm H_2O. The pressure was slowly released and consistency between the two manometer readings checked over the full inclined manometer scale.

6.7.3 Hydrogen Mass Flow Meter

The Hastings Instruments mass flow meter used for the measurement of hydrogen flow rates during this project was supplied with a current factory calibration certificate along with conversion factors. The equation used to convert the displayed flowrate in slpm N_2 to $\dot{m}_{H_2}$ is given in Appendix E.2 (Equation E.2). The manufacturer's supplied equation and calibration report were assumed to be accurate. No attempt to verify the calibration of the mass flow meter was made due to the unavailability of a device of sufficient accuracy with which to compare.

Because of the low hydrogen energy fraction's (HEF's) that the majority of the work was carried out with, it was thought that any small inaccuracies in the measured hydrogen flowrates will not have a significant effect on the accuracy of the calculated values of λ. A similar argument also applies for the calculation of HEF's.

THE LIBRARY
UNIVERSITY OF CANTERBURY
CHRISTCHURCH, N.Z.

Chapter 7

Experimental Procedures

This chapter builds on the description of the experimental apparatus described in Chapter 6. Details of fuel preparation, engine testing philosophy and spark timings used are presented. A description of the exhaust emission testing equipment and procedures used then follows. The procedures developed for the calibration of the piezo-electric pressure transducer, electronic data acquisition, engine operation and testing are then presented.

7.1 Methanol Fuel Preparation

Methanol is a fuel that has poor lubricating properties compared with gasoline. In a conventional gasoline fuelled engine system, the gasoline provides the necessary lubrication for the fuel pump. In order to improve the lubrication properties of methanol, it is common to mix 1-2 vol% castor oil with the methanol. Castor oil is used because it dissolves in methanol and does not separate as happens with mineral oils [Cree 1992].

The methanol used throughout this project was purchased in 200 liter drums from Mobil Oil NZ Limited. The bulk methanol supply was stored in the Department's fuels store adjacent to the thermodynamics laboratory. Prior to engine testing, a 15 liter tank was filled in the fuel store and 1 vol% castor oil added. The tank was shaken to ensure thorough mixing before being installed in the test cell. There has been no reports in previous investigations of castor oil having any identifiable effects on the combustion process in an engine.

7.2 Throttle Plate Position

One of the major objectives in current internal combustion engine research is the improvement of part load engine efficiency (see page 7). As was stated in Chapter 1 hydrogen, through it's high flame speed and it's wide flammability limits, allows a supplemented engine to be operated over a wide range of air/fuel ratios without requiring inlet air throttling. This reduces the volumetric efficiency and pumping losses, further enhancing

part load fuel economy. Consequently all engine testing conducted in this investigation was performed at the wide open throttle condition.

7.3 Air/Fuel Ratio

A decision was made on what changes to the engine's operating condition would be the basis for analyzing the effects of hydrogen enhanced combustion. There were three practical possibilities:

1. Maintain constant quantity of injected methanol and add varying levels of hydrogen.
2. Maintain constant total fuel energy (MeOH + H_2) and vary the overall air/fuel ratio.
3. Maintain constant overall air/fuel ratio and vary the percentage of total charge energy provided by hydrogen supplementation.

Changes in air/fuel ratio have a more pronounced effect on combustion than does changes in the total charge energy [Heywood 1988] thus any changes in combustion characteristics could be argued to be due to the change in air/fuel ratio and not the addition of hydrogen. It was decided that option three was the most suitable engine fuelling option. During testing the quantity of methanol and hydrogen supplied to the engine was varied whilst maintaining the specified overall relative air-fuel ratio. The amount of hydrogen supplementation is denoted by the % of total fuel energy that is contributed by hydrogen, the Hydrogen Energy Fraction (HEF) [Rauckis and McLean 1979]. In order to fuel the engine in the specified manner, an Excel spreadsheet was developed (LAMBDA METHANOL.xls). The spreadsheet required the following inputs:

- Atmospheric Pressure
- Overall relative air/fuel ratio required (λ)
- Required HEF
- Viscous flow meter manometer reading
- Ambient air temperature

Using these inputs along with the calibration curve for the viscous flowmeter, the spreadsheet gave the required flow rates of methanol (liters/hour) and hydrogen (SLPM N_2[1]) required for the particular test condition. The method used to fuel the engine involved operating the engine at fixed air/fuel ratios while the level of hydrogen supplementation was varied.

[1]The unusual hydrogen flow rate specification is due to the units that the mass flow meter displays the measured flow rate.

7.4 Spark Timing

Ignition timing in a spark ignited engine has a large effect on combustion, engine performance and emissions. The spark timing at each engine test point was adjusted to be that which gives the maximum brake torque (MBT) [Heywood 1988] from the engine (denoted MBT spark timing). MBT spark timing is the point at which the net work transfer to the piston is maximized (ie expansion stroke work minus compression stroke work) [Heywood 1988]. MBT spark timing depends upon the rate of flame development and propagation, the length the flame has to travel across the combustion chamber and details of the flame termination process after it reaches the combustion chamber wall. It has also been shown that MBT spark timing gives the lowest values of cyclic variation at any engine operating condition [Young 1981] , [Stone and Beckwith 1992] , [Ozdor *et al.* 1996].

The engine torque curve around the point of MBT spark timing is quite flat. It is thus quite common to retard the spark timing in order to give a 1-2% reduction in brake torque to permit a more precise definition relative to the optimum [Heywood 1988]. For this work the spark timing at each test point was advanced until a drop in engine torque was observed and then retarded until a corresponding drop was observed. The MBT spark timing was determined to be the crank-angle midway between these two points[2].

Unless specified, the spark timing used in all testing is that of MBT.

7.5 NO/NO_x Emissions Measurements

Although much of the current focus of engine research is on reducing all the various species of pollutants that are found in engine exhaust, the primary focus has been on the reduction in the oxides of nitrogen (NO_x). NO_x along with HC emissions are a primary contributor to the formation of photochemical smog [Heywood 1997].

Testing for NO_x emissions was carried out using a Beckman chemiluminescent NO / NO_x analyzer (Model 951A). Any NO_2 in the sample gas stream is decomposed into NO thereby allowing the concentration of total oxides of nitrogen (NO + NO_2) to be determined. The NO in the sample stream is reacted with ozone producing NO_2 molecules in an excited electronic state. The excited NO_2 molecules emit radiation as they decay to their ground state. This radiation is measured with a photomultiplier [Heywood 1988]

[2]NO and UHC engine emissions are known to vary significantly with spark timing [Heywood 1988]. However throughout the course of this work the trends in engine emissions obtained were found to be consistent confirming the consistent nature of the method of MBT spark timing determination employed.

whose output is proportional to the concentration of NO_x in the sample.

Several hours prior to engine testing, the NO_x meter was switched on and the supply of oxygen to the meter opened. The meter was then left to warm-up and reach a stable zero reading. Just prior to engine testing, the zero was set and the meter calibrated with the 3330 ppm total oxides of nitrogen span gas supplied by BOC gases. The calibration and operating procedures will not be detailed here but can be found in the Beckman equipment manual [Beckman 1980]. The output voltage and range setting was recorded manually (see Section 7.13) for later conversion to the actual emission level.

7.6 Unburnt Hydrocarbon Measurement

Another major pollutant of importance that was measured are the unburned hydrocarbons (UHC). UHC emissions have been found to contribute, along with NO_x emissions, to the formation of photochemical smog [Heywood 1997].

UHC emissions are most commonly measured by one of two instruments, a flame ionization detector (FID) or a nondispersive infrared (NDIR) analyzer. FID's are effectively carbon atom counters as the hydrocarbons present in the exhaust gas sample are burned in a hydrogen-air flame and produce ions in proportion to the number of carbon atoms burned (C1). The sensitivity of a FID is known to differ between different hydrocarbon species [Ferguson 1986] , [Bell *et al.* 1996]. NDIR analyzers use the infrared absorption by the hydrocarbons in the exhaust gas sample to determine their concentration. Hydrocarbon concentrations measured by a FID are about two times the concentrations measured by an NDIR analyzer thus NDIR obtained values are usually multiplied by 2 to give an estimate of the actual UHC concentrations [Heywood 1988].

The major proportion of *"hydrocarbon"* components in the exhaust of methanol fuelled engines is unburned methanol [Bernhardt 1977]. It is known that aldehydes are not detected by FID analyzers [Bernhardt 1977]. Therefore the UHC emissions of a methanol fuelled engine as measured by a FID represents unburned methanol and all other hydrocarbons excluding aldehydes.

The majority of UHC emissions in this project were measured by the department's Beckman FID. It was not available during the initial part of the work and some initial testing was conducted with the department's Horiba MEXA-GE534. Once the FID became available, it was used to make a small number of checks on the actual levels and trends in UHC emissions of the untimed manifold injection system. The calibration and operating procedures for the FID will not be detailed here but can be found in the Beckman equipment manual [Beckman 1981]. Unless specified, all UHC emission values

presented are those derived from the Beckman FID analyzer. The Horiba MEXA-GE534 emission analyzer uses the NDIR method of UHC measurement. The calibration and operating procedures for the Horiba can be found in the operating manual [Horiba 1988]. The Horiba gives UHC emission levels in ppm n-hexane equivalent which are multiplied by 6 to give ppm C1 equivalent. Brown [2001] had previously conducted an experiment on an engine comparing the UHC emission's as measured by the departments Horiba MEXA-GE534 and Beckman FID. He concluded that the concentrations measured by the Horiba must be multiplied by 2.5 before being converted to ppm C1 equivalent in order to match those given by the FID over the range of emission levels being looked at. Brown's conclusions were used throughout this work.

7.7 Aldehyde Measurement

The incomplete combustion of hydrocarbons produces emissions of aldehydes. Although the level of exhaust emissions are generally lower for vehicles fuelled on alcohols, the level of aldehyde emissions are significantly higher than that of a gasoline fuelled engine [Bernhardt 1977] , [Lipari and Colden 1987] , [Mearns and Dutkiewicz 1993]. Formaldehyde is the predominant aldehyde present in the exhaust of a methanol fuelled engine [Lipari and Colden 1987] accounting for 98% of the total aldehydes. There are two main methods by which exhaust gas aldehyde emission levels are commonly measured: the 2,4-dinitrophenylhydrazine (2,4-DNPH) method and the 3-methyl-2-benzothiazolone hydrazone (MBTH) method. Comparative investigations have found that both methods give a similar measurement accuracy [Menzies and Beltis 1982] although the MBTH method is non-selective and gives the total aldehyde concentration in terms of their formaldehyde equivalent [Lipari and Swarin 1982]. Lipari and Swarin [1982] developed a simple method for the measurement of aldehydes and ketones which involves bubbling exhaust gas through an acidic 2,4-DNPH solution contained in a set of midget impingers. An aliquot of the resulting solution containing hydrazone derivatives of the aldehydes and ketones is then quantitatively analyzed in a high-performance liquid chromatograph (HPLC). The 2,4-DNPH-HPLC method of Lipari and Swarin has become the preferred technique for the measurement of aldehyde emissions in exhaust gas [Haack *et al.* 1986] , [Mearns and Dutkiewicz 1993] , [Mori *et al.* 1993]. Smith *et al.* [1989] improved the performance of this method to eliminate the unwanted peaks due to the presence of ozone. A further improvement to the 2,4-DNPH-HPLC method has been the development of 2,4-dinitrophenylhydrazine Solid-Phase-Extraction (2,4-DNPH-SPFE) cartridges [Tejada 1986] , [de Goede *et al.* 1996]. Quantification of the resulting hydrazone derivatives is still carried out via HPLC. This eliminates the technically demanding and time consuming production of the 2,4-DNPH solutions used in the impingers. More recently Fourier transform infrared (FT-IR) spectrometry has been developed as a method of measuring both regulated and non-regulated emissions simultaneously on-line [Nichols

et al. 1988] The FT-IR method is able to quantify transient emission data where the 2,4-NDPH-HPLC method is limited to the quantification of steady state emission data [Haack *et al.* 1986].

An aldehyde sampling system based on the 2,4-DNPH-HPLC impinger method was investigated. A C_{18} HPLC column and guard column were purchased and fitted to a HPLC in the Department of Chemistry. Reference standards of the aldehydes of interest were manufactured and a suitable gradient optimized to give good separation and reproducibility. However a large amount of time would have been required to fully implement a calibrated engine exhaust gas analysis system. Due to both the time required and the amount of work that still remained to be completed in implementing the engine management system and associated data acquisition system in the test cell, it was decided that the although aldehyde exhaust emission measurements would be desirable it was beyond the scope of this investigation and it's time constraints.

It is known that aldehyde emissions decrease significantly as the air/fuel mixture becomes richer. The lower oxygen levels lead to a reduction in aldehyde concentrations despite an increase in UHC [de Goede *et al.* 1996]. Varying the spark timing has little effect on the concentration of aldehydes which indicates that aldehyde production is independent of peak combustion gas temperatures and pressures [de Goede *et al.* 1996]. It has been suggested that there is an opportunity to simultaneously reduce aldehyde and NO_x emissions through the addition of water to methanol. Bernhardt [1977] found that the addition of 10% water to methanol resulted in a 50% reduction in NO_x and a 40% reduction in aldehyde emissions with only a 10% reduction in engine output power (CR = 9.7, WOT and 3000 rpm). The explanation given is that the increase in water is responsible for an increase in hydroxyl radicals which simultaneously increase the rate of HCO production from formaldehyde and reduces the amount of atomic oxygen available for the formation of NO.

7.8 Oxides of Carbon Measurement

Two further exhaust pollutants of importance are the oxides of carbon, CO and CO_2. CO emissions has been shown to have detrimental effects to health. CO_2 emissions have been shown to contribute to the so called "global warming" phenomenon that has risen to prominence in recent years.

The CO and CO_2 emissions are measured by the Horiba MEXA-GE534 emission analyzer. Like the measurement of UHC emissions, the emissions of CO and CO_2 are measured using the NDIR principle. However the NDIR analyzer does not suffer the same under estimation of the oxides of carbon emission levels that is problematic with

NDIR UHC emission measurement. The analyzer is calibrated with a span gas containing 10.9 vol% CO_2 and 2.03 vol% CO. The emissions levels are displayed in %vol.

7.9 Oxygen Measurement

The preferred method of measuring O_2 concentrations is with a paramagnetic analyzer [Heywood 1988]. Unfortunately there were none of these available but the Horiba MEXA-GE534 emission analyzer has been previously modified to incorporate a galvanic O_2 sensor. The O_2 concentrations are displayed in %vol.

7.10 Horiba MEXA-GE534 Operating Procedure

Before use, the Horiba was calibrated against a span gas supplied for that purpose in accordance with the instructions found in the manual. A full description of the calibration procedure can be found in the Horiba technical manual [Horiba 1988].

The Horiba has it's own unheated sample line for connecting the analyzer to the exhaust pipe of the engine. A water trap was added to the sample line as it was anticipated that there would be increased amounts of water vapor in the exhaust gas resulting from combustion of the supplementary hydrogen. During preliminary engine testing it was noticed that the UHC readings would drift upwards over time. Test points completed early in a testing session when repeated near the end would give much higher UHC readings. The discrepancies in the readings seemed to be limited to the UHC and not the CO, CO_2 or O_2 readings. The explanation proposed for this observed trend is that the Horiba is not designed for continuous sampling of exhaust gas emissions over time but rather quick samples of a car exhaust at idle to determine approximately what the state of tune of the engine is. It appears that over the duration of the engine test session, the UHC build up in the analyzer and result in the observed increase in emission levels over time. To overcome this, a three way valve was plumbed into the Horiba sample line just after the water trap. The spare inlet to the valve was connected to a supply of oxygen free nitrogen. Thus when exhaust emissions are not being measured, the valve is switched so that the Horiba draws in oxygen free nitrogen to flush out any residual exhaust gas that has remained inside the analyzer. This system was found to eliminate the problem of the UHC readings drifting upwards over time.

7.11 Piezo-electric Pressure Transducer Calibration

Piezo-electric pressure transducers rely upon a change in applied pressure to produce a change in the output signal. Therefore in order to correctly calibrate, a known change

in pressure is required. The required change in pressure was applied by a Barnet dead weight tester that had been modified by Trolove [1991] to allow for the rapid release of static pressure. To ensure the highest possible accuracy of the cylinder pressure data, the piezo-electric pressure transducer and the data acquisition system was calibrated as a whole[3].

A routine called CALTRANS was written to read voltages from the piezo-electric pressure transducer channel at a frequency of 5 kHz by the on-board pacer trigger. The piezo-electric charge amplifier was set on the appropriate range and setting to give an $\approx$4 V maximum output voltage during preliminary engine testing. The calibration data acquisition procedure was as follows:

1. Apply the desired load (in increments of 5 bar from 0 to 70 bar)
2. Ground the charge amplifier
3. Run "Calibrate Pressure Transducers" from the "Hardware Test and Calibration Programs" Menu.
4. Enter the piezo-electric pressure transducer channel number
5. Start the data acquisition and immediately unload the transducer
6. Repeat until the required load range has been covered

The procedure outlined above results in 14 data files with a suffix *.piz. Each of these files is imported into Excel and the change in voltage between the transducer being loaded and unloaded is calculated. A summary of all voltage changes and the corresponding changes in pressures are entered into an Excel spreadsheet called CALIB.xls. A plot of voltage change verses pressure change is made with the slope of the line being the pressure transducer calibration constant for that particular calibration. In the pressure transducer calibration plot shown in Figure 7.1, the pressure transducer calibration constant is 17.005 bar/volt.

7.12 Data Acquisition

At each test point during engine testing two sets of combustion pressure and temperature data was taken (see page 68). Two sets were taken as it was discovered that on occasion the data acquisition system started taking data at a point in the engine cycle that did not correspond to the position of the rotary encoder index pulse (see page 65). Whether the data was good or faulty was not known until it had been post-processed. It was

[3]The transducer and cables were dried and calibrated weekly during engine testing and stored in an air-tight container with desiccant to prevent charge leakage which occurs when moisture is present.

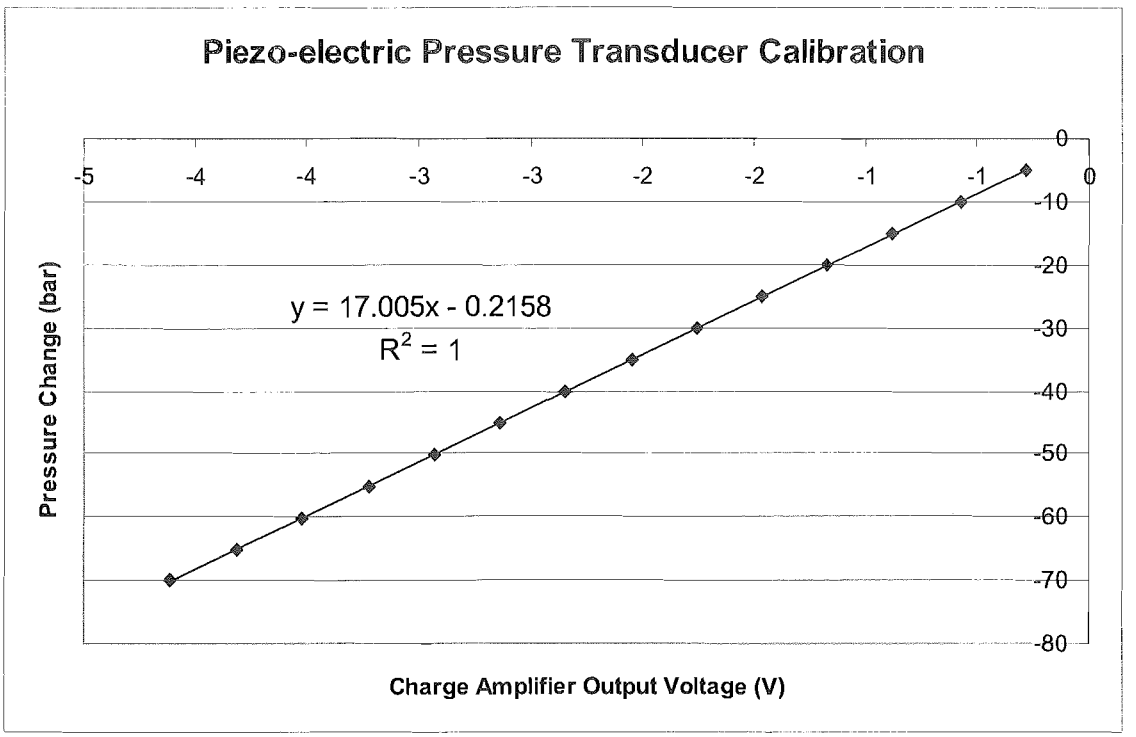

Figure 7.1 Pressure Transducer Calibration

thought that the faulty operation was caused by stray electrical noise however the cause was not investigated due to time constraints and the fact that it occurred infrequently.

The procedure for electronic engine data acquisition is as follows:

1. Run "Acquire Single Channel Data at 1800 ppr" from the "Engine Data Acquisition" Menu.
2. Enter the file name, nominal engine speed and external trigger frequency
3. Ground the charge amplifier
4. Start the data acquisition
5. Repeat to acquire a second set of data

7.13 Manually Recorded Engine Test Data

At each of the test points, a certain amount of data was recorded manually on pre-printed engine test log sheets. The data recorded was:

1. Compression ratio

2. Required lambda
3. Piezo-electric pressure transducer constant (bar/volt)
4. Atmospheric Pressure (mbar)
5. Engine speed (rps)
6. Methanol flow rate (liters/hour)
7. Hydrogen flow rate (SLPM N_2)
8. Hydrogen injector open angle (^{o}ATDC - when appropriate)
9. Hydrogen injector close angle (^{o}ATDC - when appropriate)
10. Viscous Flow Airmeter Manometer reading (mm H_2O)
11. Pressure drop across viscous air flow meter (mm H_2O)
12. Ambient air temperature (^{o}C)
13. Dynamometer scale reading (N)
14. Number of weights used on dynamometer
15. Spark timing (^{o}ATDC)
16. Air heater supply voltage (V)
17. Heater controller setting (%)
18. Mean inlet manifold pressure (mbar)
19. Inlet manifold mixture temperature (^{o}C)
20. NO_x range setting
21. NO_x meter reading (V)
22. Horiba HC emissions (ppm)
23. Horiba CO emissions (vol%)
24. Horiba CO_2 emissions (vol%)
25. Horiba O_2 emissions (vol%)
26. FID range setting
27. FID meter reading (%)

7.14 Operating Procedures

Approximately one hour before engine testing was to be commenced, the engine oil and coolant pumps and heaters were turned on to allow the engine to reach a "hot wall" condition of $\approx 60^{o}$C. The piezo-electric pressure transducer was fitted to the engine and it's coolant water turned on. The data acquisition computer, oscilloscope, charge amplifier, mass flow meter and methanol flow meter were all turned on to allow the electronic circuitry to heat up and stabilize. The water supply to the fuel system heat exchanger is turned on. The test cell fan and air conditioning unit were also activated to allow plenty of time for a steady state test cell temperature to be achieved.

Prior to engine testing, both pressure regulators were wound out (giving zero pressure) and the supply lines set to vent to the outside. The hydrogen bottles in the outside fuel cell are then opened.

When testing was due to commence, the engine was motored up to just below the required test speed before being switched to fixed speed mode. The engine speed was then adjusted to the correct value before the being left for up to 20 minutes (or longer if there was gasoline in the fuel line which had to be flushed through the system) for the engine to reach a steady state operating condition[4]. Once the engine was thoroughly warmed up, the test points were set by varying the injector close angles of both the methanol and the hydrogen injectors to achieve the desired flow-rates given by the spreadsheet LAMBDA METHANOL.xls (see page 102).

It was found during the course of the experimental work that it is necessary to ensure that the liquid fuel supply system was free from air or vapor so that stable fuel flow readings are obtained from the flow meter. The fuel system incorporates a recirculation system and a pressure regulator to supply the fuel injector with a constant supply pressure. The recirculation system can heat the fuel significantly so there is a heat exchanger incorporated in the system. Water to this heat exchanger is turned on at all times to reduce the risk of fuel vapor being formed. There is also a vapor trap located above the Bosch fuel pump in which vapor and air in the system accumulates. During engine testing this was regularly cleared[5].

At the conclusion of testing, the hydrogen supply is turned off at the bottles and the remaining hydrogen in the lines allowed to be injected into the engine and burnt. Once the hydrogen pressure has dropped to atmospheric, the hydrogen regulator is wound out

[4]It was found that even though the engine appeared to reach steady state quickly, the engine would "drift" off that particular operating condition for quite some time

[5]When the fuel pump is turned off as the pump would otherwise pull air into the system

and the hydrogen supply lines to the engine vented to the atmosphere. If the engine is not to be run for some time, the fuel supply is switched to gasoline and the engine run until the fuel system contains gasoline only. The engine is switched off and allowed to come to a standstill. All test cell services are switched off with the exception of the coolant water supply to the piezo-electric pressure transducer which is kept running until the cylinder head has cooled down and the risk of thermal damage has passed.

Chapter 8

Untimed Manifold Injection Results

In this chapter the results of an investigation into the untimed manifold injection of hydrogen will be presented. First the engine configuration and the relevant operating parameters are discussed, then the effects of hydrogen supplementation on the fluid properties are examined before the effects of hydrogen supplementation on the combustion characteristics, engine performance and emissions are presented.

8.1 Introduction

Hydrogen supplementation via untimed manifold injection is technically the simplest of the three methods under investigated. Hydrogen is supplied to the inlet manifold of the engine in a continuous, untimed manner and is induced into the engine with the engine inlet air and manifold injected methanol forming a homogeneous air/fuel mixture. Any resultant changes in the combustion, power or emissions characteristics of the engine are therefore due to the combustion properties of hydrogen alone and not due to the effects of charge stratification.

8.2 Engine Configuration

The engine's primary fuel was manifold injected methanol. The main fuel was supplemented with the untimed manifold injection of gaseous hydrogen via the low pressure hydrogen supply system described on page 94 and the manifold injection configuration described on page 35. The flow rate of hydrogen was varied as required by adjusting the supply pressure to the inlet manifold.

In order to best examine the effects of supplemented hydrogen on the combustion process the overall air/fuel ratio was kept constant and the percentage of the total charge energy provided by hydrogen supplementation (hydrogen energy fraction or HEF) varied (see page 102). The HEF of the incoming charge was varied from zero to fifty percent at each value of air/fuel ratio. At the richer air/fuel ratios, HEF's of 40% - 50% were

not always obtainable due to limitations in the ability of the manifold supply system to supply the required high hydrogen flow rates.

Inlet air heating was used to ensure adequate mixture preparation by partially offsetting the cooling effect on the inlet mixture caused by methanol's high latent heat of vaporization (see page 89). Approximately 364 Watts of heat was continuously supplied to the inlet air from a heater and associated control unit.

All results refer to testing performed at an engine speed of 1500 rpm and at a wide open throttle setting. The compression ratio was raised from 8:1 which is the optimum compression ratio for gasoline in the Ricardo E6 test engine. The compression ratio was set at 10:1. This is not necessarily the maximum compression ratio that is possible when fuelling a Ricardo E6 with combinations of methanol and hydrogen but was chosen to demonstrate the potential benefits over gasoline operation. Engine operation at higher compression ratios was problematic with pre-ignition occurring at rich air/fuel ratios with both methanol and methanol/hydrogen mixtures. The source of the pre-ignition was thought to be the spark plug which was the same heat range as used for gasoline operation (NGK BPR6HS). Due to difficulties experienced in obtaining a resistive spark-plug of the same configuration colder than the existing plug, engine testing was conducted at a compression ratio of 10:1. A resistive spark-plug is required to be used with the engine management system to prevent stray electrical noise affecting the electronics (see page 91).

8.3 Fluid Properties

Combustion in a spark ignition engine is approximated by the ideal Otto cycle named after Nicolaus Otto who built the first engine based upon a four stroke cycle in 1876. The thermal efficiency, η_{th}, for the air-standard Otto cycle is:

$$\eta_{th} = 1 - \frac{1}{r_c^{\gamma-1}} \tag{8.1}$$

The compression and expansion processes are assumed to be adiabatic isentropic processes for which:

$$pV^{\gamma} = constant \tag{8.2}$$

In a real engine however irreversiblities of the actual compression process, the addition of fuel, the effects of heat transfer and the effects of mass loss (blowby) result

in the actual compression and expansion processes being approximated by a polytropic relation:

$$pV^n = constant \tag{8.3}$$

The actual compression process in an engine is however very close to an isentropic process. Details on the calculation of these indices can be found on page 78.

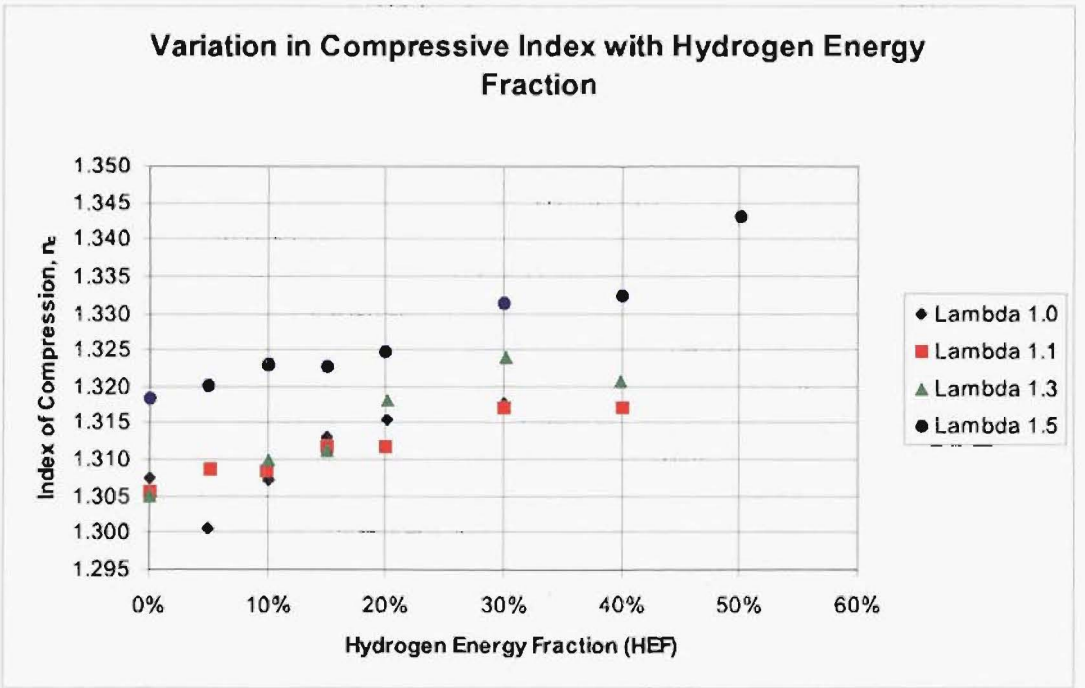

Figure 8.1 Effect of Hydrogen Supplementation on the Polytropic Index of Compression

Figure 8.1 shows the effect of hydrogen addition on the polytropic index of compression (n_c) calculated from measured cylinder pressure and crank-angle data at each test point. The polytropic index is calculated from logarithmic pressure/volume data between 220 ^{o}ATDC and 320 ^{o}ATDC. The value of compressive index for $\lambda = 1.0$ and 5% HEF is much lower than the values either side. While the reason for this is not apparent, the effect of this on the mfb durations (which are heavily dependent on the values of polytropic index used) appears to be negligible (see Figures 8.2 to 8.5). It is apparent that $\lambda = 1.5$ exhibits a value of n_c that is greater than all the richer air/fuel mixtures. The trends between the other values of λ are not that clear at lower values of HEF. At higher values of HEF however it is apparent that leaner mixtures exhibit a higher value of n_c than do richer mixtures as would be expected (see following paragraph). The addition of hydrogen has the effect of raising the polytropic index of compression for all values of λ.

Methanol vapor has a specific heat ratio of $\gamma \approx 1.16$ [Germane *et al.* 1983] compared with $\gamma \approx 1.38$ for hydrogen [McCarty *et al.* 1981] and $\gamma \approx 1.40$ for air [Rogers and Mayhew 1988]. As an air/fuel mixture becomes leaner, the proportion of methanol vapor in the mixture decreases. Thus it is to be expected that lean air/fuel mixtures will exhibit a value of n_c greater than that of richer air/fuel mixtures. For a given air/fuel ratio, the increase in n_c with HEF is due to an increase in the amount of hydrogen (with a high specific heat ratio) and the reduction in the amount of methanol vapor (with a low specific heat ratio) in the inlet air/fuel mixture. Hydrogen has a specific heat ratio value approximately equal to that of air thus as the amount of hydrogen supplementation increases, the intake fluid specific heat ratio tends towards that assumed in the ideal air standard cycle.

The addition of hydrogen to the working fluid of an engine increases the specific heat ratio of the overall air/fuel mixture and the value of the polytropic index approaches that of $\gamma = 1.4$ for the air standard Otto cycle. The theoretical thermal efficiency that can be attained from an engine (as given by Equation 8.1) is therefore increased.

How leaner air/fuel ratios and higher levels of hydrogen supplementation can contribute towards increases in thermal efficiency will be more fully discussed on page 129.

8.4 Combustion Burn Rate

The supplementation of methanol with hydrogen is expected to have a measurable effect on the combustion of the cylinder charge (see page 16). In order to elucidate changes occurring in the combustion process, a full analysis of the in-cylinder pressure data was performed on data acquired at each of the test points covered. Perhaps the most important information to be gained about the combustion process is from the mass fraction burned analysis of the cylinder pressure data (see page 75).

The Figures 8.2 to 8.5 show the effect of hydrogen addition on each different phase of combustion.

From Figures 8.2 to 8.5, the following points can be noted. For the range of values of λ tested, in all phases of combustion the richest mixtures burn faster than do the leaner mixtures as would be expected to occur for any fuel or combination of fuels. Increasing the HEF reduces the burn duration of all phases of combustion resulting in faster overall combustion (refer to Figure 8.5). Similar observations were made by Rauckis and McLean [1979] and Jordan [1979] in their work dealing with hydrogen supplemented gasoline as well as Schafer [1981] with methanol. The reason for the increased rate of

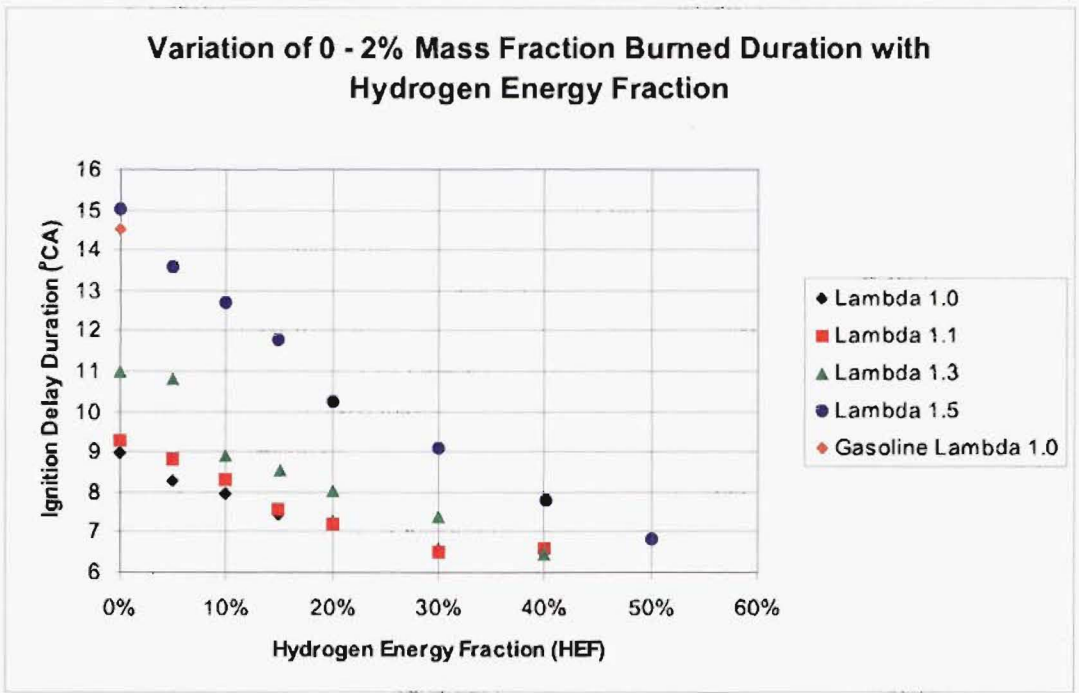

Figure 8.2 Effect of Hydrogen Supplementation on 0-2% mfb

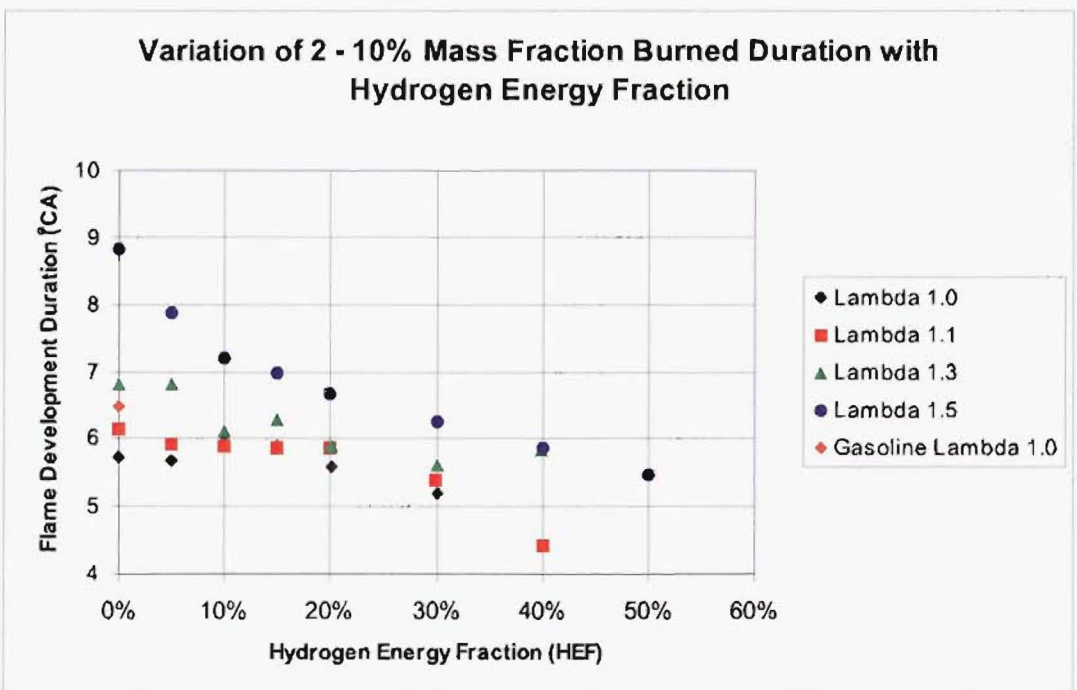

Figure 8.3 Effect of Hydrogen Supplementation on 2-10% mfb

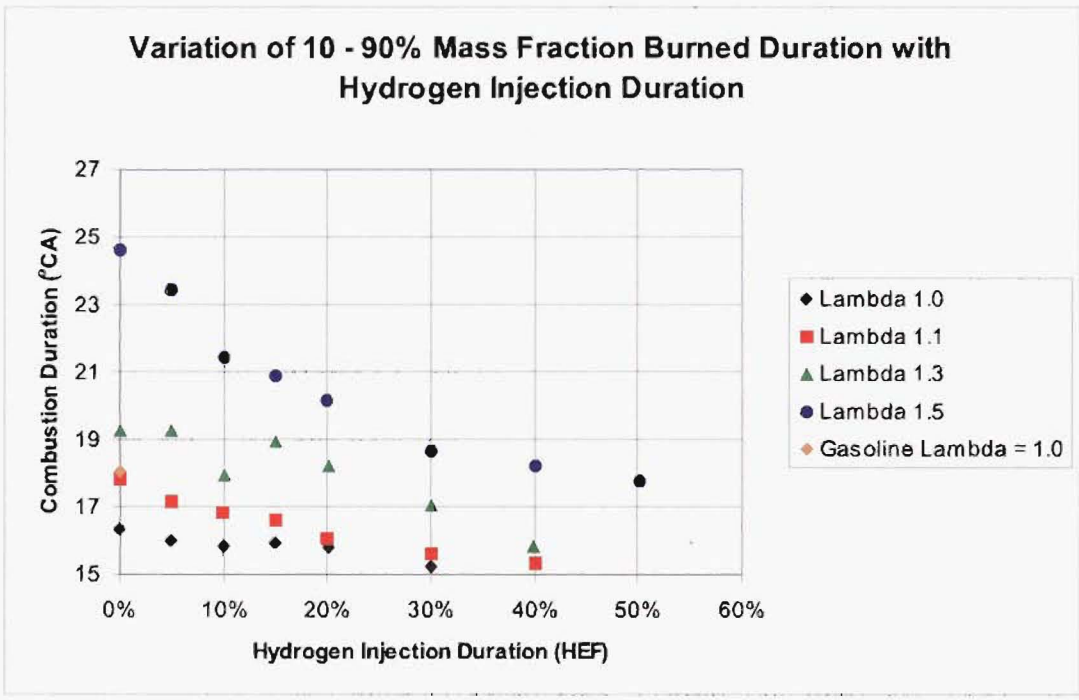

Figure 8.4 Effect of Hydrogen Supplementation on 10-90% mfb

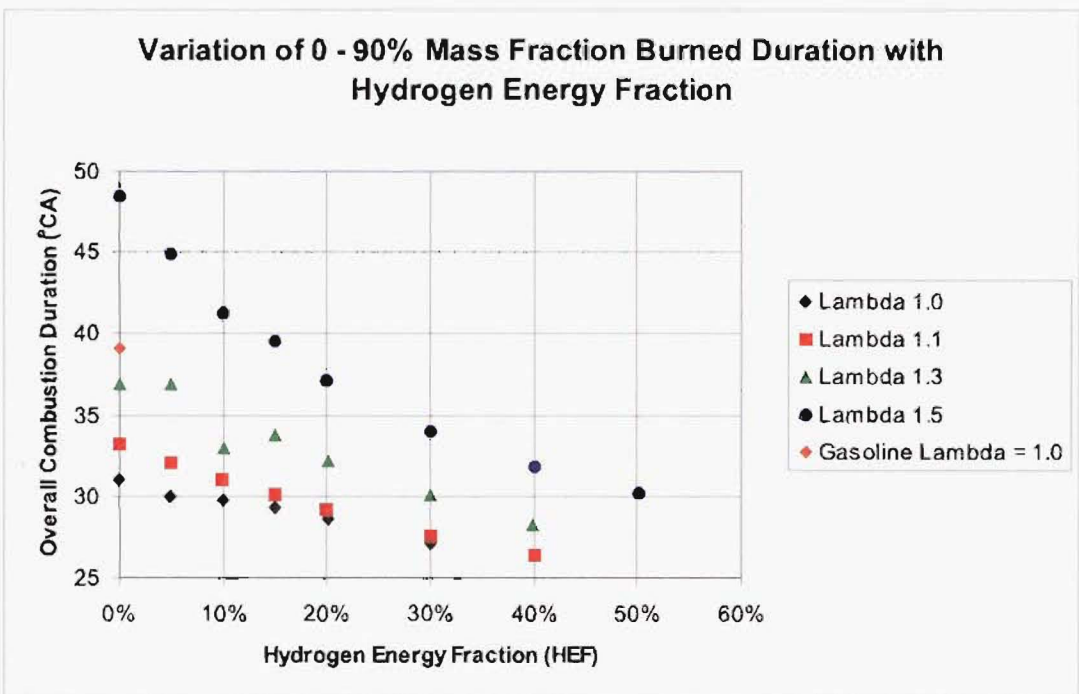

Figure 8.5 Effect of Hydrogen Supplementation on 0-90% mfb

combustion is thought to be due to the substantially higher laminar flame speed of hydrogen (265 - 325 cm/sec) compared to that of methanol (44 - 46 cm/sec) [Rauckis and McLean 1979] , [Sher and Hacohen 1987]. Lu *et al.* [1994] investigated the effect of intermediate species left in the combustion chamber from the previous cycle on autoignition in a 4-stroke, spark ignition, hydrogen fuelled engine. They found that the addition of HO_2, OH and H_2O_2 all reduced the ignition delay period in an engine. However HO_2 and OH were found to be unstable at low temperatures and would therefore be unlikely to exist in the chamber at the start of a new cycle leaving H_2O_2 as the likely cause of the observed reduction in ignition delay. Swain *et al.* [1990] and co-workers investigated the emission levels of H_2O_2 from a hydrogen fuelled engine. They found that H_2O_2 is only formed in significant concentrations in mixtures near the lean flammability limit and concluded that H_2O_2 is a product of incomplete combustion. Over the majority of test points that will be covered in this investigation the production of H_2O_2 will be negligible and therefore have no influence on the ignition delay duration. The observed increase in combustion rate with increasing HEF could also be attributed to the turbulence induced in the inlet manifold as hydrogen is injected into the inlet air. There would be no disruption to the flow of the inlet air at 0% HEF. As the HEF is increased to 50%, the disruption to the inlet air increases in a corresponding manner. It is however thought that the effect of the manifold injection of hydrogen on the level of turbulence in the engine during combustion will be negligible for the following reasons. Firstly the hydrogen is introduced continuously into the manifold over the full 720 ^oCA of the engine cycle at relatively low velocity through a 4 mm diameter pipe. Secondly the hydrogen is only induced into the cylinder during the 224 ^oCA that the inlet valve is open along with the inlet air. Thirdly it is known that rapidly converging flow causes the velocity to become more uniform over a cross-section i.e. turbulence is reduced [Massey 1989]. For the Ricardo E6 the ratio of minimum valve throat area to inlet manifold area is ≈ 0.55. This will significantly reduce the level of any turbulence present in the inlet manifold [Huntsman 2000]. Fourthly the majority of turbulence in the cylinder immediately after the inlet valve closes is due to the induction process itself past the inlet valve. The effect of turbulence induced by manifold injection of hydrogen on the combustion process is therefore thought to be minimal and the observed increases in combustion rate are due to the higher flame speed of hydrogen.

For comparison, the 0-90% mfb duration for gasoline (CR = 8:1, $\lambda = 1.0$) is also plotted with the 0-90% mfb duration data. It is apparent that methanol combustion at CR = 10:1 is much faster than that of gasoline. Combustion durations are however known to reduce with an increase in compression ratio [Ferguson 1986]. Figures 8.2 to 8.5 suggest that the combustion process for $\lambda = 1.3$ and 10% HEF was burning at a faster rate than would be expected given the trends of the data points either side. It is expected that the cause of a faster burn rate is a slightly richer air/fuel mixture than the test points

either side. This is in fact the case. The value of λ is 1.30 for 10% HEF and 1.31 for the data points either side. This difference however is very small and it seems unlikely that a difference of this magnitude would have had such a pronounced effect on the burn rate. The air/fuel ratio may well have been richer than this but is not reflected in the fuel flow readings recorded at the time. This seems a likely scenario with the corresponding values of $IMEP_g$ and CO_2 (see Figures 8.13 and 8.26 respectively) being slightly higher than expected and the value of O_2 slightly lower than expected (see Figure 8.29).

Looking at Figures 8.2 to 8.5, it is difficult to discern whether hydrogen addition has had a more pronounced effect on any one particular phase of the combustion process. A clearer way of presenting the mass fraction burned data is to normalize values with respect to the zero hydrogen addition case [Apostolescu and Chirac 1996]. Presenting the data in this manner allows the percentage change in combustion duration for each combustion phase to be plotted for a particular air/fuel ratio. Thus the relative effect of supplementation on each of the phases of combustion can be compared.

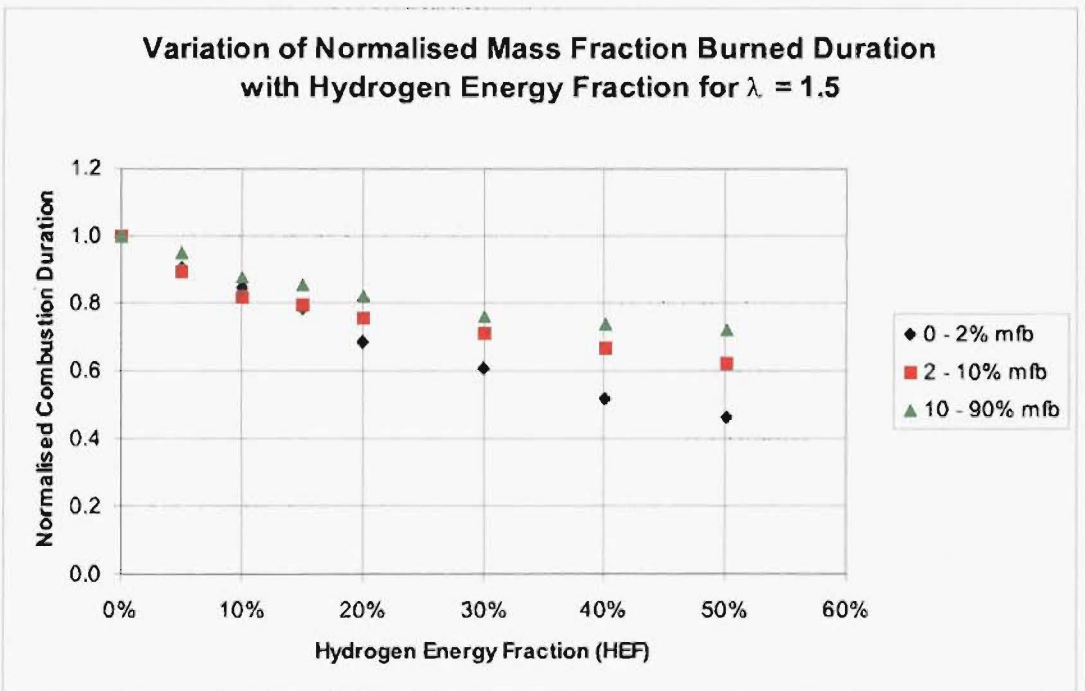

Figure 8.6 Effect of Hydrogen Supplementation on Different Combustion Phases

Figure 8.6 shows how normalized combustion duration varies with HEF at λ =1.5. This result is typical for any air/fuel ratio. It is readily apparent that although hydrogen supplementation reduces the combustion duration in all phases of combustion, hydrogen supplementation has a far more pronounced effect on the 0-2% mfb phase. This finding is in agreement with the findings of Rauckis and McLean [1979] who also found a

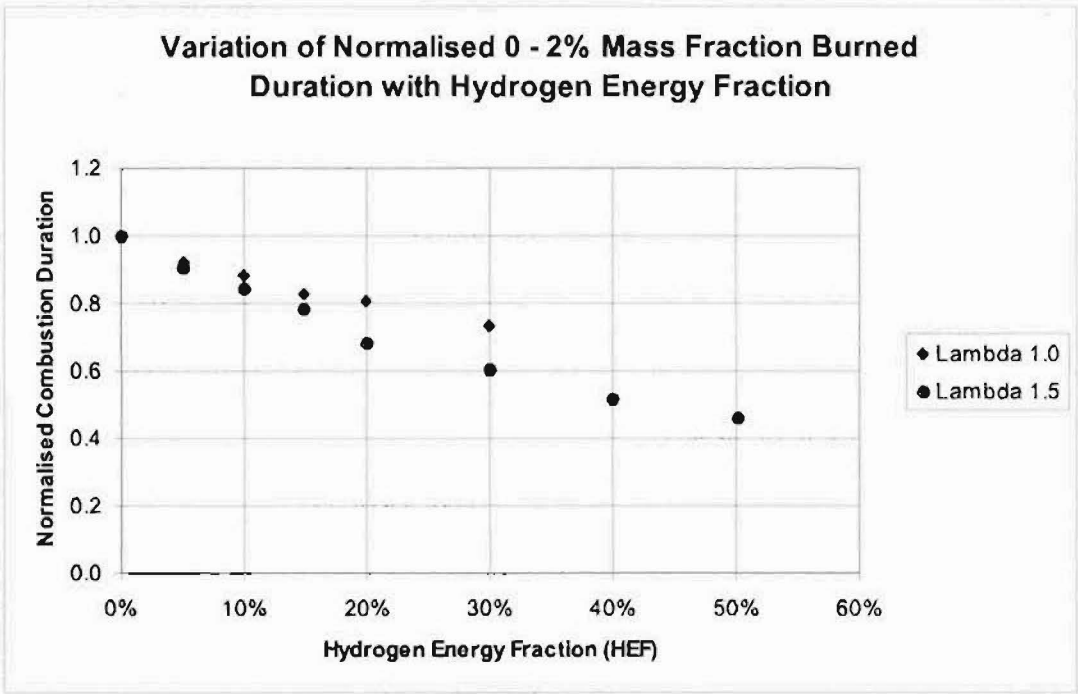

Figure 8.7 Effect of Hydrogen Supplementation on Normalized 0-2% mfb

more pronounced effect on the 0-2% mfb phase. The ignition delay duration portion of the overall flame burn duration (represented by the 0-2% mfb duration) is thought to be largely dominated by the laminar flame speed of the burning mixture [Rauckis and McLean 1979] , [Heywood 1988]. Once established the flame kernel develops into a turbulent flame, the propagation rate of which is dominated primarily by large scale turbulent transport effects and to a much lesser extent the laminar flame speed of the mixture. The results of more recent modelling of hydrogen enriched combustion processes suggests that while the "eddy burning" model is able to accurately predict overall combustion durations, it underestimated the pronounced effect of hydrogen addition on the ignition delay duration [Sher and Hacohen 1989]. A possible explanation given is that the "eddy burning" model does not take into consideration the rapid dissociation of hydrogen into active radicals especially near the spark plug.

The concept of hydrogen dissociating into active radicals which have a substantial impact on the initial stages of combustion is investigated as part of the investigation into hydrogen supplementation via direct injection in Chapter 9.

Figure 8.7 shows the variation of normalized 0-2% mfb with HEF for two different values of λ. This result is typical for any phase of combustion. It can be concluded that hydrogen supplementation has a greater effect on the 0-2% mfb in leaner mixtures than it does in richer mixtures. This result is also in agreement with the findings of Rauckis

and McLean [1979] who concluded that the rapid chain branching ignition process of hydrogen stimulates the otherwise slow thermal ignition processes of the hydrocarbon fuel.

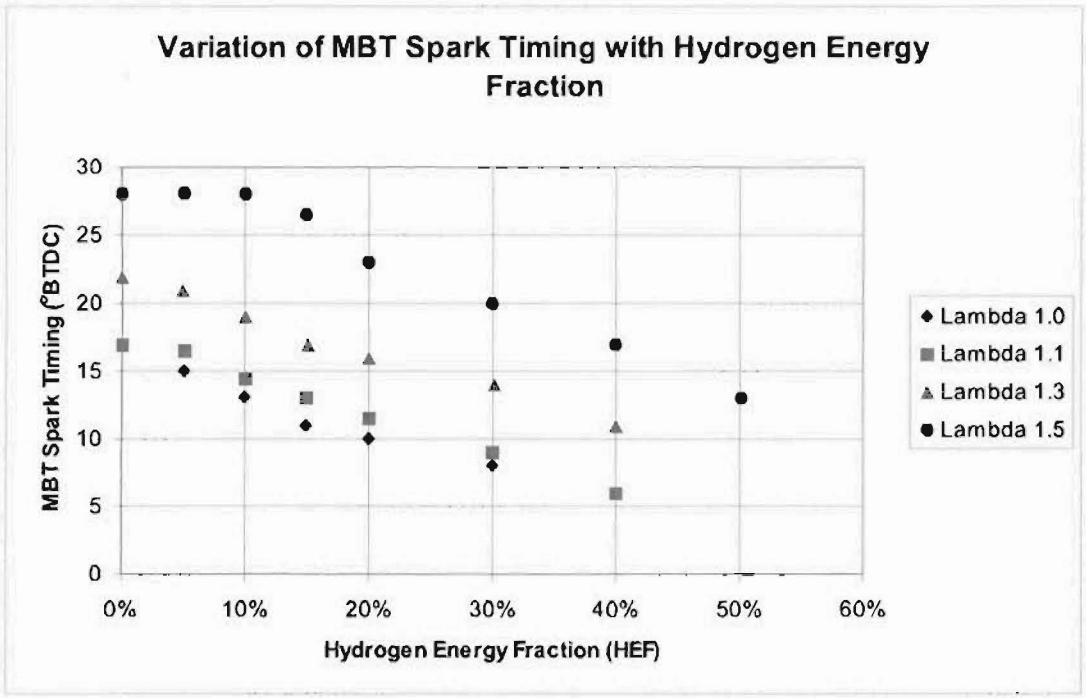

Figure 8.8 MBT Spark Timing verses Hydrogen Energy Fraction

An increase in the overall rate of combustion will require the spark timing to be retarded in order to maintain the MBT condition. This is in fact what was found to occur. Figure 8.8 shows the variation in MBT spark timing with HEF for various air/fuel ratios and reflects the reduction in combustion duration that is evident in Figures 8.2 to 8.5. The MBT spark timing becomes further retarded as the air fuel ratio becomes richer for any value of hydrogen supplementation. For each air/fuel ratio, MBT spark timing is progressively retarded with increasing hydrogen supplementation, probably due to the increased rate of combustion. One feature of Figure 8.8 is that the MBT spark timings for $\lambda = 1.5$ with 0, 5 and 10% HEF are identical. The reason for this is that at $\lambda = 1.5$, the torque curve is very flat and MBT spark timing is very difficult to determine accurately. When performing the engine testing at $\lambda = 1.5$, detecting changes in MBT spark timing between 0, 5 and 10% HEF was not possible and the timing was left unchanged.

It is possible that the more retarded MBT spark timings that occur due to the increase in combustion rate result in the spark occurring at a more favorable position from the point of view of flame kernel initiation and growth. The mixture is at a higher pressure (and therefore density and temperature) at the point where the spark occurs. Swain

et al. [1993] noted in their study of hydrogen supplemented natural gas that flame initiation became a problem at lean air/fuel ratios with advanced spark timings (as evidenced by large cycle to cycle variations in the onset of pressure rise). They noted that further advancing the spark timing did not help and concluded that further spark advance resulted in attempting to ignite a less compressed (cooler, less dense) mixture, probably increasing flame ignition problems.

The faster observed combustion rates and resultant retarded spark timings will have an impact on the magnitude and location of peak cylinder pressures. Figure 8.9 shows the variation of peak cylinder pressure with HEF while Figure 8.10 shows the variation of peak pressure location with HEF for a range of values of λ. The 0% and 5% HEF values for $\lambda = 1.5$ are suspect as the corresponding values of MBT spark timing are the same in both cases (see Figure 8.8). Ignoring the suspect data, the value of peak cylinder pressure decreases in an approximately linear fashion with increasing HEF for all values of λ. It would be expected that peak cylinder pressures would decrease as the total energy input is decreased and peak cylinder position is retarded with increasing HEF. An interesting feature is that for HEF's of >20%, the values of peak cylinder pressure are approximately the same value for all values of λ.

It is apparent from Figure 8.10 that the trends in peak cylinder pressure for each value of λ are a mirror image of the trends in peak cylinder pressure position as observed in Figure 8.9. Again ignoring the suspect values noted in the previous paragraph, the position of peak cylinder pressure moves further after TDC in an approximately linear fashion with increasing HEF (and decreased combustion durations) in order to maintain the MBT condition. It can also be seen that the position of peak cylinder pressure occurs closer to TDC as λ increases (mixture becomes weaker) for a particular value of HEF. As the combustion duration lengthens as the mixture becomes leaner, the location of peak cylinder pressure moves closer to TDC in order to maintain the MBT operating condition.

8.5 Engine Power Output

Now that the gross effects of hydrogen on the various phases of combustion have been identified, the effect of untimed manifold hydrogen supplementation on the power output of the engine will be investigated. The effect of HEF on the volumetric efficiency of the engine and the energy of the charge induced into the engine is presented in Figures 8.11 and 8.12.

From Figure 8.11 the following trends are apparent. Firstly the volumetric efficiency decreases as the HEF increases for all air/fuel ratios. This thought to be due to

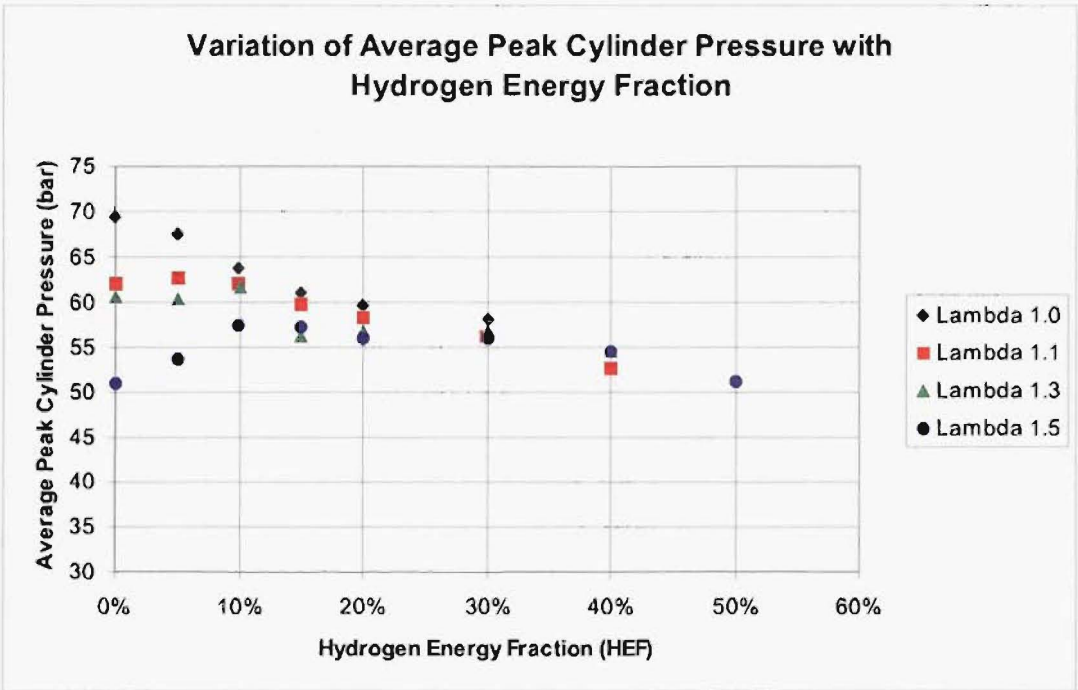

Figure 8.9 Effect of Hydrogen Supplementation on Peak Cylinder Pressure

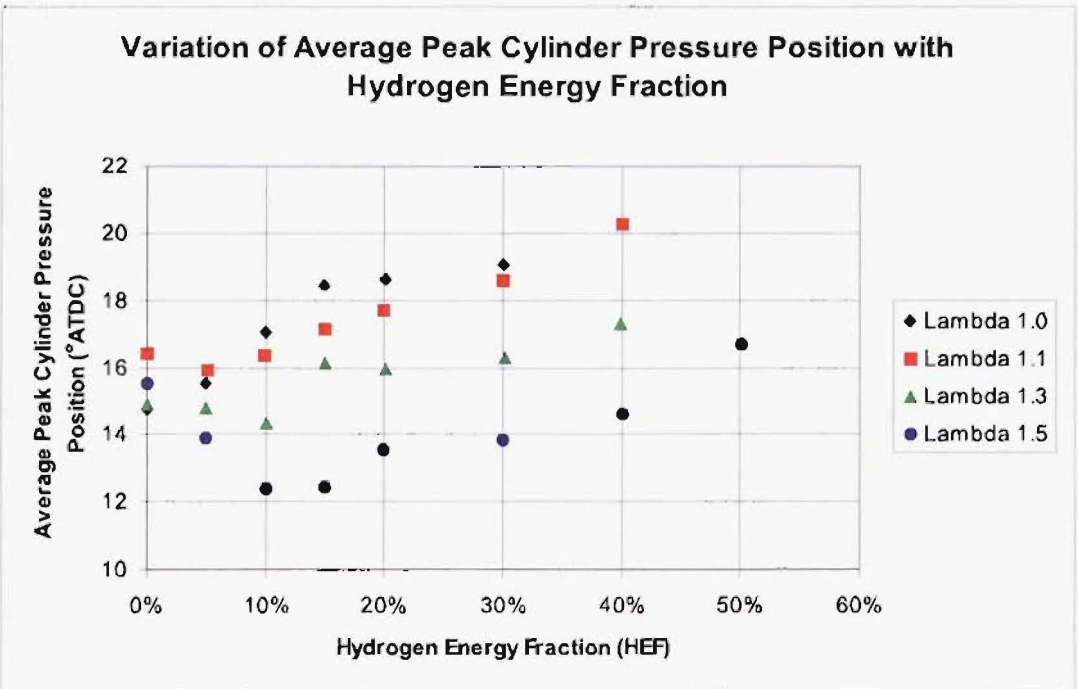

Figure 8.10 Effect of Hydrogen Supplementation on Peak Cylinder Pressure Position

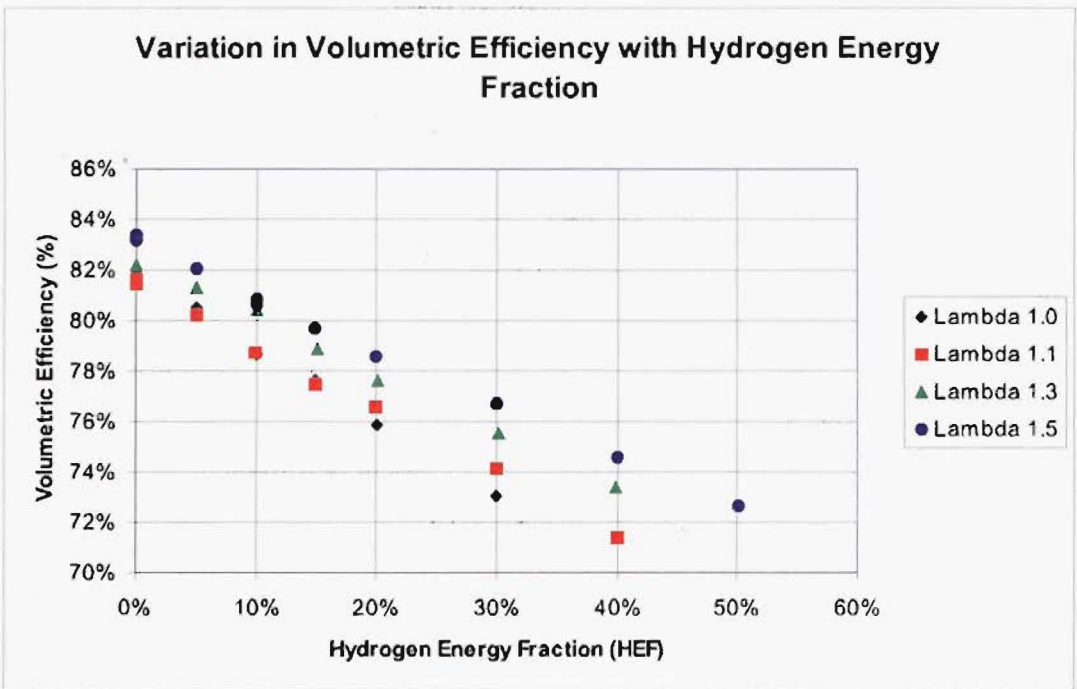

Figure 8.11 Volumetric Efficiency verses Hydrogen Energy Fraction

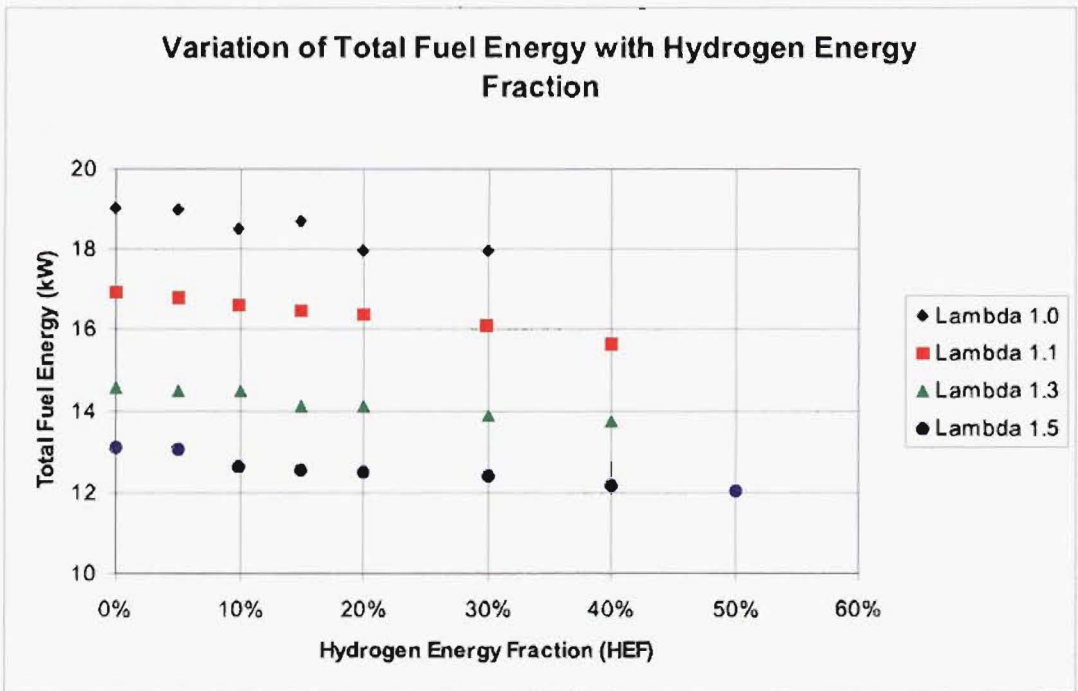

Figure 8.12 Total Fuel Energy verses Hydrogen Energy Fraction

the manifold induced hydrogen displacing inlet air that would have, in the absence of hydrogen supplementation, been induced into the engine. Thus increasing the rate of hydrogen supplementation increases the displacement of inlet air and correspondingly reduces the volumetric efficiency. The second trend is that the volumetric efficiency for leaner mixtures is always greater than that for richer mixtures. It has been shown that both methanol vapor and hydrogen gas have a significant detrimental effect on the volumetric efficiency of an engine [Heywood 1988]. This effect becomes increasingly pronounced as the air/fuel mixture becomes richer. The reduction in volumetric efficiency with increasing HEF will be shown to be responsible for a reduction in engine power output with increasing HEF. The volumetric efficiency and power losses associated with hydrogen supplementation via untimed manifold injection will be overcome by injecting the supplementary hydrogen directly into the combustion chamber (see Chapter 9).

Figure 8.12 shows the effect of increasing HEF on the total fuel energy. The total fuel energy is greatest for richer air/fuel ratios and decreases as the air/fuel ratio becomes leaner, as would be expected. The total fuel energy decreases as the HEF increases for all air fuel ratios. This trend can be explained as follows. As the HEF increases, the volumetric efficiency of the engine decreases. Thus in order to maintain a particular overall air-fuel ratio, the total energy content of the fuel mixture must therefore decrease.

Figures 8.13 to 8.15 show how varying the HEF affects three different measures of engine power output, IMEP_g, corrected brake power and brake mean effective pressure.

The same trends in engine output power are evident in all three of the figures. IMEP_g has been identified as the most appropriate measure of engine output power (see page 75). The plots of corrected brake power and brake mean effective pressure are therefore presented at this point for completeness only. As they convey essentially the same information as the plot of IMEP_g, plots of corrected brake power and brake mean effective pressure will not be presented again. As expected, the highest values of IMEP_g occur with the richest mixtures and decrease as the mixture becomes leaner. Increasing levels of hydrogen supplementation result in a decrease in IMEP_g for any air/fuel ratio. The trends demonstrated in Figures 8.13 to 8.15 can be explained as follows. Firstly increasing the amount of hydrogen being introduced through the inlet manifold results in inlet air being displaced. Thus the volumetric efficiency of the engine is adversely affected (see Figure 8.11). This effect has also been observed by Houseman and Voecks [1980] in their work with hydrogen enrichment. The reduction in volumetric efficiency causes a reduction in the total charge energy that can be induced while maintaining a particular air/fuel ratio (see Figure 8.12) and so the engine output power is adversely affected. As will be seen in the next chapter, this loss of power can be overcome through the use of early direct injection of hydrogen into the combustion chamber.

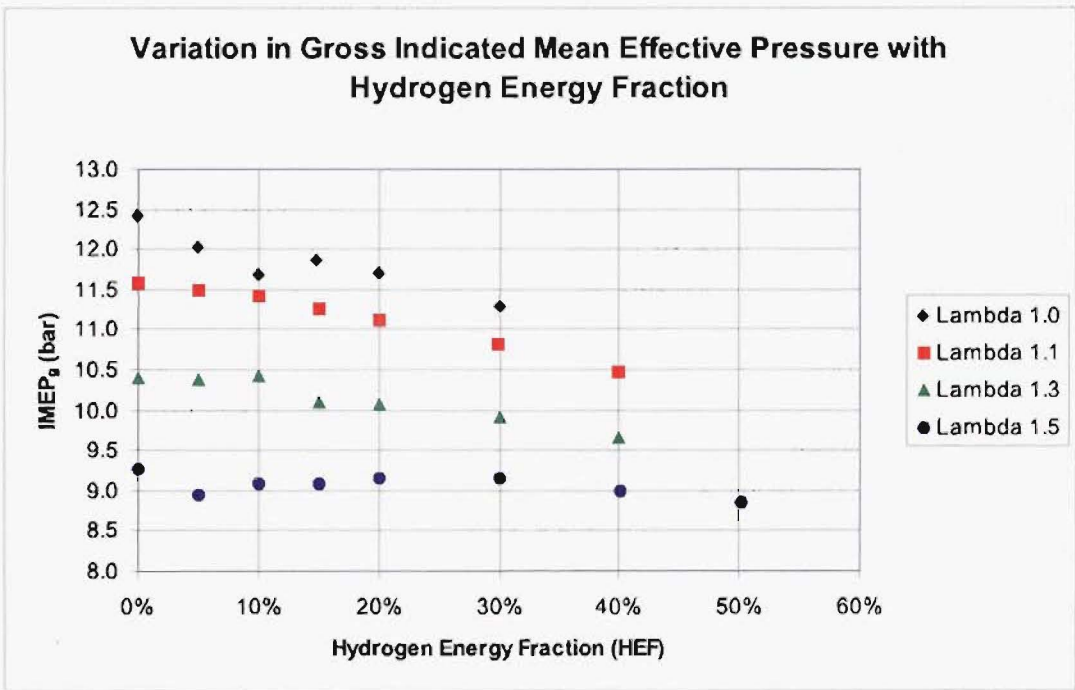

Figure 8.13 Effect of Hydrogen Supplementation on Gross Indicated Mean Effective Pressure

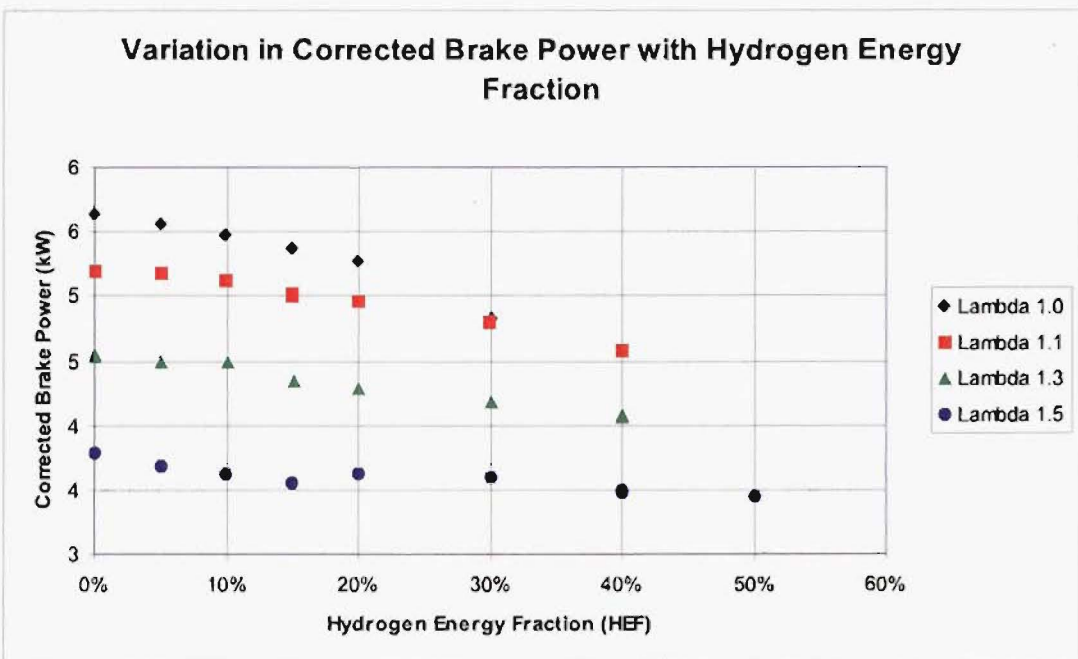

Figure 8.14 Corrected Brake Power verses Hydrogen Energy Fraction

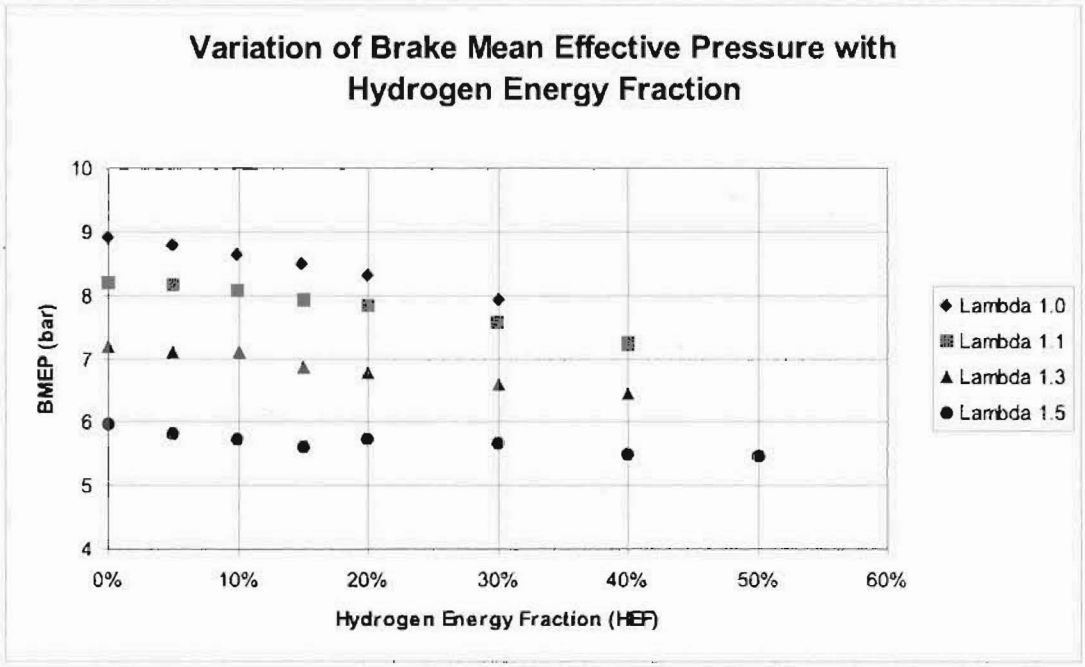

Figure 8.15 Brake Mean Effective Pressure verses Hydrogen Energy Fraction

The value of the co-efficient of variation of IMEP$_g$ (COV$_{IMEPg}$) is often used as a gauge of the cycle-by-cycle variability of combustion in an engine (see page 81). Figure 8.16 shows the variation in COV$_{IMEPg}$ with HEF. It can be seen that the cyclic variability increases as the air/fuel mixture becomes leaner. This is a well reported trend [Young 1981] , [Ozdor *et al.* 1994] and results from a large number of both physical and chemical factors. The slower flame propagation rates that occur with lean air/fuel ratios are thought to be a major contributing factor. As the HEF is increased for all air/fuel ratios, the value of COV$_{IMEPg}$ decreases with leaner mixtures being affected to a far greater extent than richer mixtures. Rauckis and McLean [1979] also reported this finding in their work. It is also clear that the addition of a small amount of hydrogen to a lean mixture has a significant effect on the COV$_{IMEPg}$. Increasing the level of hydrogen supplementation leads to diminishing returns as far as the beneficial effects on COV$_{IMEPg}$ in lean mixtures is concerned.

The mechanism by which hydrogen supplementation reduces COV$_{IMEPg}$ is not so clear. It is well recognized that cycle-by-cycle variability is at a minimum with MBT spark timing and rich air/fuel mixtures [Young 1981]. During the earlier discussion on the influence of hydrogen supplementation on MBT spark timing (see page 122), it was proposed that the conditions at the point of spark are more favorable for flame initiation when using more retarded spark timings. The most likely reason for the reduction in

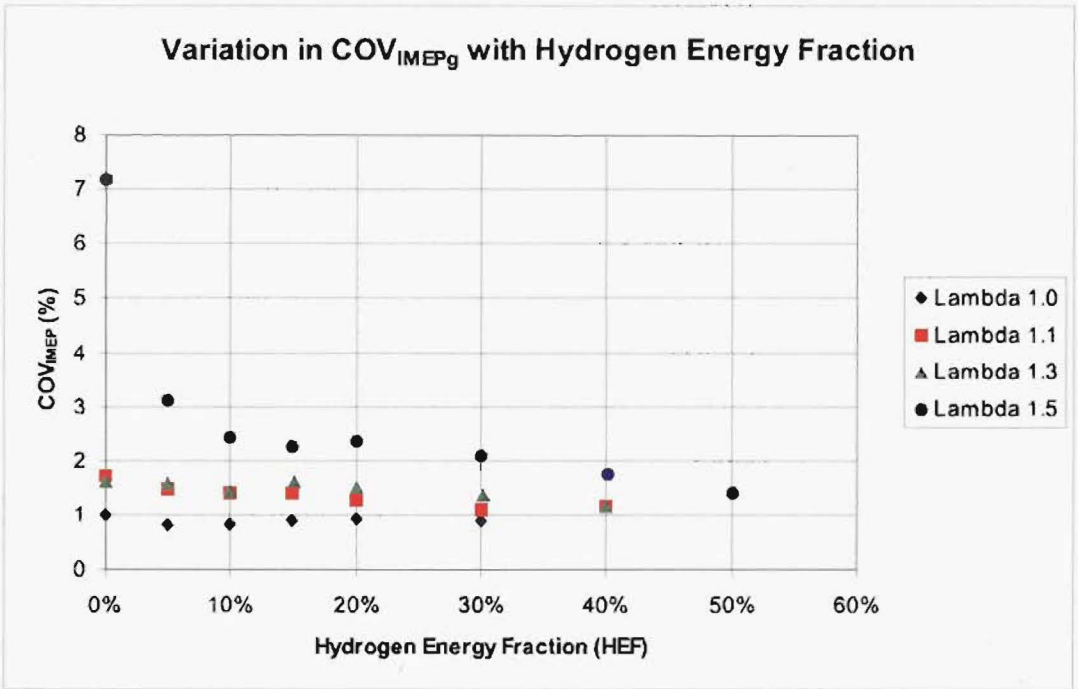

Figure 8.16 Effect of Hydrogen Supplementation on the Coefficient of Variation of Gross Indicated Mean Effective Pressure

COV_{IMEPg} however is due to the increase in combustion rate with increasing HEF. It is known that the magnitude of the variations in the rate of combustion are decreased as the burning rate is increased [Heywood 1988]. As a consequence, the effect of variations in the rate of combustion on engine torque are reduced.

A value of 10% COV_{IMEPg} has been suggested as being an acceptable limit for driveability in a vehicle [Matekunas 1983] , [Atkinson *et al.* 1995]. As can be seen from Figure 8.16 that even at $\lambda = 1.5$ and 0% HEF, the COV_{IMEPg} is less that this value. This indicates the potential for operating the engine unthrottled at much leaner air/fuel ratios than has currently been demonstrated, especially with what seems to be significant improvements in COV_{IMEPg} in lean air/fuel mixtures with hydrogen supplementation.

8.6 Engine Thermal Efficiency

The thermal efficiency of an internal combustion engine increases as the air/fuel ratio increases (becomes leaner) reaching a theoretical maximum at an infinitely lean air/fuel ratio [Germane *et al.* 1983]. The theoretical expression for the thermal efficiency of the air-standard Otto cycle previously stated in Section 8.3 (Equation 8.1) is given again here to facilitate the ease of discussion.

$$\eta_{th} = 1 - \frac{1}{r_c{}^{\gamma-1}} \tag{8.4}$$

Increasing the compression ratio (r_c) of the engine and the value of γ both lead to increases in the theoretical thermal efficiency of the engine. As was demonstrated on page 114, increasing the HEF at any air/fuel ratio leads to an increase in the value of γ thus increasing the theoretical efficiency. The compression ratio of the Ricardo E6 was also increased from 8:1 to 10:1 to take advantage of the higher octane rating of methanol compared with gasoline thus further increasing the theoretical efficiency.

The actual engine thermal efficiency that can be achieved is lower than the theoretical thermal efficiency due to the deviation of the actual combustion process from the theoretical Otto cycle.

Actual engine thermal efficiency can be increased by the use of lean air/fuel mixtures due to the beneficial effects of improved thermodynamic properties and the resultant lower combustion temperatures of the air/fuel mixture as listed below:

1. Increase in specific heat ratio using lean mixtures
2. Reduced dissociation losses
3. Reduced heat transfer with the combustion chamber walls

Actual engine thermal efficiencies can also be improved by reducing the duration of the combustion process. The ideal Otto cycle assumes that combustion occurs at constant volume. The actual combustion process in an engine takes place over a period of many degrees of crank-angle rotation. As leaner air-fuel mixtures are used, the combustion duration increases as the flame speed of lean air/fuel mixtures is slower than that of richer mixtures. Improvements to the rate of combustion at lean air/fuel ratios will therefore result in a closer approximation to the ideal Otto cycle while reducing the so called time losses by reducing the time available for heat transfer to occur.

η_{ith} is used throughout this work because all engine testing was performed at constant speed not constant load. At constant speed, the parasitic engine losses change in proportion to the load changes and are thus not the same for each test point. The gross indicated engine power, P_i (see page 241), is preferred as this is the power applied to the piston as a direct result of the combustion process before any parasitic losses occur. Thus η_{ith} is a more accurate representation of the effects of hydrogen supplementation on the combustion process. η_{ith} is calculated as follows:

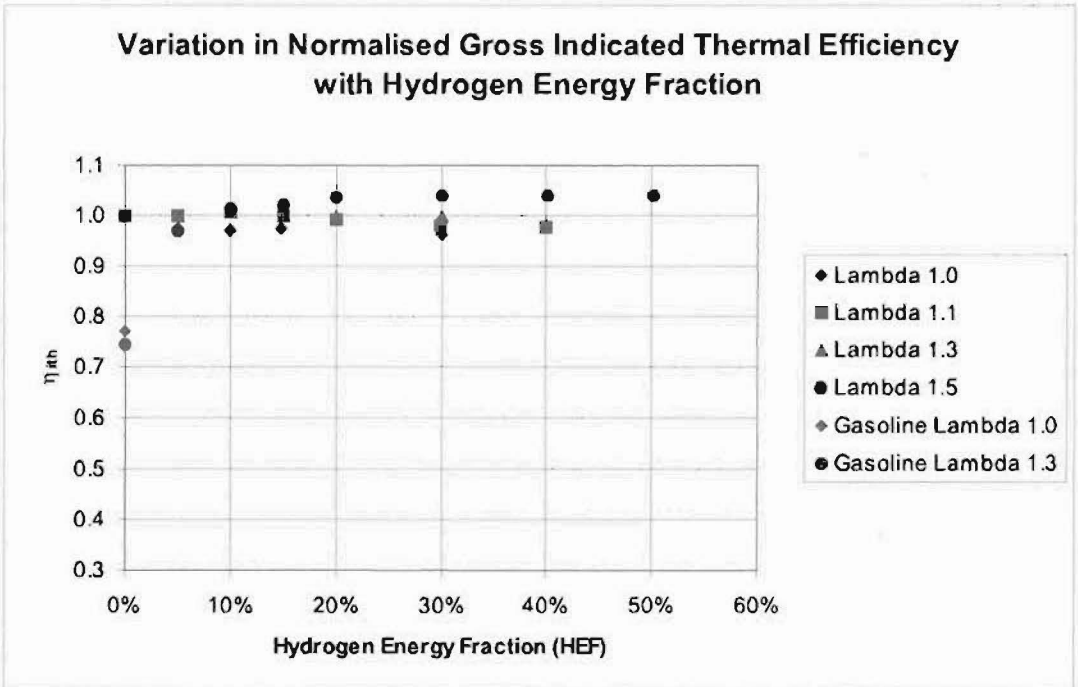

Figure 8.17 Normalized Gross Indicated Thermal Efficiency verses Hydrogen Energy Fraction

$$\eta_{ith} = \frac{P_i\ [kW]}{Total\ Fuel\ Energy\ [kW]} \tag{8.5}$$

Figure 8.17 shows the variation in normalized gross indicated thermal efficiency (η_{ith}) with HEF. Also plotted for comparison are the normalized 91 octane gasoline data points for $\lambda = 1.0$ and 1.3 taken at a compression ratio of 8:1 c.f. 10:1 for the methanol data.

The data in this figure has been normalized with respect to the 0% HEF case for each value of λ. The reason for this is that a systematic error in the acquired combustion pressure data was discovered to have occurred during the untimed manifold injection testing. Thus pressure derived data from this chapter cannot be compared directly with data presented later in the thesis. This error was corrected before any of the early direct injection or comparative testing was undertaken. A fuller description of the pressure data error can be found on page 157. Further untimed manifold injection η_{ith} data is presented on page 189 when comparing the different injection systems.

At the same engine speed, the increased compression ratio (10:1 c.f. 8:1) and the faster combustion characteristics of methanol are evident in the greatly improved gross indicated thermal efficiencies achieved over those obtained with gasoline. This highlights the benefit of using methanol fuel in an engine whose compression ratio has been raised

to take advantage of the increase in octane rating over that of gasoline.

The anticipated gains in thermal efficiency of methanol with hydrogen supplementation due to improved combustion and fluid thermodynamic properties were not apparent. The reasons for this are thought to be as follows. Both the total energy content of the fuel supplied and the power produced by the engine decrease as the HEF is increased (see Figures 8.12 and 8.13). Whether the thermal efficiency increases or decreases depends on which quantity is decreasing faster, P_i or Q_{HV}. Any inaccuracies in the measurement or calculation of either of these quantities will lead to variation in the calculated result. The changes in the value of the indicated efficiency with HEF for each value of λ is relatively small ($< 3\%$) with the trends unclear except in the case of $\lambda = 1.5$ which appears to show an increase in indicated efficiency with increasing HEF reaching a maximum at approximately HEF = 30%.

As indicated specific fuel consumption (isfc) is the numerical reciprocal of indicated thermal efficiency, there will be no discussion of isfc.

8.7 Engine Emissions

Minimizing the level of exhaust emissions from an engine is becoming increasingly important with rising concerns about the detrimental impact automobile emissions are having on the environment. As the supplementation of methanol with hydrogen via untimed manifold injection has been shown to result in a decrease in engine power output, the most relevant way of presenting engine emission data is as specific emissions. The measure of power used in calculating specific emissions is $IMEP_g$. Details on the calculation of specific emissions can be found in Appendix F on page 243.

The discussion on the emissions from the engine will begin with the exhaust gas temperature. Figure 8.18 shows the variation of exhaust gas temperature with HEF. Exhaust gas temperatures at 0% HEF are highest for $\lambda = 1.0$ and decrease as the mixture becomes leaner. This is expected as exhaust gas temperatures are known to decrease as the mixture is richened and leaned on either side of stoichiometric [Heywood 1988]. There is not much variation between the exhaust gas temperatures for $\lambda = 1.0$ and $\lambda = 1.1$. All air/fuel ratios exhibit a slight increase in exhaust gas temperature with increasing HEF although the increase for the $\lambda = 1.0$ case is not as pronounced as that of the leaner air/fuel ratios.

The increase in the rate of combustion would result in there being less time available for heat transfer to occur from the burnt combustion gases to the cylinder walls i.e. a reduction in the so called time losses. This would be expected to lead to an increase in

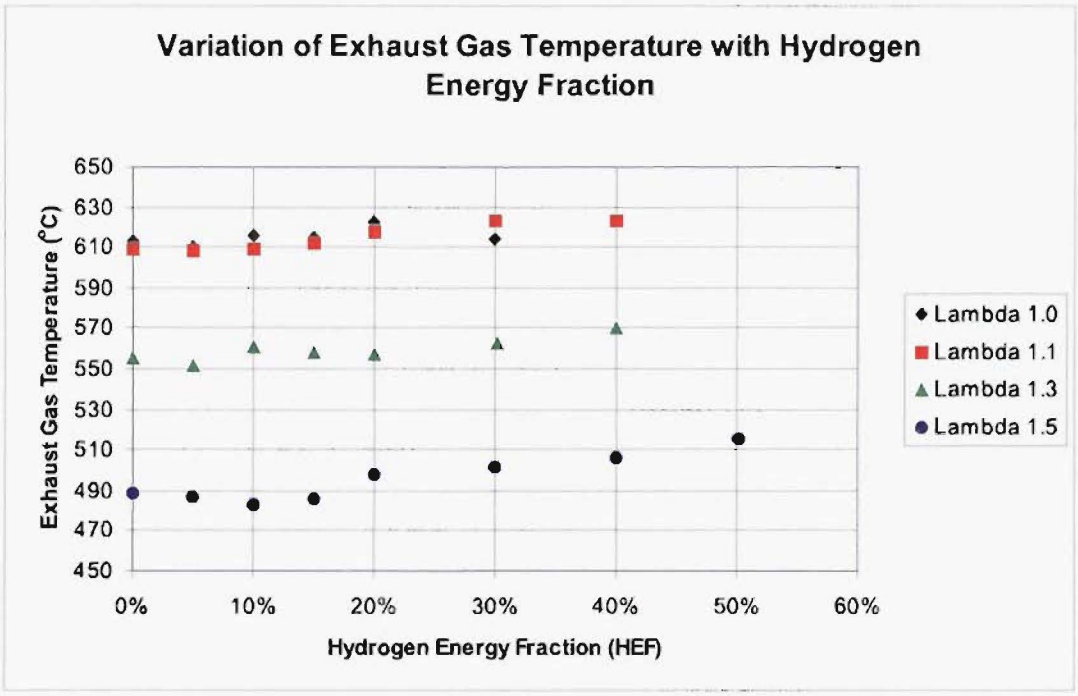

Figure 8.18 Effect of Hydrogen Energy Fraction on Exhaust Gas Temperature

the exhaust gas temperature.

Retarding the spark timing is known to increase the exhaust gas temperature along with increases in load and engine speed [Heywood 1988]. As the engine speed remained constant during these tests, the effect of changes in engine speed can be ignored. As has been observed, the engine load decreases as the HEF increases therefore this would be expected to lead to a reduction in the exhaust gas temperature. Conversely as the HEF is increased, the spark timing has to be retarded due to the increased rate of combustion and this would be expected to result in an increase in the exhaust gas temperature.

To summarize therefore, several factors have been identified as having an effect on the exhaust gas temperature. They are:

1. Increase in rate of combustion resulting in less time for heat transfer.
2. Decrease in load on the engine as a result of deteriorating volumetric efficiency.
3. Retarding of the ignition timing due to increase in rate of combustion.

The observed trends in exhaust gas temperatures can not be attributed to any one of the factors listed above but is more than likely a result of a combination of them.

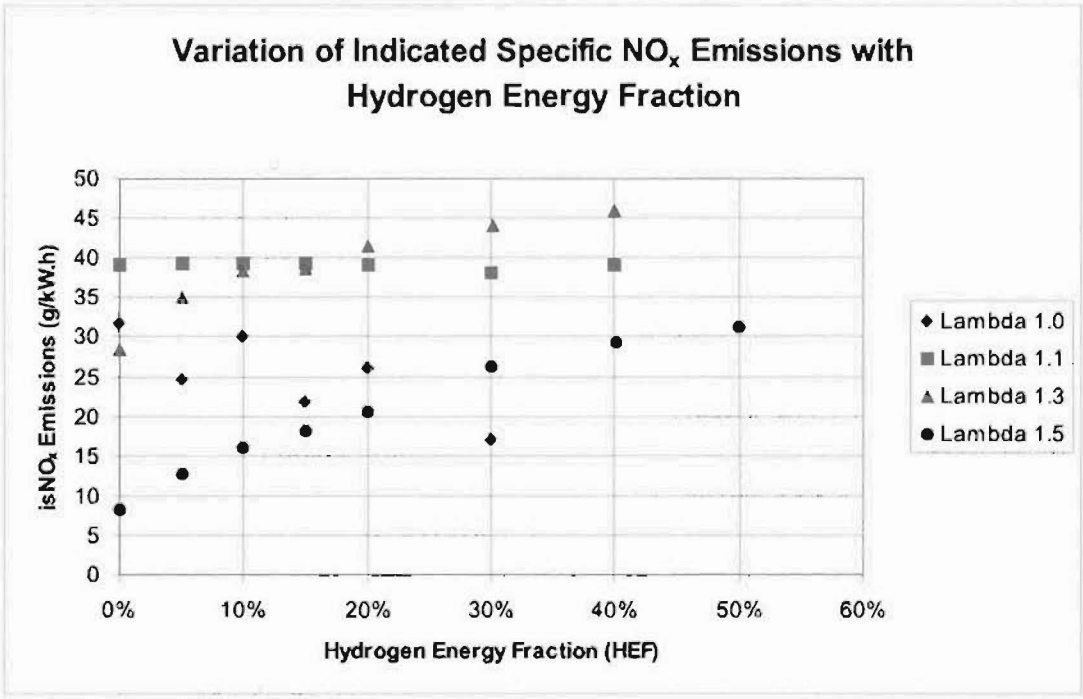

Figure 8.19 Indicated Specific NO_x Emissions verses Hydrogen Energy Fraction

The variation in indicated specific isNO_x emissions with HEF is shown in Figure 8.19 for various air/fuel ratios. There are several interesting features in Figure 8.19. Firstly the NO_x emissions for leaner mixtures (i.e. $\lambda = 1.3$ and $\lambda = 1.5$) increase significantly with increasing HEF . The curve for $\lambda = 1.1$ shows no appreciable change in NO_x emissions with HEF. The curve for $\lambda = 1.0$ displays a trend opposite to all the leaner air/fuel ratios; as the HEF increases the level of NO_x emissions decrease. The NO_x emissions recorded for $\lambda = 1.0$ also display considerable variability as the HEF is increased in contrast to the NO_x measurements obtained for the leaner mixtures. This variation is also apparent in the corresponding plot of isCO emissions in Figure 8.25. As will be discussed with the engine CO emissions (see page 140), the cause of these variations are thought to be small changes in the air-fuel ratio of the mixture. Near stoichiometric conditions, both NO_x and CO emissions are sensitive to small changes in air-fuel ratio. Slightly richer mixtures result in higher levels of CO and lower levels of NO_x. In order to facilitate a discussion on the causes of the observed trends, a brief summary of NO_x formation mechanisms will now be presented.

The principle reactions governing the formation of NO from molecular nitrogen are known as the extended Zeldovich mechanism [Heywood 1988]. The principle reactions are as follows:

$$O + N_2 \rightleftharpoons NO + N \tag{8.6}$$

$$N + O_2 \rightleftharpoons NO + O \tag{8.7}$$

$$N + OH \rightleftharpoons NO + H \tag{8.8}$$

The reaction rates for formation of NO by these mechanisms are strongly temperature dependent. Equations 8.6 to 8.8 also highlight the necessity of having oxygen present in the burnt combustion gases to allow the formation of NO. The formation of NO when operating rich of stoichiometric is consequently low. It has also been demonstrated that the formation of NO proceeds much slower than the initial combustion reactions that convert the air/fuel mixture into combustion products [Newhall and Shahed 1971]. The formation of NO is thus dependent on the time that the burnt gases spend at elevated temperatures before piston motion and the ensuing expansion process results in a cooling of the gases (usually termed the residence time). To summarize, the factors which affect the formation of NO are therefore:

1. Temperature
2. Oxygen availability
3. Residence time

NO is the predominant oxide of nitrogen formed in an engine as a result of the combustion process [Flagan and Seinfeld 1988] , [Heywood 1988]. It is formed in both the flame reaction zone (prompt-NO) and in the burned gases (thermal-NO). The flame reaction zone is very thin so residence times are short. The amount of prompt-NO formed is therefore small and can be neglected except when dealing with lean, slow burning mixtures [Heywood 1988]. The vast majority of the NO is thermal-NO formed in the burned gases [Flagan and Seinfeld 1988] , [Heywood 1988]. The burnt gases formed early in the combustion process are compressed to much higher pressures (and therefore temperatures) than those formed later in the combustion process. Therefore during the combustion process, there exists in the combustion chamber a temperature gradient between the first and last portions of the charge to be burnt with the first portion to burn having the highest temperature. The magnitude of this temperature gradient can be several hundred degrees Celsius [Lewis and Von Elbe 1987]. Therefore the earlier burning fractions of the charge contribute much more to NO formation than do the later burning fractions of the charge. Variables that affect NO formation in an engine are:

- Air/fuel ratio. Maximum burned gas temperatures occur at $\lambda \approx 0.9$ (rich). Oxygen concentrations are however low. As the mixture is leaned out, the increasing oxygen concentration initially offsets the falling gas temperatures and NO emissions peak

at $\lambda \approx 1.1$ (slightly lean) before decreasing as the mixture is leaned out further [Heywood 1988].

- Burned gas fraction. The burned gas fraction of the in-cylinder unburned mixture reduces flame temperatures by increasing the heat capacity of the cylinder charge per unit mass of fuel. While there are always some unburnt gases in the cylinder from the previous cycle, the amount can be increased by recycling exhaust gases into the intake system of the engine (known as exhaust gas recirculation or EGR) as a means of controlling NO_x emissions [Heywood 1988].

- Spark timing has a considerable effect on NO emissions. Advancing the timing so combustion occurs earlier in the cycle increases the peak cylinder pressure (and burned gas temperatures) therefore increasing the formation rate of NO. Retarding the spark timing reduces peak cylinder pressures (and burned gas temperatures) therefore decreasing the formation rate of NO. NO emissions steadily decrease as the spark timing is retarded from MBT timing and moved closer to TDC. Since the exact determination of MBT spark timing is difficult, there is often considerable uncertainty in NO emissions at MBT timing.

The amount of oxygen present in the exhaust gas has been found to decrease as HEF increases for all overall air/fuel ratios (see Figure 8.29 on page 147). The increase in NO_x emissions for the leaner mixtures must therefore be due to changes in the bulk temperature as the HEF is increased. An increase in exhaust gas temperature with increasing HEF has been observed for lean overall air/fuel ratios indicating higher in-cylinder gas temperatures (see Figure 8.18). Thus for leaner overall air/fuel ratios, the increase in NO_x formation rate due to higher in-cylinder gas temperatures would appear to offset the decrease in NO_x formation rate due to the reduced availability of oxygen. For the case of $\lambda = 1.0$, the decrease in NO_x formation rate due to the reduced availability of oxygen appears to be dominating the increase in NO_x formation rate due to higher in-cylinder gas temperatures. The end result is a decrease in NO_x emissions with increasing HEF.

Figure 8.20 shows the variation in isUHC emissions with HEF for various air/fuel ratios as measured via the NDIR analyzer. It is apparent that for a particular air/fuel ratio, as the HEF is increased, the level of isUHC emissions decreases. This is expected because as the amount of hydrogen energy substitution is increased, the amount of methanol (and thus C atoms) induced is correspondingly reduced. There is no clear trend however as to what happens as the air/fuel ratio is varied. It would be expected that UHC emissions be highest for richer air/fuel ratios and reduce as the mixture becomes leaner. These results possibly reflect the inadequacy of using the Horiba gas analyzer in engine research especially when comparing test runs from day to day.

In order to better quantify the trends in UHC emission levels as the overall air/fuel ratio is varied, a flame ionization detector (FID) was used to provide clearer trends (see page 104). The UHC emission readings derived from the FID are presented in Figure 8.21 along with the NDIR results from the same test points. The value for $\lambda = 1.1$ NDIR, 0% HEF looks to be too low compared with the rest of the $\lambda = 1.1$ NDIR results and should be actually very close to the $\lambda = 1.1$ FID, 0% HEF case. The second point of interest from Figure 8.21 is that for HEF = 0%, the values of UHC obtained for each detection method are similar (exact in the case of $\lambda = 1.5$). As HEF increases however, the FID UHC emissions levels decrease at a far greater rate than do the NDIR UHC emission levels. The testing was conducted starting with the 0% HEF case and finishing with the 50% HEF points. This indicates that even with a nitrogen flushing system for use between emission readings, there is still an error in results obtained with the Horiba analyzer resulting in UHC emissions levels that are overestimated. These results highlight the inadequacy of using the Horiba exhaust gas analyzer for accurate UHC exhaust gas emissions measurement. As far as can be determined from the results obtained, the measurement of emissions of CO and CO_2 are not affected in the same manner as the measurement of UHC emissions over time.

Figure 8.22 shows the variation in isUHC emissions as measured by the FID with HEF for two values of λ. The 0% HEF for $\lambda = 1.5$ gives the highest value of isUHC. This is in part due to the reduced power output at this test point. Also as was observed for isUHC emissions measured by NDIR, isUHC emissions levels decrease with increasing HEF for both overall air/fuel ratios. The rate at which the isUHC emission levels decrease with increasing HEF however differs between the two overall air/fuel ratios. The $\lambda = 1.1$ curve exhibits an almost linear decrease in isUHC emissions with increasing HEF. The $\lambda = 1.5$ curve however exhibits large decreases in the level of isUHC emissions with the addition of hydrogen initially but further hydrogen addition produces increasingly smaller reductions in isUHC emissions. In addition, between 0 and 20% HEF there is a $\approx 24\%$ reduction in the mass flow-rate of methanol. Over the same range however the isUHC emissions reduce by $\approx 43\%$ for $\lambda = 1.1$ and by $\approx 76\%$ for $\lambda = 1.5$! Clearly there is an additional mechanism or mechanisms involved in the reduction of isUHC emissions as the reduction of methanol flow-rate does not account for all of the observed decrease.

There are many mechanisms by which fuel can escape burning and contribute to UHC emissions. These mechanisms are listed below [Heywood 1997].

1. Air/fuel mixture compressed into the combustion chamber crevice volumes.

2. Fuel absorbed in oil layers on the cylinder liner.

3. Fuel absorbed by, and/or contained within, deposits on the cylinder head and piston

crown.

4. Quench layers on the combustion chamber wall left as the flame extinguishes close to the walls.

5. Air/fuel mixture left unburned when the flame extinguishes prior to reaching the walls.

6. Liquid fuel within the cylinder that does not evaporate and mix with sufficient air to burn prior to the end of combustion.

7. Leakage of unburned mixture through the (nominally) closed exhaust valve.

Of these mechanisms, the most significant is the effect of crevice volumes. Examples of crevice volumes (and relative contribution to UHC emissions) in an engine are [Heywood 1988]:

1. Piston ring and pack crevice (80%).

2. Cylinder head gasket crevice (13%).

3. Spark plug thread crevice (5%).

4. Valve seat crevice and any other crevices (2%).

The amount of unburnt air/fuel mixture that is compressed into the crevice volume of an engine is dependent on the magnitude of the peak cylinder pressure that occurs during the engine cycle. The density of the unburned air/fuel mixture ahead of the flame front is approximately 4 times that of the burned mixture therefore a significant amount of unburnt fuel can be compressed into the crevice volumes. As the cylinder pressure falls during the expansion stroke, the unburned mixture compressed in the crevice volumes expands into the cylinder. A significant fraction of the unburnt mixture is oxidized in the cylinder or the exhaust port and thus does not contribute to the measured engine emissions. All the unburned mixture that is compressed into crevice volumes and does not oxidize during the main combustion duration represents a loss in efficiency of the engine.

Figure 8.23 shows the variation of peak cylinder pressure with HEF for the UHC data measured with the FID. Figure 8.23 shows similar trends as the peak cylinder pressure data previously presented in Figure 8.9 on page 124 and can be explained in the same manner. It can be seen from Figure 8.23 that for HEF's $< 10\%$ it would be expected that the contribution to UHC emission levels from crevice volume effects are being underestimated, more so for $\lambda = 1.5$, due to the lower than expected peak cylinder pressures. For HEF's greater than 10%, the peak cylinder pressure decreases with increasing HEF

and the cylinder pressures for both values of λ are approximately the same. It would therefore be expected that the mechanism of crevice volume UHC emissions would have a greater effect on $\lambda = 1.1$ due to the greater mass of methanol contained within the cylinder. The reduction in peak cylinder pressures between HEF = 15% and 40% is only 8% where as the UHC emissions reduced by 66% for both $\lambda = 1.1$ and 1.5! Bell *et al.* [1996] found in their investigation into the use of alcohol fuels that advancing the ignition timing resulted in increased combustion pressures and UHC emissions. They suggested that the observed increase in UHC emissions was due to increased amounts of fuel being forced into the crevice volumes. It can be concluded that UHC emissions arising from the crevice volume mechanism will be contributing to the overall reduction in UHC emissions but it appears not to be the dominating mechanism.

The fourth mechanism listed on page 137 is that of UHC emission formation due to quenching on the combustion chamber wall. As the flame approaches the relatively cool combustion chamber wall it is quenched leaving a layer of unburned mixture near the combustion chamber wall. The quench distance is inversely proportional to the laminar flame speed [Heywood 1988]. Therefore an increase in flame speed such has been observed with hydrogen supplementation would be expected to lead to a reduction in the quench distance adjacent to the combustion chamber wall. This would result in reduced hydrocarbon emissions. The curve in Figure 8.22 for FID measured UHC emissions at $\lambda = 1.5$ is similar to the curve for the variation of overall burn duration for $\lambda = 1.5$ with increasing HEF in Figure 8.5. Both the 0 - 90% mfb duration and the FID measured UHC emissions initially display large reductions in value with hydrogen supplementation. Additional hydrogen supplementation however provides diminishing benefits. Figure 8.24 shows FID isUHC emissions plotted against 0-90% mfb duration. Both $\lambda = 1.1$ and $\lambda = 1.5$ exhibit a roughly linear relationship between UHC and 0 - 90% mfb. The difference in the slopes of the two plots could be due to differences in the rate of methanol mass flow rate reduction and effects of peak pressure reduction on crevice UHC formation between the two values of λ. Thus it appears that the mechanism of UHC emission formation due to quenching on the combustion chamber wall plays a significant role in UHC emissions from a hydrogen supplemented engine.

A reduction in hydrocarbon emissions would be expected to be accompanied by an small increase in oxygen utilization as the portion of previously unburned hydrocarbons are oxidized in the combustion process. This is in fact what was observed to occur. Figure 8.29 (on page 147) shows a reduction in oxygen emissions as the HEF is increased.

To summarize, the trends observed in UHC emissions are for UHC emissions to decrease as HEF increases. The mechanisms responsible for the decrease in UHC emissions are thought to be:

1. Reduction in mass flow rate of methanol.
2. Decrease in peak cylinder pressures resulting in a reduction in UHC formed in crevice volumes.
3. Increase in flame speed reducing the UHC formed due to quenching of the flame on the combustion chamber walls.

The relative magnitude of each mechanism is unknown but from the data obtained it appears that the reduction in UHC due to wall quenching could be the dominant mechanism.

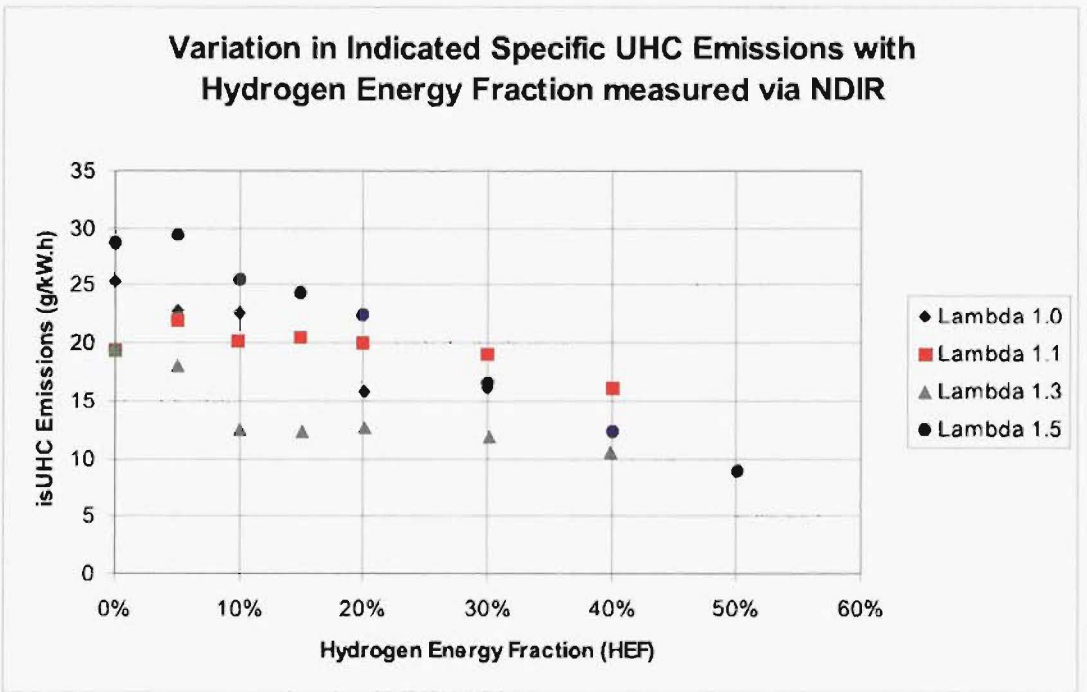

Figure 8.20 NDIR Measured Indicated Specific UHC Emissions verses Hydrogen Energy Fraction

The variation of indicated specific CO emissions with increasing HEF is presented in Figure 8.25. Figure 8.25 displays the same trends in CO emissions as a plot of vol % CO emissions which has been omitted for brevity. The engine CO emission levels increase as the air/fuel ratio becomes richer with the most significant CO emissions occurring at the stoichiometric air/fuel ratio ($\lambda = 1.0$). There are large variations evident in the level of CO emissions for $\lambda = 1.0$ as the HEF is increased. These variations are due to slight variations in the air/fuel ratio that occurred during the test run. The formation of CO is controlled primarily by the air/fuel ratio [Heywood 1988]. At operating conditions of near stoichiometric and with rich air/fuel ratios, the level of CO production varies considerably with changes in air/fuel ratio. The value of λ for the HEF's of 5, 15 and

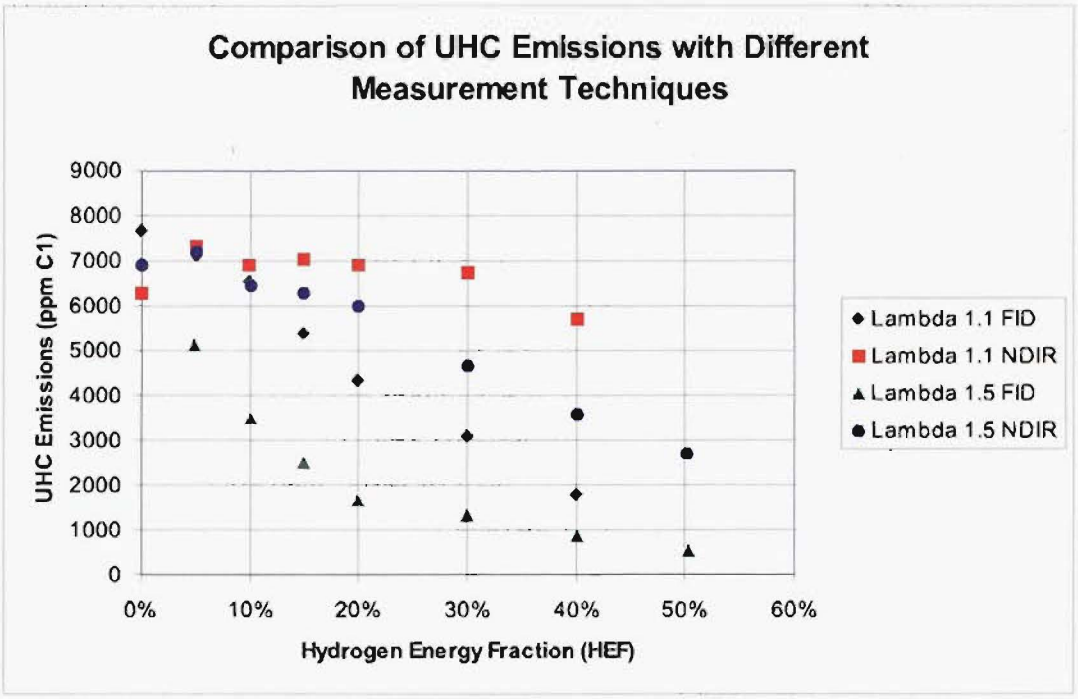

Figure 8.21 Comparison of UHC Emissions with Different Measurement Techniques

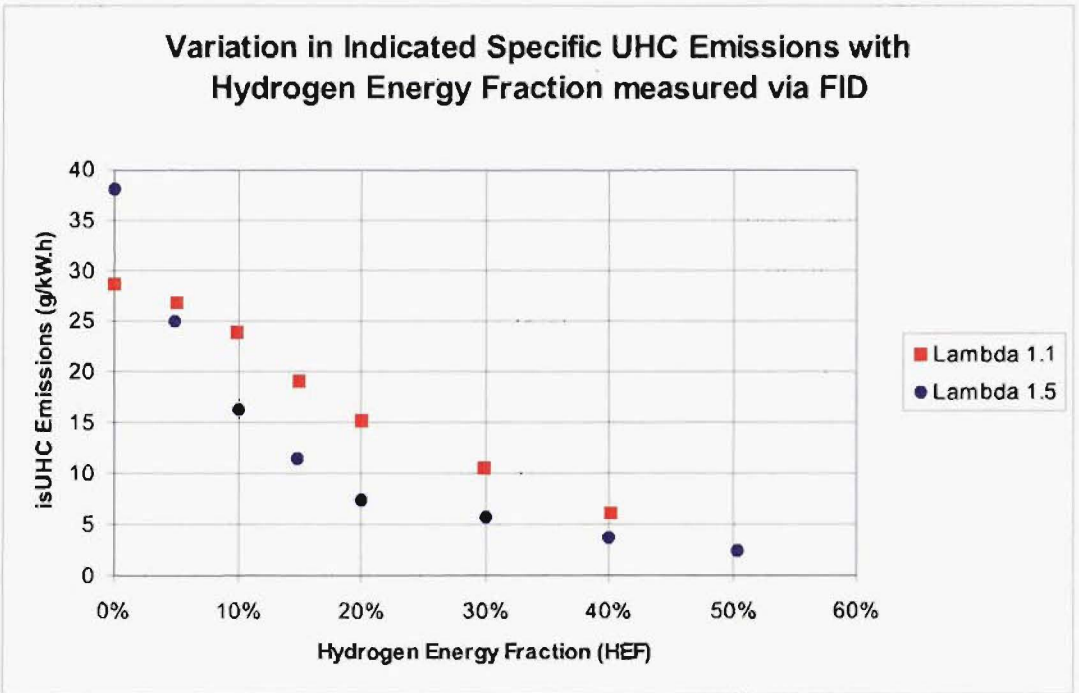

Figure 8.22 FID Measured Indicated Specific UHC Emissions verses Hydrogen Energy Fraction

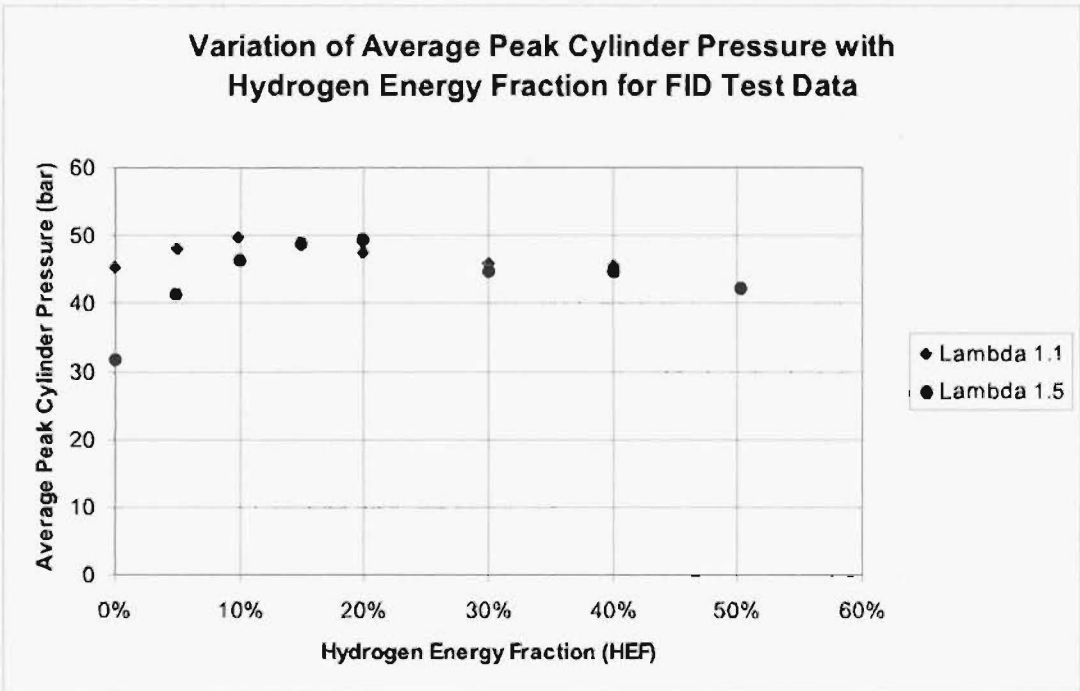

Figure 8.23 Effect of Hydrogen Supplementation on Peak Cylinder Pressure for FID Measured UHC Data

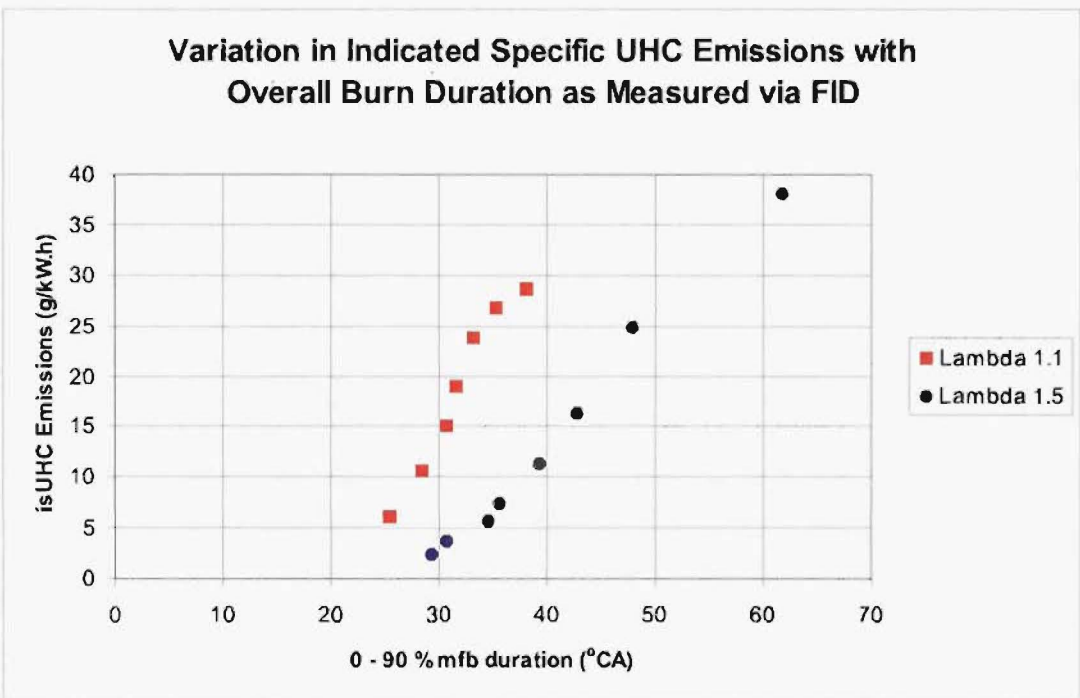

Figure 8.24 FID Measured isUHC Emissions verses 0-90% mfb Duration

30% were 1.0, 0.99 and 0.99 respectively whereas the values of λ for the HEF's of 0, 10 and 20% were 1.01 in all cases. Thus the richer air/fuel ratios resulted in higher levels of CO production. These results highlight the sensitivity of CO production to slight changes in air/fuel ratio with stoichiometric and rich air/fuel ratios. The low CO emission level is to be expected for the leaner air fuel ratios as there is excess oxygen available to ensure that the majority of the CO produced during combustion is oxidized to CO_2. As the CO data for $\lambda = 1.0$ exhibits a large amount of scatter, drawing any conclusions on the trend in emissions with increasing HEF cannot be made with any certainty. In the leaner mixtures ($\lambda = 1.1$, 1.3 and 1.5) there appears to be a slight decrease in CO emissions with increasing HEF. This is thought to be due to a reduction in the amount of methanol (and therefore carbon) present as the HEF is increased. Another possible contributing factor in the observed trend could lie with the water gas reaction [Ferguson 1986] , [Kyaw 1989].

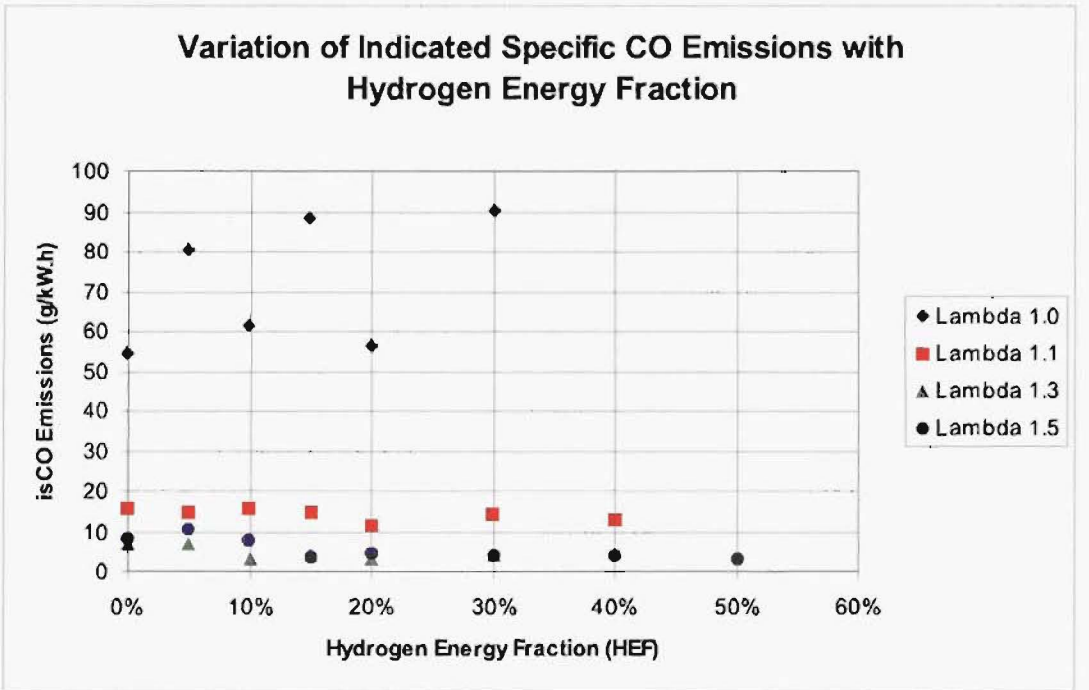

Figure 8.25 Indicated Specific CO Emissions verses Hydrogen Energy Fraction

$$CO + H_2O \quad \rightleftharpoons \quad CO_2 + H_2 \tag{8.9}$$

It was found from the stoichiometric combustion equation for a dual fuel mixture of methanol and hydrogen (see Appendix G on page 250) that for a given value of λ the predicted exhaust gas concentration of water increased with increasing HEF[1] (see page

[1]This was observed to actually occur during engine operation. The water traps in the exhaust gas sampling system required more frequent checking and emptying as the HEF was increased

250). It has been suggested by Kyaw [1989] that the higher concentrations of H_2O in the exhaust gas shifts the reaction in Equation 8.9 to the right favoring the formation of CO_2 and H_2 thereby reducing the level of CO. The trends observed in the data presented here are so slight that a conclusion as to whether this is happening or not cannot be made with certainty.

Figure 8.26 shows clear trends in the variation of CO_2 emissions with HEF for various values of λ. The level of CO_2 emissions are greatest for $\lambda = 1.0$ and decrease as the air/fuel ratio becomes leaner. For all values of λ, the level of CO_2 emissions decrease with increasing HEF. This trend is similar to that exhibited by the UHC emissions and again reflects the reduction in methanol (and thus C atoms) being induced into the engine as the HEF is increased. The level of CO_2 emissions were predicted from the stoichiometric combustion equation for methanol and hydrogen and are plotted in Figure 8.27 against the experimental results. It can be seen that the trends in the experimental data are in good agreement with the trends predicted from the stoichiometric combustion equation. The levels of CO_2 emissions for the experimental data however are greater than those predicted by the stoichiometric combustion equation for all values of λ. The stoichiometric combustion equation would be expected to overestimate the level of CO_2 in the exhaust as it assumes complete oxidation of all the fuel present and therefore does not take into consideration the presence of unburned hydrocarbons or carbon monoxide. It is known that CO and CO_2 concentration measurements via the NDIR technique are susceptible to errors due to the presence of water vapor [Heywood 1988]. Water vapor infrared (IR) absorption overlaps both the CO and CO_2 absorption bands requiring exhaust gas samples to be dried before entering the NDIR analyzer. Thus water vapor in the sample would result in the concentrations of CO and CO_2 being overestimated. The NDIR sample line included a water trap in addition to the built in water trap to ensure that the exhaust sample was dry. In addition, the overestimation of the CO_2 emissions was found not to increase with increasing HEF (and therefore H_2O vapor in the exhaust gas). This indicates that the cause more than likely lies in the calibration of the NDIR analyzer. Figure 8.28 shows the variation in indicated specific CO_2 emissions with HEF for various values of λ. It is apparent that isCO_2 emissions do not show much variation with air/fuel ratio but are reduced significantly as the HEF is increased. Comparing Figures 8.25 and 8.28, it is apparent that the level of isCO_2 emissions are much larger than the emissions of isCO which is to be expected for an engine operating with lean overall air/fuel ratios.

Figure 8.29 shows the variation in the level of O_2 emissions with HEF for various air/fuel ratios. The O_2 emission levels increase as the overall air/fuel ratio becomes leaner as would be expected with plenty of excess air being available for combustion. For a particular air/fuel ratio the level of O_2 emissions decreases as the HEF increases. The

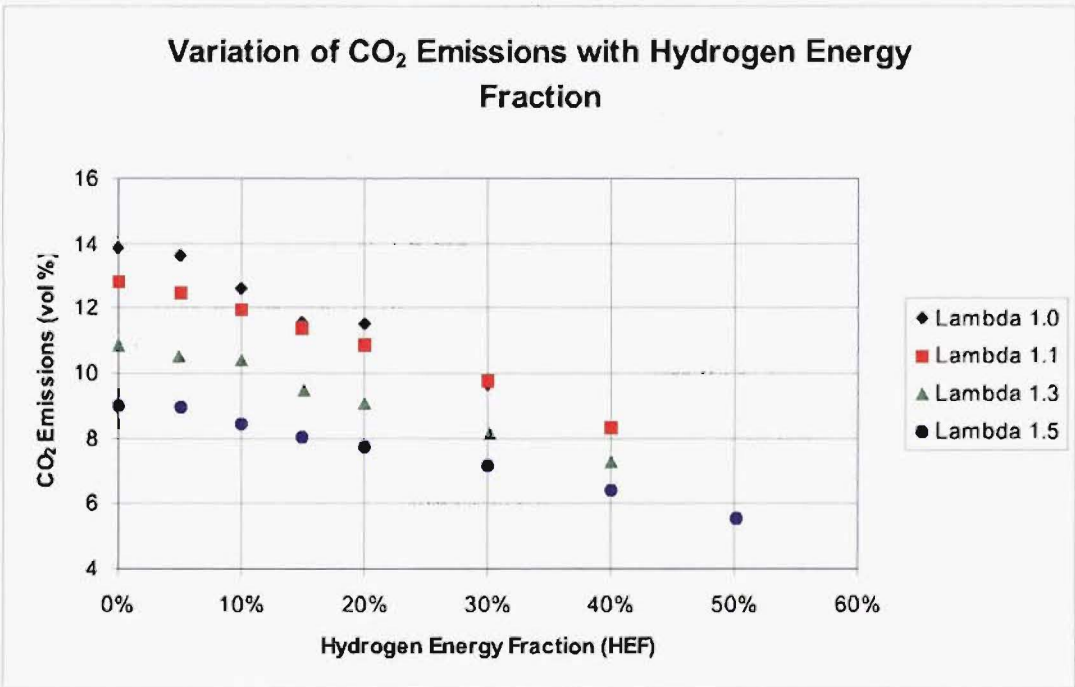

Figure 8.26 CO_2 Emissions verses Hydrogen Energy Fraction

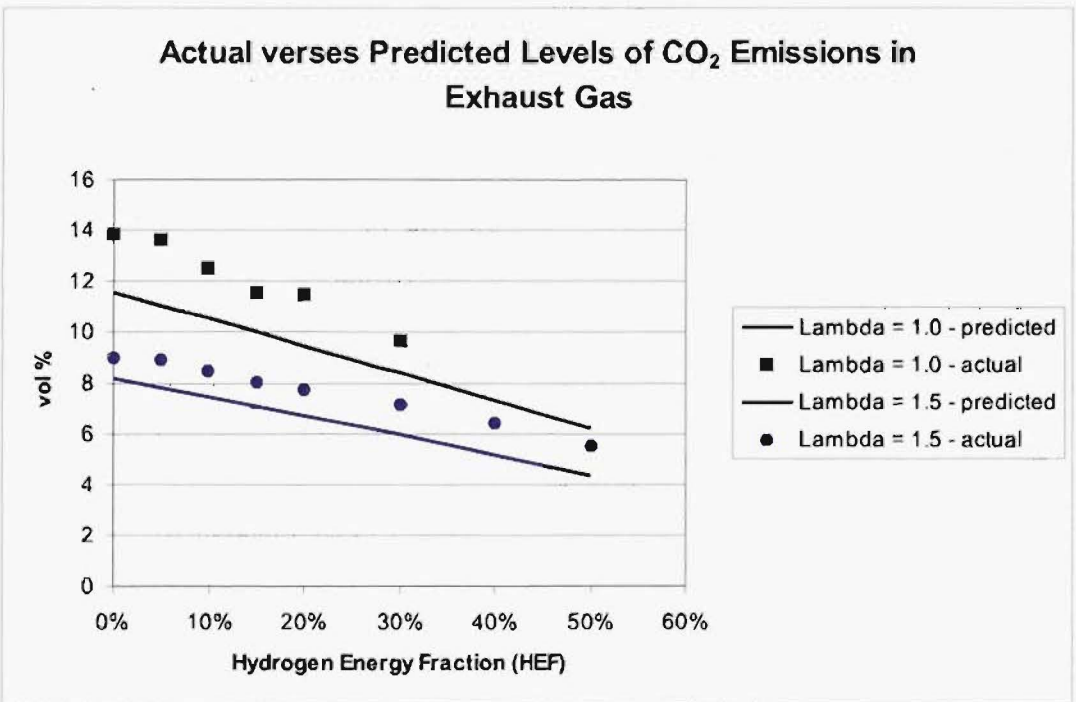

Figure 8.27 Actual verses Predicted Levels of CO_2 Emissions in Exhaust Gas

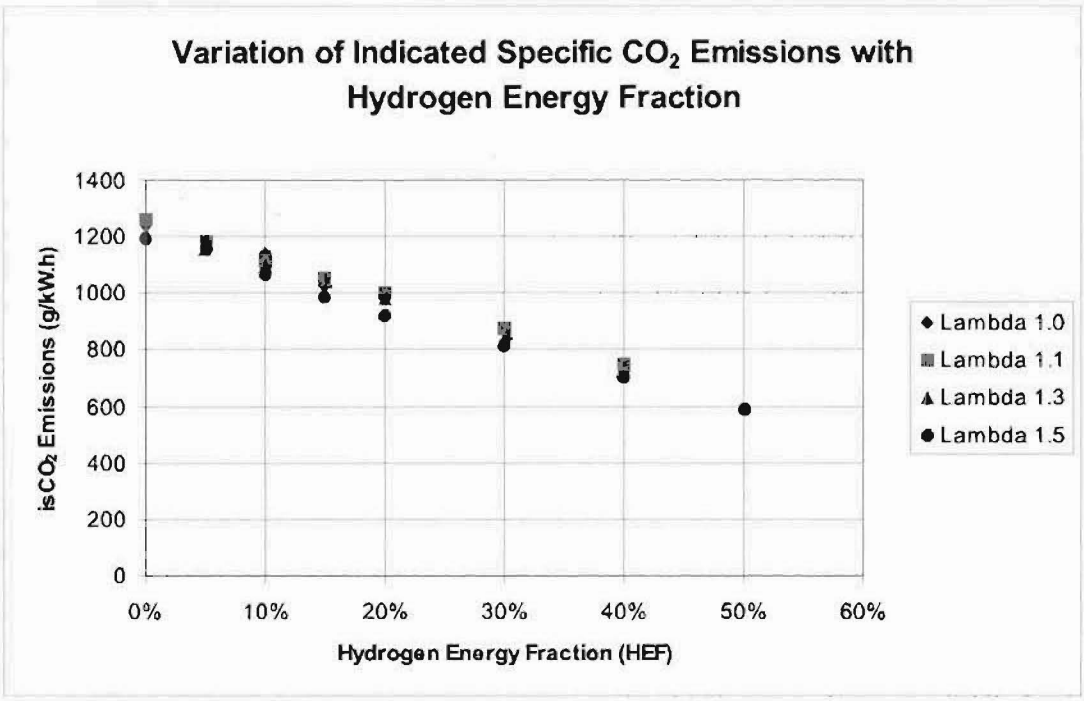

Figure 8.28 Indicated Specific CO_2 Emissions verses Hydrogen Energy Fraction

actual level of O_2 emissions are plotted against the values predicted from the stoichiometric combustion equation (see Appendix G) in Figure 8.30. The actual experimental results follow a similar trend to the predicted O_2 emissions with the leaner air/fuel mixture's exhaust containing more oxygen than that of the richer air/fuel ratios. The predicted emission levels for a particular air/fuel ratio however remain constant with increasing HEF in contrast to the actual experimental results which show a decrease with increasing HEF. This decrease in emissions with increasing HEF could be resulting from a more complete combustion occurring due to the higher flame speed of hydrogen compared to methanol (see page 140). Whether the predicted more complete combustion process is entirely responsible for the increase in oxygen utilization or not is not known but it will be a contributing factor. From Figure 8.30 it is apparent that the predicted values for O_2 emissions compare fairly well for $\lambda = 1.0$. However the stoichiometric combustion equation underestimates the actual experimental values obtained for $\lambda = 1.5$ more than it does with the $\lambda = 1.0$ case. This could be due $\lambda = 1.5$ having a bigger quench distance due to a slower burning mixture resulting in a significant reduction in the extent of completion of the combustion process. This would account for the observed increase in both UHC and O_2 emissions for $\lambda = 1.5$. In general, the stoichiometric combustion equation should underestimate the level of O_2 emissions in the exhaust due to the actual combustion process not oxidizing 100% of the fuel.

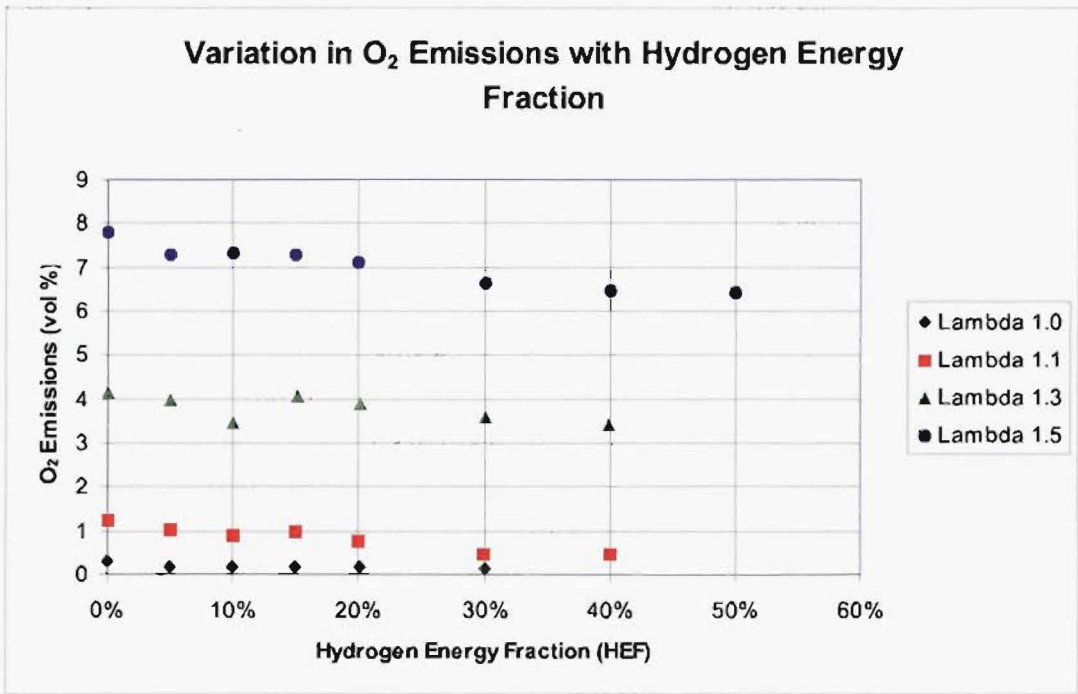

Figure 8.29 O_2 Emissions verses Hydrogen Energy Fraction

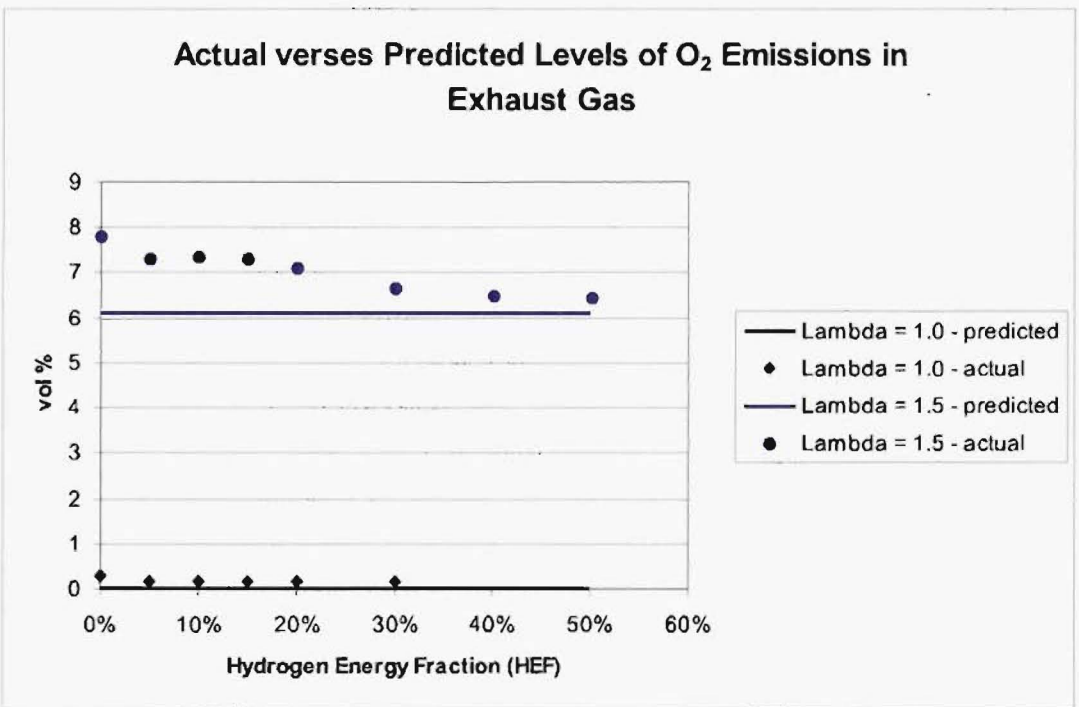

Figure 8.30 Actual verses Predicted Levels of O_2 Emissions in Exhaust Gas

8.8 Summary

The key results of the investigation into the untimed manifold injection of hydrogen can be summarized by the following points.

1. Increasing the HEF resulted in an increase in the rate of combustion for each value of λ investigated. The effect of hydrogen addition was most significant on the 0-2% mass fraction burned duration with leaner mixtures being affected to a greater extent than richer mixtures.

2. The MBT spark timing was retarded at each value of λ as the HEF was increased due to the increased rate of combustion.

3. Increasing the HEF at a particular value of λ results in reduced power outputs due to manifold injected hydrogen displacing inlet air.

4. Increasing the HEF at a particular air/fuel ratio reduces COV IMEP$_g$ with leaner mixtures being affected to a greater extent than richer mixtures.

5. Gross indicated brake thermal efficiency (η_{ith}) is highest with leaner mixtures and shows no clear trends as the HEF is increased.

6. isNO_x emissions were greatest for $\lambda = 1.1$ and decreased as the mixture became richer or leaner. Increasing the HEF lead to decreased emissions for $\lambda = 1.0$ and increased emissions for all leaner mixtures.

7. isUHC emissions are greatest for the richest mixtures and decrease as the mixture becomes leaner. Increasing HEF results in decreased UHC emissions for all values of λ investigated.

8. isCO emissions are only significant for $\lambda = 1.0$ and decrease as the mixture becomes leaner. For all other values of λ, CO emissions decrease as the HEF is increased.

9. isCO_2 emissions are greatest for $\lambda = 1.0$ and decrease as the mixture becomes leaner. Increasing HEF results in reduced CO_2 emissions for all values of λ investigated.

10. O_2 emissions are greatest for $\lambda = 1.5$ and decrease as the mixture becomes leaner. Increasing HEF results in reduced O_2 emissions for all values of λ investigated.

The untimed manifold injection of hydrogen resulted in the expected benefits on the combustion process with an increase in combustion rate and reduced cyclic variability. The engine performance characteristics are dominated however by the reduction in volumetric efficiency resulting from the injection of hydrogen into the inlet manifold. This resulted in reduced engine power outputs as the level of hydrogen supplementation was increased. There was no clear trend in thermal efficiency with an increase in HEF

as values remained fairly constant. All engine emissions except for NO_x were reduced as the level of hydrogen supplementation increased. One interesting result was that in leaner mixtures, the addition of smaller quantities of hydrogen appeared to result in large improvements in cyclic variability and UHC emissions. This indicates that the greatest potential benefits of hydrogen supplementation appear to lie in operating the engine with lean mixtures, i.e. at part load. In addition to this, hydrogen supplementation by reducing cyclic variability would allow the lean operating limit of the engine to be extended, further improving the engine efficiency and emissions. Although untimed manifold injection is technically very easy to implement, the major drawback of the system is the loss of volumetric efficiency and hence power output of the engine. This drawback will be overcome by the early direct injection of hydrogen into the combustion chamber which is the subject of the next chapter.

Chapter 9

Early Direct Injection Results

In this chapter the results of an investigation into the early direct injection of hydrogen into the combustion chamber will be presented. Preliminary investigations into early direct injection, early direct injection timing and lean air/fuel mixtures are discussed. A schlieren investigation looking at the injected hydrogen distribution of both the early direct injector and the modified spark-plug injector is outlined. A set of engine test results comparing the three methods of supplying supplementary hydrogen to an engine including the effects on the combustion characteristics, engine performance and emissions are presented and discussed. The results of an investigation into the effects of injection duration on the performance of the modified spark-plug injector is then presented.

9.1 Introduction

The initial aim of early direct injection of supplementary hydrogen was to overcome the volumetric efficiency and resulting power losses that are the major detrimental feature of hydrogen supplementation via untimed manifold injection as discussed in the preceding chapter. Direct injection also offers the potential to form stratified air/fuel mixtures in the combustion chamber.

9.2 Preliminary Engine Testing

Glasson [1992], during his investigation into the fuelling of a Ricardo E6 engine with hydrogen, determined that a delay of 9 ms (the time between the start of injection at 260 ^{o}ATDC and ignition at 345 ^{o}ATDC at 25 rps) is required for the formation of an apparently homogeneous charge. Glasson's injection duration was 14 ^{o}CA.

A simple experiment was conducted operating the engine at $\lambda = 1.0$, HEF = 10% with early direct injection of hydrogen and progressively retarding the injection timing. The NO_x emissions were observed to increase when hydrogen injection commenced at 260 ^{o}ATDC and ended at 290^{o}ATDC. As the longest estimated injection duration was

≈70 °CA, commencing hydrogen injection immediately following the closure of the inlet valve (at 220 °ATDC) should result in a homogeneous mixture being formed as was the case with untimed manifold injection.

9.2.1 Engine Configuration

The engine's primary fuel is manifold injected methanol. The main fuel can be supplemented with the early direct injection of gaseous hydrogen via the high pressure hydrogen supply system described on page 94 and the hydrogen injector configurations described from page 39. In all cases, the injection of hydrogen into the combustion chamber commenced at 220 °ATDC, the inlet valve having closed at 216 °ATDC, in order to achieve a homogeneous air/fuel mixture[1]. A constant hydrogen supply pressure of 48.2 bar (700 psi) was used to achieve sonic injection thus negating the influence of variations in combustion chamber pressure upon the injected flow-rate (see page 28). Varying the hydrogen injection duration therefore varied the quantity of hydrogen injected. As in the untimed manifold injection investigation described in the previous chapter, testing was carried out over a range of HEF's at each value of λ. Due to flow rate limitations of the direct injection hydrogen fuel injector at the supply pressure being used (see page 34), the maximum HEF obtainable at $\lambda = 1.0$ and 1.1 was 20%. The maximum obtainable HEF at $\lambda = 1.3$ and 1.5 was 30%. The injection durations varied from 13.6 °CA ($\lambda = 1.5$, 5% HEF) to 66.2 °CA ($\lambda = 1.3$, 30% HEF). The amount of each fuel being delivered was varied so as to maintain the same overall air/fuel ratio (or relative air/fuel ratio, λ). As with the manifold injection engine testing, all engine testing was carried out at a compression ratio of 10:1, at an engine speed of 1500 rpm and at wide open throttle. The level of inlet air heating used was approximately 364 Watts. Thus the operating conditions are the same as those used in the untimed manifold injection investigation.

9.2.2 Results

Preliminary engine testing of the early direct injection system was completed over the same test matrix as was used for the untimed manifold injection testing. When the data were analyzed, certain results were unexpected given the clear results that were obtained from the untimed manifold injection system. Only these key results will be presented here to form the basis for discussion. A full set of direct injection results with accompanying discussion will be presented later this chapter.

[1] Note:- The schlieren photography investigation of the early direct injector performance (see Section 4.4) indicated that there is a delay of approximately 1.8 ms between the start of injection and when the hydrogen plume is first visible entering the combustion chamber. At an engine speed of 1500 rpm, this equates to a delay of approximately 16.2 °CA. Thus as the hydrogen injection was commenced at 220 °ATDC, the hydrogen would not actually be entering the combustion chamber until approximately 236.2 °ATDC!

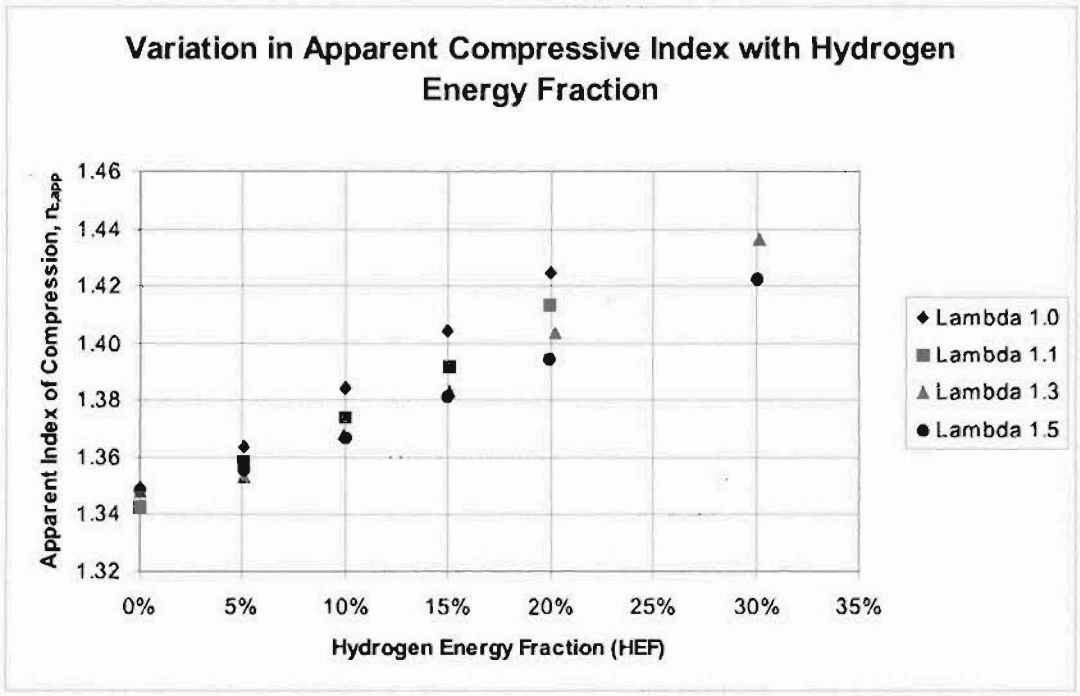

Figure 9.1 Effect of Hydrogen Supplementation on the Apparent Polytropic Index of Compression

Figure 9.1 shows the effect of hydrogen addition on the polytropic index of compression calculated from measured cylinder pressure and crank-angle data at each test point. The polytropic index is calculated from logarithmic pressure/volume data between 220 °ATDC and 320 °ATDC. The polytropic index of compression values for 0% HEF cannot be compared directly with those presented in Figure 8.1 for untimed manifold injection. The reason for this is that a systematic error in the acquired combustion pressure data was discovered to have occurred during the untimed manifold injection testing. Thus while absolute values from Figure 8.1 cannot be compared with, a comparison between the trends is still valid. This error was corrected before any of the early direct injection or comparative testing was undertaken. A fuller description of the pressure data error can be found on page 157.

The addition of hydrogen has the effect of raising the polytropic index of compression for all air/fuel ratios as was found in the untimed manifold injection investigation. It is also quite clear that the trends followed for the various overall air/fuel ratios are quite different from those trends observed with untimed manifold injection (see Figure 8.1 on page 115). At 0% HEF, n_c is greatest for the lean mixtures and smallest for the rich mixtures as was observed with untimed manifold injection. As the HEF is increased to 20%, the observation is reversed with the richer mixtures having a greater value of n_c. The value of n_c varied 0.02 between 0 and 50% HEF in the untimed manifold case but varies 0.07 between 0 and 30% HEF in the early direct injection case. The different

trends and degrees of influence can be explained as follows: In the untimed manifold injection case, no additional mass enters or leaves the combustion chamber after the inlet valve closes[2]. Thus the changes in n_c from test point to test point are due to changes in charge composition and heat transfer. For the early direct injection case however, after the inlet valve shuts supplementary hydrogen is injected into the combustion chamber. This injection of hydrogen occurs over varying durations of crank-angle depending on the HEF, adding mass to that which had been induced through the inlet manifold. Thus the value calculated by fitting a line of best fit to the compression part of the logarithmic p-V diagram (see page 78) is no longer representative of the index of compression. The value of n_c calculated during the early direct injection work will be referred to as being the apparent index of compression, $n_{c,app}$. The added mass increases the value of $n_{c,app}$ resulting in the observed change from lean mixtures having the greater $n_{c,app}$ at 0% HEF to rich mixtures having the greater $n_{c,app}$ at higher levels of HEF.

The effect of changes in n_c on the efficiency of an engine has been discussed previously for manifold injection on page 114. With manifold injection, the increase in the value of n_c reflected the increase in the specific heat (γ) of the air/fuel mixture. With direct injection, the increase in the value of $n_{c,app}$ reflects both the increase in specific heat of the mixture and the mass which is injected into the cylinder after the inlet valve is closed. Hence while the value of n_c for manifold injection can be used in Equation 8.1 to determine the theoretical cycle efficiency, the value for $n_{c,app}$ for direct injection cannot.

Increasing the HEF via direct injection will result in an increase in the Otto cycle efficiency of the engine as was the case with manifold injection due to the increase in the ratio of specific heats for the mixture. The mass of hydrogen added after the inlet valve has shut would be expected to also result in a higher pressure after compression and higher overall cycle pressures.

A mass fraction burned (mfb) analysis was carried out on the cylinder pressure data acquired at each test point. Figures 9.2 to 9.4 present the results of this analysis showing the effect of hydrogen addition on each different phase of combustion.

The trend in 0-2% mfb durations with increasing HEF as shown in Figure 9.2 in particular is very different from that obtained with untimed manifold injection. With untimed manifold injection, increasing the HEF at a particular value of λ resulted in large reductions in the 0-2% mfb duration. This is not apparent for early direct injection where the 0-2% mfb durations only reduce very slightly with increasing HEF. In addition, it appears that the 0-2% mfb durations for $\lambda = 1.3$ and 1.5 at 30% HEF are greater than

[2] Assuming that any blow-by effects are negligible

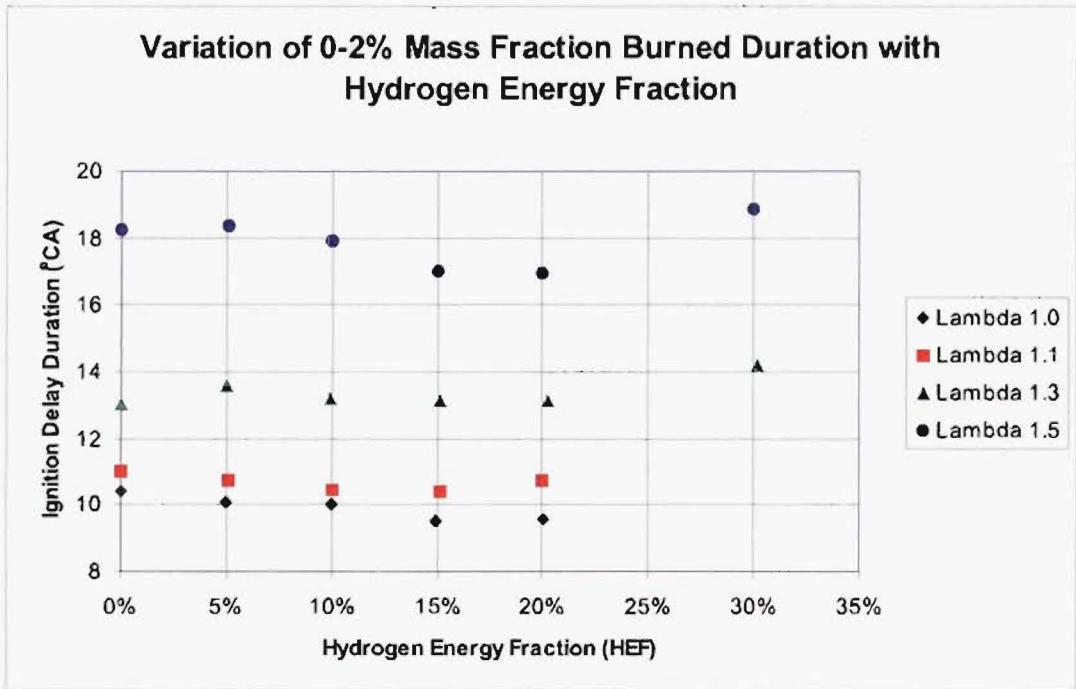

Figure 9.2 Effect of Hydrogen Supplementation on 0-2% mfb

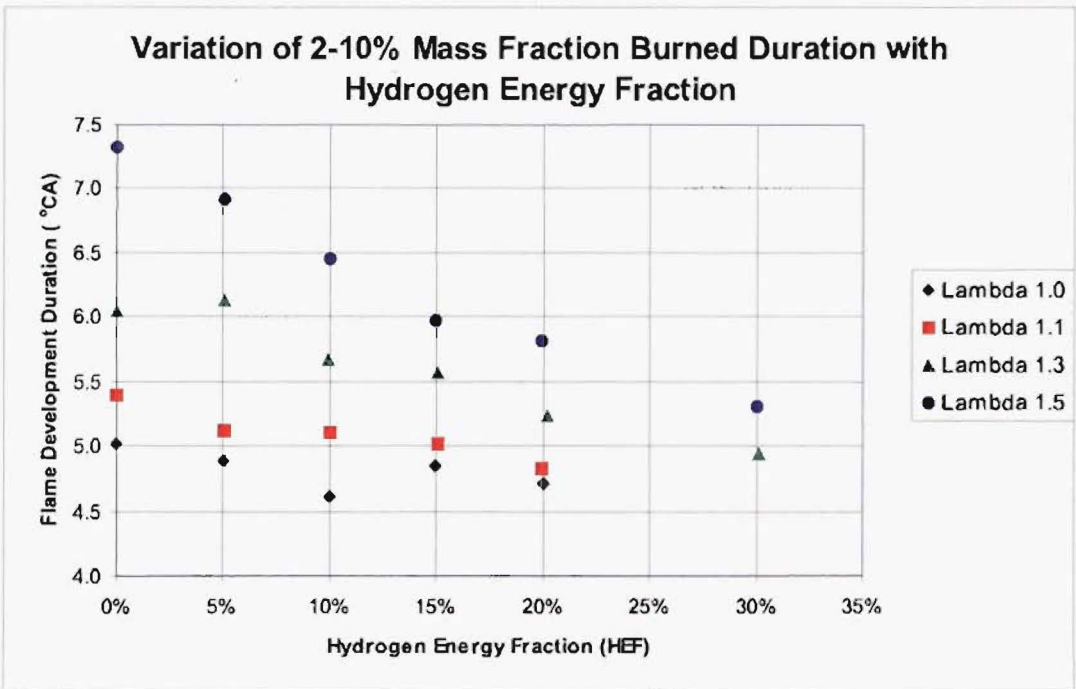

Figure 9.3 Effect of Hydrogen Supplementation on 2-10% mfb

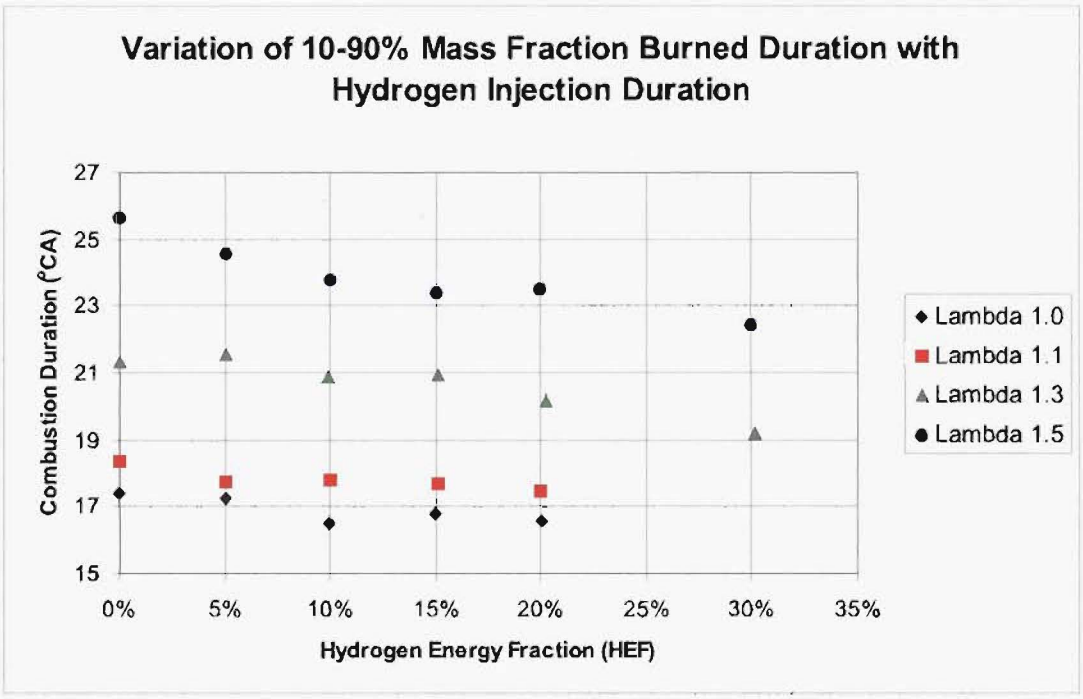

Figure 9.4 Effect of Hydrogen Supplementation on 10-90% mfb

would be expected given the trends exhibited for the lower HEF's. The principle reason for a substantially slower burn duration would be because of a leaner air/fuel mixture. If a leaner homogeneous mixture was the cause, it would be expected that all the various mfb durations would be affected in a similar manner (as was found to be the case with a manifold injection test point that was slightly richer than required). Referring to Figures 9.3 and 9.4, this is clearly not the case. Incorrectly specified spark timings when post processing the pressure data would result in differences to the 0-2% mfb duration without affecting the subsequent 2-10% and 10-90% mfb durations. This was investigated and the correct spark timings were found to have been used when post processing the data, eliminating this possible cause. As these test points were acquired on separate days the fact that both the points in question occur at HEF = 30% would appear not to be due to experimental error. The actual reason for these two points being higher than expected and the lack of effect that increasing HEF's have on the 0-2% mfb durations cannot be deduced from the data presented to date. Evidence will be presented in the following sections that shows that these slower 0-2% mfb durations are due to the injected hydrogen not reaching the spark-plug by ignition time. Thus as the HEF is increased, the mixture being ignited is a progressively leaner mixture of methanol and air. Compared to the corresponding plots for the untimed manifold injection case (see pages 117 to 118), Figures 9.3 and 9.4 exhibit similar trends but with distinctly different magnitudes. For both these phases of combustion, the burn duration decreases with increasing levels of HEF. The reduction in burn duration with increasing HEF is however not as pronounced

as was the case with untimed manifold injection.

The other key result is the variation in COV_{IMEPg} with HEF. Figure 9.5 shows the variation in COV_{IMEPg} with HEF for various air/fuel ratios. The values for $\lambda = 1.5$ with HEF = 20% and 30% are greater than would be expected given the trend of the values at lower HEF's. As noted previously, the 0-2% mfb duration for $\lambda = 1.5$, 30% HEF is also greater than would be expected. For all other values of λ, the COV_{IMEPg} is reduced as the HEF is increased although not to such an extent as was the case for untimed manifold injection of hydrogen (see Figure 8.16 on page 129).

Assuming that a homogeneous air/fuel mixture is formed by both the untimed manifold and the early direct injection systems, there are two differences between the two systems. The first is the duration that the hydrogen is resident in the cylinder. The second is that in the case of hydrogen being injected directly into the combustion chamber, the injected hydrogen jets will induce localized turbulence that is not present in the untimed manifold injection system. The effects of changing injection duration (and consequently the level of localized turbulence) on the combustion process will be investigated in the next section.

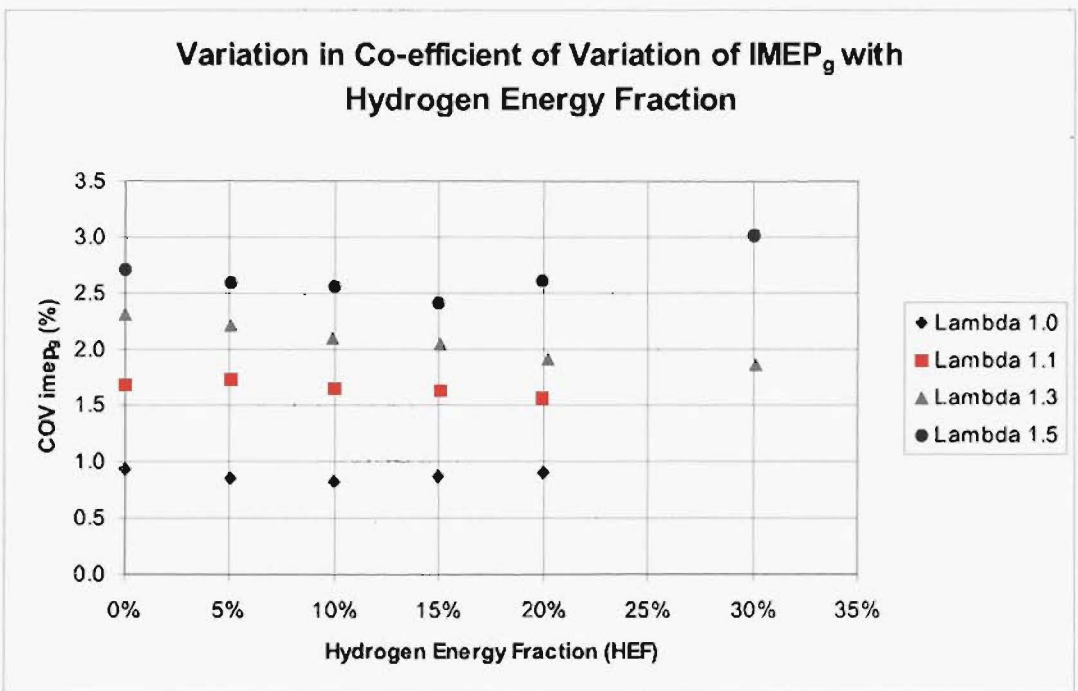

Figure 9.5 Effect of Hydrogen Supplementation on the Coefficient of Variation of Gross Indicated Mean Effective Pressure

At this point, as processed results from preliminary testing of the first two fuelling

η_m	$\lambda = 1.0$	$\lambda = 1.1$	$\lambda = 1.3$	$\lambda = 1.5$
Untimed Manifold	72%	71%	68%	65%
Early Direct	77%	76%	73%	70%

Table 9.1 Comparison of Mechanical Efficiencies

systems were compared against each other, it became apparent that the values for 0% HEF cases were not in reasonable agreement (allowing for experimental error). The engine parameters of concern were:

1. Brake Power
2. All mfb Durations
3. $IMEP_g$
4. η_{ith}

Investigation revealed that the differences in brake power could seemingly be accounted for by the substantially different inlet conditions the existed between when each of the systems were tested. Confidence can be placed in the values of $P_{corrected}$ obtained during engine testing as the measuring system employed is a mechanical one comprising of a spring balance and weights on a torque arm.

It therefore seemed that the problem could lie with incorrect pressure data. The mechanical efficiencies (see page 242 for calculation details) of the untimed manifold and early direct injection cases at 0% HEF for the range of λ's were calculated to gain further insight into the problem. The results are presented in Table 9.1.

Table 9.1 shows for both the untimed manifold and the early direct injection cases, the mechanical efficiency decreases as the mixture becomes leaner. This result is expected because as gross indicated power decreases with decreasing mixture strength at the same speed and throttle setting, the pumping work remains the same and is reflected in the value of corrected brake power. Thus at lower loads a greater proportion of the engine power produced is being used to pump mixture in and out of the cylinder and η_m decreases. The most interesting point in Table 9.1 is that although both systems exhibit the same decrease in η_m with increasing λ, they are offset from each other by 5%. It would be expected that both systems should have the same η_m at a particular value of λ. Thus it appeared that the combustion pressure data was suspect.

The following parameters all affect the value of combustion pressure that is measured and calculated via post processing software:

1. Clearance volume
2. Compression ratio
3. Piezo-electric pressure transducer calibration
4. Phasing of the data

Investigations revealed all to have been accurately specified and that no rotation of the rotary encoder relative to the crank-shaft had occurred. Further investigation revealed that an electronic circuit that had been added between the charge amplifier and the screw terminal accessory board during the untimed manifold injection testing to reduce the impedance of the charge amplifier output voltage signal was faulty. A time delay was being introduced to the combustion pressure voltage signal resulting in an incorrectly phased graph of the motored log(P) verses log(V) being observed when tested. The time delay being introduced could not be accurately measured but was estimated to be $\approx 1.2\ ^{o}$CA. This circuit had been replaced by one of the Department's multipurpose operational amplifier units before the main engine testing was carried out and thus no other electronic data was affected. The trends shown in the preliminary manifold injection investigation were found to be consistent with the trends found when further comparative testing between all three injection systems was carried out. As none of the data presented in the preliminary manifold injection investigation were used in drawing conclusions between any of the three injection systems, these results were presented to form the basis for discussion on the effect of increasing HEF's on methanol combustion.

9.3 Injection Duration Investigation

9.3.1 Introduction

This section of work was undertaken to elucidate what (if any) effects changing the duration hydrogen was injected over has on the combustion process.

The residence time of hydrogen in the combustion chamber is longer for low levels of HEF compared to the hydrogen injected later in the compression stroke with higher levels of HEF. In addition to this, for the same HEF the end of hydrogen injection is much later for richer overall air/fuel ratios than for leaner overall air/fuel ratios.

The possible effects of lengthening the injection duration are:

- Stratification of the charge due to late injection and poor in-cylinder mixture motion.
- Decreased residence time of the hydrogen in the cylinder possibly resulting in reduced dissociation of hydrogen and subsequent formation of H^+ and OH^- radicals, therefore resulting in a reduction in pre-flame reactions, adversely affecting the combustion of the charge.
- Higher levels of localized turbulence being induced in the combustion chamber by the high velocity hydrogen jet.

An experiment was devised that enabled the injection duration of the injected hydrogen to be varied with all other engine operating parameters remaining constant.

9.3.2 Experimental Procedure

The hydrogen injection system being used achieved sonic injection with careful selection of supply pressure and thus negated the influence of variations in combustion chamber pressure. The hydrogen injection duration and supply pressure (within limits) are therefore the only factors influencing the quantity of hydrogen that is injected.

The overall relative air/fuel ratio chosen for this investigation is $\lambda = 1.3$ as it would allow the effects of any stratified charge combustion of the injected hydrogen (which would burn with a locally rich A/F ratio) to be easily distinguished from that of the lean manifold induced methanol charge.

The HEF used was 10% so that a relatively low pressure could be used and still inject the required quantity of hydrogen before charge stratification was thought to become likely. The hydrogen supply pressure could then be raised to allow the same quantity of hydrogen to be injected but over a much reduced duration, increasing both the residence time and turbulence in the combustion chamber.

The first experimental run was conducted with a hydrogen supply pressure of 27.5 bar (400 psi). It was determined that an injection duration of 40 degrees crank-angle was required to give a HEF of 10%. The second experimental run was conducted with a hydrogen supply pressure of 48.3 bar (700 psi). With this increased supply pressure, an injection duration of only 24.6 degrees crank-angle was required to give a HEF of 10%. Thus without changing any other engine parameters, the residence time in the cylinder was able to be altered. The third experimental run was conducted with a hydrogen supply pressure of 37.9 bar (550 psi) to give an injection duration of 29 ^oCA.

For the first test point in each run, injection started at 220 ^{o}ATDC and the start of injection for successive test points was retarded progressively by 10 degrees from the previous.

9.3.3 Engine Configuration

The engine's primary fuel was manifold injected methanol. The amount of each fuel being delivered was kept constant so as to maintain an overall air/fuel ratio, $\lambda = 1.3$. The main fuel was supplemented with the early direct injection of gaseous hydrogen.

All engine testing was carried out at a compression ratio of 10:1, an engine speed of 1500 rpm and at wide open throttle. The level of inlet air heating used was approximately 364 Watts. Thus the operating conditions are the same as those used in both the untimed manifold injection and preliminary early direct injection investigations.

The spark timing was set to 16^{o}BTDC (MBT for 10% HEF when the start of injection was 220 ^{o}ATDC at $\lambda = 1.3$) and remained at this value for all of the tests. If the injection duration does have an effect on the combustion process, it will be highlighted by the use of a constant spark timing.

9.3.4 Results

In order to understand what effect (if any) changes in hydrogen injection duration has, the combustion process will be examined.

Figures 9.6 to 9.8 show the effect of differing hydrogen injection durations and timing on each of the mass fraction burned durations. Each of these graphs shows a clear general trend that for shorter injection durations, the combustion of the charge is faster than that for longer injection durations.

Figure 9.6 exhibits some other distinguishing features that are not present in Figures 9.7 and 9.8. For each of the three injection durations, as the start of injection is progressively retarded, the 0-2% mass fraction burned duration steadily increases before reaching a plateau. For the 40 degree crank-angle injection case this occurs with a start of injection of approximately 240 ^{o}ATDC. For the 29 and 24.6 ^{o}CA degree crank-angle injection cases, this occurs slightly later with a start of injection of approximately 260 ^{o}ATDC. Bearing in mind that the hydrogen injector is located in the spare spark-plug hole which is on the opposite side of the combustion chamber from the spark plug being used, the observed insensitivity to the injection duration being retarded past 260 ^{o}ATDC suggests that there is insufficient time for the 0-2% mfb duration to be affected by the

hydrogen injection. Thus the observed differences in the mfb durations appear to be caused by either differences in the residence time in the cylinder and/or localized turbulence due to the injected hydrogen jets and/or some degree of charge stratification.

Figures 9.7 and 9.8 show the effect of injection duration on the 2-10% and 10-90% mfb durations respectively. An interesting feature of Figure 9.8 is that for the 24.6 ^{o}CA injection duration, advancing the injection timing beyond 240 ^{o}ATDC does not result in the 10-90% mfb duration being further reduced. Again the results suggest that the variations in combustion duration are due to differences in the time available for mixing/chemical reactions to occur before combustion is initiated and/or the level of locally induced turbulence.

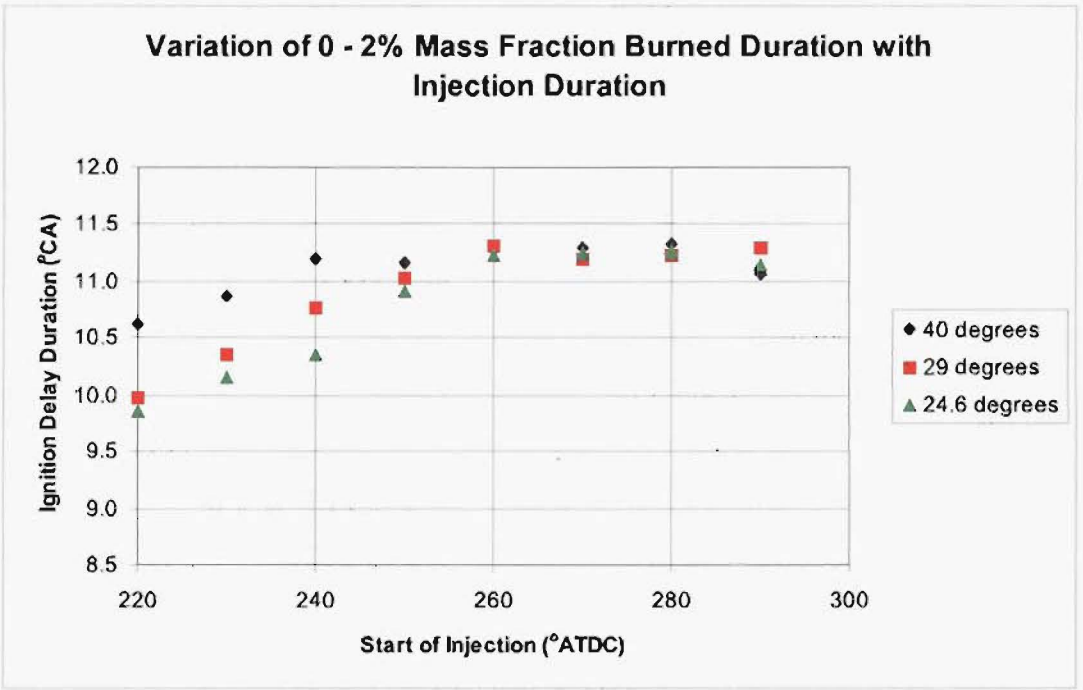

Figure 9.6 Effect of Injection Duration on 0-2% mfb

The first possible explanation for the observed differences in combustion rate is that longer in-cylinder residence time allows the supplemented hydrogen to dissociate and form intermediate species to a greater degree, increasing the pre-flame reaction rate and increasing the rate of combustion of the charge. Karim and Watson [1971] investigated the compression ignition of a homogeneous mixture of hydrogen and air both experimentally and using a kinetic model. They concluded that no significant chemical reactions began until the cylinder temperature rose above 550 K. A simplified calculation on the compression process in the engine assuming polytropic compression of an ideal gas (γ = 1.4) indicates that the cylinder temperature would not reach 550 K until approximately

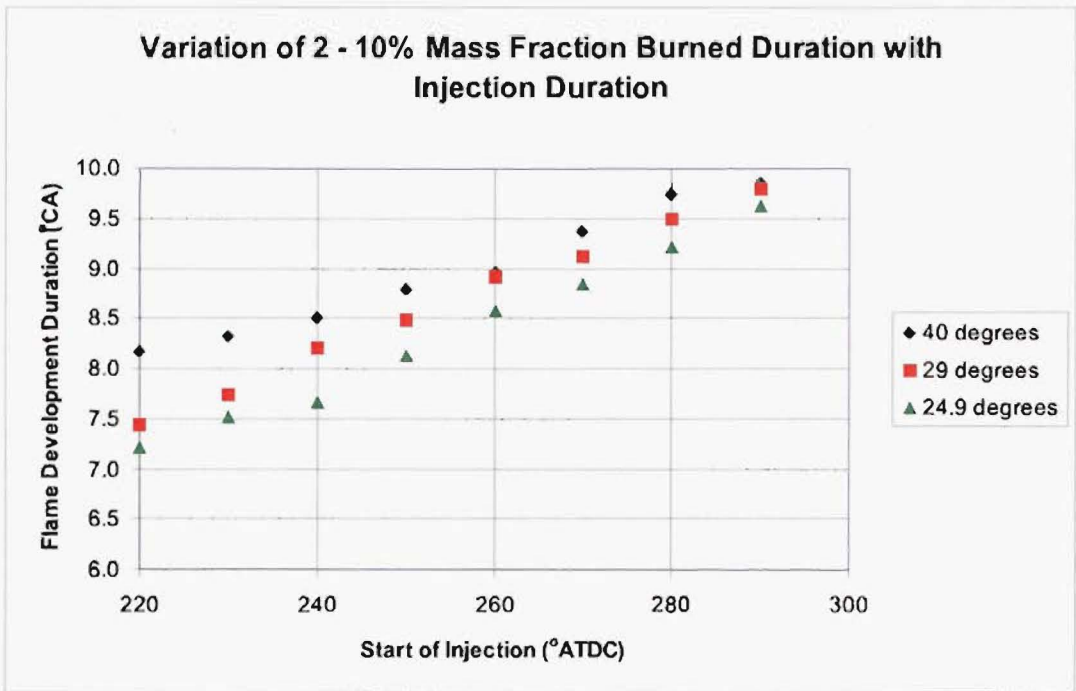

Figure 9.7 Effect of Injection Duration on 2-10% mfb

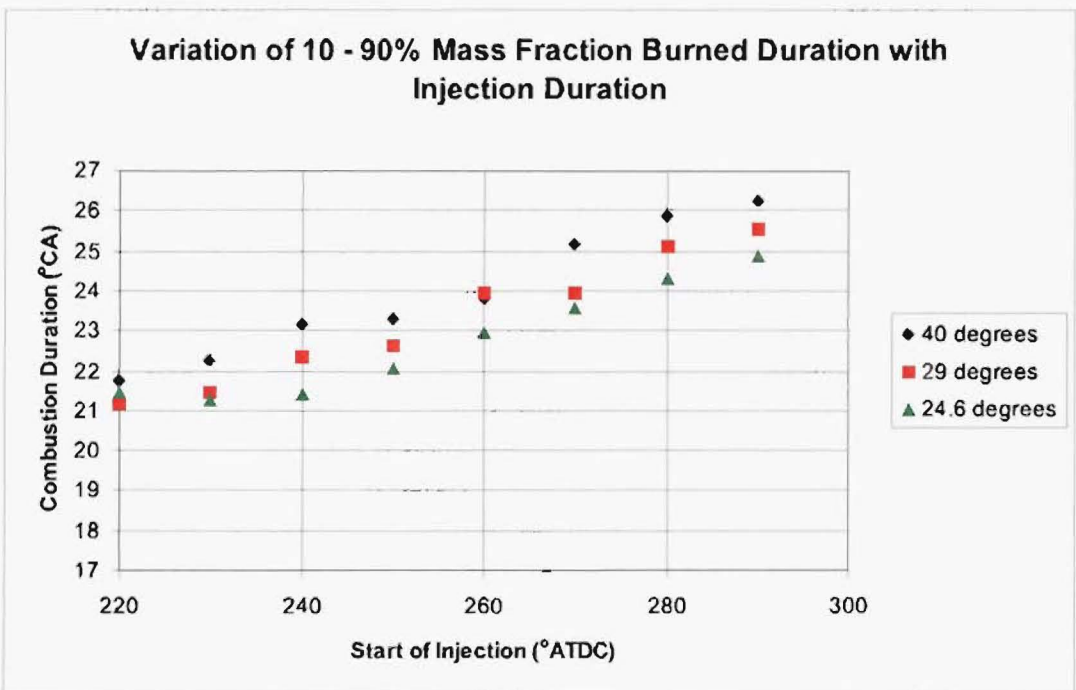

Figure 9.8 Effect of Injection Duration on 10-90% mfb

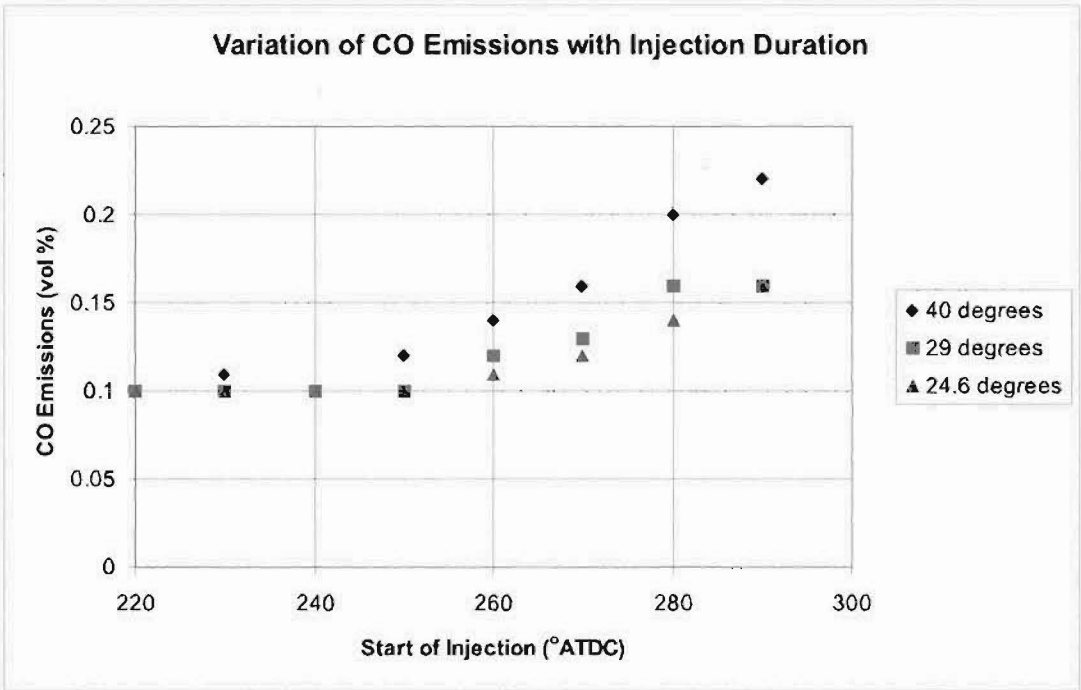

Figure 9.9 Effect of Injection Duration on CO Emissions

325 °ATDC (or 35 °BTDC). At this point in the compression stroke, the injection of hydrogen in all three cases (except the 40 °CA injection which starts at 290 °ATDC) is complete. Therefore the differing injection durations will not have any effect on the extent of hydrogen dissociation or pre-flame reactions and can therefore not be responsible for the observed differences in combustion duration.

Another possible explanation for the observed trends is that the injected hydrogen does not have time to form a homogeneous mixture with the existing homogeneous charge of methanol and air in the cylinder. Thus the charge is stratified to some degree. This being the case there will be a region in the cylinder closest to the hydrogen injector containing methanol, hydrogen and air. There will also be a region furthest from the hydrogen injector (i.e. closest to the spark-plug) containing only methanol and air. The emission levels of CO should increase as the former region burns richer than the latter region. Referring to Figure 9.9, it can be observed that the emission levels of CO increase for injection timings after 240 °ATDC for the 40 °CA injection case and after 250 °ATDC for the 24.6 and 29 °CA cases. This indicates that there is some degree of charge stratification as the start of injection is increasingly retarded. The shorter injection durations which have higher flow-rates and more time for mixing would result in reduced levels of stratification. As the hydrogen injector and spark-plug are diametrically opposite each other on either side of the combustion chamber, reduced stratification would result in more hydrogen in the vicinity of the spark-plug. This would be expected to result in

reduced ignition delay durations as has been shown to occur in Figure 9.6 as the 0-2% mfb duration in hydrogen supplemented mixtures is known to be dominated by the high laminar flame speed of hydrogen [Rauckis and McLean 1979] , [Heywood 1988]. With the earliest injection timings, the level of stratification could be relatively slight, showing up as longer 0-2% mfb combustion durations but not producing significantly increased CO emissions. The trends apparent in Figure 9.9 would indicate that lower injection pressures and the associated longer injection durations lead to greater degrees of charge stratification than do higher injection pressures and reduced injection durations. The injection pressure used for the preliminary early direct injection work was 48.2 bar (700 psi) and the injection was started at 220 ^{o}ATDC. In most cases, injection had ended before 270 ^{o}ATDC with the latest end of injection being 286.2 ^{o}ATDC. Thus based on these results, any charge stratification in the preliminary early direct injection testing would not have been evident in the engine emissions but possibly evident in the 0-2% mfb results.

The third possibility for the observed differences in combustion rate is the turbulence that is induced in the cylinder by the jet of injected hydrogen. Increased in-cylinder turbulence is known to increase the rate of combustion in an engine. Increasing in-cylinder turbulence is a commonly used technique for increasing the combustion rate in lean burn engines which suffer from inherently slow combustion rates [Heywood 1988]. Referring to the schlieren photographs of the five hole nozzle arrangement on page 51, it was found that the injected hydrogen jets have a high initial velocity. A later schlieren investigation with a much enlarged field of view revealed that the injected hydrogen jets had low momentum and the jet velocity decreased markedly after the completion of injection (see page 171). At the projected time of ignition the mixture in the schlieren bomb appeared to be close to quiescent with very little localized turbulence remaining. The direct injection of hydrogen into the combustion chamber will therefore have very little effect on the level of localized turbulence in the cylinder. It is thought that this mechanism would be contributing very little to the observed differences in combustion duration.

The trends observed in the mass fraction burned durations are also reflected in the behavior of other engine combustion parameters in a manner that is expected and has previously been discussed in the untimed manifold injection results.

9.3.5 Conclusions

From this investigation into the effect of injection duration on the combustion processes, the following conclusions can be drawn:

1. The duration of hydrogen injection has a significant effect on the observed combustion durations. For a given injection timing, shorter injection durations lead to

reduced combustion durations.

2. The injection timing has an effect on the combustion duration. Retarded timings result in longer combustion durations.

3. There is little variation in 0-2% mfb duration with injection duration when retarding the injection timing beyond 260 ^{o}ATDC.

4. Advancing the injection duration beyond 260 ^{o}ATDC results in no further reduction in the 10-90% mfb duration for the shortest injection duration.

5. Differences in injection duration will not be contributing to the degree or extent of the dissociation of hydrogen or pre-flame combustion reactions.

6. The extent to which turbulence induced by the injected hydrogen jet is affecting the combustion process is unknown but it is thought to be minimal.

7. There appears to be some degree of charge stratification occurring in the combustion chamber which is especially evident in the 0-2% mfb duration results. It is thought that charge stratification is the dominant mechanism responsible for the observed combustion phenomena.

9.4 Lean Mixture Investigation

The results from the untimed manifold injection and preliminary early direct injection investigations indicated that hydrogen supplementation was particularly beneficial in leaner mixtures. An investigation was therefore undertaken to determine the effects of hydrogen supplementation in lean mixtures. The value of HEF used was 30% as this is the maximum value obtainable using early direct injection at $\lambda = 1.5$. The hydrogen supply pressure was 48.2 bar (700 psi) and the start of injection 220 ^{o}ATDC as was used in the preliminary early direct injection investigation.

Initial attempts to operate the engine at $\lambda = 2.2$ and 2.0 with 30% HEF failed as the mixture was obviously outside of the engine's equipment lean limit. At $\lambda = 1.8$ however, the engine was able to be run albeit extremely roughly with significant misfire and backfire. The mixture was set to $\lambda = 1.8$, 40% HEF in order to achieve better combustion but the engine performance deteriorated further. At $\lambda = 1.8$, 50% HEF the engine would not run at all. It was apparent that the supplementary hydrogen was barely reaching the spark plug if at all in the 30% case and as the HEF was increased (and the methanol flowrate decreased), the spark was having to try to ignite an increasingly lean methanol/air mixture. Returning to $\lambda = 1.8$ and 30% HEF, the start and finish of injection were progressively advanced while keeping all other engine operating parameters constant.

The combustion became more stable as the injection timing was advanced thus allowing more time for the injected hydrogen to reach the spark-plug. It was concluded that there was indeed a stratified mixture being formed in the combustion chamber with the early direct injection system contrary to the assumptions that had previously been made.

An experiment was devised to investigate the level of stratification present in the engine and see if it could be overcome by injecting earlier in the compression stroke before the inlet valve shuts. How far the injection could be advanced from inlet valve closure before the volumetric efficiency of the engine started to become adversely affected would be the limiting factor. The engine configuration was changed so that either the early direct injection injector or the modified spark plug injector could be used (but never both at the same time) by switching the injection signal from the engine management system to the appropriate injector. The engine was again run at 1500 rpm at $\lambda = 1.8$ and 30% HEF with an initial start of injection of 230 ^{o}ATDC. The data was taken from the engine at this injection timing using both the early direct injector and the modified spark-plug injector. The MBT spark timings for the early direct injector and the modified spark-plug injector were found to be 320 ^{o}ATDC and 340 ^{o}ATDC respectively. These spark timings were used for their respective system throughout the test.

Figure 9.10 shows the effect that varying the start of injection has on both the COV_{IMEP_g} and the volumetric efficiency for the early direct injection system. It can be seen that injected hydrogen starts to adversely effect volumetric efficiency when the start of injection is advanced past 180 ^{o}ATDC (i.e. 36 ^{o}CA before the inlet valve closes). A start of injection of 170 ^{o}ATDC corresponds to the point at which the COV_{IMEP_g} reaches a point where further advancing the injection timing results in negligible improvements in the combustion stability. Thus using a start of injection of 170 ^{o}ATDC with the early direct injection system appears to result in a homogeneous air/fuel mixture with only a very slight adverse effect on the volumetric efficiency.

Figure 9.11 compares the effects of varying the injection timing on the value of COV_{IMEP_g} between each injection system. It can be seen that with an injection timing of 230 ^{o}ATDC the combustion in the early direct injection system is very rough compared to that in the modified spark-plug injector system. Advancing the injection timing in the early direct injection case gives the marked reduction in combustion variability already shown in Figure 9.10. For the modified spark-plug system however, the combustion variability is already very low with an injection timing of 230 ^{o}ATDC and further advancing the injecting timing has little effect. As the injection timing is advanced past 170 ^{o}ATDC there is little difference between the values of COV_{IMEP_g} for each system. The COV_{IMEP_g} for the modified spark-plug system however is always slightly lower than that of the early direct injection system. These results clearly indicate that unless the

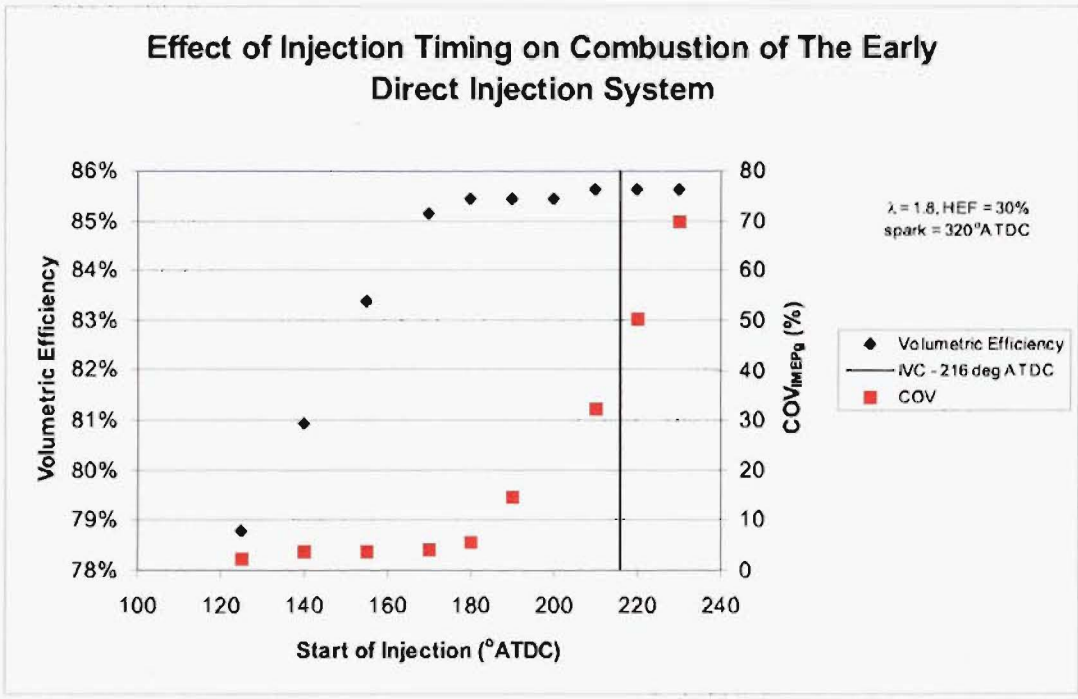

Figure 9.10 Effect of Injection Timing on Combustion of the Early Direct Injection System

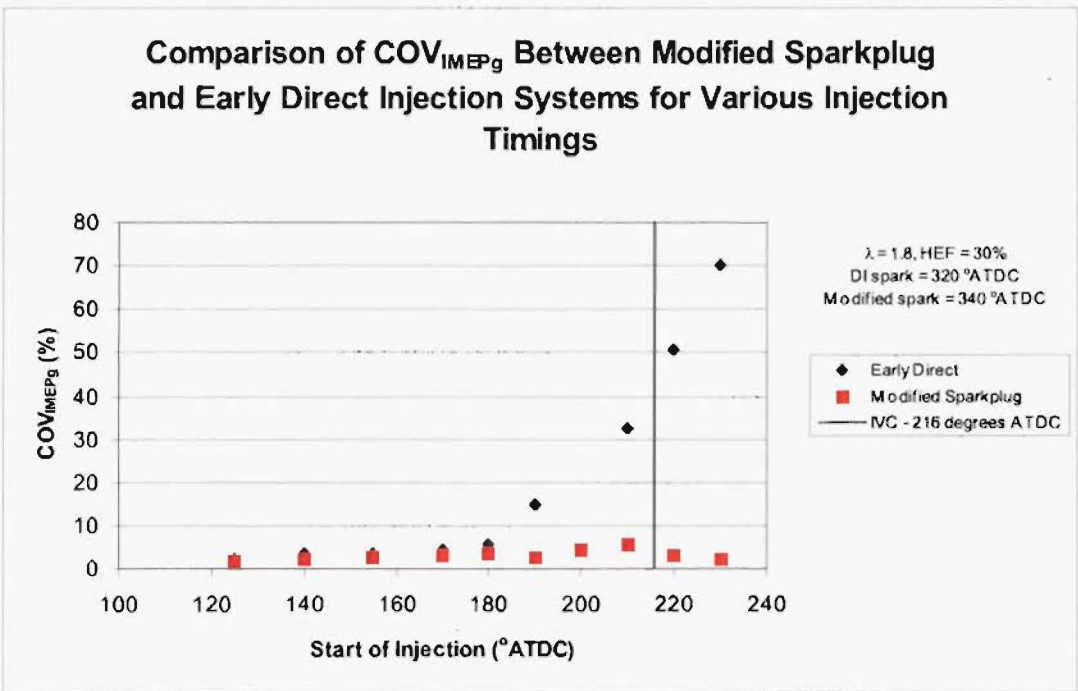

Figure 9.11 Effect of Injection Timings on COV_{IMEPg}

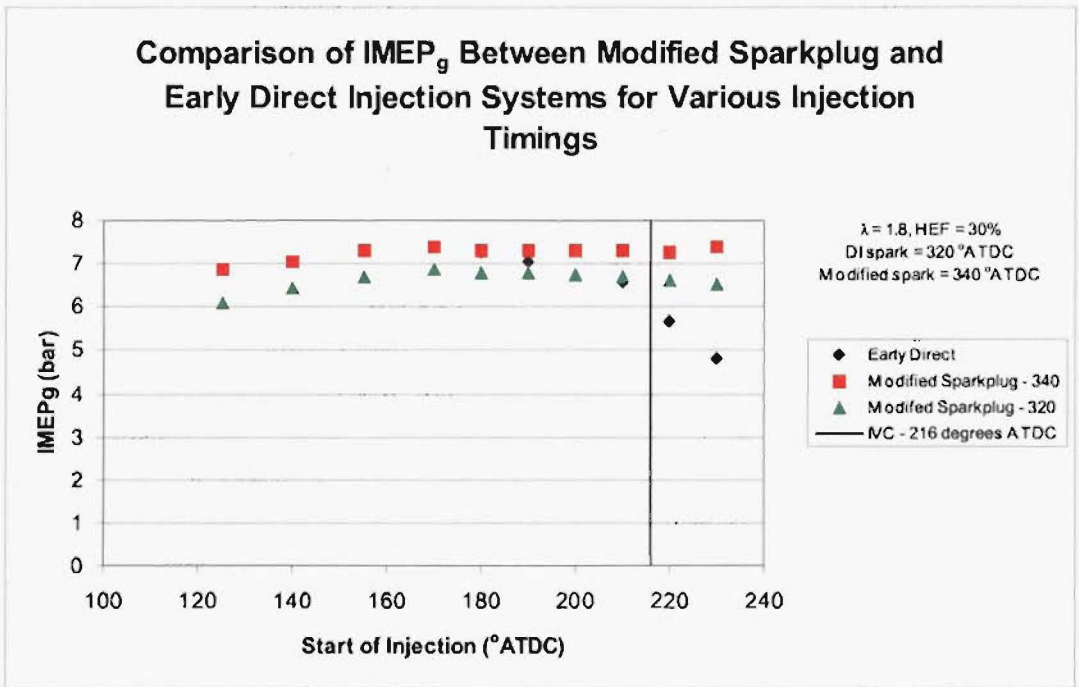

Figure 9.12 Effect of Injection Timings on IMEP$_g$

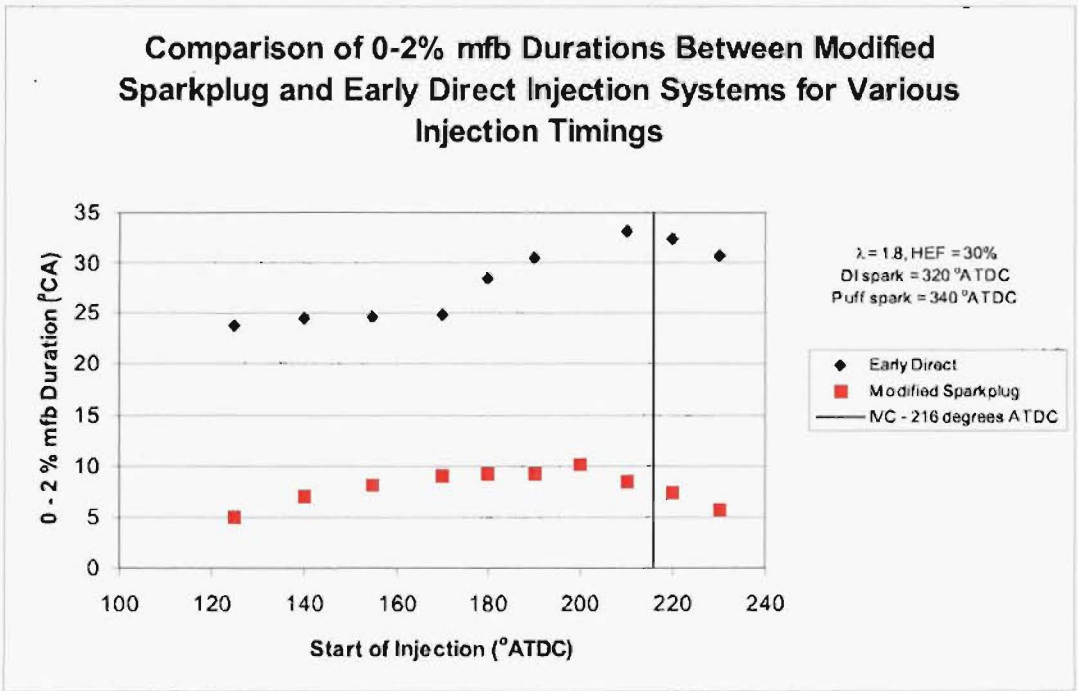

Figure 9.13 Effect of Injection Timings on the 0-2% mfb Duration

supplementary hydrogen is injected before 170 ^{o}ATDC with the early direct injection system, the resultant air/fuel mixture will be stratified.

Figure 9.12 shows the effect of varying the injection timing on IMEP$_g$ between each injection system. During engine testing it was found that if the engine was operated with the modified spark-plug system and a spark timing of 320 ^{o}ATDC (MBT for the early direct injection system), the combustion phasing was too advanced. Thus combustion data was acquired for spark timings of 320 ^{o}ATDC (for comparative purposes) and 340 ^{o}ATDC (MBT spark timing for the modified spark-plug arrangement). For injection timings advanced of 170 ^{o}ATDC, the values of IMEP$_g$ for both systems with MBT spark timings coincide. The values of IMEP$_g$ for the early direct injection system with injection timings retarded past 170 ^{o}ATDC fall away dramatically from the values obtained with the modified spark-plug system. This is due to the increase in combustion variability resulting from attempting to burn an increasingly stratified charge. The values of IMEP$_g$ for the modified spark-plug system with a spark timing of 320 ^{o}ATDC are clearly lower than those obtained with a spark timing of 340 ^{o}ATDC, reflecting the over advanced combustion phasing observed during engine testing. An interesting point to note is that for injection timings advanced of 170 ^{o}ATDC, the same values of IMEP$_g$ were obtained from the early direct injection and the modified spark-plug injection systems with spark timings of 320 ^{o}ATDC and 340 ^{o}ATDC respectively. This implied that combustion is occurring at a faster rate in the modified spark-plug injection system than it is in the early direct injection system with the same level of hydrogen supplementation.

Figure 9.13 shows the effect of varying the injection timing on the 0-2% mfb duration between each injection system. The 0-2% mfb duration for the modified spark-plug system is 15 - 20 ^{o}CA lower that that for the early direct injection system for the same injection timing. The 2-10% and 10-90% mfb durations for both systems are close in magnitude and plots of these quantities have been omitted for brevity. Thus it appears that it is the faster 0-2% mfb duration of the modified spark-plug arrangement that is responsible for the more retarded MBT spark timing of modified spark-plug system. The shorter 0-2% mfb duration would also be likely to be responsible for the lower value of COV$_{IMEPg}$ compared to the early direct injection system as observed in Figure 9.11. The most likely reason for the observed short 0-2% mfb duration is that there is a hydrogen rich region remaining near the spark-plug at the time of combustion initiation. To further investigate the injection process of hydrogen into the combustion chamber, a further schlieren photography investigation was carried out.

9.5 Schlieren Photography Investigation

In order to further investigate the injection of hydrogen into the combustion chamber by both of the direct injection systems used, a further schlieren investigation was undertaken. The constant volume bomb used in the preliminary schlieren investigation had since been modified to allow a much enlarged field of view to be observed during an injection event.

For the modified spark-plug arrangement, the injector was fitted in a custom made end of the bomb which allowed the electrodes of the spark-plug to be visible in the resultant schlieren photograph. Due to physical limitations in the construction of the bomb, the angle of the modified spark-plug arrangement is 60^o from the horizontal compared to 40^o in the actual head of the engine. In addition, the electrode is approximately 10 mm closer to the center of the combustion chamber than is the case in the actual engine. These differences were not thought to be of consequence for the modified spark-plug injector arrangement as the primary interest was in the area around the spark-plug at the projected time of ignition. For the photographs of the early direct injection system, a spare Ricardo E6 engine head was fitted to the top of the schlieren bomb. Due to the physical layout of the bomb this meant that the end of the injector could not be seen in the resulting photographs. This was not seen as being problematic as the primary interest was in how close the injected hydrogen was getting to the spark-plug at the projected time of ignition. The advantage of using the Ricardo E6 head was that the orientation of the injector with respect to the combustion chamber is as it was in the engine.

All timings and injection quantities used in the schlieren investigation were chosen to replicate the engine operating parameters used in the engine testing described previously at $\lambda = 1.8$ and 30% HEF (see page 166). The first pair of schlieren photographs simulate an injection timing of 230 ^{o}ATDC while the second pair simulate an injection timing of 170 ^{o}ATDC. All photographs were taken at a simulated ignition timing of 320 ^{o}ATDC. The injection duration used throughout was 5 ms which simulated the $\approx$ 45 ^{o}CA injection duration that was used in the engine testing (1 ms equals 9 ^{o}CA at 1500 rpm).

In order to clearly visualize the location of the early direct injection nozzle with respect to the spark-plug, refer to Figure 9.14. The early direct injection injector nozzle can be seen in the lower left corner of the head while the spark-plug is located at the top right. It can clearly be seen that the nozzle and the spark plug are on opposite sides of the combustion chamber from each other. The pressure transducer tapping can be seen on the right hand side. The holes around the perimeter of the head are coolant passages. Also of relevance when considering the formation of a localized hydrogen rich air/fuel mixture in the vicinity of the spark-plug is that the spark-plug is located in a recess in

head as can be seen in Figure 9.14. The location of the spark-plug in the recess can be seen more clearly in the recess in the cutaway view shown in Figure 3.7 on page 42. This recess would provide some measure of protection to any injected hydrogen remaining in the vicinity of the spark-plug from the influence of combustion chamber mixture motion.

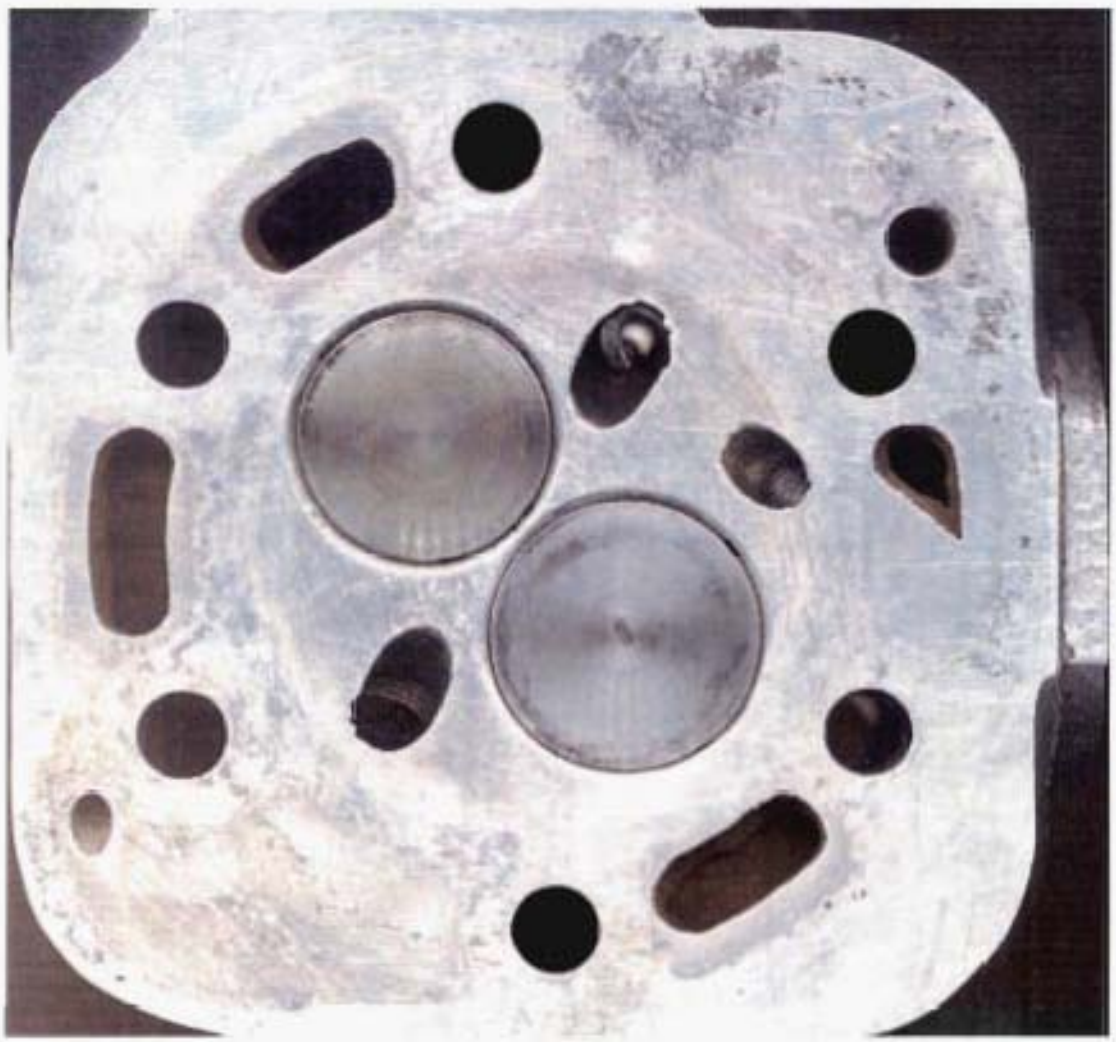

Figure 9.14 View of the Ricardo E6 Head

Figures 9.15 and 9.16 show the distribution of injected hydrogen from the early direct injection and modified spark-plug systems respectively at the projected time of ignition with an injection timing of 230 °ATDC. For the early direct injection case, the photograph shows two jets emanating from the 5 hole nozzle in the top right hand corner of the photograph. The jet emanating from the central hole in the nozzle can be seen having traversed the combustion chamber and impacted on the left hand combustion chamber wall. One of the 45° jets can be seen propagating down the right hand wall. The spark plug is located above the top of the photograph in the left hand corner. It can be seen that when injecting into a quiescent mixture with an injection timing of 230 °ATDC, no

hydrogen is in the vicinity of the spark plug at the time of ignition. From the engine test results presented earlier (starting on page 166) it can be inferred that even with the bulk fluid motion in the engine, the injected hydrogen is still not reaching the spark plug by the time of ignition. For the modified spark-plug case, it is apparent that when injecting into a quiescent mixture at the time of ignition there is hydrogen present in the vicinity of the spark-plug. Again referring to the engine results presented earlier it is apparent that the hydrogen has not been displaced from the vicinity of the spark-plug at the time of ignition. Comparing Figures 9.15 and 9.16 it is apparent also that the injected hydrogen jet of the early direct injection system has a far greater velocity compared to the modified spark plug system and propagates further into the combustion chamber. This should result in a more homogeneous mixture being formed in a given period of time that is available for injection and mixing.

Figures 9.17 to 9.18 show the distribution of injected hydrogen from the early direct injection and modified spark-plug systems respectively at the projected time of ignition with a simulated injection timing of 170 ^{o}ATDC and an ignition timing of 320 ^{o}ATDC. By simulating the advancing of the start of injection by 60 ^{o}CA, it can be seen that in both the early direct and the modified spark-plug injection systems the injected hydrogen has propagated far further into the combustion chamber than had been the case with an injection timing of 230 ^{o}ATDC. While the injected hydrogen appears to have again not reached the spark plug in the early direct injection case, it was apparent from the engine test results presented earlier that the bulk fluid motion in the engine does in fact result in the hydrogen reaching the spark-plug. For the modified spark-plug system, there is still hydrogen in the vicinity of the spark plug at the time of ignition as was found previously with a simulated injection timing of 230 ^{o}ATDC. Previous work within the department [Zavier 1991] (see page 4.5) showed, using hot wire anemometry, that there is motion of the mixture in the cylinder in the vicinity of the sparkplug. The cause of this motion is likely to be a combination of swirl induced during the inlet stroke and motion of the piston rising during the compression stroke. Disk type combustion chambers such as that of the Ricardo E6/Mk6 are known to have relatively low levels of bulk in-cylinder motion compared to more modern designs [Heywood 1988]. However vortices are known to form at the interface between the piston face and the cylinder wall which act to mix the cylinder contents at the periphery of the combustion chamber along with swirl induced in the inlet process [Heywood 1988]. It is a combination of induced swirl and piston induced mixture motion that is thought to be responsible for ensuring the injected hydrogen does in fact reach the spark-plug by the time of ignition.

From the evidence gathered from the preliminary engine testing, the injection duration investigation, the lean mixture investigation and the schlieren photography investigation, it is apparent that using an injection timing of 220 ^{o}ATDC with the early direct

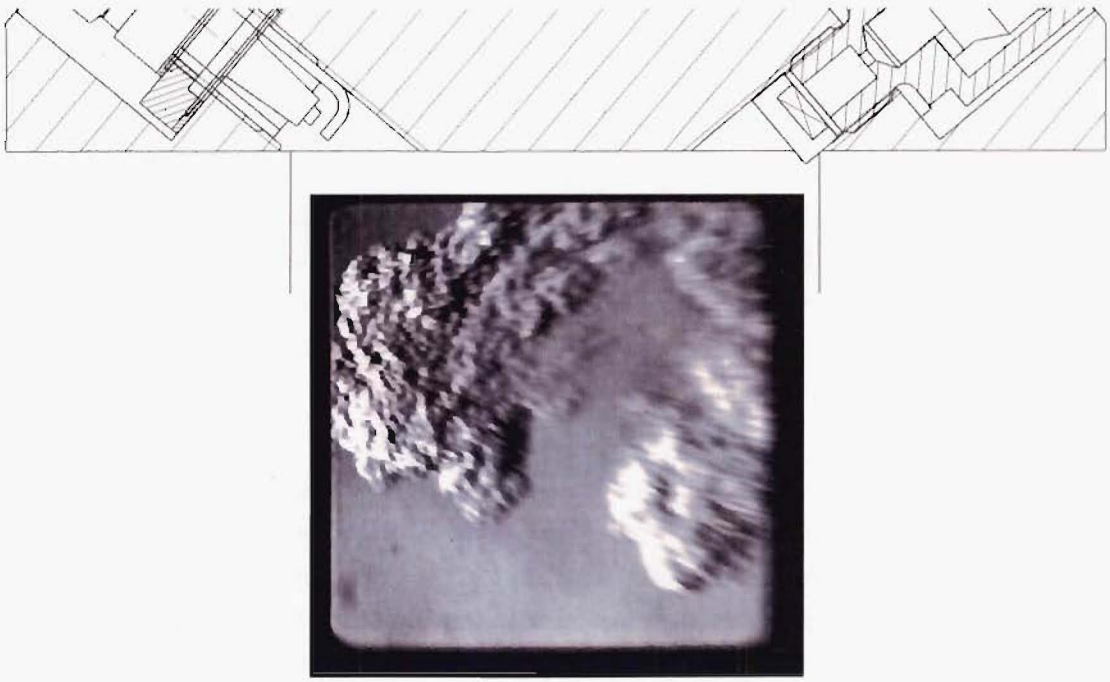

Figure 9.15 Early Direct Injection, HEF = 30%, Θ_{inj} = 230 °ATDC

Figure 9.16 Modified Spark-plug Injection, HEF = 30%, Θ_{inj} = 230 °ATDC

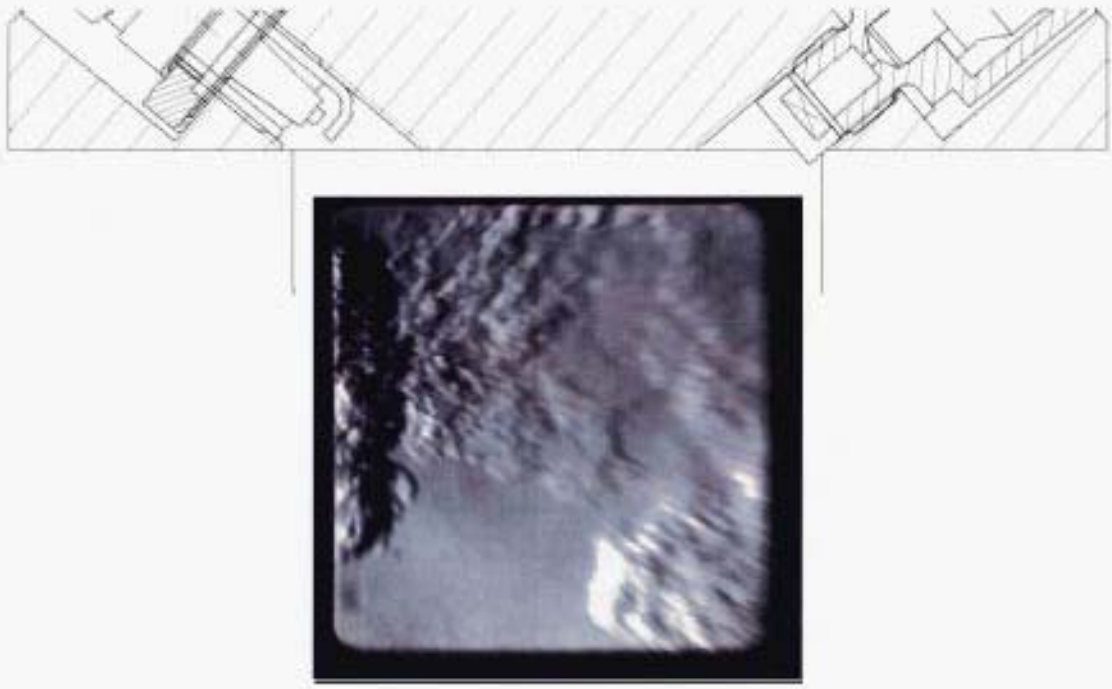

Figure 9.17 Early Direct Injection, HEF = 30%, Θ_{inj} = 170 °ATDC

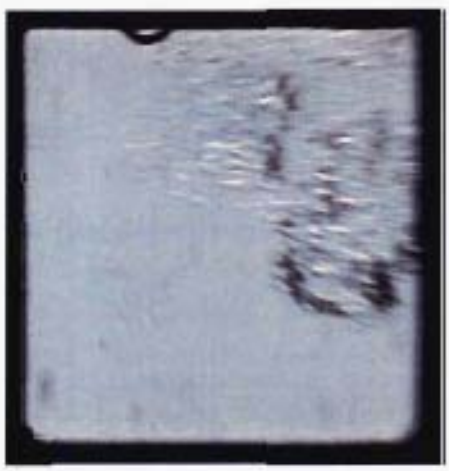

Figure 9.18 Modified Spark-plug Injection, HEF = 30%, Θ_{inj} = 170 °ATDC

injection system results in the formation of a stratified charge. It has been shown that the injection timing can be advanced to 170 ^{o}ATDC resulting in a low level of cyclic variability while not adversely affecting the volumetric efficiency of the engine. Using the modified spark-plug injection system results in a much faster 0-2% mfb duration than is the case with the early direct injection system. This is thought to be due to a localized fuel rich mixture of hydrogen/air in the vicinity of the spark-plug at the time of ignition. Based upon these results an injection timing of 170 ^{o}ATDC will be used for the ensuing comparative testing between the three fuelling systems.

9.6 Comparative Testing Between Systems

9.6.1 Introduction

The previous sections have shown that hydrogen supplementation using the early direct injection system does not provide a homogeneous air/fuel mixture as was originally intended. Instead the air/fuel mixture appears to be inversely stratified, adversely affecting the critical ignition and flame kernel development phase of the combustion process compared with the un-supplemented case. Further, when the modified spark-plug was used to inject the supplementary hydrogen, it appeared that the resulting air/fuel mixture was stratified with a hydrogen rich mixture remaining in the vicinity of the spark-plug at the time of ignition. Both the ignition and flame kernel development phases of combustion were affected beneficially.

Both the early direct injection and the modified spark plug injection systems were tested, along with the untimed manifold injection system, over a similar test matrix as was used in the preliminary untimed manifold case, with more emphasis on the lean mixtures where hydrogen supplementation has been shown to have a more pronounced effect. The $\lambda = 1.1$ and 1.3 cases are omitted from the test matrix and $\lambda = 1.8$ added as the area of interest is in the lean air/fuel mixtures.

Combustion features particular to the early direct injection systems will be discussed where appropriate but the majority of the explanation of trends with increasing HEF are as previously discussed for the untimed manifold injection of hydrogen. The majority of the discussion will focus on comparisons between the three fuelling systems.

9.6.2 Engine Configuration

The engine's primary fuel was manifold injected methanol. The main fuel can be supplemented with either the early direct injection of hydrogen via the early direct injection and the modified spark-plug injection systems, or the untimed manifold injection of hydrogen.

In all direct injection cases, the injection of hydrogen into the combustion chamber commenced at 170 ^{o}ATDC, the earliest injection could begin without adversely affecting the volumetric efficiency of the engine. A constant hydrogen supply pressure of 48.2 bar (700 psi) was again used to achieve sonic injection thus negating the influence of variations in combustion chamber pressure. Varying the hydrogen injection duration therefore varied the quantity of hydrogen injected.

As in the untimed manifold injection investigation described in the previous chapter, testing was carried out over a range of HEF's at each value of λ. Due to the earlier injection timing and consequently longer time for mixing, the maximum HEF obtainable at $\lambda = 1.0$ was extended to 30%. The maximum HEF used for untimed manifold injection was limited to 30% HEF in order to only provide test points where a comparison between all three systems was possible[3]. The injection durations varied from 11.6 ^{o}CA ($\lambda = 1.8$, 5% HEF) to 79.6 ^{o}CA ($\lambda = 1.0$, 30% HEF). The amount of each fuel being delivered was varied so as to maintain the same overall air/fuel ratio (or relative air/fuel ratio, λ).

A second Mitsubishi GDI injector had been obtained allowing both the early direct injection and modified spark-plug injection systems to be fitted to the engine at the same time (see also page 167). Both injection systems were plumbed into the same high pressure hydrogen supply line allowing flow rate measurement on either system. A switch was fitted to the injector power supply lead from the engine management unit allowing either one of the injection systems to be actuated but never both at the same time. The low pressure hydrogen regulator supplying the untimed manifold injection system was also plumbed into the high pressure supply after the flow-meter. A shut-off valve was fitted close to the manifold allowing the untimed manifold injection system to be employed at will. Thus at a particular test point, all three fuelling systems could be tested consecutively ensuring that an accurate comparison between systems would be possible.

As with the preliminary engine testing, all engine testing was carried out at a compression ratio of 10:1, at an engine speed of 1500 rpm and at wide open throttle. The level of inlet air heating used was approximately 364 Watts. Thus the operating conditions are the same as those used in the untimed manifold and preliminary early direct injection investigations.

[3]Due to an electronic failure during engine testing, no pressure data was obtained at $\lambda = 1.8$, 30% HEF for the modified spark-plug or manifold injection systems. These missing test points were not obtained at a later stage as is was apparent from earlier testing that it was low levels of supplementation that were primarily of interest.

9.6.3 Fluid Properties

The effect of hydrogen supplementation on the fluid properties of the air/fuel mixture has been discussed in the case of untimed manifold injection on page 114 and in the case of the early direct injection on page 152. Further discussion on fluid properties does not add to the discussion and will thus be omitted for brevity.

9.6.4 Combustion Burn Rate

As in the untimed manifold injection and preliminary early direct injection investigations, a mfb analysis was carried out on the cylinder pressure data acquired at each test point. Figures 9.19 to 9.23 present the results of this analysis showing the effect of hydrogen addition on each different phase of combustion.

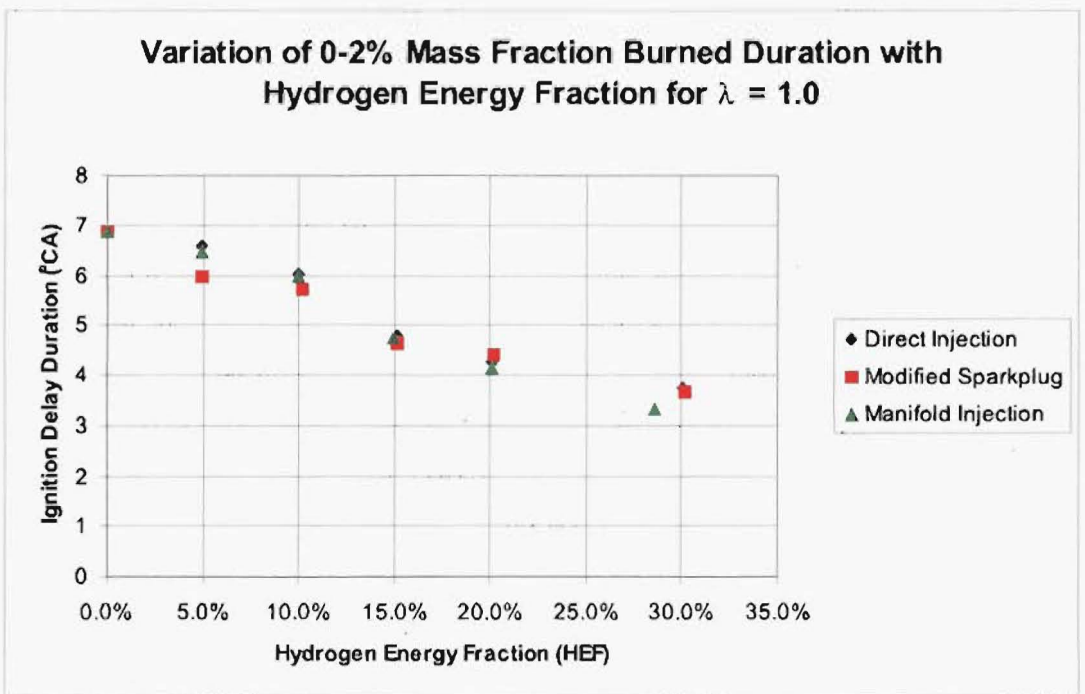

Figure 9.19 Effect of Hydrogen Supplementation on 0-2% mfb, $\lambda = 1.0$

From Figure 9.19 it can be seen that as the HEF is increased at $\lambda = 1.0$, the ignition delay duration is reduced in a linear fashion for all three injection systems. The ignition delay duration values are similar in magnitude and do not exhibit any clear trend as to which system is more beneficial than another. Figure 9.20 shows the variation of the 0-2% mfb duration at $\lambda = 1.8$. It is apparent that the modified spark-plug injection system has a distinct advantage in reducing the ignition delay duration over the others with the addition of 5% HEF. As discussed previously, this is thought to be due to the presence of a localized rich mixture of hydrogen in the vicinity of the spark-plug at the

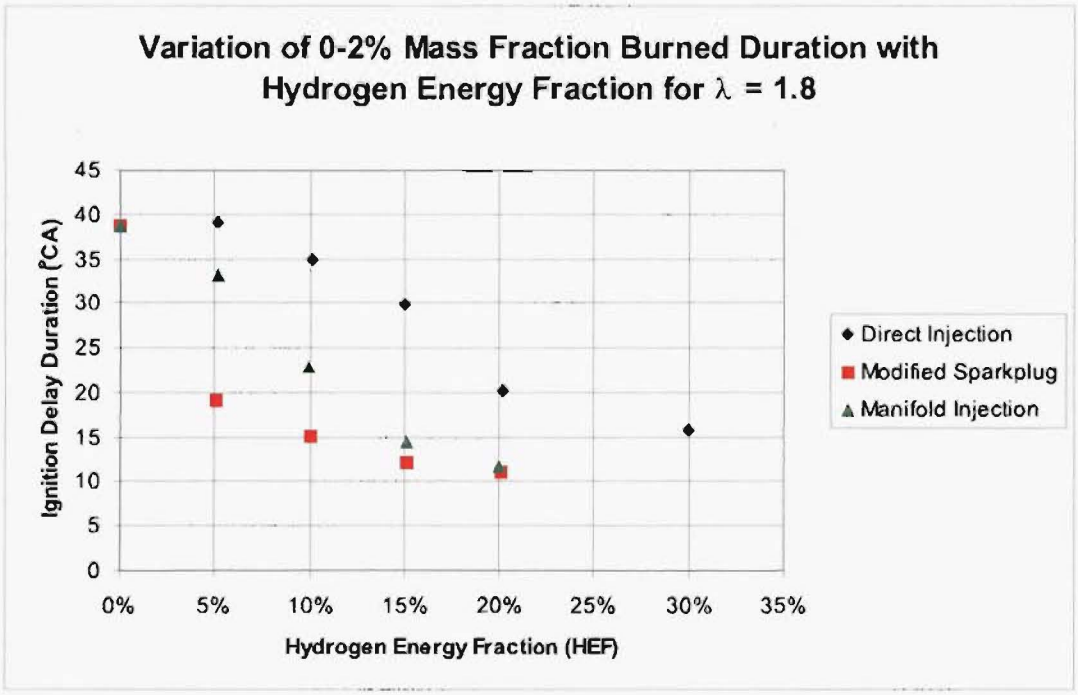

Figure 9.20 Effect of Hydrogen Supplementation on 0-2% mfb, $\lambda = 1.8$

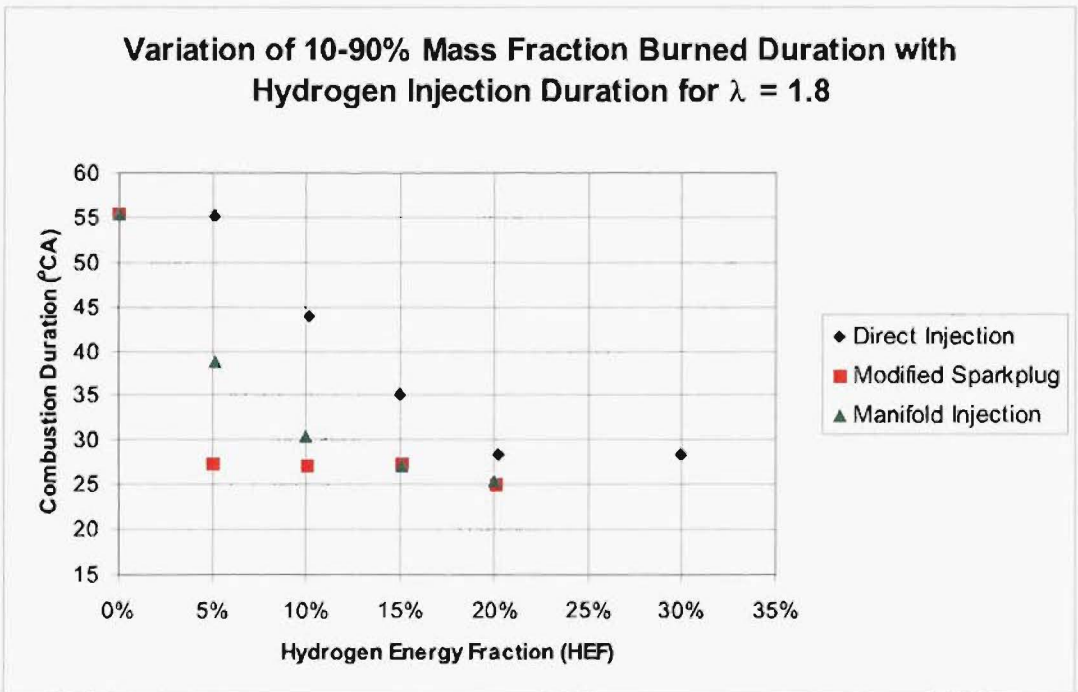

Figure 9.21 Effect of Hydrogen Supplementation on 10-90% mfb, $\lambda = 1.8$

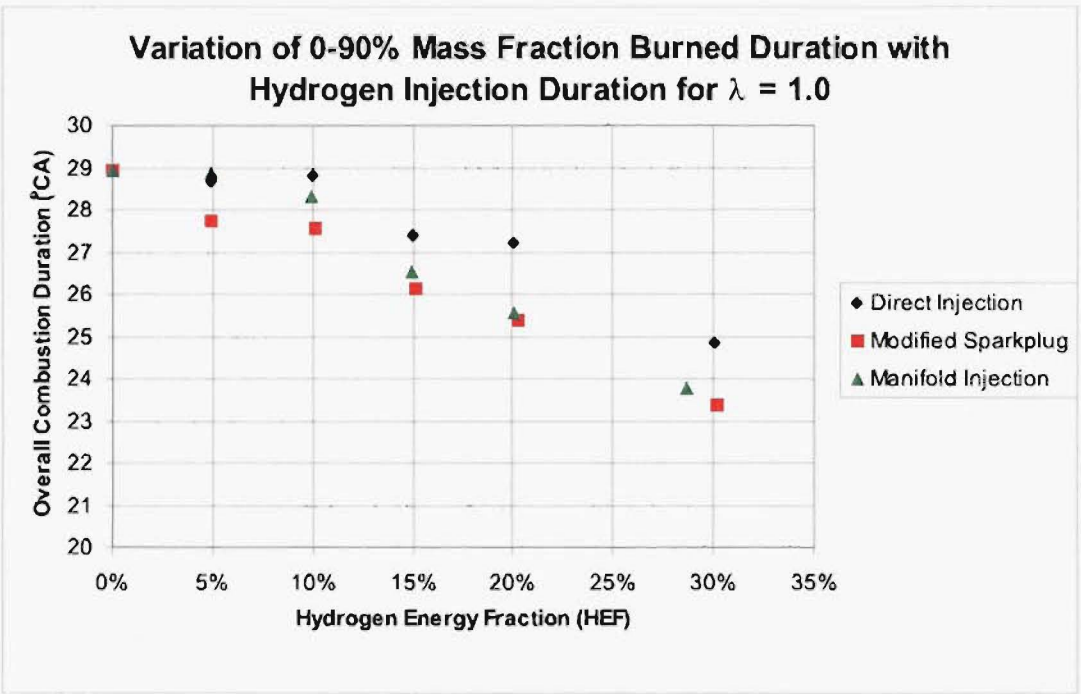

Figure 9.22 Effect of Hydrogen Supplementation on 0-90% mfb, $\lambda = 1.0$

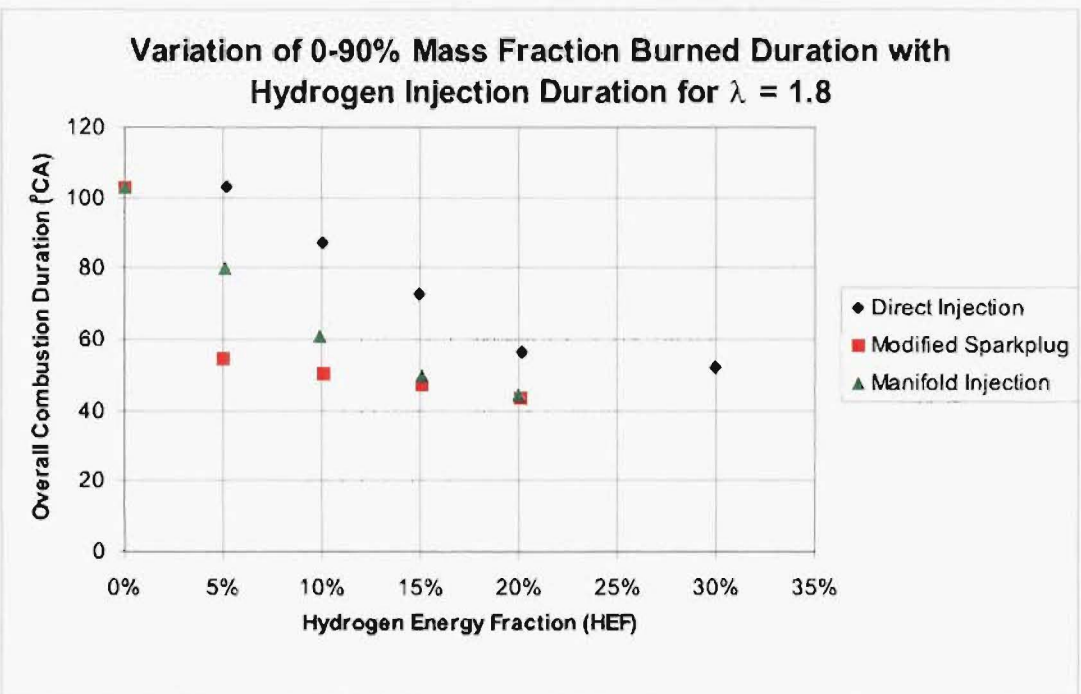

Figure 9.23 Effect of Hydrogen Supplementation on 0-90% mfb, $\lambda = 1.8$

time of ignition. As the HEF increases the 0-2% mfb duration reduces further but not to the same extent as was observed with the initial 5% addition. The inverse stratification of the early direct injection system is apparent as it is unaffected by the addition of 5% HEF but reduces in a linear fashion with HEF's greater than 5%. The homogeneous charge formed by the untimed manifold injection system gives ignition delay values between the two extremes of stratification and the values tend towards those of the modified spark-plug system as the HEF is increased. It is expected that the 0-2% mfb duration for the untimed manifold injection case will approach that of the modified spark-plug system as the HEF is increased but should not become smaller as the stratified charge should always ensure a faster ignition delay duration.

The 2-10% mfb durations show a small reduction with all injection systems with increasing HEF but do not show any clear trends between the systems. For brevity, these plots have been omitted.

The effect of hydrogen supplementation at $\lambda = 1.0$ on the 10-90% mfb duration, like that of the 0-2% mfb duration, is minimal and this plot has been omitted for brevity. Figure 9.21 shows the effect of increasing hydrogen supplementation on the 10-90% mfb duration for $\lambda = 1.8$. It can be seen that as in the $\lambda = 1.8$, 0-2% mfb case the addition of 5% HEF via the modified spark-plug system causes a large reduction in combustion duration. Further increases in HEF result in negligible further reductions in burn duration. This is thought to be due to the fast propagating flame kernel initially formed being able to quickly propagate through the remaining lean air/fuel mixture in the combustion chamber. The early direct injection system again demonstrates a considerably poorer response initially to increasing HEF. However by 30% HEF the 10-90% mfb duration has reduced to a value that is only slightly higher than that obtained with the modified spark-plug and the untimed manifold injection systems. The 10-90% mfb duration of the untimed manifold system decreases rapidly with increasing HEF reaching similar values as obtained with the untimed manifold injection system at 15% HEF. Again these results highlight the advantages of a small quantity of stratified hydrogen over the same quantity of hydrogen as a homogeneous mixture in reducing combustion durations in lean air/fuel mixtures.

Figures 9.22 and 9.23 show the variation of overall combustion duration with increasing HEF for both the $\lambda = 1.0$ and 1.8 cases. Clearly for both mixture strengths the spark advance will have to be retarded as the HEF is increased. However the amount of spark advance will be much greater for $\lambda = 1.8$ than $\lambda = 1.0$. Further for both values of λ and a given HEF the spark advance will be greater for the early direct injection system than the untimed manifold injection system with the modified spark-plug injection system having the least spark advance of all the systems, especially in lean mixtures with low HEF's.

From Figures 9.19 to 9.23 it may be concluded that hydrogen supplementation has a greater effect on leaner mixtures than it does upon richer mixtures of near stoichiometric strength.

The increase in observed combustion rate indicates that the spark timing would need to be retarded in order to maintain MBT spark timing as was the case with the untimed manifold injection of hydrogen. This is what was seen to occur. Figure 9.24 shows the variation in MBT spark timing with HEF for $\lambda = 1.8$. As expected spark timings are progressively retarded at a particular HEF from the early direct injection system to the untimed manifold injection system to the modified spark-plug system reflecting the increase in the rate of combustion. Although the substitution of 5% HEF with the modified spark-plug injection system resulted in an approximately 45°CA faster overall combustion duration compared to the 0% HEF case, this was not reflected the MBT spark timings plotted in Figure 9.24. This is due to the engine operating with such a high level of combustion variation, the determination of an accurate MBT timing was impossible. From the 5% HEF mfb results it appears that the 0% case was in fact too retarded.

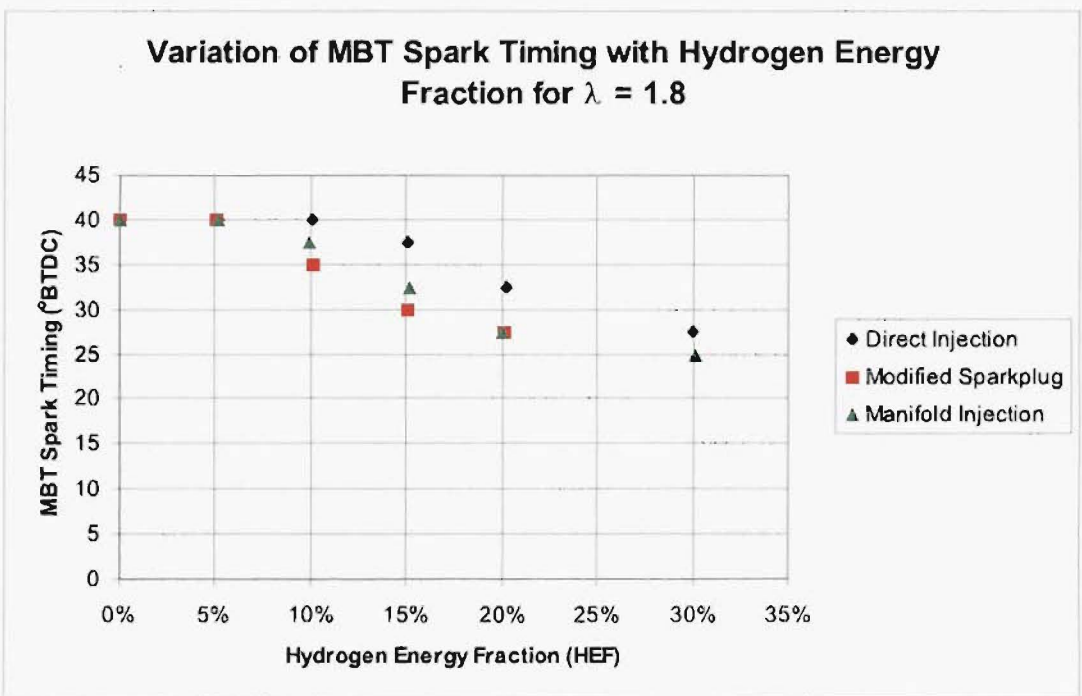

Figure 9.24 MBT Spark Timing verses Hydrogen Energy Fraction for $\lambda = 1.8$

Fuel	Stoichiometric A/F Ratio $\left(\frac{kg_a}{kg_f}\right)$	LCV $\left(\frac{MJ}{kg_f}\right)$	LCV of Stoichiometric Mixture $\left(\frac{MJ}{kg_a}\right)$
Methanol	6.4	19.7	3.078
Hydrogen	34.4	120	3.488

Table 9.2 Relevant Properties of Methanol and Hydrogen

9.6.5 Engine Power Output

One objective of injecting supplementary hydrogen directly into the combustion chamber of the engine was to overcome the volumetric efficiency penalty that dominated the engine performance characteristics of the untimed manifold injection system.

Figure 9.25 shows the variation of volumetric efficiency with HEF for $\lambda = 1.0$. Only $\lambda = 1.0$ will be used for the purposes of discussion as the volume of hydrogen injected is greater than that for the $\lambda = 1.8$ case and the resulting trends are clearer. The trends for the $\lambda = 1.8$ case are similar with the volumetric efficiency of lean mixtures being greater than that of richer mixtures. As was discussed in the untimed manifold case, this is due to the reduction of fuel vapor in the inlet mixture. From Figure 9.25 it can be seen that as the HEF increases, the volumetric efficiency remains essentially constant for the early direct injection and modified spark-plug injection systems. This is the desired effect of direct injection where increasing the levels of hydrogen supplementation has no adverse effect on the breathing of the engine. For the untimed manifold injection system however the volumetric efficiency can be observed to decrease as the HEF is increased. This result was found previously with untimed manifold injection and is thought to be due to the manifold induced hydrogen displacing inlet air that would have, in the absence of hydrogen supplementation, been induced into the engine. A slight increase in volumetric efficiency would be expected for the early direct and modified spark-plug injection systems as HEF increases due to a reduction in the volume of air being displaced in the inlet manifold by methanol vapor. This gain however would be offset by a reduction in the beneficial effect of charge cooling provided by the methanol. These two effects appear to have cancelled each other out resulting in constant volumetric efficiency with increasing HEF. On the basis of these observations, the decrease in volumetric efficiency with increasing HEF observed with untimed manifold injection (see page 123) can be attributed primarily to the addition of hydrogen to the inlet manifold of the engine.

The observed improvement in volumetric efficiency with direct injection over manifold injection with increasing HEF will have an impact on the quantity of fuel that can be burnt in each engine cycle. Figure 9.26 shows the variation of the total fuel energy con-

sumed (both methanol and hydrogen) with HEF again at $\lambda = 1.0$. The following trends can be observed. First, the amount of energy consumed by the direct injection systems reduces slightly then increases with increasing HEF. The reduction in total fuel energy is because the value of λ for the 0% HEF case was 0.995 while the value of λ for HEF's of 5% and above was $\approx$1.01 thus accounting for the slightly higher energy consumption at 0% HEF. The trend of increasing energy consumption with increasing HEF can be explained in terms of the respective stoichiometric air/fuel ratios and calorific values of the two fuels which are given in Table 9.2. It can be seen from Table 9.2 that the Lower Calorific Value (LCV) of a stoichiometric mixture of hydrogen and air is higher than a corresponding mixture of methanol and air (3.488 (MJ/kg$_a$) verses 3.078 (MJ/kg$_a$)). For a given mass of air and at a given air/fuel ratio, using hydrogen supplementation results in a charge with a higher energy content than would be achieved if methanol alone was the fuel. When supplementing the engine with directly injected hydrogen the volumetric efficiency remained essentially constant (constant mass of air induced) as the HEF is increased. Thus while maintaining the same overall air/fuel ratio, the total energy of the charge must increase as the HEF is increased. The second major trend is in the untimed manifold injection case where the amount of energy decreased as the HEF increased for HEF's $< 30\%$, reflecting the decrease in volumetric efficiency with increasing HEF. The value at 30% HEF however does not fit the trend of the lower HEF's and has a higher value than the both the 15% and 20% HEF's. This is due to the 30% HEF test point having a value of λ of 0.96 while the rest of the untimed manifold test points have were taken at $\lambda \approx 1.01$.

Figure 9.27 shows the variation in IMEP$_g$ with increasing HEF for $\lambda = 1.0$. The increase in total fuel energy for the direct injection systems with increasing HEF has not resulted in increasing IMEP$_g$ with HEF as would be expected. Instead the IMEP$_g$, at best, stays constant with increasing HEF in the early direct injection case and slightly decreases with increasing HEF in the modified spark-plug injection case. Both direct injection systems would be expected to give very similar values of IMEP$_g$. The observed slight differences in IMEP$_g$ as well as the failure to produce increasing IMEP$_g$ values with increasing HEF could be due to the either system or both having an over advanced or retarded spark timing. The values of IMEP$_g$ for the manifold injection system reduce with increasing HEF as was expected from Figure 9.26. The 30% HEF test point however failed to show an increased value of IMEP$_g$ despite having an increased energy consumption compared to the 20% HEF case. This again is likely to be due to the spark timing being too advanced (see also the discussion on isNO$_x$).

Figure 9.28 shows the variation in IMEP$_g$ with increasing HEF for $\lambda = 1.8$. The trends exhibited in this Figure are very different from those shown for the $\lambda = 1.0$ case in Figure 9.27. The value of IMEP$_g$ is low for the 0% HEF case and increases rapidly as the

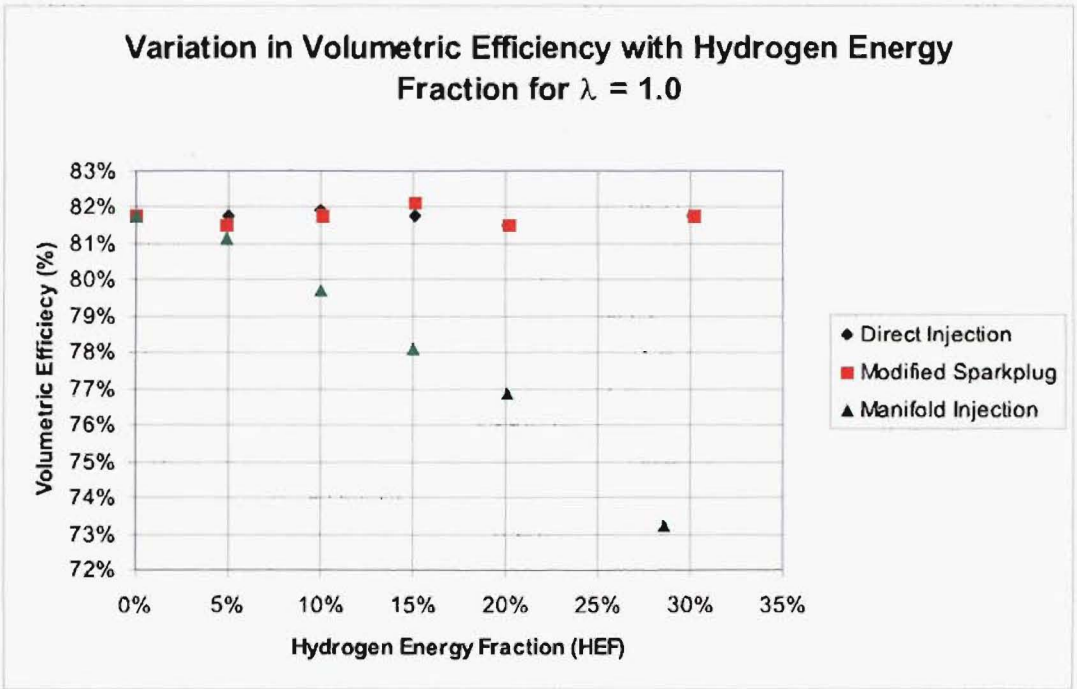

Figure 9.25 Volumetric Efficiency verses Hydrogen Energy Fraction for $\lambda = 1.0$

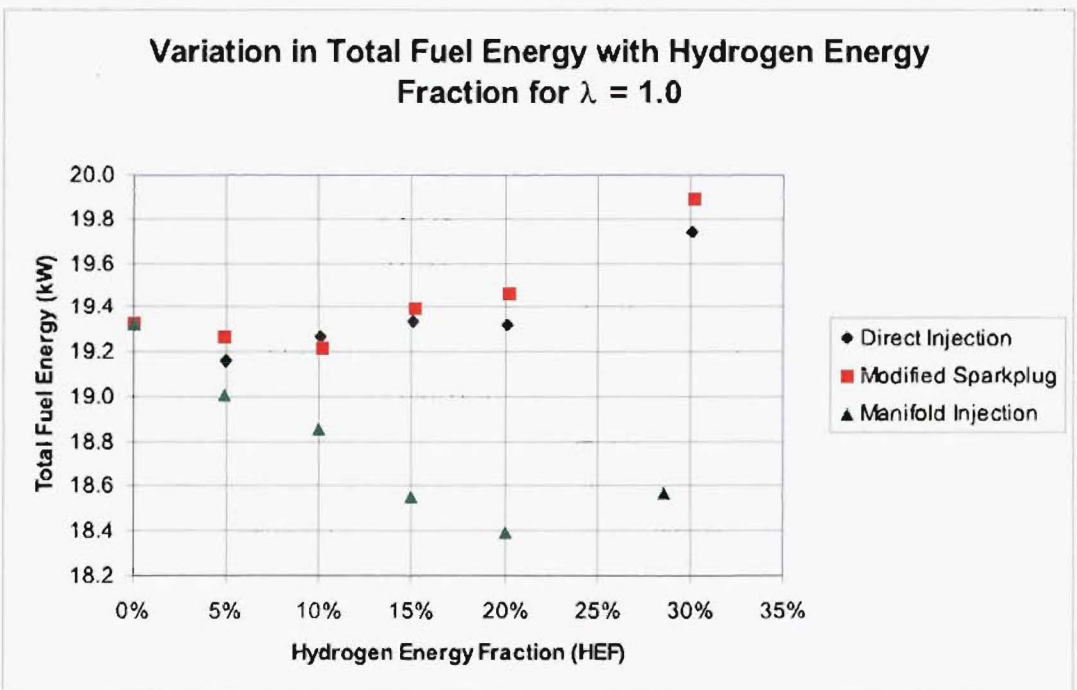

Figure 9.26 Total Fuel Energy verses Hydrogen Energy Fraction for $\lambda = 1.0$

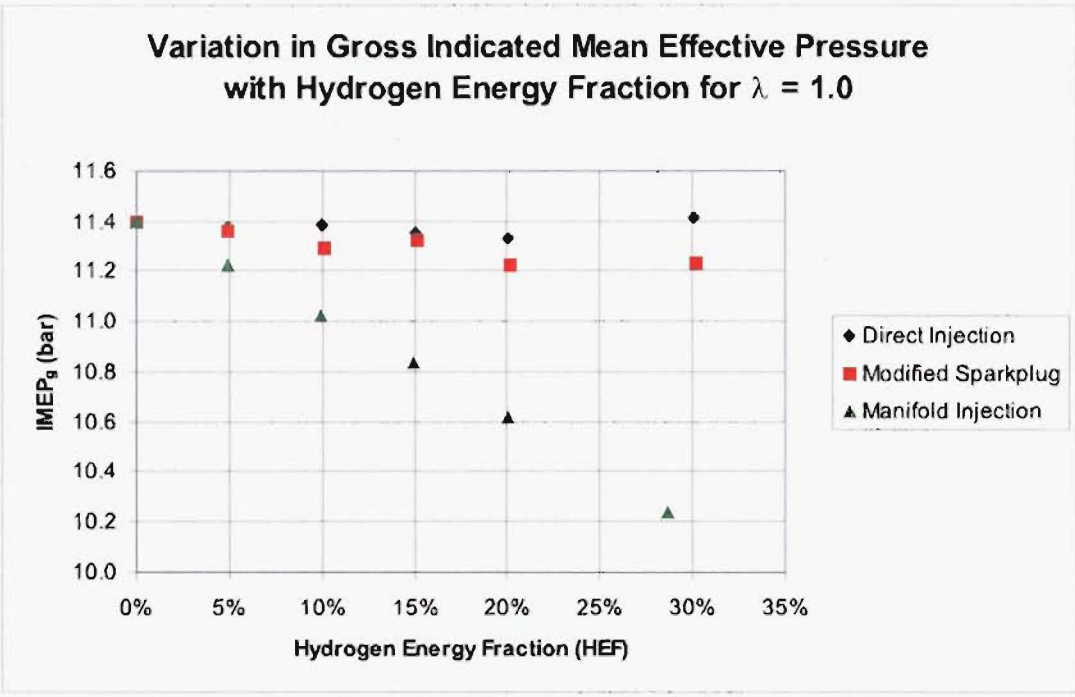

Figure 9.27 Effect of Hydrogen Supplementation on Gross Indicated Mean Effective Pressure for $\lambda = 1.0$

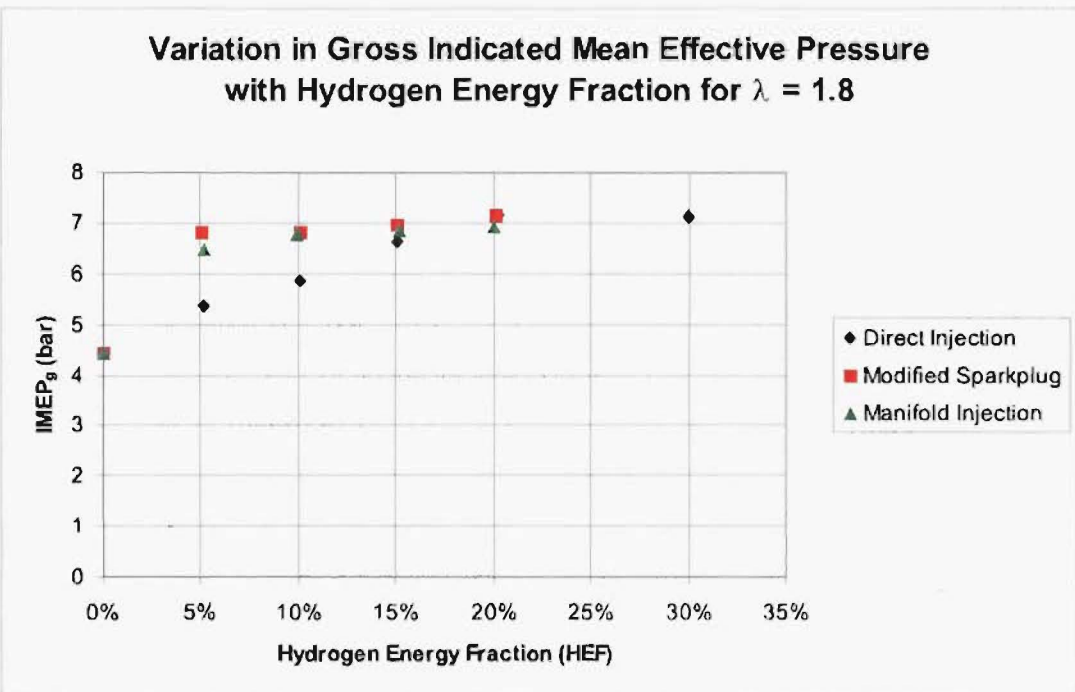

Figure 9.28 Effect of Hydrogen Supplementation on Gross Indicated Mean Effective Pressure for $\lambda = 1.8$

HEF is increased. The modified spark-plug injection system shows the largest increase in $IMEP_g$ with the addition of 5% HEF followed by the untimed manifold injection system and the early direct injection system. For HEF's greater than 5% the modified spark-plug system and the untimed manifold injection system only slowly increase in value. The early direct injection system however increases steadily with increasing HEF until 20% HEF where it reaches a value comparable to the other two injection systems. The trends in $IMEP_g$ are thought to be largely due to the reduction in COV_{IMEPg} with increasing HEF as shown in Figure 9.29. The plot of COV_{IMEPg} in Figure 9.29 is a virtual mirror image of the plot of $IMEP_g$ in Figure 9.28. Increased cyclic variability is known to result in a reduction in power in an engine [Young 1981]. There are two key results that can be obtained from Figure 9.28. First, the near maximum level of power obtainable from the engine at $\lambda = 1.8$ can be achieved with the minimum level of hydrogen substitution if the hydrogen is injected early in the compression stroke through the modified spark-plug injection system. Secondly, operating the engine at higher levels of HEF with the modified spark-plug injector system does not significantly improve the power produced by the engine. Thus it appears that it is optimal to use the minimum level of hydrogen substitution with the modified spark-plug injector system.

The values of COV_{IMEPg} for $\lambda = 1.0$ are low ($\approx$1.2%) as would be expected for a stoichiometric air/fuel mixture and show very little improvement with increasing HEF. This plot has been omitted for brevity, as it is the effect of hydrogen supplementation in lean air/fuel mixtures that is of interest. Figure 9.29 shows the variation in COV_{IMEPg} with HEF for $\lambda = 1.8$. It is apparent that the addition of 5% HEF with the modified spark-plug system results in a dramatic reduction in COV_{IMEPg} and further increasing the HEF does not result in a significant improvement in the COV_{IMEPg}. The value of COV_{IMEPg} for the untimed manifold injection system also decreases rapidly with HEF reaching a plateau with a value slightly below that of the modified spark-plug system at HEF = 15%. The reason for the value of COV_{IMEPg} being lower than that of the modified-spark plug system at higher levels of HEF is thought to be as follows. Although the modified spark-plug system has faster 0-2% duration than the untimed manifold injection system for HEF's of >10%, the untimed manifold injection system exhibits less variability for the 0-2% mfb duration (see Figure 9.30). The reasons for the higher COV 0-2% mfb duration of the modified spark-plug injection system are thought to lie in cycle-by-cycle variations in the composition and distribution of the stratified charge around the spark-plug. The values of COV_{IMEPg} for the early direct injection system reduce in an approximately linear fashion before reaching a plateau at HEF = 20%. The minimum value of COV_{IMEPg} for the early direct injection system is however higher than the minimum value of COV_{IMEPg} attained for the other two injection systems possibly reflecting the inverse stratification of the charge formed.

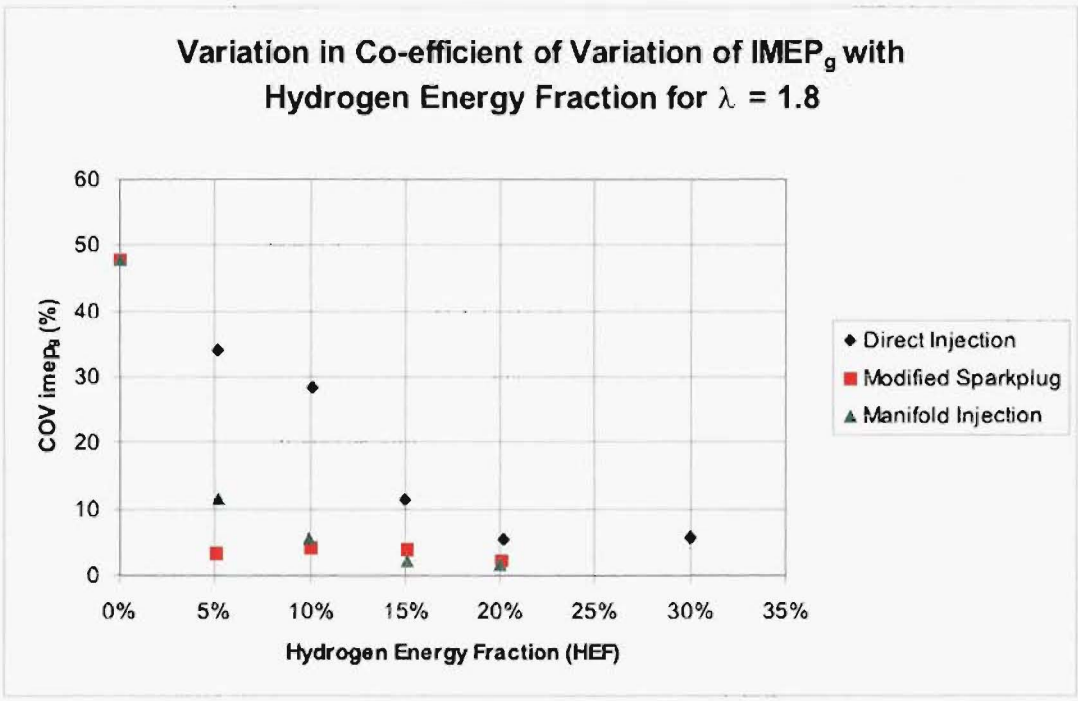

Figure 9.29 Effect of Hydrogen Supplementation on the Coefficient of Variation of Gross Indicated Mean Effective Pressure for $\lambda = 1.8$

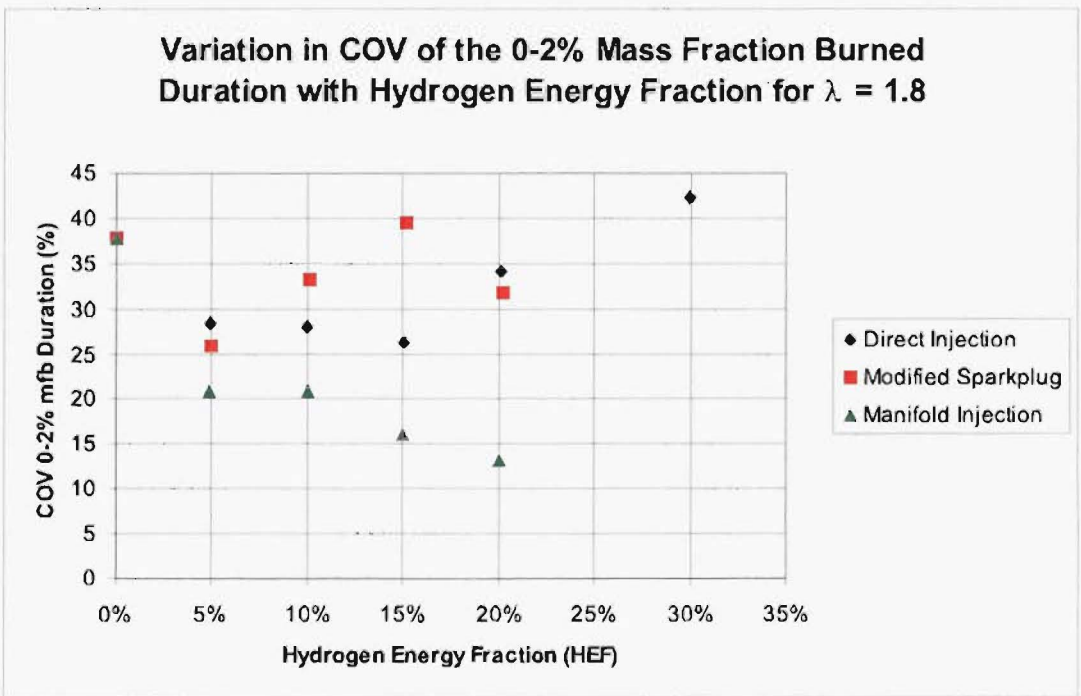

Figure 9.30 Effect of Hydrogen Supplementation on the Coefficient of Variation of 0-2% mfb Duration for $\lambda = 1.8$

9.6.6 Engine Thermal Efficiency

Figure 9.31 shows the variation in gross indicated thermal efficiency with HEF for $\lambda = 1.0$. An in depth discussion on the thermal efficiency of an engine was presented during the discussion on the untimed manifold injection of hydrogen (page 129). As was the case for the untimed manifold injection results, the anticipated gains in thermal efficiency due to improved combustion and fluid thermodynamic properties were not apparent. It can be seen that η_{ith} is at a maximum at 5% HEF and decreases slightly as the HEF is increased. This trend is due to the value of $IMEP_g$ remaining constant as the HEF and energy input increases. Figure 9.31 also indicates that there is little point from an efficiency point of view in operating at $\lambda = 1.0$ with high levels of HEF.

Figure 9.32 shows the variation in gross indicated thermal efficiency with HEF for $\lambda = 1.8$. This follows the trends previously observed in $IMEP_g$ for $\lambda = 1.8$. Again as was the case for $IMEP_g$, it is optimal to use the minimum level of hydrogen substitution with the modified spark-plug injector system. Using higher levels of HEF do not lead to significant improvements in η_{ith}.

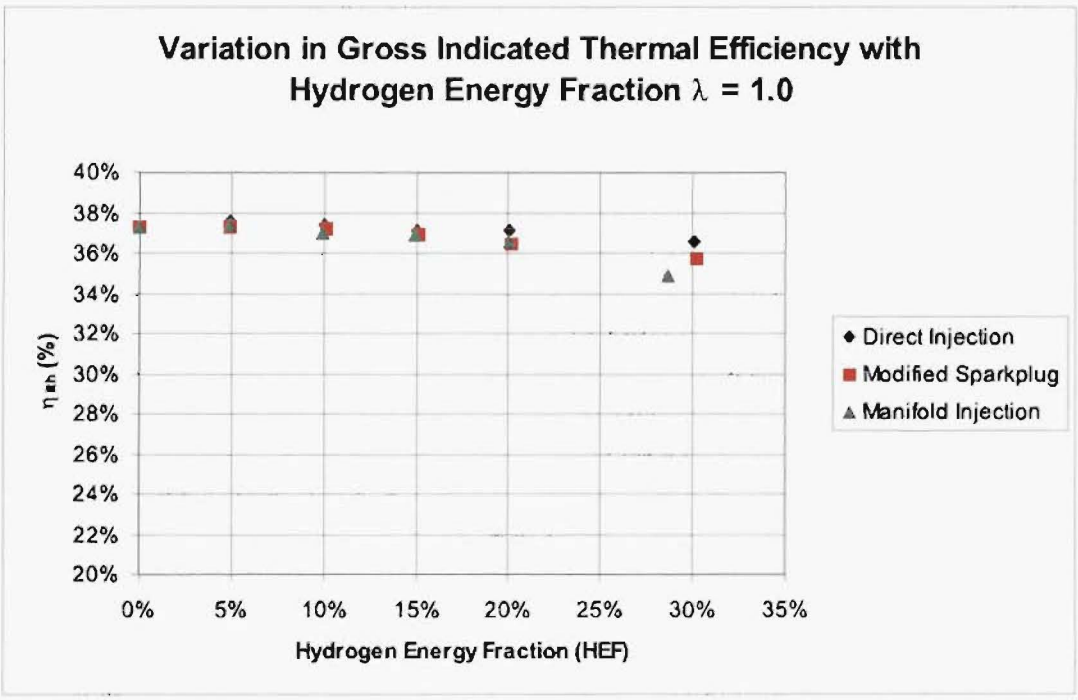

Figure 9.31 Effect of Hydrogen Supplementation on Gross Indicated Thermal Efficiency for $\lambda = 1.0$

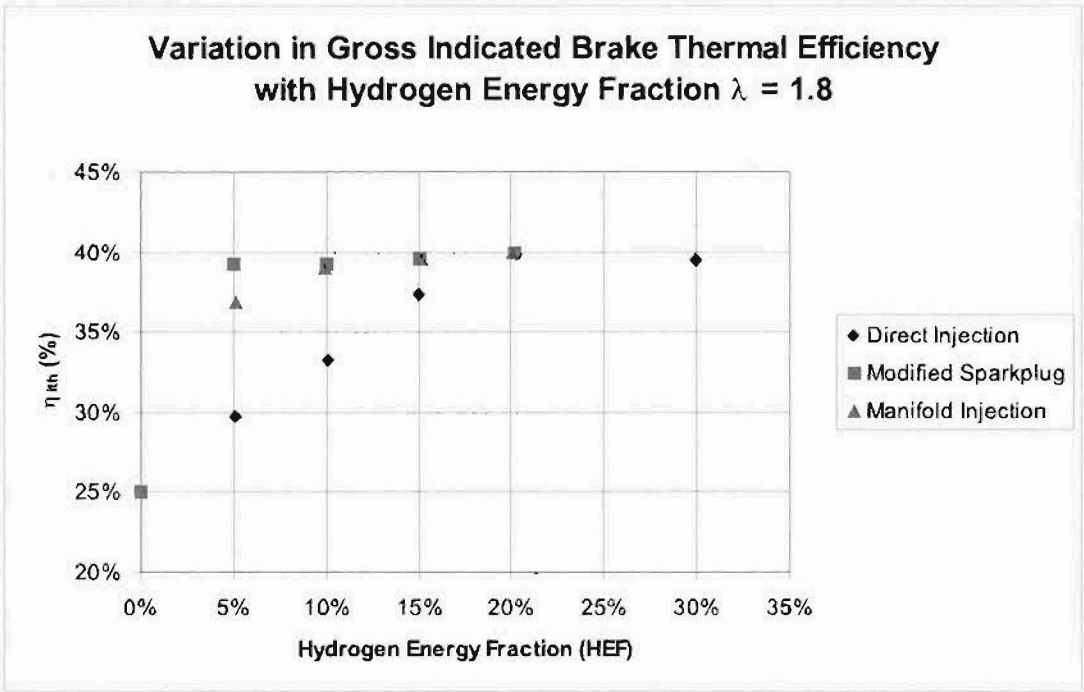

Figure 9.32 Effect of Hydrogen Supplementation on Gross Indicated Thermal Efficiency for $\lambda = 1.8$

9.6.7 Engine Emissions

The trend in exhaust gas temperature with increasing HEF are similar to those already discussed with the untimed manifold injection hydrogen.

The variation in isNO_x emissions with HEF are shown in Figure 9.33 for $\lambda = 1.0$. The peak isNO_x emissions occur at HEF = 0% and are reduced as the HEF is increased. The value of isNO_x for the 30% HEF untimed manifold injection case is however much higher than the values for the other injection systems. It was noted previously that this test point is richer than the other manifold injection test points (see Figure 9.26). As the air/fuel mixture is richer, is thought that the spark timing at this point could be too advanced as previously discussed with $IMEP_g$. The increased isNO_x could to be due to the spark timing being advanced from MBT resulting in reduced power and higher peak cylinder pressures (and therefore temperatures) resulting in higher levels of NO_x production. The reduction in isNO_x emissions is thought to be due to a reduction in oxygen availability as the HEF is increased. For a more in depth discussion on isNO_x formation mechanisms, refer to the untimed manifold discussion on page 134.

The variation in isNO_x emissions with HEF are shown in Figure 9.34 for $\lambda = 1.8$. When comparing Figures 9.33 and 9.34 it can be seen that operating the engine at λ = 1.8 results in much reduced levels of isNO_x than when the engine is operated at λ =

1.0 highlighting one of the important reasons for the desire to operate an engine in the lean region. It is also apparent that the levels of $isNO_x$ decrease rapidly with increasing HEF and appear to reach a plateau at HEF $\geq$ 20%. At $\lambda = 1.8$ one of the main dominating influences on NO_x production, peak cylinder temperature, is not conducive to NO_x formation. Therefore it is thought that the reduction in $isNO_x$ is due mainly to a combination of increased $IMEP_g$ and reduced COV_{IMEP_g} as the HEF is increased.

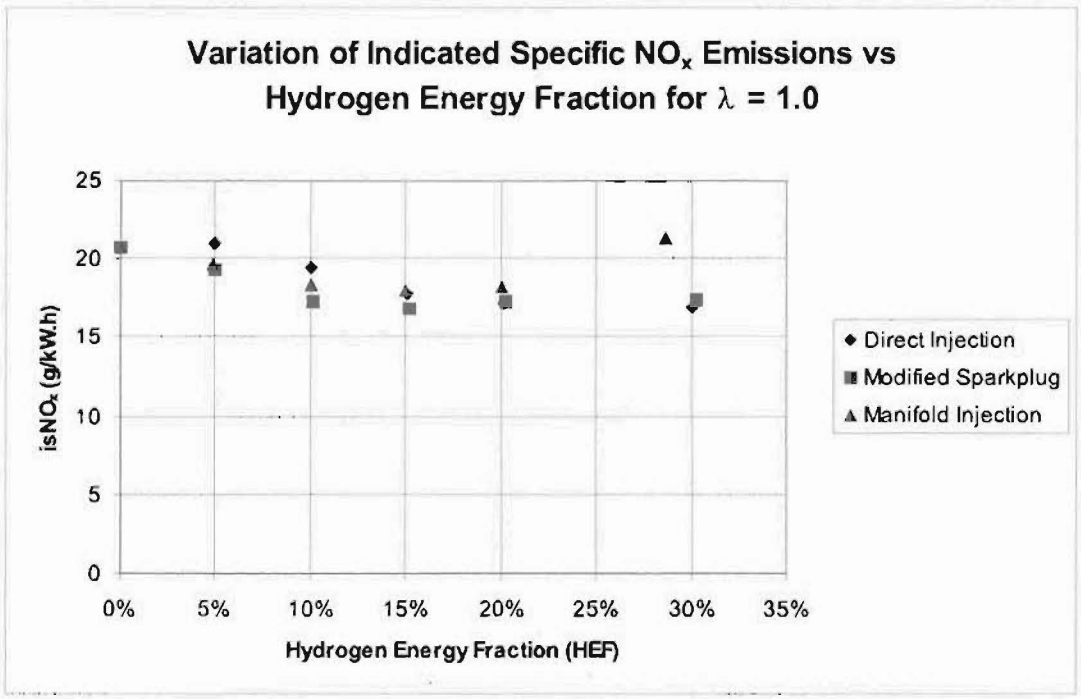

Figure 9.33 Indicated Specific NO_x Emissions verses Hydrogen Energy Fraction for $\lambda = 1.0$

Figure 9.35 shows the variation in isUHC emissions with HEF as measured with the FID for $\lambda = 1.0$. It can be seen that the isUHC emissions for all three injection systems reduce as the HEF is increased as was expected and found previously with the untimed manifold injection of hydrogen. It is expected that the same mechanisms as were highlighted in the untimed manifold case are responsible for the observed decreases in UHC with increasing HEF for a particular value of λ. These mechanisms are:

1. Reduction in mass flow rate of methanol.

2. Decrease in peak cylinder pressures resulting in a reduction in UHC formed in crevice volumes.

3. Increase in flame speed reducing the UHC formed due to quenching of the flame on the combustion chamber walls.

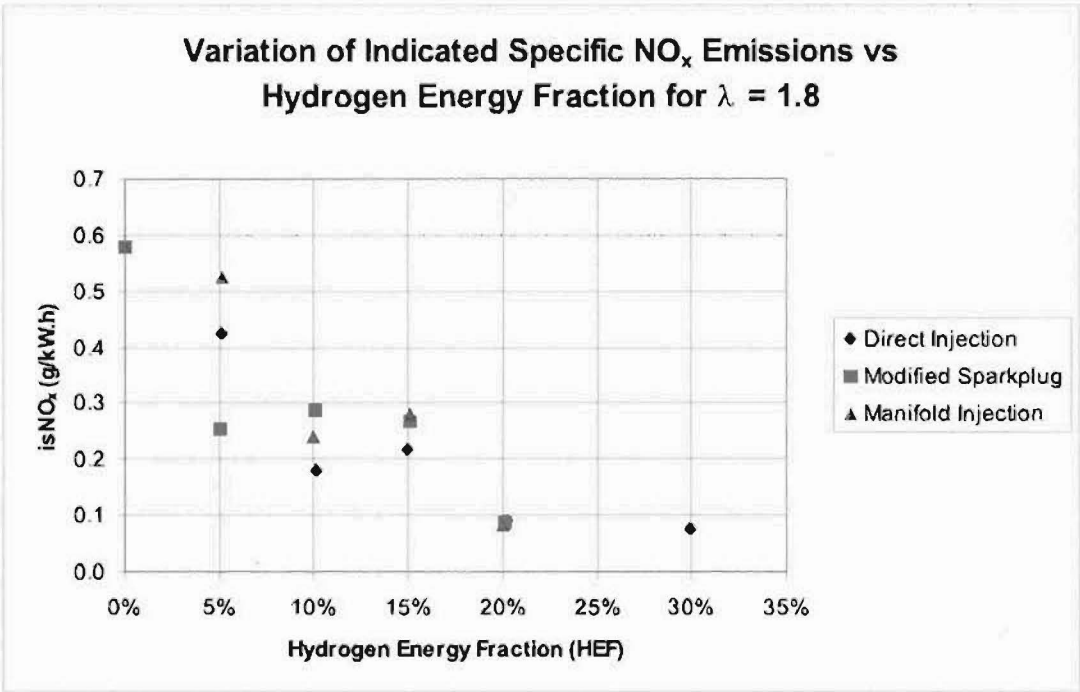

Figure 9.34 Indicated Specific NO_x Emissions verses Hydrogen Energy Fraction for $\lambda = 1.8$

As was the case with untimed manifold injection, the relative magnitude of each mechanism is unknown but the observed reduction in UHC is likely to be a combination of all three of these mechanisms. The level of isUHC emissions are of a similar level for both the early direct injection and the modified spark plug injection systems over the range of HEF's. The isUHC levels for the modified spark-plug system are slightly higher than that of the early direct injection system. This difference could be due to the modified spark-plug arrangement producing a slightly lower value of $IMEP_g$ than the early direct injection system (see Figure 9.27). If the increased dead volume contained in the hypodermic of the modified spark-plug system was causing an increase in crevice hydrocarbon emissions over the early direct injection system, it is only very slight. This is somewhat surprising given that the major source of UHC emissions at near stoichiometric operating conditions is crevice volumes [Cheng *et al.* 1993]. It was thought that when operating with the modified spark-plug arrangement the hypodermic would contain mostly unburned hydrogen and compressed hydrogen rich products of combustion. When operating with the early direct injection system however it was thought that a greater proportion of gas containing products of methanol combustion would have been compressed into the hypodermic increasing the UHC emissions. This does not appear to be the case and is an area that requires further investigation. The isUHC values for the untimed manifold system are higher that those for the direct injection systems due to the lower values of $IMEP_g$ produced at a given HEF by the untimed manifold injection system.

Figure 9.36 shows the variation in isUHC emissions with HEF as measured with the FID for $\lambda = 1.8$. When comparing Figures 9.35 and 9.36 it can be seen that operating the engine at $\lambda = 1.8$ results in much higher levels of isUHC emissions than when the engine is operated at $\lambda = 1.0$. As the HEF is increased the level of isUHC emissions are reduced significantly. Comparing Figure 9.36 to Figure 9.29 it is thought that the reduction in isUHC emissions for $\lambda = 1.8$ with increasing HEF is due largely to the corresponding reduction in cycle-by-cycle variability of the combustion process. The mechanisms listed above will all also play a role in the formation of UHC emissions but is appears that for $\lambda = 1.8$, the formation of UHC emissions is dominated by the cyclic variability in the combustion process as the engine operates near it's effective lean limit. While this investigation has not focused on UHC emissions in particular, this is an area that would benefit from further in depth study.

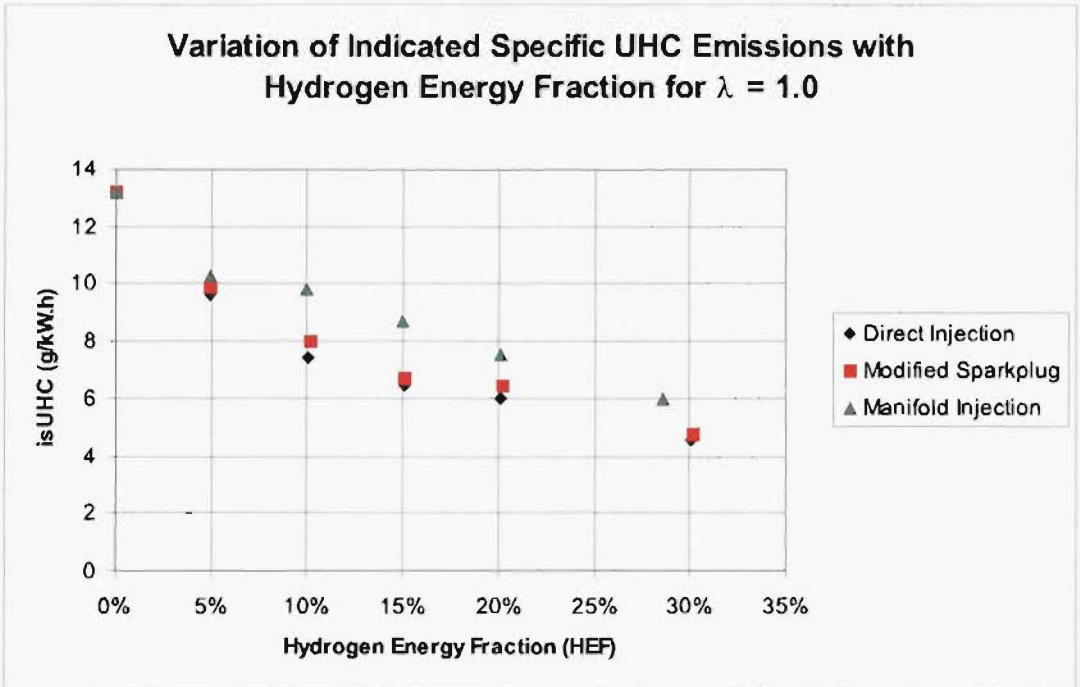

Figure 9.35 Indicated Specific UHC Emissions verses Hydrogen Energy Fraction for $\lambda = 1.0$

The variation of isCO emissions with increasing HEF is presented in Figure 9.37 for $\lambda = 1.0$ and in Figure 9.38 for $\lambda = 1.8$. As was found with untimed manifold injection CO emissions are high for the $\lambda = 1.0$ case as expected as CO production is only significant in stoichiometric and rich mixtures where there is a shortage of oxygen present to fully oxidize the carbon to CO_2. The isCO emissions for $\lambda = 1.0$ are reasonably scattered reflecting small differences in the actual value of λ between each of the test points. The isCO results remain approximately constant with increasing HEF as they would be ex-

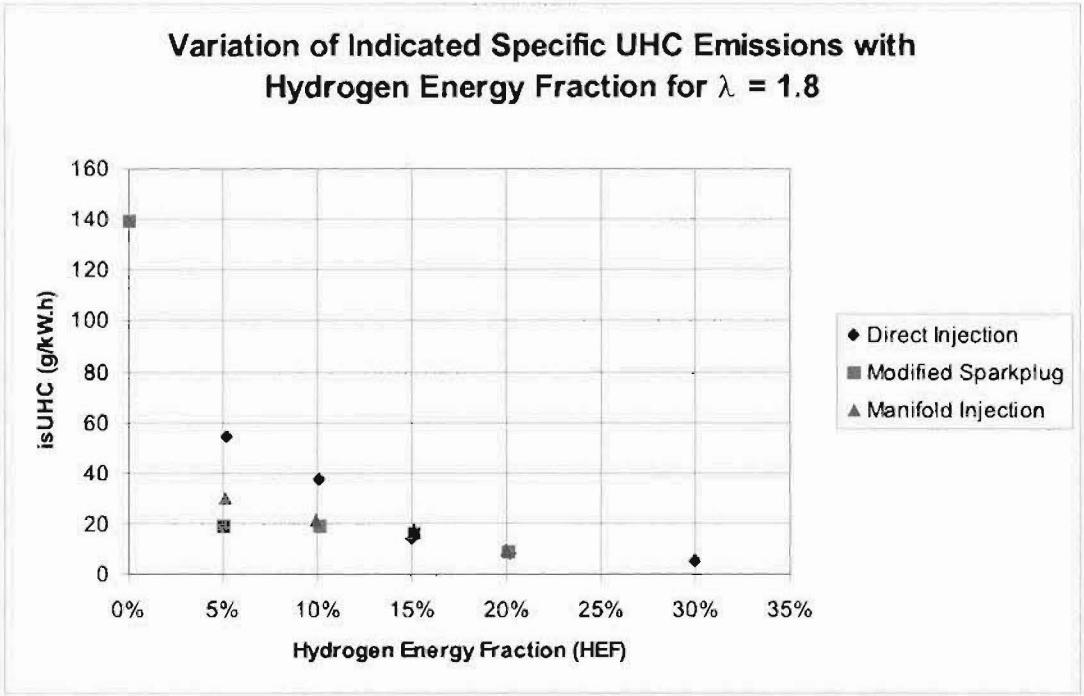

Figure 9.36 Indicated Specific UHC Emissions verses Hydrogen Energy Fraction for $\lambda = 1.8$

pected to do. The $\lambda = 1.8$, 0% HEF case demonstrates a isCO level of a similar value to those obtained with $\lambda = 1.0$ reflecting the level of incomplete combustion occurring. As the HEF is increased however cyclic variability decreases, the level of isCO emissions rapidly decreases reflecting the increase in combustion stability and therefore a more complete oxidization of CO to CO_2.

Figure 9.39 shows the variation in isCO_2 emissions with HEF for $\lambda = 1.0$ while Figure 9.40 shows the variation in isCO_2 emissions with HEF for $\lambda = 1.8$. Both figures show that the isCO_2 emissions decrease as the HEF increases as expected and the quantity of methanol being oxidized is reduced. In the case of $\lambda = 1.8$, the low levels of $IMEP_g$ produced are reflected in the higher values of isCO_2 for the 0% HEF case and in the early direct injection values for HEF's < 20%. Not withstanding the test points exhibiting low values of $IMEP_g$, the isCO_2 emission levels for $\lambda = 1.8$ are very similar to those for $\lambda = 1.0$.

The trends in oxygen emissions with increasing HEF are similar to those already discussed with the untimed manifold injection hydrogen. Further discussion will not add anything and the reader is referred to the untimed manifold injection discussion on page 144.

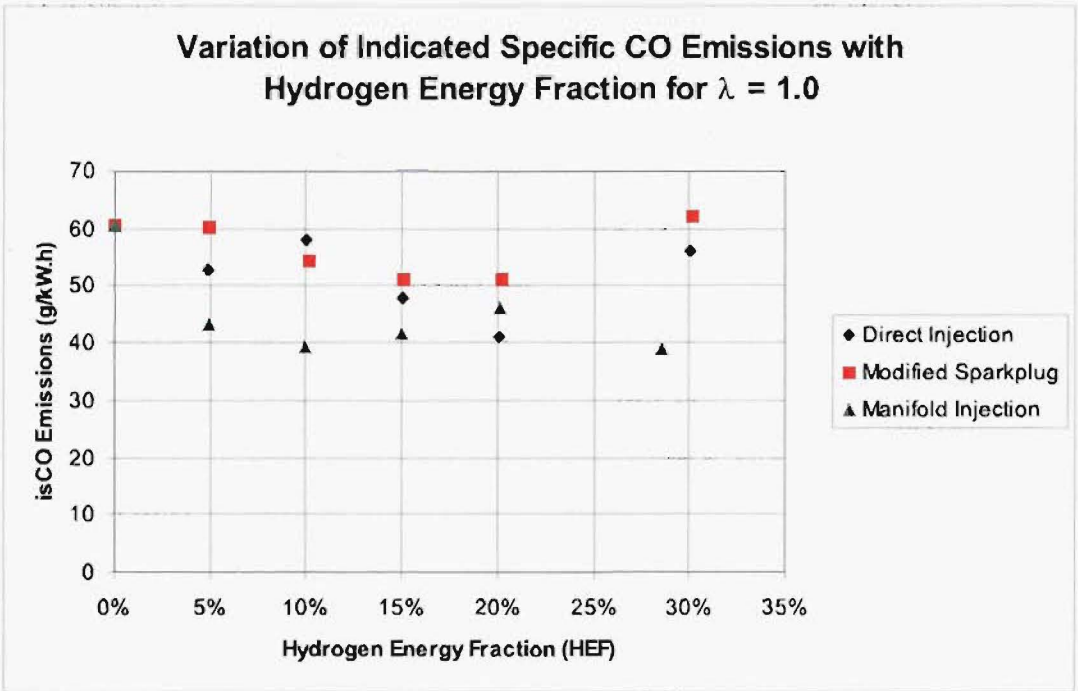

Figure 9.37 Indicated Specific CO Emissions verses Hydrogen Energy Fraction for $\lambda = 1.0$

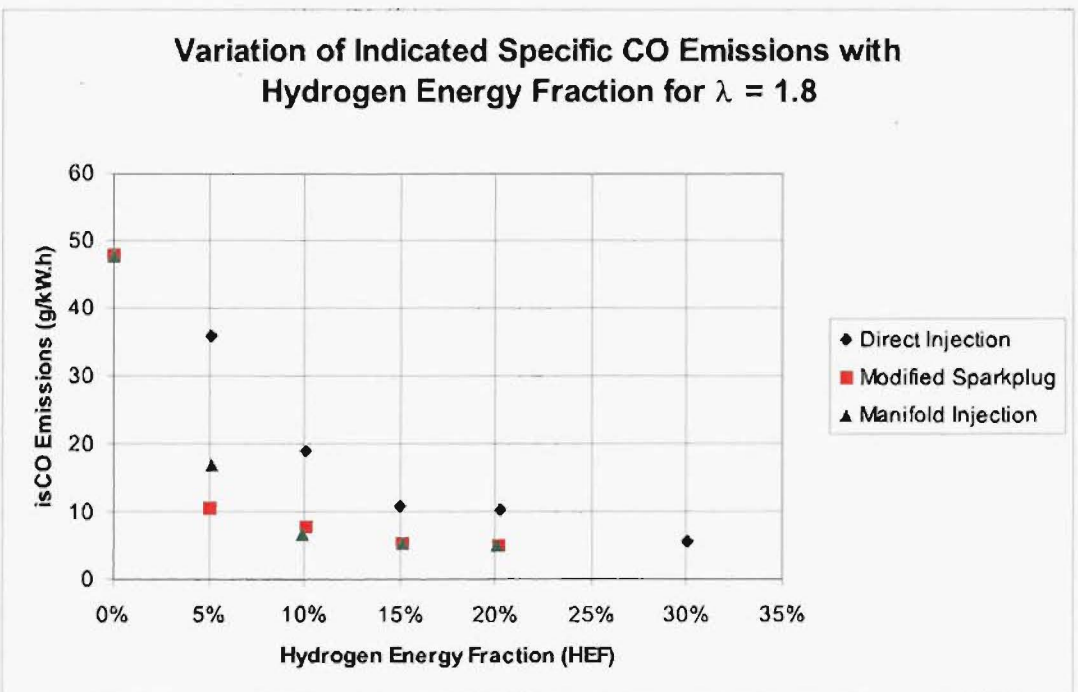

Figure 9.38 Indicated Specific CO Emissions verses Hydrogen Energy Fraction for $\lambda = 1.8$

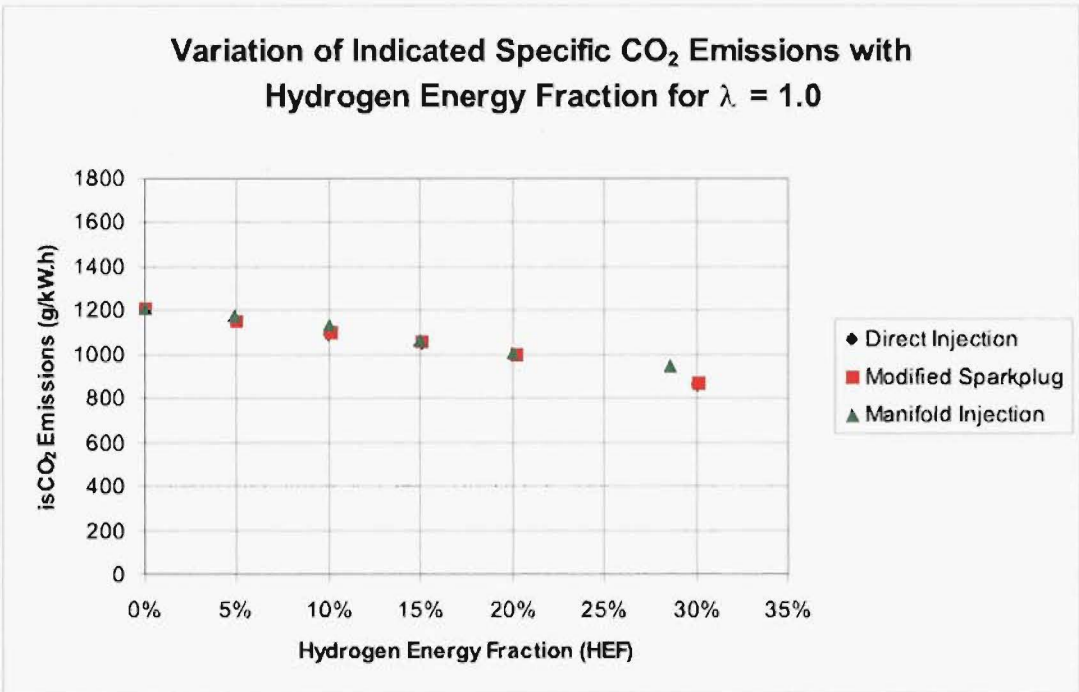

Figure 9.39 Indicated Specific CO_2 Emissions verses Hydrogen Energy Fraction for $\lambda = 1.0$

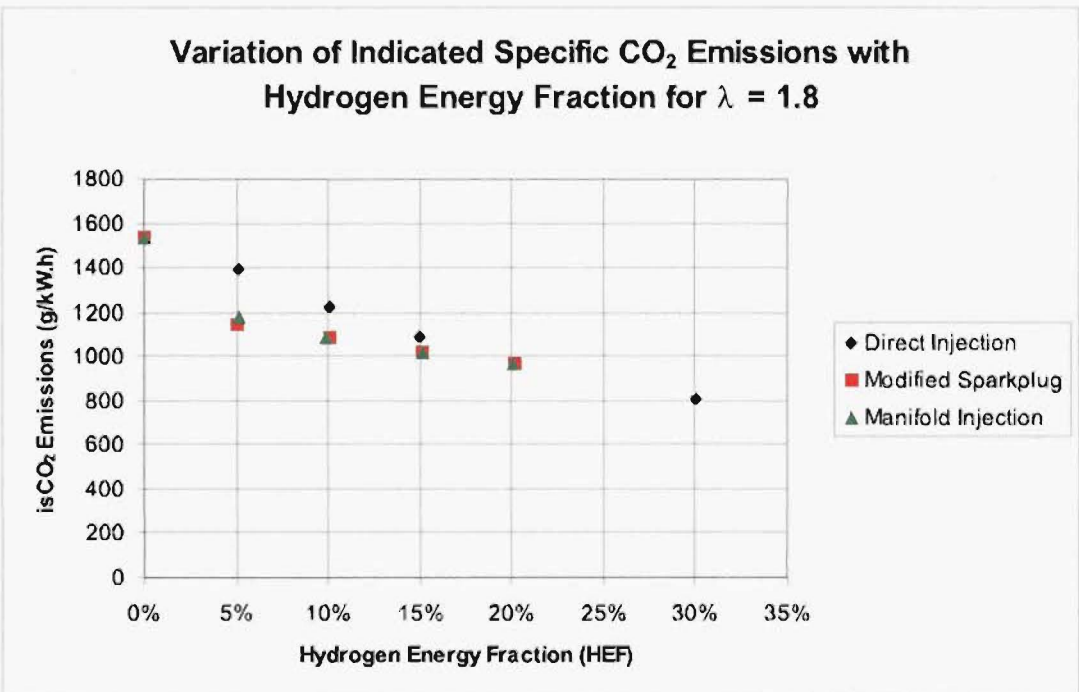

Figure 9.40 Indicated Specific CO_2 Emissions verses Hydrogen Energy Fraction for $\lambda = 1.8$

9.6.8 Summary

This section of work has demonstrated that the most effective method for introducing supplementary hydrogen is early direct injection via the modified spark-plug injection system. The more pronounced effect of the modified spark-plug injection system, for a given level of hydrogen supplementation, is thought to be due to an easily ignitable hydrogen/air in the vicinity of the spark-plug at the time of ignition. The effect of hydrogen addition was most significant on lean air/fuel mixtures. The utilization of HEF's greater than 5% with the modified spark-plug system resulted in only a very slight further improvement in combustion, engine performance and emissions.

9.7 Modified Spark-plug Injection Timing Investigation

Charge stratification has historically been investigated as a method of allowing the lean operating limit of an engine to be extended. The benefits of extending the lean operating limit of an engine lie in improved fuel economy and reduced emissions that can be obtained with the combustion of lean, unthrottled air/fuel mixtures. Charge stratification can be achieved by one of two main methods: the use of a pre-chamber, or direct injection into the combustion chamber (direct injection stratified charge or DISC).

Pre-chamber designs, although effective, generally suffer from reduced efficiencies due to greater heat losses compared to conventional designs. The higher heat losses result from increased surface area and higher turbulence in the pre-chamber. The spark plug ignites a locally rich, easily ignitable mixture in the pre-chamber which then propagates out into the main combustion chamber igniting the lean main charge.

DISC engines are mechanically simpler and as the combustion process is initiated by spark ignition, they offer a wide tolerance to fuel composition and can be operated with a wide range of liquid fuels. The fuel is generally sprayed into a bowl-in-piston combustion chamber where it is swept past the spark plug operating with a long duration discharge.

It was found in the previous section that when the modified spark-plug injector arrangement was used to inject the supplementary hydrogen early in the compression stroke, a hydrogen rich region remained in the vicinity of the spark-plug. It was thought that this localized stratified charge was responsible for the observed decreases in 0-2% mfb duration and the COV_{IMEPg} (see page 176). It is known that the early period of flame development largely dictates how the remainder of the combustion process will proceed. It is also known that the laminar flame speed of the mixture has a large influence

on early flame kernel development [Rauckis and McLean 1979] , [Heywood 1988].

Having established that the most effective method of introducing the supplementary hydrogen into the combustion chamber was via the modified spark plug injector, a short investigation was conducted to determine what the optimum timing of the injection of hydrogen was.

9.7.1 Engine Configuration

The engine's primary fuel is manifold injected methanol. The main fuel can be supplemented with a stratified charge of gaseous hydrogen via the modified spark-plug injection system. For the majority of the testing a hydrogen supply pressure of 41.3 bar (600 psi) was used. This is somewhat lower than the 48 bar that was calculated on page 28. It was determined during the schlieren photography investigation (see page 53) that this pressure gave a good distribution of hydrogen around the spark-plug without creating a jet into the combustion chamber as higher pressures did. As it was found that the puff of hydrogen will not actually enter the combustion chamber until 9 - 18 ^{o}CA after injection is initiated[4], it was thought that injection timings more retarded than 330 ^{o}ATDC would be unlikely to occur. At 330 ^{o}ATDC the minimum pressure required to give sonic flow was calculated to be 22.7 bar. Thus 41.3 bar is sufficiently above this value to ensure that variations in cylinder pressure will not affect the mass of hydrogen being injected. The relative air/fuel ratio chosen for the experimental work was $\lambda = 1.8$ as at this condition the effects of charge stratification are readily apparent. The HEF employed was 5% as it was determined from the preceding investigation that there was little benefit to be gained from using higher levels of HEF with the modified spark-plug injection system. The spark timing was kept constant for all test points at 330 ^{o}ATDC (30 ^{o}BTDC). This value is the MBT value that was found for 5% HEF at $\lambda = 1.8$ with an injection timing of 170 ^{o}ATDC. This value of MBT spark timing is 10^{o}CA more retarded than was previously found for this test condition (see page 182) reflecting the fact that the torque curve is flat near MBT especially in lean mixtures. Determination of accurate values of MBT spark timing is thus very difficult. A constant value of spark timing was used throughout so any changes to the combustion process as a result of changes to the injection timing would be easily identified without having to separate out the effects of changes to the spark timing. The injection timing was initially set at 170 ^{o}ATDC, the value used in the previous testing, and progressively retarded. The methanol flow rate was kept constant for all test points and the injection timing varied. All engine testing was carried out at a compression ratio of 10:1, at an engine speed of 1500 rpm and at

[4]Note:- The schlieren photography investigation of the late puff injector performance (see page 53) indicated that there is a delay of between 1.0 ms and 2.0 ms between the start of injection and when the hydrogen puff is first visible around the spark plug electrode. At an engine speed of 1500 rpm, this equates to a delay of between 9 and 18 ^{o}CA.

wide open throttle. The level of inlet air heating used was approximately 364 Watts. Thus the operating conditions are the same as those used in the untimed manifold and preliminary early direct injection investigations.

9.7.2 Results

Figures 9.41 and 9.42 show the variation in the 0-2% mfb and 0-90% mfb durations as the start of injection is progressively advanced. Also plotted are the values for the 0% HEF case for comparison. The 0-2% mfb duration can be seen to decrease to a minimum at 290 °ATDC before sharply rising as the injection timing is retarded further. As the 0-2% mfb duration is strongly affected by the local air/fuel ratio and mixture motion, it can be surmised that injection at 290 °ATDC results in the optimum conditions for early flame development. As the injection timing is retarded further from 290 °ATDC, it is thought that the injection is occurring too close to the time of ignition resulting in a slower burning rich air/fuel mixture. Figure 9.42 shows that the 0-90% mfb duration is also decreased as the injection timing is retarded. Thus the combustion process as a whole is faster (≈8 °CA) and this occurs with an injection timing of 270 °ATDC.

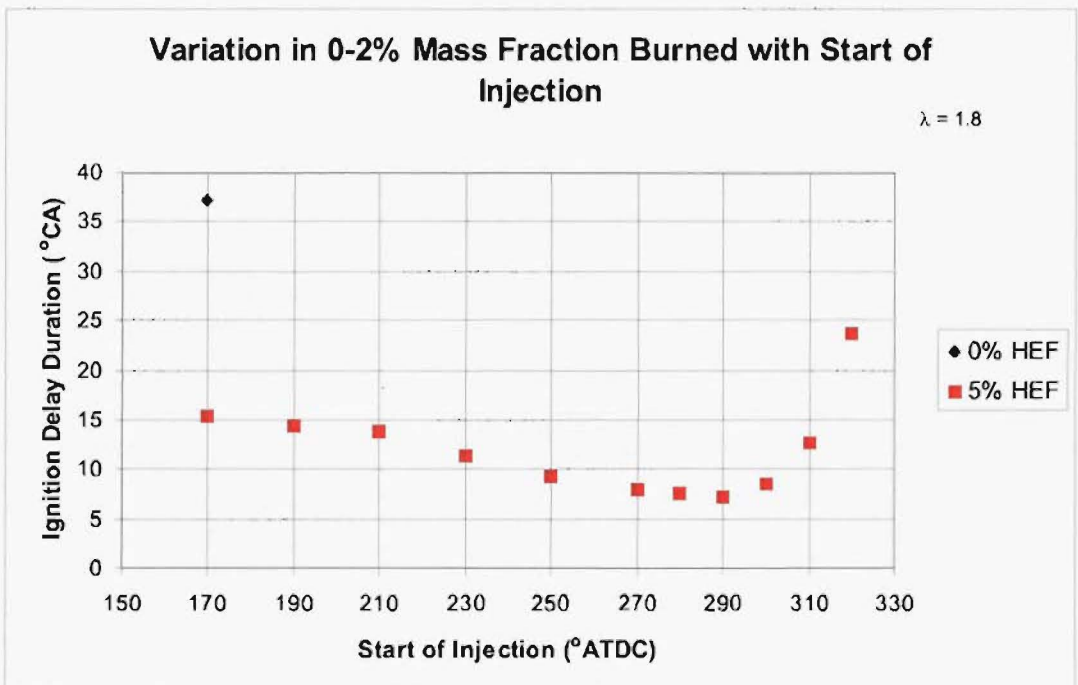

Figure 9.41 Effect of Injection Timing on 0-2% Mass Fraction Burned

The effect of injection timing on the gross indicated mean effective pressure is shown in Figure 9.43. It can be seen that the $IMEP_g$ remains essentially constant as the start of injection is retarded. As the injection timing is retarded past 290 °ATDC the value of

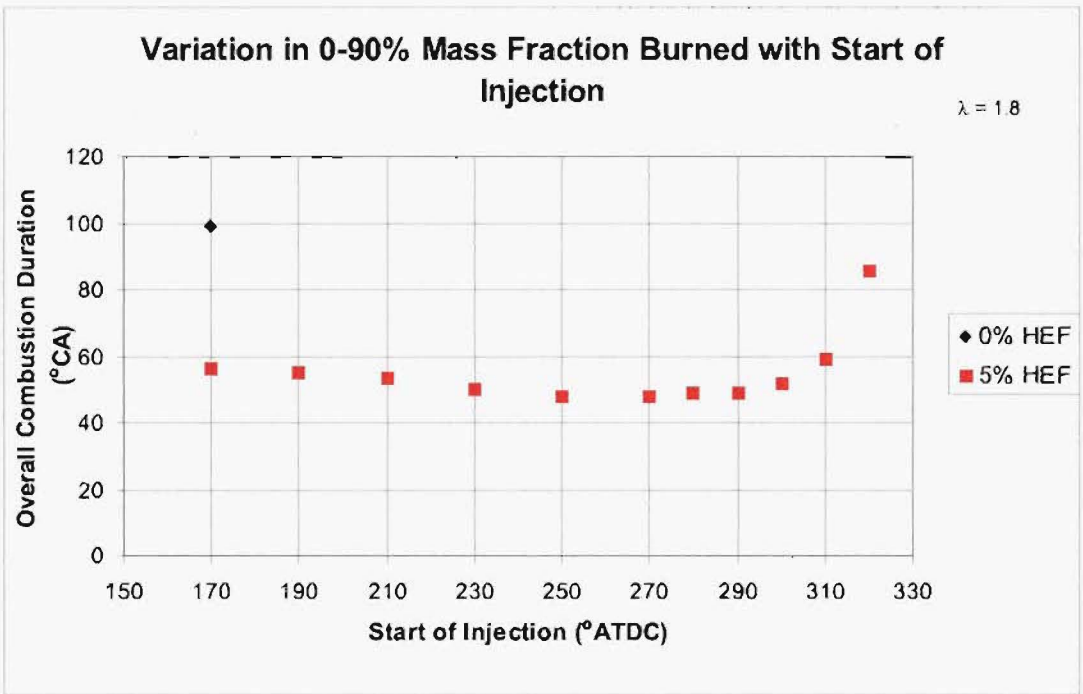

Figure 9.42 Effect of Injection Timing on 0-90% Mass Fraction Burned

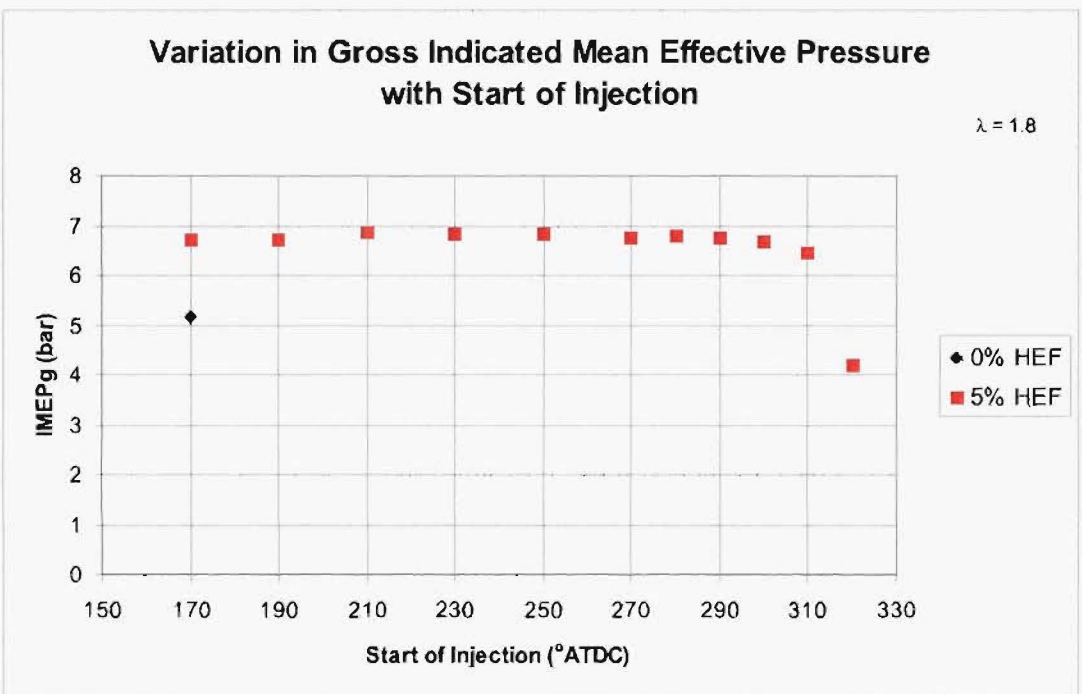

Figure 9.43 Effect of Injection Timing on Gross Indicated Mean Effective Pressure

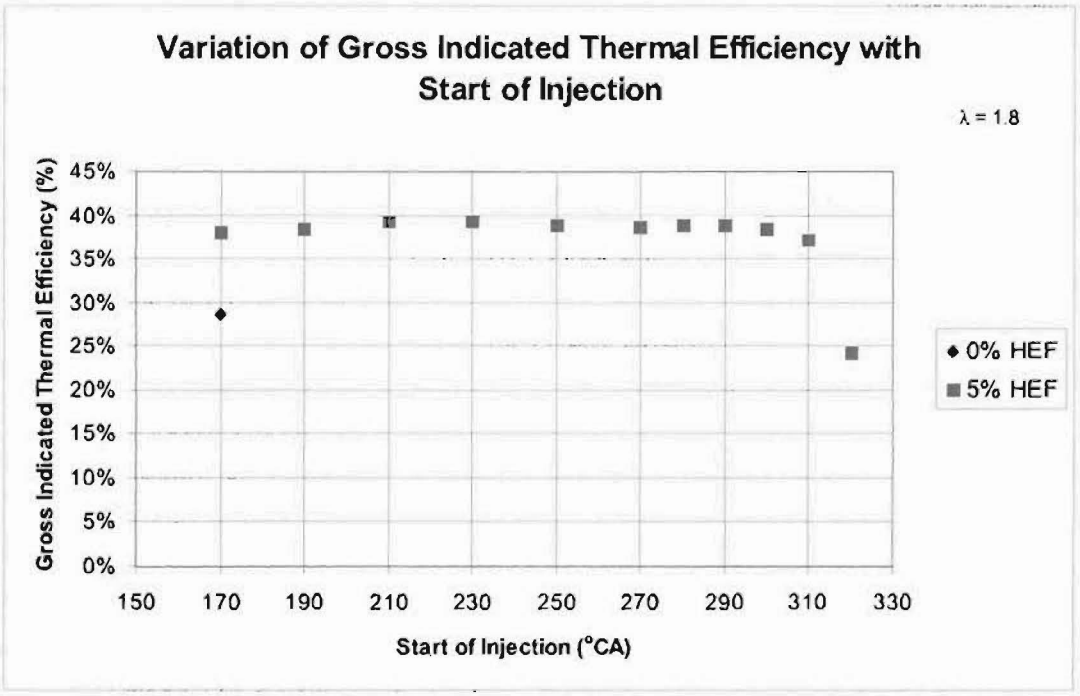

Figure 9.44 Effect of Injection Timing on Gross Indicated Thermal Efficiency

$IMEP_g$ quickly drops due to the slow overall combustion that is occurring and the spark timing no longer being at MBT for that combustion duration.

Figure 9.44 shows the effect of injection timing on gross indicated thermal efficiency. It can be seen that η_{ith} reaches a maximum with an injection timing of 210 ^{o}ATDC before reducing slowly until 290 ^{o}ATDC where the value of η_{ith} quickly falls away following the trend in $IMEP_g$.

Figure 9.45 shows the effect of injection timing on gross indicated specific NO_x emissions. It can be seen that isNO_x emissions reach a maximum with an injection timing of $\approx$210 ^{o}ATDC which corresponds with the shortest overall combustion duration. The spark timing will be advanced from MBT and hence result in higher combustion temperatures and NO_x formation. As the injection timing is retarded further the levels of isNO_x fall away quickly as a result of the lengthening combustion process.

Figure 9.46 shows the effect of injection timing on gross indicated specific UHC emissions. The isUHC emission levels remain fairly constant as the injection timing is retarded until the overall combustion increases after 290 ^{o}ATDC where they sharply increase as would be expected given the much slower combustion process.

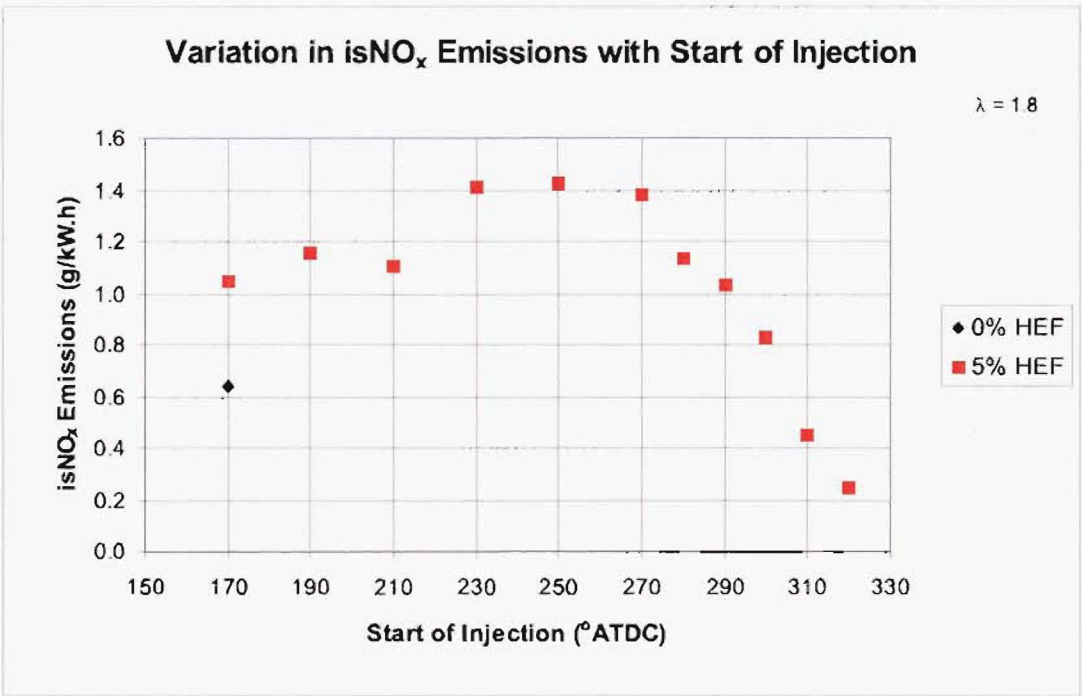

Figure 9.45 Effect of Injection Timing on Indicated Specific NO_x Emissions

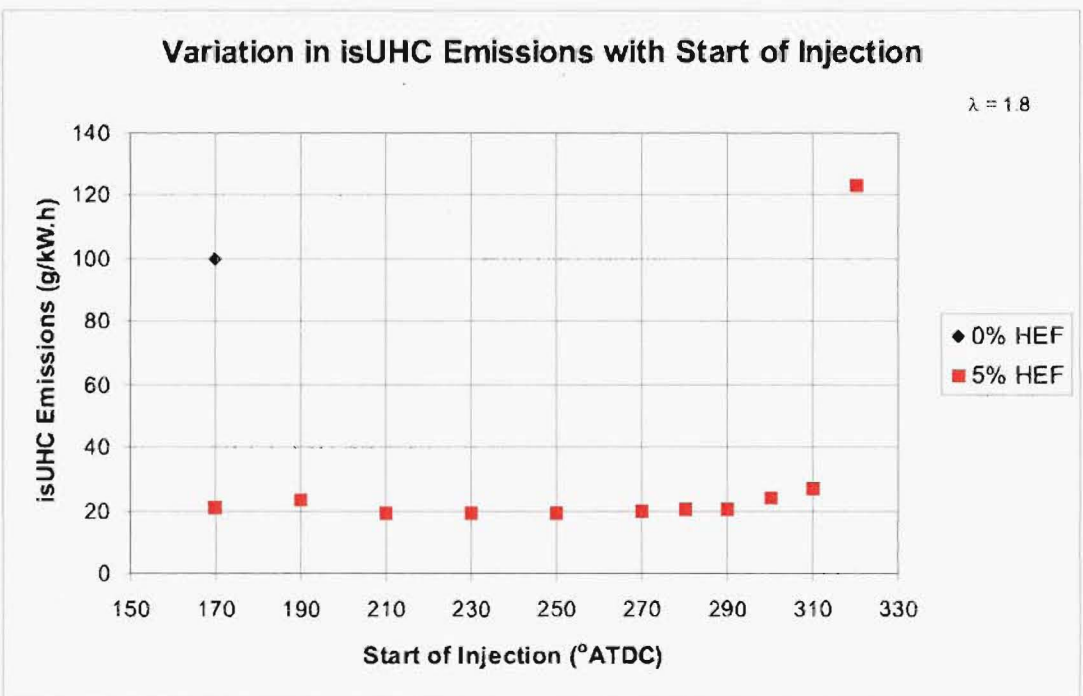

Figure 9.46 Effect of Injection Timing on Indicated Specific UHC Emissions

9.7.3 Summary

From the results of the investigation into the timing of the injection of supplementary hydrogen through the modified spark-plug arrangement the following conclusion can be made. While it is apparent that no large gains can be expected to be made by optimizing the injection timing, it appears that there could be scope for some very small gains in thermal efficiency and power. With MBT spark timings being employed at the resulting optimum injection timing, it is unlikely that there will be any significant improvement or worsening of engine emission levels. As there is no significant advantage in injecting late in the compression stroke, the injection of the supplementary hydrogen should still occur early in the compression stroke. This offers the possibility of using much reduced injection pressures while still ensuring that the injection process is sonic. The technical requirement of the hydrogen injector used is also therefore reduced as it would not have to actuate against such a substantial supply pressure. The injector would still be required to withstand substantial back-pressures resulting from the combustion process.

9.8 Early Direct Injection Summary

The key results of the investigation into the early direct injection of hydrogen can be summarized by the following points.

1. The early direct injection of hydrogen into the combustion chamber results in the formation of a stratified charge, not a homogeneous charge as was the intention.
2. The early direct injection of hydrogen can be commenced as early as 170 ^{o}ATDC without adversely affecting the volumetric efficiency of the engine.
3. The effect of hydrogen addition was most significant on lean air/fuel mixtures.
4. The most effective method for supplementing hydrogen is early direct injection via the modified spark-plug injection system.
5. Using the modified spark-plug injection system, the addition of only 5% HEF resulted in a dramatic improvement in all aspects of combustion, engine performance and emissions.
6. Using the modified spark-plug injection system, the utilization of HEF's greater than 5% resulted in only a very slight further improvement in combustion, engine performance and emissions.
7. Varying the injection timing employed with the modified spark-plug system offers the potential for only very small improvements in combustion, engine performance and emissions.

Chapter 10

Optimum Fuelling System

This chapter outlines the optimum method of fuelling an engine on supplementary hydrogen via early direct injection through a modified spark-plug injector as determined in the previous chapter. The results of a series of tests comparing the baseline engine operation with the optimum fuelling system is then presented. A possible vehicular engine fuelling regime is then discussed.

10.1 Introduction

In the previous chapter, the conclusion was reached that the optimum method of introducing supplementary fuel to the engine is with a modified spark-plug injection arrangement. Furthermore it was also found that hydrogen supplementation had the most beneficial effect on lean air/fuel mixtures. The supplementation of lean air/fuel mixtures with 5% HEF was found to result in a dramatic improvement in the combustion process, engine performance and engine emissions. Supplementation with higher HEF's however resulted in only slight further improvements. Varying the injection timing had little effect on the engine performance. In order to illustrate the benefits of hydrogen supplementation in an engine, the modified spark-plug injection system was used with HEF's of 5% and 10%.

10.2 Engine Configuration

The engine's primary fuel was manifold injected methanol. The supplementary hydrogen was introduced into the engine via the modified spark-plug arrangement.

The injection of hydrogen into the combustion chamber commenced at 170 ^{o}ATDC. A constant hydrogen supply pressure of 48.2 bar (700 psi) was again used to achieve sonic injection thus negating the influence of variations in combustion chamber pressure. Varying the hydrogen injection duration therefore varied the quantity of hydrogen injected.

Engine testing was carried out over a range of values of λ at each value of HEF by varying the quantity of each fuel being delivered. No further testing was completed at HEF = 0%. The values for HEF = 0% that are plotted for comparison with the 5% and 10% HEF cases were taken from the engine test results presented in the previous chapter.

All engine testing was carried out at a compression ratio of 10:1, at an engine speed of 1500 rpm and at wide open throttle. The level of inlet air heating used was approximately 364 Watts. Thus the operating conditions are the same as those used in the untimed manifold and preliminary early direct injection investigations.

10.3 Results

Figure 10.1 shows the variation in gross indicated thermal efficiency as the overall relative air/fuel ratio is varied for three different levels of hydrogen supplementation. It can be seen that peak η_{ith} occurs at approximately $\lambda = 1.5$. This is expected as engine efficiency is known to peak at a value of λ that is lean of stoichiometric. The values of η_{ith} for the 0% HEF case appear to be slightly higher than the values plotted for the 5% HEF case. This is attributed to the fact that the 0% points were obtained during a separate set of testing. For the 0% HEF case the η_{ith} falls away rapidly after $\lambda = 1.5$ as the equipment lean limit is approached when the engine is fuelled on methanol alone. The η_{ith} curve for 5% HEF demonstrates the ability of hydrogen supplementation to extend the equipment lean limit of the engine. Where the value of η_{ith} drops away rapidly for the 0% case after $\lambda = 1.5$, the value of η_{ith} for the 5% HEF remains high and slowly falls away as the mixture is further leaned out. It is also apparent that at $\lambda = 1.8$ the value of η_{ith} for both the 5% and 10% HEF cases are approximately the same. As the mixture is leaned out past $\lambda = 1.8$ however the η_{ith} of the 10% HEF is higher than that of the 5% HEF case. This demonstrates the ability of the higher levels of hydrogen supplementation to increasingly extend the engine's equipment lean limit. Lean limit extension has been demonstrated in the past when utilizing untimed manifold injected supplementary hydrogen. This is the first time lean limit extension results via the direct injection of a stratified charge of hydrogen have been presented. As was demonstrated in the previous chapter, supplementation via direct injection through a modified spark-plug gives superior results compared to untimed manifold injection, particularly with reduced levels of supplementation.

Figure 10.2 shows the variation in gross indicated mean effective pressure as the overall relative air/fuel ratio is varied for three different levels of hydrogen supplementation. As expected the engine power output decreases as the value of λ is increased. As discussed for η_{ith}, the higher values for the 0% HEF case compared to the 5% HEF case are thought to be due to the fact that the 0% HEF points were obtained during a separate set

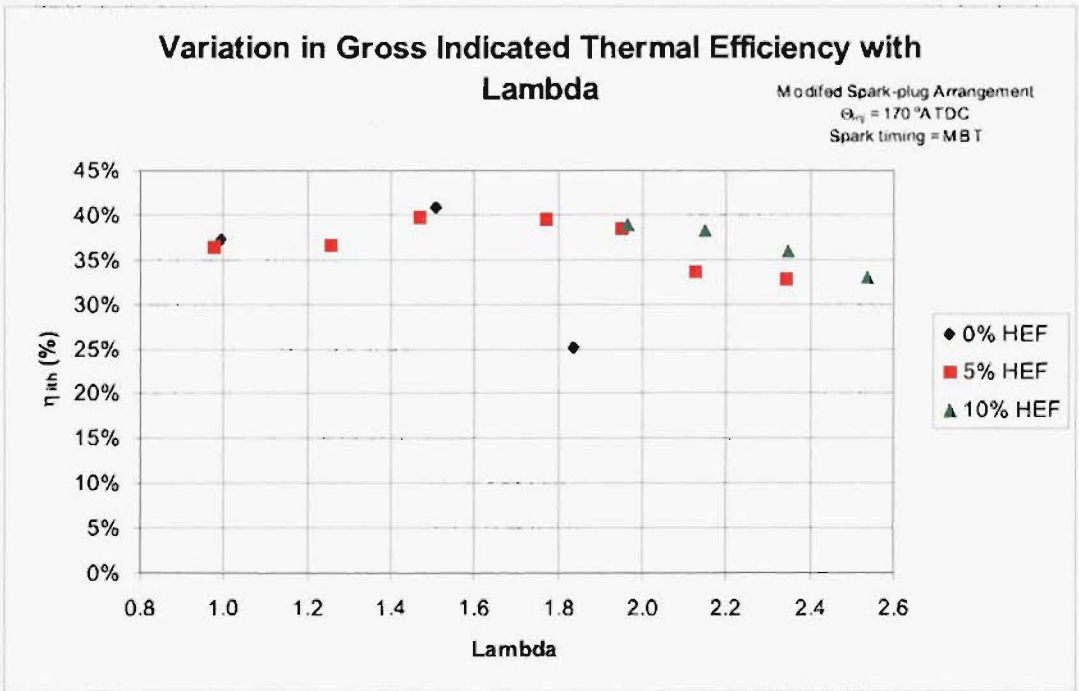

Figure 10.1 Variation in Gross Indicated Thermal Efficiency with Lambda

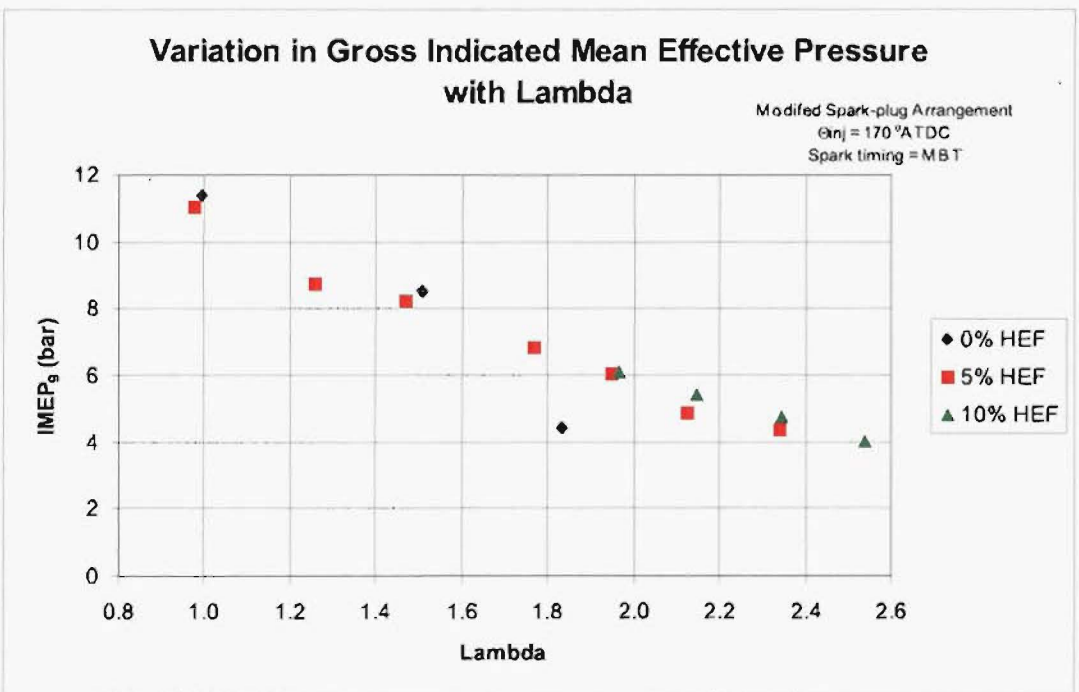

Figure 10.2 Variation in Gross Indicated Mean Effective Pressure with Lambda

of testing. At values of λ greater than 1.5 the 5% HEF case demonstrates higher levels of $IMEP_g$ than the 0% HEF case. At values of λ greater than 1.8 the 10% HEF case demonstrates higher levels of $IMEP_g$ than the 5% HEF case. These results again demonstrate the ability of hydrogen supplementation to extend the equipment lean limit of the engine.

The variation in the coefficient of variation of gross indicated mean effective pressure with the overall relative air/fuel ratio is shown in Figure 10.3 for three different levels of hydrogen supplementation. The magnitude of the value of COV_{IMEPg} can be used to define combustion stability. A value for COV_{IMEPg} of 10% has been proposed as defining the upper limit for acceptable driveability [Atkinson *et al.* 1995]. It can be observed from Figure 10.3 that the value of COV_{IMEPg} for the 0% HEF case is of the order of 2-3% until between $\lambda = 1.5$ and 1.8 where the value rises rapidly. This corresponds with the already identified equipment lean limit of the engine when fuelled by methanol alone. The value of COV_{IMEPg} for the 5% HEF case is $\approx$2% until $\lambda = 1.5$ after which it slowly rises, reaching 10% at approximately $\lambda = 2.1$. The 10% HEF values for $\lambda = 1.9$ and 2.15 are somewhat higher than would be expected. The results presented in the previous chapter showed that increasing the HEF resulted in the COV_{IMEPg} being reduced slightly further than was the case with 5% HEF. Accepting that these values are higher than expected, it can be seen that the values of COV_{IMEPg} for the 10% HEF case do not reach the 10% threshold until $\lambda \approx 2.5$. Figure 10.3 demonstrates that it is possible to operate an engine unthrottled considerably leaner than would be possible with methanol alone and still maintain the combustion stability within acceptable limits.

Figure 10.4 shows a plot of how the gross indicated thermal efficiency varies with gross indicated mean effective pressure. This plot demonstrates that when the engine is producing low levels of output power, it can do so more efficiently when utilizing 5 or 10% HEF. This result realizes one of the major objectives of current engine research (see page 7), improving part load engine efficiency. Improvements in part load efficiency have been achieved in the past with hydrogen supplementation using untimed manifold hydrogen injection [Houseman and Hoehn 1974] , [MacDonald 1976] , [Finegold 1978] , [Rauckis and McLean 1979] , [Jamal and Wysznski 1994] , [Apostolescu and Chirac 1996]. This current work however has demonstrated that the same improvements in part load efficiency can be attained using far smaller amounts of hydrogen if utilized as a stratified charge in the vicinity of the spark-plug electrodes. It should be stressed again at this point that these results were obtained with the engine operating unthrottled. At all load points at a given speed, the ideal value of λ to run an engine at is that which gives the minimum bsfc (highest efficiency) at the required load [Heywood 1988]. As can be seen from Figure 10.4 for the 0% HEF case that at low values of IMEP_g the η_{ith} is considerably reduced from what it was at higher values of IMEP_g. Thus it would be expected that the engine would be operated with some throttle at 0% HEF for values of IMEP_g below

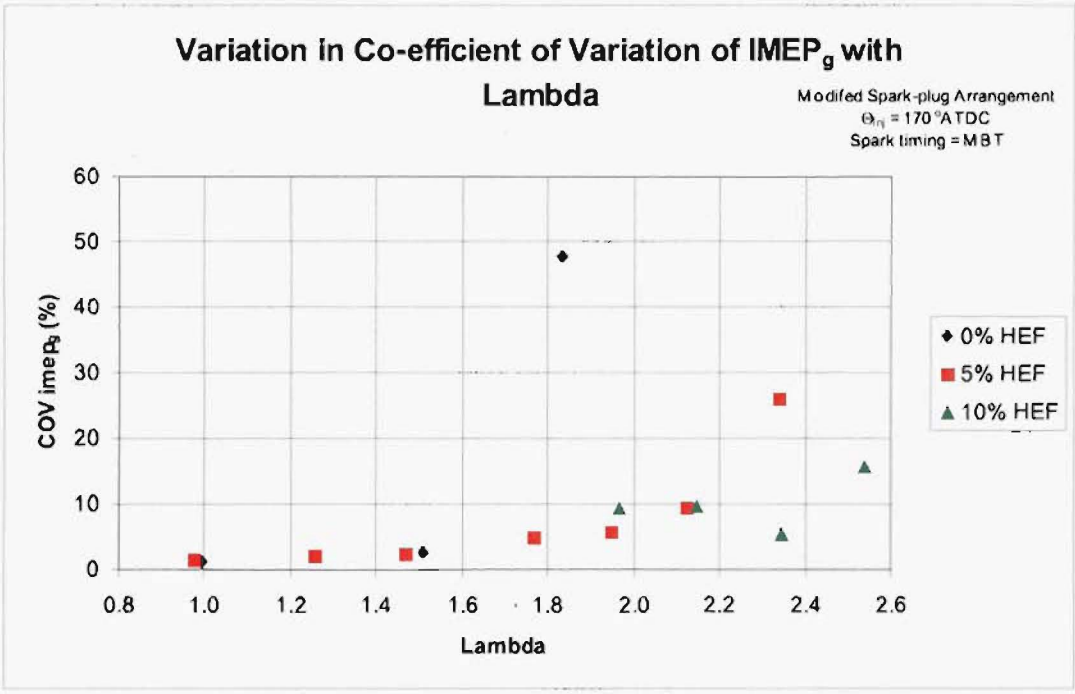

Figure 10.3 Variation in the Coefficient of Variation of Gross Indicated Mean Effective Pressure with Lambda

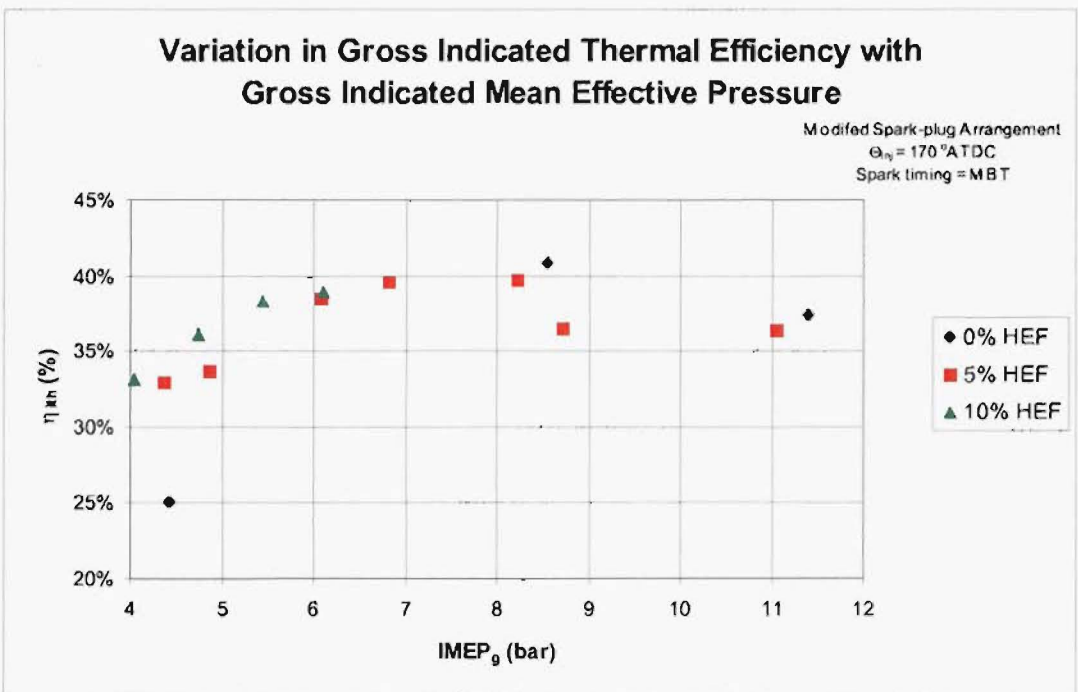

Figure 10.4 Plot of Gross Indicated Thermal Efficiency verses Gross Indicated Mean Effective Pressure

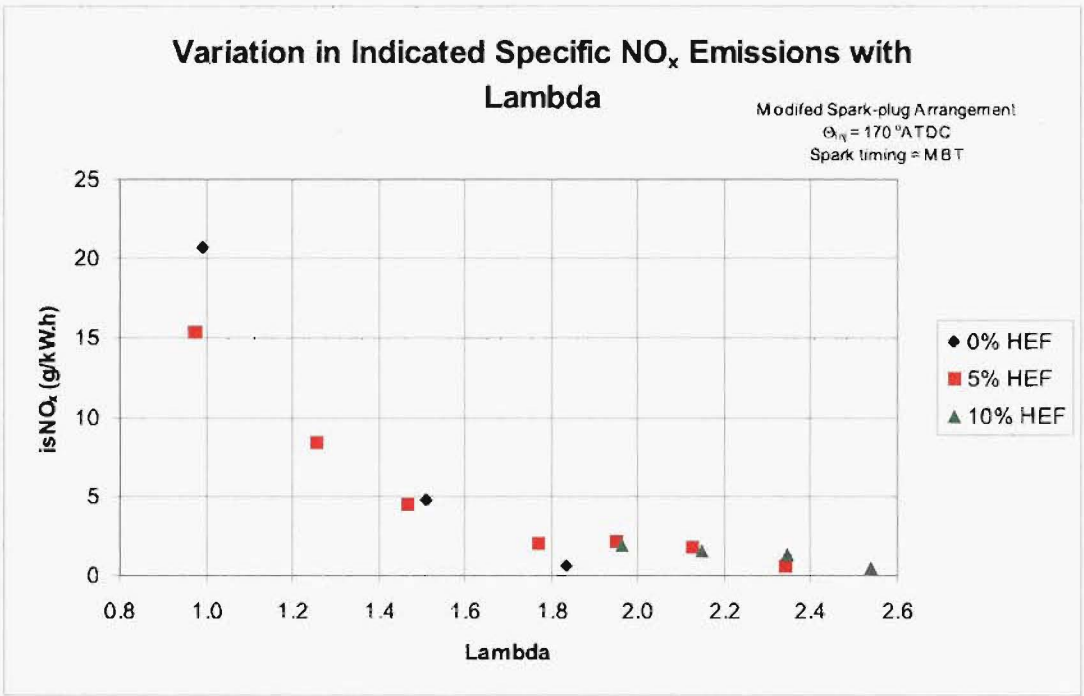

Figure 10.5 Variation in Indicated Specific NO_x Emissions with Lambda

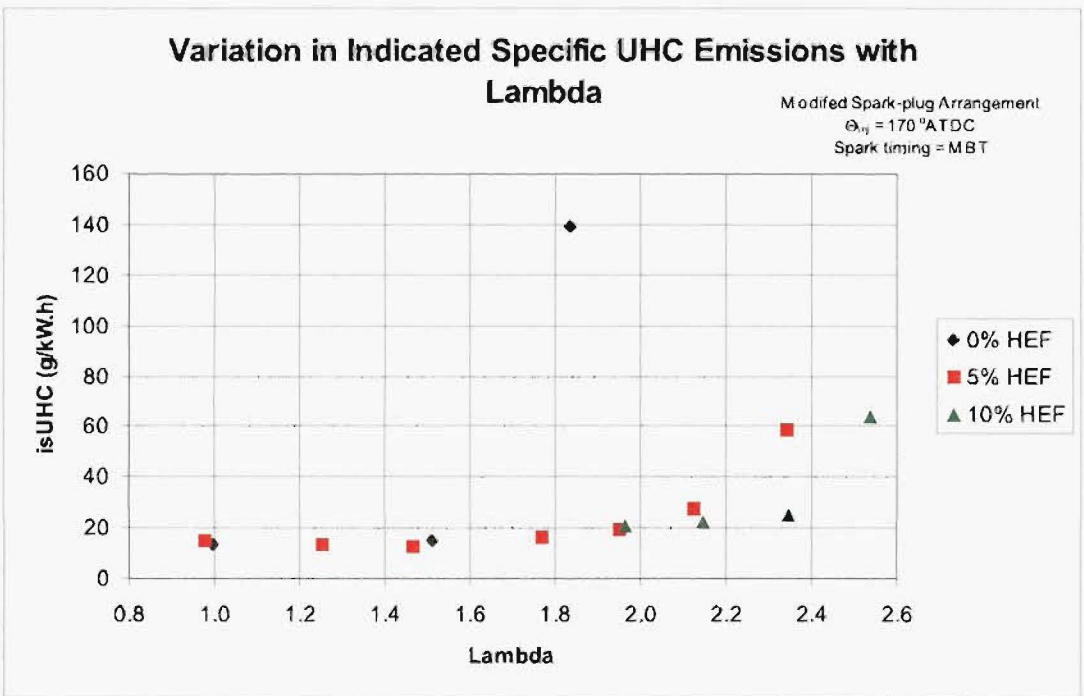

Figure 10.6 Variation in Indicated Specific UHC Emissions with Lambda

approximately 7 bar. It is also apparent that operating the engine with a HEF of 5 or 10% allows the engine to be operated at low $IMEP_g$ values without a large reduction in η_{ith}. This demonstrates that a hydrogen supplemented engine can be operated unthrottled over a larger operating range than can an engine operating on 100% methanol alone. At which exact point operating the engine throttled, with or without hydrogen supplementation, is more advantageous for lower output power levels is not known from this investigation. If a hydrogen supplementation system is to be utilized on a vehicle, an investigation into throttled engine operation will need to be undertaken. This was considered to be outside the scope of the current investigation.

Figure 10.5 shows the variation in indicated specific NO_x emissions as λ is varied. As expected the level of $isNO_x$ emissions reduces rapidly as λ increases demonstrating the well known benefit of operating an engine in a lean burn regime. The use of hydrogen supplementation allows the engine to be operated past it's usual equipment lean limit, further reducing the level of $isNO_x$ emissions.

The variation in indicated specific UHC emissions with λ is shown in Figure 10.6. The values for the 0% HEF case show the characteristic sharp increase in isUHC emissions as the equipment lean limit is reached between $\lambda = 1.5$ and 1.8. It is also apparent that operation with 5% and 10% HEF allows the engine to be operated progressively leaner before the equipment lean limit is approached and the isUHC emission levels begin to rise. This demonstrates that the engine can be operated leaner than previously possible with no hydrogen supplementation without an excessive increase in UHC emission levels.

Depending on the intended use of the engine, the use of lean air/fuel ratio's allows the possibility of using higher compression ratio's. The engine could be optimized for the maximum allowable compression ratio at maximum power output to take full advantage of the higher octane rating of methanol over gasoline. At the leaner air/fuel ratio's, the effective compression ratio of the engine could be raised using a variable valve timing mechanism such as that developed by Mitsubishi Motors Ltd [Hatano *et al.* 1993] to gain further advantages in both power and efficiency.

10.4 Summary

It has been demonstrated that low levels of hydrogen supplementation can extend the equipment lean limit from that of a 100% methanol fuelled engine when using the modified spark-plug injector. A high value of indicated thermal efficiency was maintained with a reduced value of $IMEP_g$, low cycle-by-cycle variability and low isUHC emissions. It was shown that a hydrogen supplemented engine offers the potential to be operated unthrottled over a larger operating range than an engine operating on 100% methanol

alone could be thus improving part load engine efficiency. Increasing the level of hydrogen supplementation allowed the effective lean limit to be extended leaner still.

10.5 Possible Vehicular Engine Fuelling Regimes

Based upon the findings of the research program, some suggestions as to a possible vehicular fuelling regime can be made.

As the hydrogen used for supplementation will have to be either stored or manufactured on-board the vehicle from the main fuel, the level of hydrogen supplementation should be kept to the minimum required to achieve the desired result. The optimal system for hydrogen supplementation amongst those tested is the modified spark-plug injection system with the injection of supplementary hydrogen occurring early in the compression stroke.

For each engine speed, the maximum value of λ that the engine is required to be able to run at unthrottled will be determined and the minimum level of hydrogen supplementation required to ensure an acceptable level of cyclic variability at that value of λ found. As the main benefits of hydrogen supplementation are to be found in lean mixtures, it it proposed that the flow rate of hydrogen employed at the maximum value of λ be set constant to reduce the control complexity and used for all values of λ. Thus the leaner air/fuel mixtures which are significantly affected by hydrogen supplementation benefit from a higher level of HEF. The richer air/fuel mixtures which are only slightly affected by hydrogen supplementation are thus operating with a much reduced HEF.

Depending on the method employed to provide supplementary hydrogen to the engine, it may be advantageous to only supply hydrogen supplementation when the value of λ falls below a particular value to conserve hydrogen. Doing so would sacrifice very little in terms of engine performance or emissions levels when operating with richer air/fuel ratios.

Chapter 11

Conclusions and Recommendations for Future Work

In this chapter, the key achievements of the thesis are summarized. Conclusions are drawn as to the performance of each of the hydrogen injection systems employed. The optimal hydrogen supplementation system for the Ricardo E6 engine is presented along with a suggested fuel management scenario for the engine. Recommendations for further work that could be undertaken as a result of this research project are then presented.

11.1 Conclusions

The use of hydrogen as a supplementary fuel is recognized as being an effective way of extending the lean limit of an engine. The benefits of doing so lie in improved fuel consumption and reduced engine exhaust emissions. Almost all work to date in this area has focused on the use of the technically undemanding untimed manifold injection of hydrogen to achieve these goals. In recent years, advances in technology have resulted in the direct injection of both liquid and gaseous fuels becoming the increasingly preferred option in automotive engine combustion systems.

Two schlieren photography investigations were undertaken to improve the performance of each of the direct injection systems as well as provide performance data. In the first, delay durations between the injection signal being sent and the first visible sign of hydrogen entering the combustion bomb were determined. The results of the schlieren visualization were used to develop the nozzle discharge hole geometry for the early direct injection system. The performance of the modified spark-plug injector, when used to inject a late "puff" of hydrogen, was investigated and the design of the arrangement improved. Suitable injection pressures and durations were determined for the modified spark-plug arrangement. In the second schlieren investigation the combustion bomb was modified to have a much wider field of view. This investigation focused on providing visual evidence to confirm experimental results indicating that both the early direct injection system and the modified spark-plug injector, when used as an early direct injection injector, produced stratified charges.

A data acquisition system was developed and installed in the test-cell. Data acquisition was triggered externally by the output from an incremental rotary encoder mounted on the crank-shaft. Electronic hardware was developed to ensure the acquired pressure data were accurately phased with respect to the crank-angle. At each test point, 350 consecutive engine cycles of combustion pressure data were acquired and analyzed using software routines developed during the course of this work.

The untimed manifold injection of hydrogen resulted in increased rates of combustion and reduced cyclic variability as the HEF was increased. The engine performance characteristics are however dominated by the reduction in volumetric efficiency resulting from the injection of hydrogen into the inlet manifold. This resulted in reduced engine power output as the level of hydrogen supplementation was increased. The addition of small quantities of supplementary hydrogen resulted in both reduced cyclic variability and isUHC emissions especially in lean mixtures where large reductions of these parameters were observed. The highest values of indicated thermal efficiency occurred in the leanest air/fuel mixtures. There were no clear trends in indicated thermal efficiency with increases in HEF except in $\lambda = 1.5$ where the maximum value occurred at HEF = 30%. It was later determined that superior thermal efficiency values could be achieved in lean mixtures using much lower HEF's with an alternative fuelling system so no further investigation into manifold injection thermal efficiencies was undertaken. The isNO_x engine emissions were reduced for $\lambda = 1.0$ but increased for all values of $\lambda > 1.0$ as the level of hydrogen supplementation increased. This increase was thought to be due to an increase in combustion temperatures with increasing HEF. The untimed manifold injection results indicated that the greatest potential benefits of hydrogen supplementation appear to lie in operating the engine with lean mixtures i.e. at part load. In addition to this, hydrogen supplementation, by reducing cyclic variability, would allow the lean operating limit of the engine to be extended, offering further potential for improvements in engine efficiency and emissions. Although untimed manifold injection is technically very easy to implement, the major drawback of the system is the loss of volumetric efficiency and hence power output of the engine. This drawback was addressed by injecting supplementary hydrogen directly into the combustion chamber of the engine.

The use of the early direct injection system to inject supplementary hydrogen into the combustion chamber was found to result in the formation of a stratified charge, not a homogeneous charge as was the original intention. The resultant stratified charge was the inverse of what is required for improved combustion i.e. the leaner air/fuel mixture is located closest to the spark-plug. This is thought to be due, in part, to the hydrogen injector being located diametrically opposite the spark-plug in the head of the engine on the other side of the combustion chamber. The early direct injection of hydrogen can be commenced as early as 170 ^{o}ATDC (46 ^{o}CA before the inlet valve closed) without

adversely affecting the volumetric efficiency of the engine. Even with such an early start of injection, the early direct injection system was found to still form a stratified charge indicating that the Ricardo E6 engine has low levels of bulk mixture motion.

The most effective method for introducing supplementary hydrogen in the Ricardo E6 engine, of those investigated, is early direct injection via the modified spark-plug injection system. The more pronounced effect of the modified spark-plug injection system, for a given level of hydrogen supplementation, is thought to be due to an easily ignitable hydrogen/air mixture in the vicinity of the spark-plug at the time of ignition. The higher flame speed of hydrogen is thought to be responsible for greatly reducing the 0-2% mfb duration forming a rapidly propagating flame kernel which in turn reduces cyclic variability of the combustion process as a whole. The effect of hydrogen addition was most significant on lean air/fuel mixtures where a given HEF level had an increasingly beneficial effect on both the 0-2% mfb duration and the COV_{IMEPg} as the mixture was made leaner. Using the modified spark-plug injection system the addition of 5% HEF to mixtures leaner than $\lambda \approx 1.5$ resulted in a dramatic improvement in all aspects of combustion, engine performance and emissions. The utilization of HEF's greater than 5% with the modified spark-plug system resulted in only a very slight further improvement in combustion, engine performance and emissions. Varying the injection timing employed with the modified spark-plug system offers the potential for only very small improvements in combustion, engine performance and emissions.

The Ricardo E6 was operated un-throttled over a range of values of air/fuel ratios from stoichiometric to very lean utilizing the modified spark-plug as the optimum fuelling system. The ability of low levels of hydrogen supplementation to extend the equipment lean limit from that of a 100% methanol fuelled engine was demonstrated. The practical lean limit (as defined by 10% COV_{IMEPg}), of the engine running on 100% methanol was found to be $\lambda \approx 1.6$. Utilizing a HEF of 5% resulted in the practical lean limit being extended to $\lambda \approx 2.1$. The major benefits of the practical lean limit extension were the ability to maintain a high value of indicated thermal efficiency with a reduced value of $IMEP_g$, low cycle-by-cycle variability and low isUHC emissions. Emissions of isCO are only significant with air/fuel mixtures close to stoichiometric and are thus very low with the lean air/fuel mixtures of interest. Similarly $isNO_x$ emissions reduce with increasing values of λ and the corresponding reduction in peak combustion temperatures. As a high value of indicated thermal efficiency was shown to be able to be maintained in lean mixtures with increasing levels of hydrogen supplementation, the problem of a tradeoff between a high engine thermal efficiency and low NO_x emissions is reduced with hydrogen supplementation. Increasing the level of hydrogen supplementation above 5% allowed the practical lean limit to be extended leaner still.

A simple vehicular fuelling regime was proposed whereby for a given engine speed, the flow rate of hydrogen is set as constant. The flow rate specified would be the minimum required to maximize thermal efficiency at a given output power level within predetermined maximum levels of cyclic variability and bsUHC emissions (for the specified speed). Operating over a range of mixture strengths (i.e. employing quality regulation where applicable) with this constant hydrogen flow rate would result in the leanest air/fuel mixtures (which benefit most from hydrogen supplementation) having the highest HEF and the richest air/fuel mixtures (which benefit least from hydrogen supplementation) having the lowest HEF. The supplementary hydrogen is thus used to best advantage.

11.2 Recommendations for Future Work

On the basis of experience gained from this research project, there are several areas in which further work would be appropriate.

The method by which the rotational speed of the Ricardo E6 engine is controlled could be improved. During testing the speed drifted by up to 12 rpm from the desired setting of 1500 rpm. This had a measurable effect on both the amount of air being induced into the engine and the amount of fuel being injected. Improved control over engine speed would allow the air/fuel ratio of the injected mixture to be more precisely set and improve the consistency of the results.

The combustion chamber geometry is not particularly well suited to optimal combustion. The current spark plug location, at the side of the combustion chamber, results in a long distance that flame must traverse. Redesign of the head to incorporate two camshafts would allow the spark-plug to be positioned centrally in the head reducing the path the flame must travel. Thus the combustion chamber will be more representative of that of a modern automotive engine. Combustion will take place over a shorter crank-angle interval, improving the performance of the engine especially with leaner air/fuel ratios.

The emission of aldehydes in the exhaust of a methanol fuel engine is an area of concern if methanol engines are to become common place. Aldehyde emissions and measurement techniques were discussed in Chapter 7. As aldehyde emissions are greatest at leaner air/fuel ratios, which is where it is most advantageous to operate an engine, the effect of hydrogen supplementation on the aldehyde emissions should be investigated. It has been suggested by Bernhardt [1977] that the addition of water to methanol has the effect of reducing aldehyde emissions. As the combustion of supplementary hydrogen forms water vapor as a product of combustion, hydrogen supplementation could result in reduced aldehyde emissions in addition to the beneficial effects on combustion that have

been observed in this thesis.

The effect of the modified spark-plug injection arrangement on the emissions of UHC needs further investigation. Despite an increase in the crevice volume of the engine resulting from modifications to the spark-plug and the hypodermic tube, the level of UHC emissions were not observed to be increased over that of the other fuelling systems. Testing with and without the modified spark-plug in the engine as well as varying the internal volume of the arrangement will result in the effect of the modified spark-plug arrangement on UHC emissions to be evaluated. It is anticipated that the effect of the modified spark-plug arrangement to be greatest at near-stoichiometric air/fuel ratios where engine crevice volumes are a major source of UHC emissions. At leaner air/fuel ratios, wall quenching effects become the dominant source of UHC emissions.

As it has been demonstrated that the effective lean limit of the Ricardo E6 engine can be extended by the use of hydrogen supplementation, an investigation into the potential increase in useful compression ratio that can be employed with leaner air/fuel ratios should be undertaken. It is expected that the compression ratio should be able to be raised at leaner air/fuel ratios from the value of 10:1 that was used for this work resulting in an increase in the thermal efficiency that can be obtained from the engine. The effect of engine speed on the optimal level of hydrogen supplementation needs to be evaluated as increasing engine speed will result in less time for the combustion process to occur. Hence at leaner air/fuel ratios increased hydrogen supplementation is likely to be required as the engine speed is increased.

An investigation into various physical embodiments of the injection through the spark-plug concept, to provide improved control over the hydrogen/air mixture in the vicinity of the spark-plug could be undertaken. This would include an investigation into varying the injection pressure when using a modified spark-plug system to inject early in the compression stroke. Implicit in this investigation would be comparing the effects of the degree of stratification that can be achieved, by varying the injection pressure, on the various mass fraction burned durations. The effect of the size and shape of the recess where the spark-plug is currently positioned should be investigated in particular with a view to possible application in a combustion chamber design with increased turbulent mixture motion.

Considerable scope also exists for extending the findings of this more fundamental evaluation by application on a commercial multi-cylinder engine. The effects of a more turbulent combustion chamber design on the formation of the stratified charge, in particular the hydrogen/air mixture in the vicinity of the spark-plug, will need to be in-

vestigated along with the effects of engine speed. Optimization of inlet air heating levels over the range of speeds and loads would improve the engine performance when fuelled with methanol as the main fuel.

Appendix A

Manufacturing Drawings

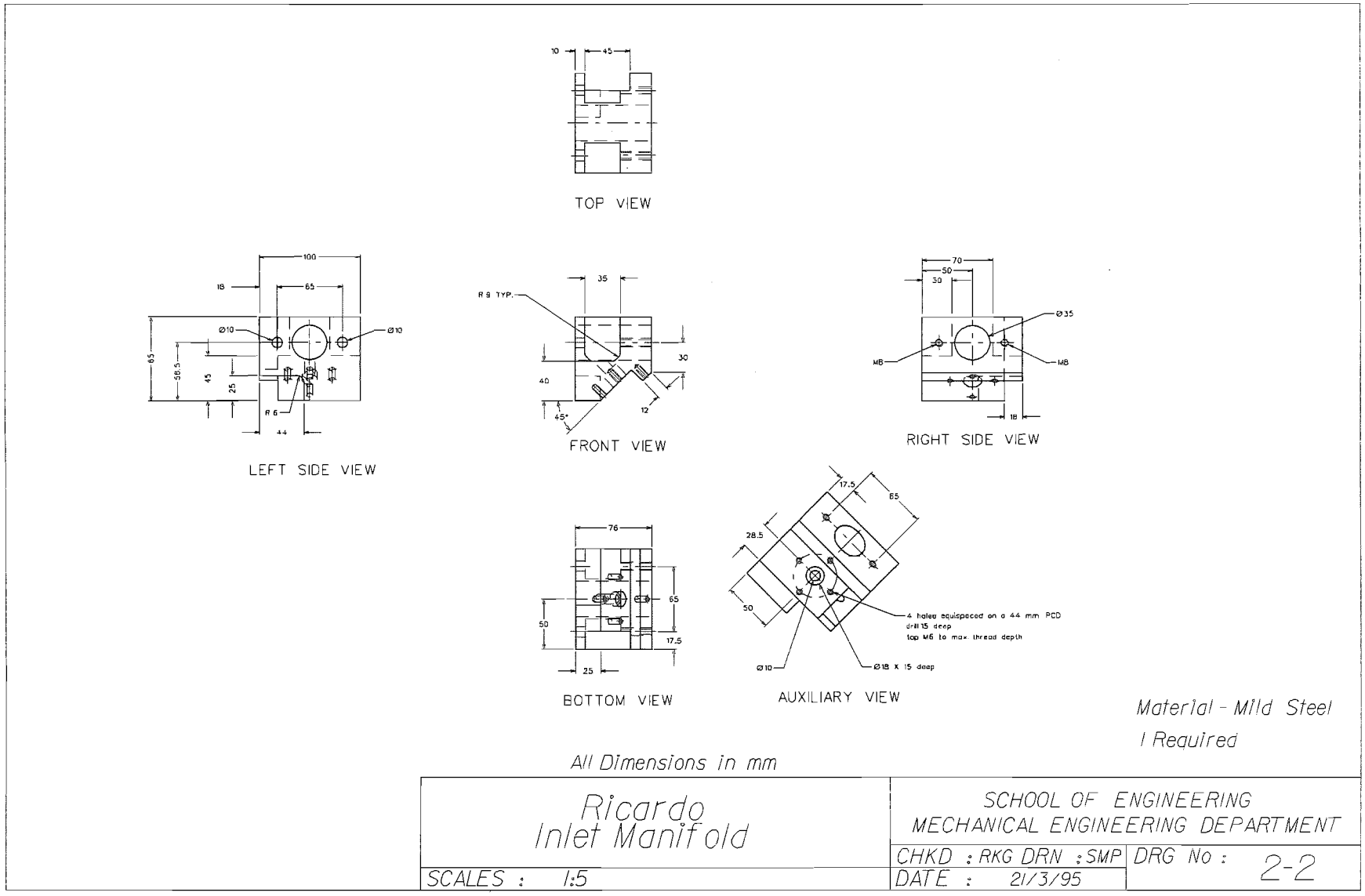

Figure A.1 Inlet Manifold Workshop Drawing

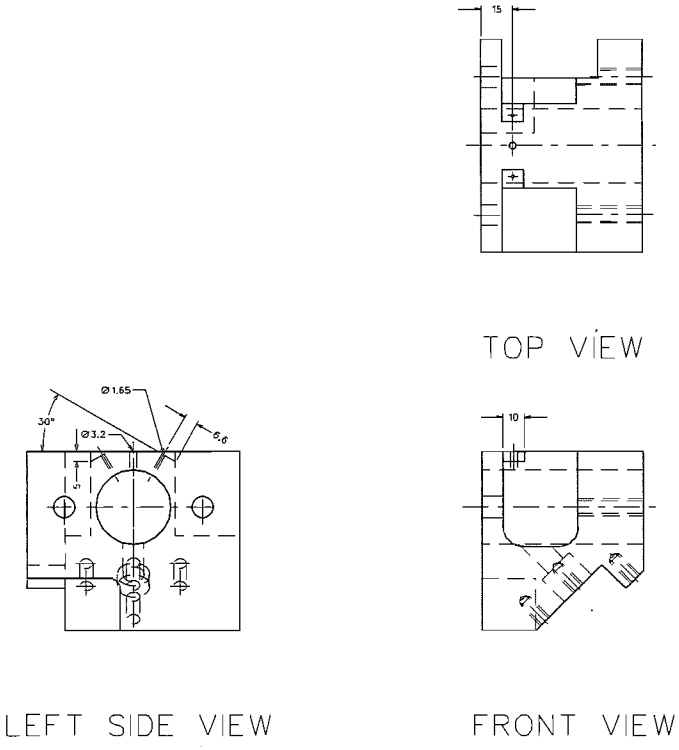

Figure A.2 Inlet Manifold Modifications Workshop Drawing

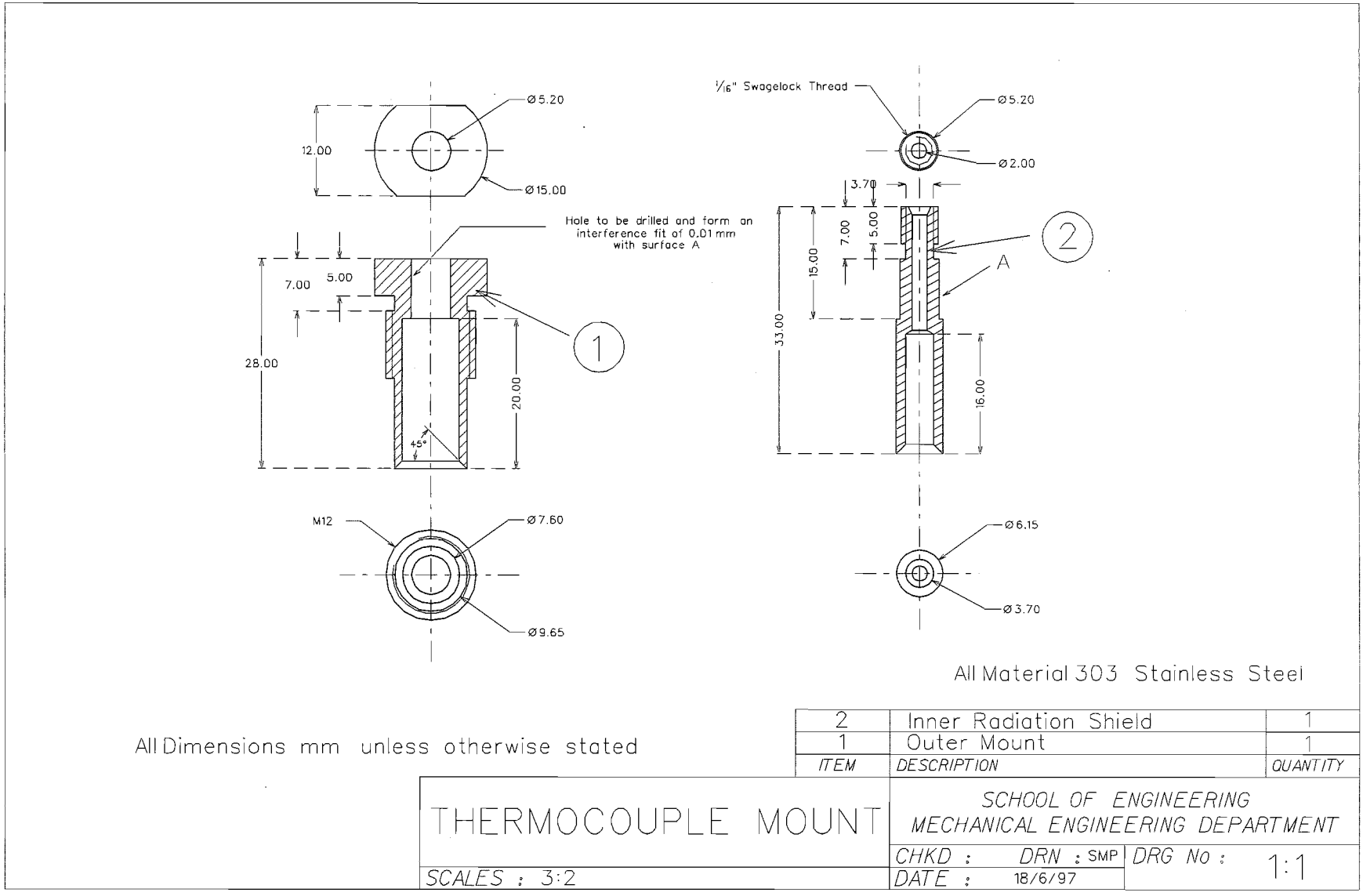

Figure A.3 Thermocouple Workshop Drawing

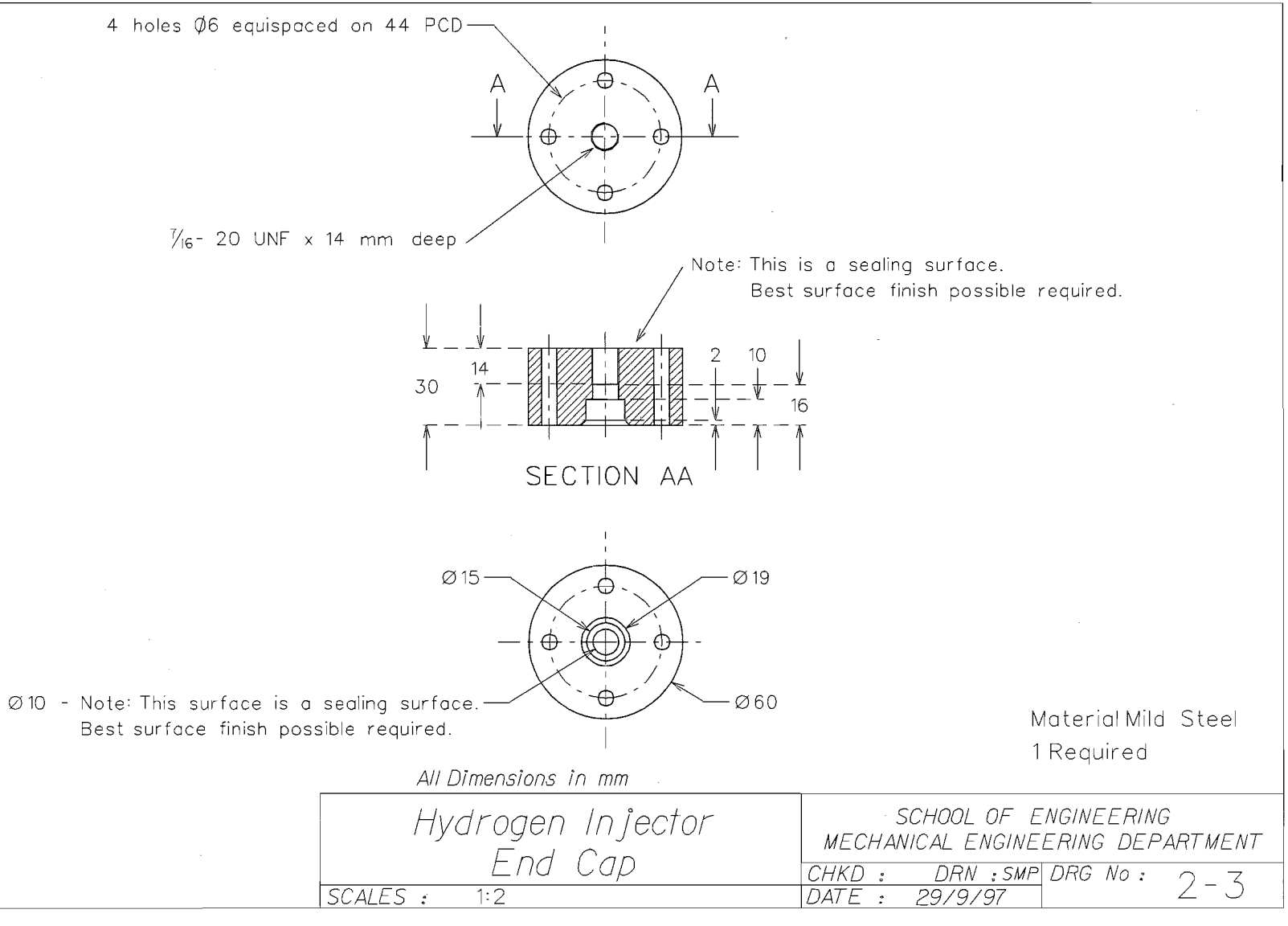

Figure A.4 Endcap Workshop Drawing

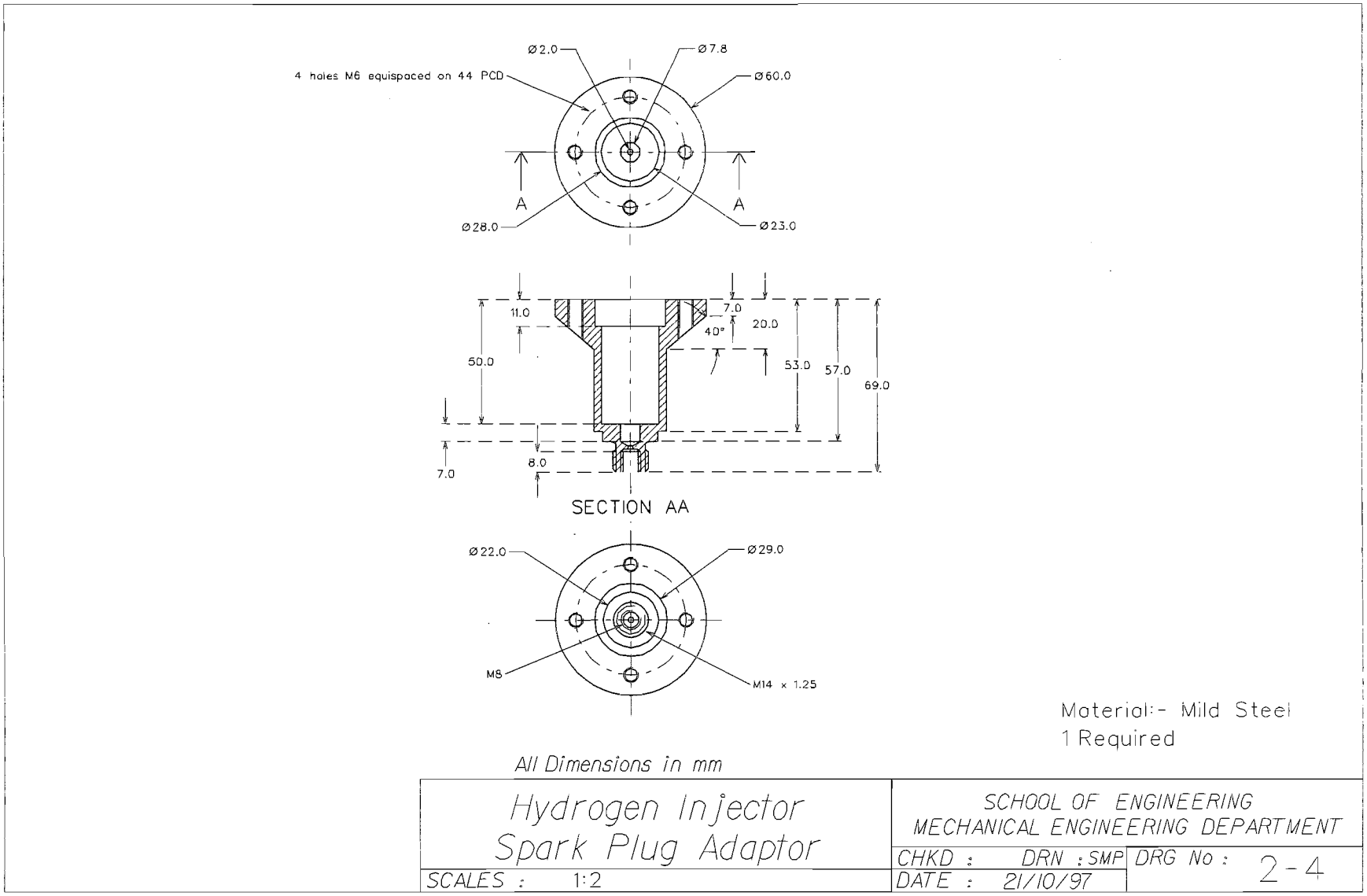

Figure A.5 Direct Injection Hydrogen Injector Workshop Drawing

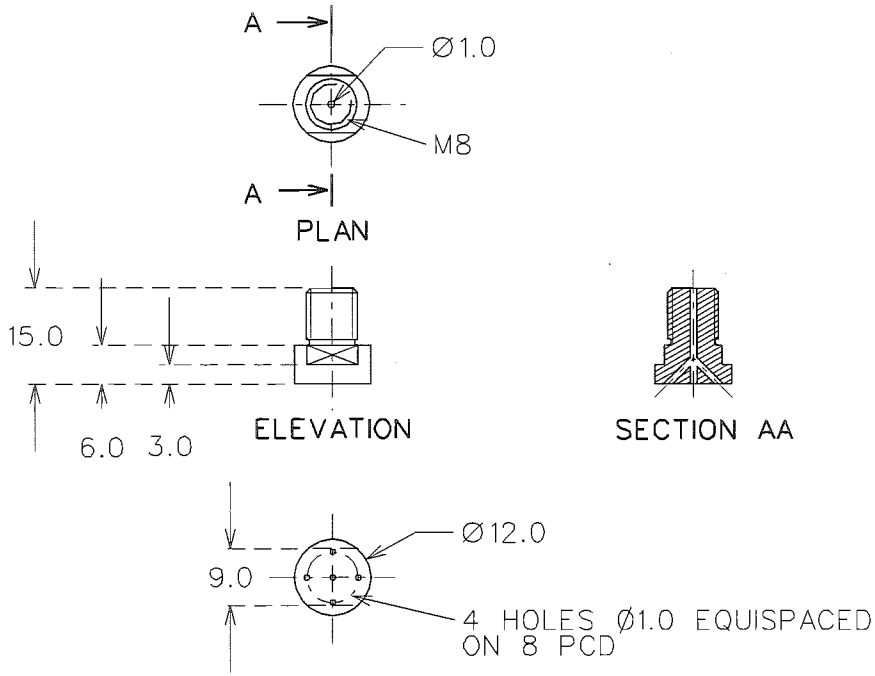

Material:- Mild Steel
1 Required

All Dimensions in mm

Hydrogen Injector Direct Injection Nozzle	SCHOOL OF ENGINEERING MECHANICAL ENGINEERING DEPARTMENT	
SCALES : 1:1	CHKD : DRN : SMP DATE : 7/4/98	DRG No : 2-5

Figure A.6 Five Hole Nozzle Workshop Drawing

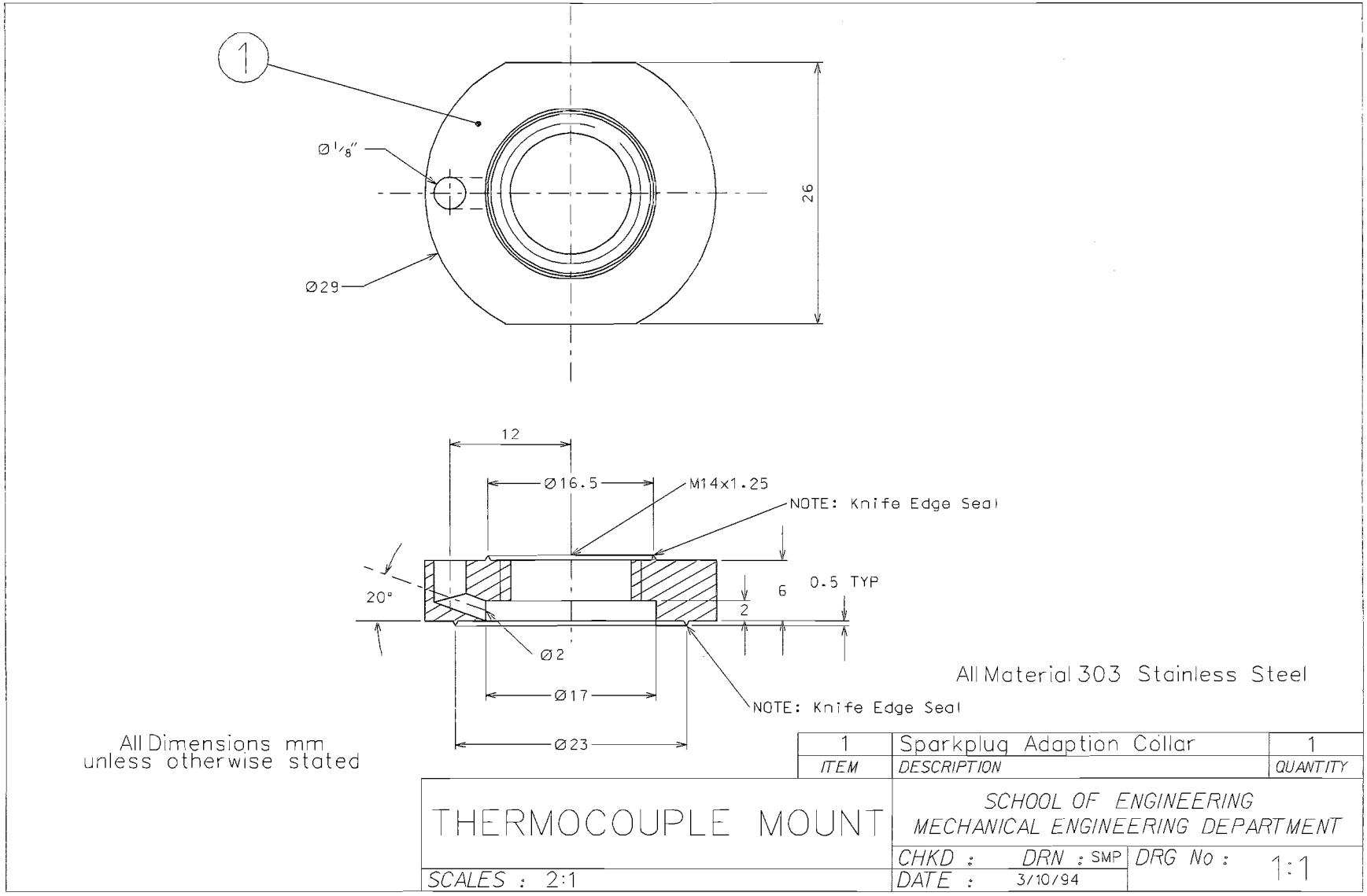

Figure A.7 Spark-plug Adaption Collar Workshop Drawing

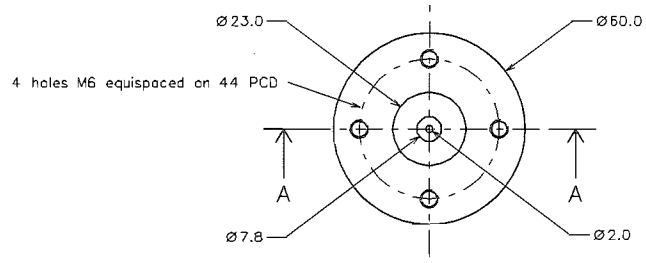

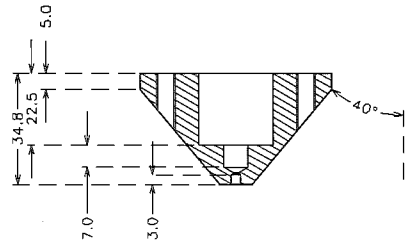

SECTION AA

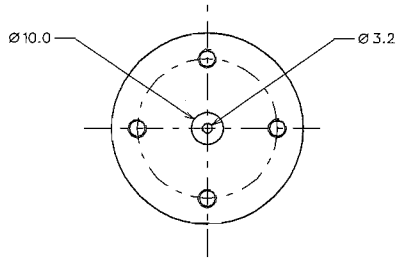

All Dimensions in mm

Material:- Mild Steel
1 Required

Hydrogen Injector Puff Injection Adaptor	SCHOOL OF ENGINEERING MECHANICAL ENGINEERING DEPARTMENT	
SCALES : 1:2	CHKD : DRN : SMP DATE : 20/11/97	DRG No : 2-5

Figure A.8 Modified Spark-plug Injection Adaptor Workshop Drawing

Appendix B

Fuel Properties and Engine Specification

B.1 Fuel Properties

The following values are generally accepted values from the literature. The sources of the values given are McCarty *et al.* [1981] , EMA [1982] , Lewis and Von Elbe [1987] , Unich *et al.* [1993] , Das and Mathur [1993].

	Gasoline	Methanol	Hydrogen
Molecular weight	107	32.04	2.016
Heat of combustion (low) (MJ kg^{-1})	42 - 44	19.7	120
Density (kg/litre)	0.72 - 0.78	0.79	N/A
Octane number	91 - 98	112	-
Latent heat of vaporization (kJ/kg)	330 - 400	1100	N/A
Boiling point (^oC)	30 - 225	78	-253
Reid vapor pressure @ 100 ^oF(psi)	9 - 13	4.6	N/A
Specific energy, LCV/AFstoich (MJ/kg_{air})	2.92	3.08	3.49

Table B.1 Thermodynamic Properties of Various Fuels

	Gasoline	Methanol	Hydrogen
Limits of Flammability in air (vol%)	1.0 - 7.6	7.3 - 36	4.0 - 75.0
Stoichiometric composition in air (kg/kg)	14.5 - 14.7	6.4	34
Autoignition temperature (K)	501 - 744	867	858
Flame temperature in air (K)	2470		2045
Burning Velocity in NPT air (cm s^{-1})	37 - 43	44 - 46	265 - 325
Quenching gap in NPT air (cm)	0.2		0.064

Table B.2 Combustion Properties of Various Fuels

B.2 Ricardo E6/Mk6 Variable Compression Engine Specification

Serial Number		138/82	
Number of Cylinders		1	
Bore		76.2	mm
Stroke		111	mm
Connecting Rod Length		241	mm
Swept Volume		507	cm^3
Compression Ratio		4.5:1 - 20:1	
Valve Timing			
	Inlet Opens	8	^{o}BTDC
	Inlet Closes	36	^{o}ABDC
	Exhaust Opens	42	^{o}BBDC
	Exhaust Closes	8	^{o}ATDC
Gasoline Pump	Bosch	0580 646 008	12 Volt
Spark Plug	NGK	BPR6ES	0.7 mm gap

Table B.3 Ricardo E6/Mk6 Variable Compression Engine Specification

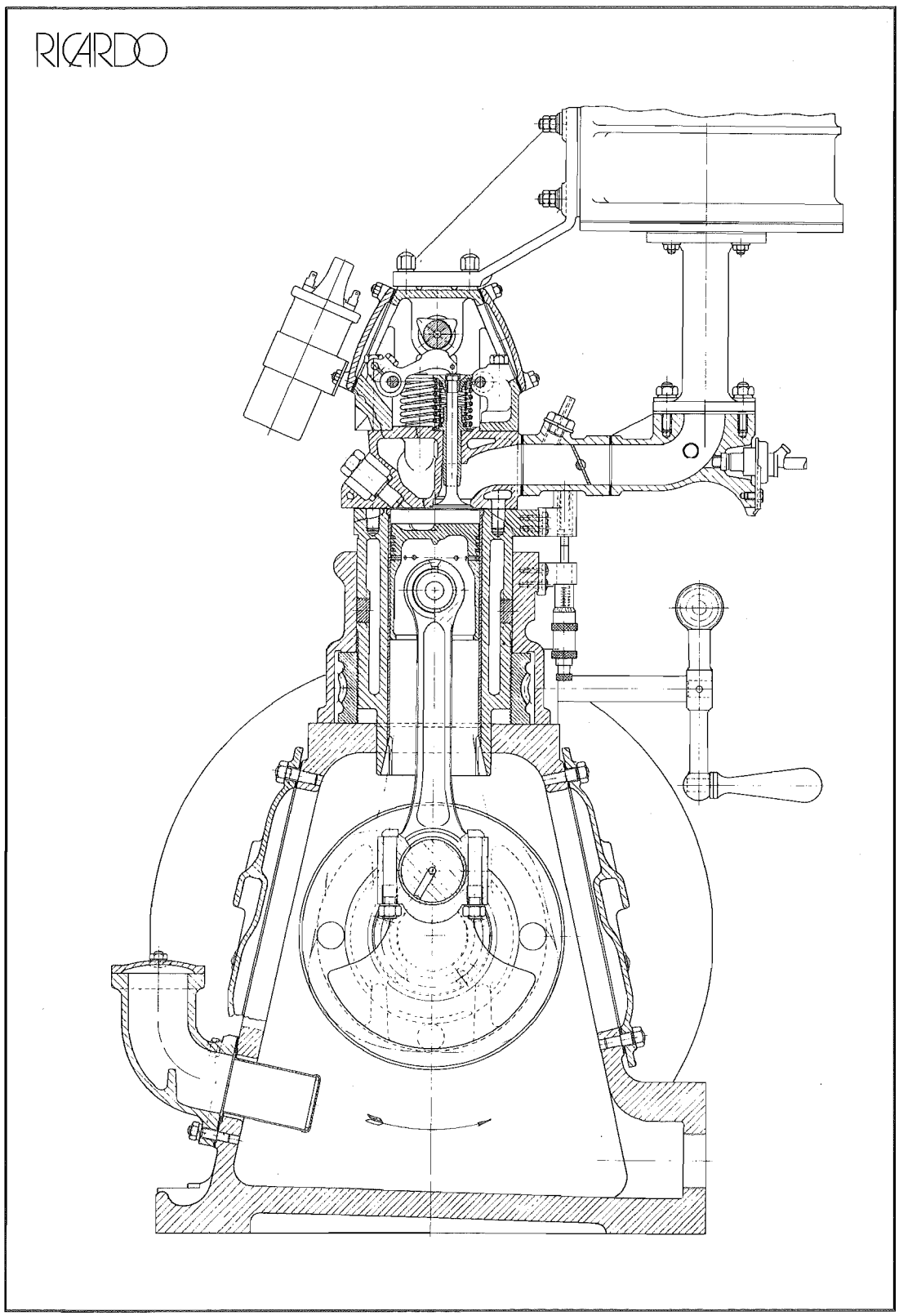

Figure B.1 Cross Sectional Arrangement of a Ricardo E6 Variable Compression Research Engine

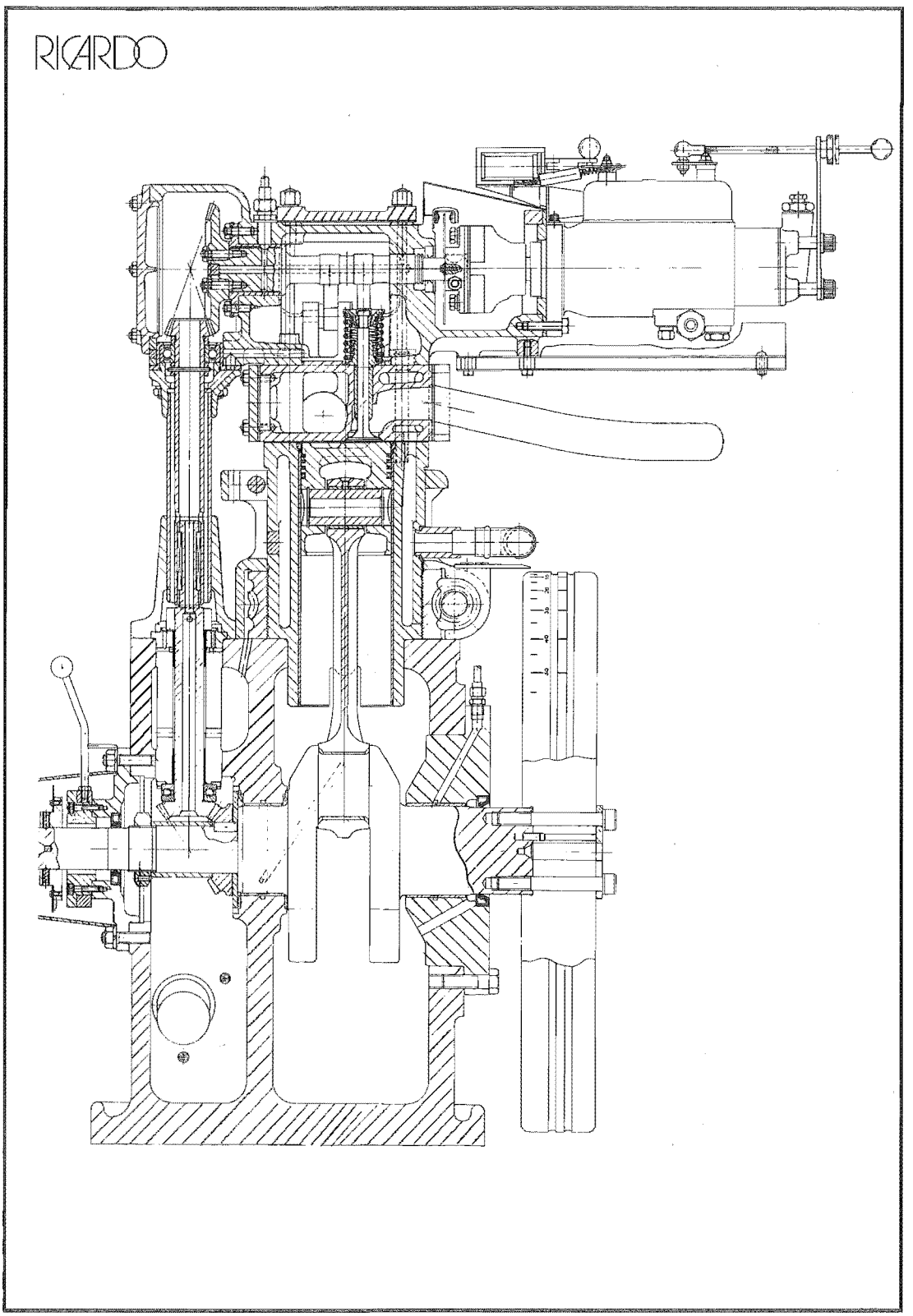

Figure B.2 Longitudinal Sectional Arrangement of a Ricardo E6 Variable Compression Research Engine

Appendix C

Data Acquisition Hardware

The Ricardo Data Acquisition System consists of the pieces of hardware that are listed below along with their relevant specifications.

- Advantech PCL 818HG High Performance DAS Card
  - 100kHz max sampling rate
  - digital inputs
  - digital outputs
  - 16 single ended analogue inputs
  - 8 differential analogue inputs
  - fifo buffer
- Advantech PCLD 889 Multiplexing Card
  - 8 input channels
  - CJC compensation circuit
- PCLD 8115D Wiring Terminal Board
- Cussons Charge Amplifier
- Hewlett Packard 54601 A Oscilloscope
  - 100MHz
  - 4 channel
- 486 DX66 Computer
  - 8 MB RAM
- Color Monitor

Appendix D

Data Acquisition and Processing Programs

All software used for data acquisition, post-processing and combustion analysis in this investigation was written in the Borland C^{++} programming language. All software routines are contained in the project file RICARDO.PRJ. The files contained in the project file are listed below.

- MENU.C
- ANALYSE.C
- FOURSTR1.C
- FIFO118.C
- MASSFRAC.C
- CALIBRAT.C
- CALDATA.C
- CALTRANS.C
- QUIT.C
- CONVERT.C
- STEADY.C
- DATA.C
- VOLUME.C
- FUNCTION.C
- 3DGRAPH.C
- IMEP.C
- 818HCL.LIB

In addition to this, the header file RICARDO.H must be located in the current directory (i.e. with the rest of the *.C files).

The program RICARDO.C is driven by a series of menus which lead the user to the subroutine they require. Although there were many subroutines written, there are only three that were used extensively in this research. The purpose of the other subroutines fall under one of the broad categories listed below.

1. Menus

2. Analysis of two stroke engine combustion pressure traces

3. Analysis routines written but not incorporated into the main analysis subroutine (for example simplified heat release analysis subroutines)

4. Calibration subroutines

The three main subroutines used in the acquisition and analysis of combustion pressure data will be briefly described below. For more in depth information on data acquisition and post-processing procedure used refer to Chapter 5, Data Acquisition and Post-Processing.

D.1 FIFO118.C

This routine was written to acquire high frequency combustion chamber pressure data during engine testing. Acquisition of a piece of data is triggered externally by the rising edge of a trigger pulse from the incremental rotary encoder. The routine is configured to acquire data from 350 consecutive engine cycles with an external trigger pulse frequency of 1800 pulses per engine revolution. The raw data is saved in binary form to a RAM drive before being saved to the hard drive after the 350 cycles have been acquired. All the relevant steady state engine temperatures are also sampled and saved to a file for later reference.

D.2 FOURSTR1.C

This routine was written to completely analyze the raw binary combustion data and create output files summarizing the results. A series of output files are produced containing the results of the analysis along with relevant statistical data.

D.3 CALTRANS.C

This routine was written to acquire the piezo-electric pressure transducer calibration data and convert the raw data to a voltage before saving to a file. The voltage data was later manually analyzed to determine the calibration constant for use in the post-processing software.

Appendix E

Engine Performance Data Analysis

E.1 Methanol Consumption

$$\dot{m}_{MeOH}\ (kg/sec) = \frac{\dot{V}_{MeOH}\ (l/hr) \times SG_{MeOH}\ (kg/l)}{3600\ (sec/hr)} \tag{E.1}$$

where SG_{MeOH} = 0.793 (kg/l)

E.2 Hydrogen Consumption

$$\dot{m}_{H_2}\ (kg/sec) = \frac{slpm\ N_2 \times TBE\ conversion\ factor \times density\ \ of\ H_2\ @\ NPT\ (kg/m^3)}{1000\ (l/m^3) \times 60\ (sec/min)} \tag{E.2}$$

where TBE conversion factor = 1.03

Density of H_2 at 101.325 Pa and 20°C = 0.083764 kg/m^3

E.3 Hydrogen Energy Fraction

A convenient way to express the amount of hydrogen substitution is by the percentage of the total fuel energy that is contributed by hydrogen, denoted the Hydrogen Energy Fraction (HEF) [MacDonald 1976] , [Rauckis and McLean 1979].

$$HEF(\%) = \frac{H_2\ energy}{total\ fuel\ energy} \times 100 \tag{E.3}$$

$$HEF(\%) = \frac{\dot{m}_{H2} \times LCV_{H2}}{\dot{m}_{MeOH} \times LCV_{MeOH} + \dot{m}_{H2} \times LCV_{H2}} \times 100 \tag{E.4}$$

E.4 Volumetric Air Flowrate

From the Alcock Viscous Flow Air Meter No. 1092V operating instructions, p9:

$$\dot{V}_{air}\ (m^3/sec) = 7.7 \times 10^{-5} \times manometer\ reading\ (mm\ H_2O) \times temp.\ correction\ factor \quad \text{(E.5)}$$

E.5 Air Mass Flowrate

$$\dot{m}_{air}\ (kg/sec) = \frac{p_{atm}\ (Pa) \times \dot{V}_{air}\ (m^3/sec)}{R_{air}\ (J/kg\ K) \times T_{air}\ (K)} \quad \text{(E.6)}$$

where R_{air} = specific gas constant of air
= 287 J/kg K

E.6 Volumetric Efficiency

From the basic definition given in Heywood [1988] p54:

$$\eta_v\ (\%) = \frac{2\ (rev/cycle) \times \dot{V}_{air}\ (m^3/sec)}{V_d\ (m^3) \times N\ (rev/sec)} \quad \text{(E.7)}$$

E.7 Relative Air/Fuel Ratio, λ

For a single fuel, λ is defined as:

$$\lambda = \frac{\dot{m}_{air}}{\dot{m}_{fuel} \times (\frac{A}{F}_{stoich})} \quad \text{(E.8)}$$

For an air/fuel mixture comprising of two fuels [Finegold 1978]:

$$\lambda = \frac{\dot{m}_{air}}{[\dot{m}_{MeOH} \times (\frac{A}{F})_{stoichMeOH}] + [\dot{m}_{H2} \times (\frac{A}{F})_{stoichH2}]} \quad \text{(E.9)}$$

E.8 Brake Power

From the Ricardo E6/Mk6 Variable Compression Engine Serial Number 138/82 manual, p12:

$$P\ (kW) = \frac{((20.1 \times No.\ of\ weights) - Dynamometer\ Scale\ Reading) \times N\ (rps)}{348.1} \tag{E.10}$$

E.9 Corrected Brake Power

All brake power readings are corrected [Bosch 1986] to account for test conditions differing from standard conditions of 20°C and 101.325 kPa. This also provides a common basis for comparison of engine performance.

$$P_{corrected}\ (kW) = P\ (kW) \times \frac{1013}{p_{atm}\ (mbar)} \times \sqrt{\frac{T_{air}\ (K)}{273}} \tag{E.11}$$

E.10 Gross Indicated Power

$$P_i\ (kW) \quad = \quad \frac{IMEP_g(bar) \times 100 \times V_d(l) \times N(rev/sec)}{n_R \times 1000} \tag{E.12}$$

where:

$$\begin{aligned} n_R &= 1\ for\ two\ stroke\ cycles \\ &= 2\ for\ four\ stroke\ cycles \end{aligned}$$

E.11 Gross Indicated Thermal Efficiency

$$\eta_{ith} = \frac{P_i\ (kW)}{Total\ Fuel\ Energy\ (kW)} \tag{E.13}$$

E.12 Mechanical Efficiency

From Heywood [1988] page 49:

$$\eta_m = \frac{P_{corrected}\,[kW]}{P_i\,[kW]} \tag{E.14}$$

Appendix F

Calculation of Specific Emissions

Specific engine emissions relate the level of exhaust gas emissions to the power output of the engine. For the purposes of this work, raw engine emissions were converted to specific emissions using the method presented by Coates and Lassanske [1990]. The equations used are summarized below.

F.1 Converting Dry Concentration Data into Wet Terms

All the exhaust gas samples pass through water traps before reaching the emissions analyzers. In the case of the NO_x meter, the exhaust gas sample also passes through a refrigerator unit to condense out any remaining water. The emissions readings must be converted from dry values to wet values before being used in the analysis.

$$[\,]_w = K \times [\,]_d \tag{F.1}$$

where:

$$K = \frac{1}{1 + 0.005\left([CO]_d(\%) + [CO_2]_d(\%)\right) y - 0.01[H_2]} \tag{F.2}$$

and

$$[H_2] = \frac{0.5y[CO]_d(\%) \times \left([CO]_d(\%) + [CO_2]_d(\%)\right)}{[CO]_d(\%) + 3[CO_2]_d(\%)} \tag{F.3}$$

F.2 Conversion to Mass Emission Units

$$\dot{m}_{UHC}\ (g/hr) = 10^{-4} \times [UHC]_w(ppmC) \times \frac{\dot{m}_{fuel}(g/hr)}{[TC]} \quad \text{(F.4)}$$

$$\dot{m}_{CO}\ (g/hr) = [CO]_w(\%) \times \frac{\dot{m}_{fuel}(g/hr)}{[TC]} \times \frac{M_{CO}}{M_C + yM_H} \quad \text{(F.5)}$$

$$\dot{m}_{CO2}\ (g/hr) = [CO2]_w(\%) \times \frac{\dot{m}_{fuel}(g/hr)}{[TC]} \times \frac{M_{CO2}}{M_C + yM_H} \quad \text{(F.6)}$$

$$\dot{m}_{NOx}\ (g/hr) = 10^{-4} \times [NOx]_w(ppm) \times KH \times \frac{\dot{m}_{fuel}(g/hr)}{[TC]} \times \frac{M_{NOx}}{M_C + yM_H} \quad \text{(F.7)}$$

where:

$$\begin{aligned}
[TC] &= [CO2]_w(\%) + [CO]_w(\%) + 10^{-4} \times [UHC]_w(ppmC) \\
KH &= \frac{1}{1 - 0.0329(h - 10.714)} \\
h &= \frac{621.97 p_w}{P - p_w} \\
M_C &= 12.011 \\
M_H &= 1.008 \\
M_{CO} &= 28.010 \\
M_{CO2} &= 44.009 \\
M_{NOx} &= 46.005 \\
y &= \textit{Number of hydrogen atoms in fuel molecule} \\
&= 4 \textit{ for methanol}
\end{aligned}$$

F.3 Calculation of Gross Indicated Power

$$P_i\ (kW) = \frac{IMEP_g(bar) \times 100 \times V_d(l) \times N(rps)}{n_R \times 1000} \quad \text{(F.8)}$$

where:

$$\begin{aligned}
n_R &= 1 \textit{ for two stroke cycles} \\
&= 2 \textit{ for four stroke cycles}
\end{aligned}$$

F.4 Calculation of Indicated Specific (is) Emissions

$$isUHC\ (g/kW.h) \quad = \quad \frac{\dot{m}_{UHC}\ (g/hr)}{P_i\ (kW)} \tag{F.9}$$

Appendix G

Combustion Stoichiometry

During the analysis of the emissions produced by the engine, it was thought that knowledge of the level of emissions produced by the ideal combustion of methanol/hydrogen mixtures would be of benefit. The ideal emission levels were compared to the actual engine emission levels to help elucidate the effects of hydrogen addition. The overall complete combustion equation for a dual fuel mixture of methanol and hydrogen was derived. An equation has previously been presented by Kyaw [1989]. Kyaw's analysis is accurate for the addition of small mass fractions (<2%[1]) of hydrogen to methanol but becomes inaccurate as the mass fraction of hydrogen is increased. The equation that was derived during this investigation is accurate for a mixture containing any fraction of hydrogen (i.e. from 0% to 100% hydrogen substitution). In deriving this equation the molar masses of methanol and hydrogen were assumed to be 32 and 2 respectively[2]. The number of moles of hydrogen being reacted was multiplied by 16 so that the molecular masses of the two reacting fuels were made to be equal. This allowed the fraction of hydrogen to be expressed as a mass fraction (f) and thus be able to be related to the hydrogen energy fraction (HEF) which has been used as the measure of hydrogen supplementation throughout this work.

The equation derived is:

$$\begin{aligned}(1-f)\,CH_3OH + 1.5\,(1-f)\,\lambda\,O_2 + 1.5\,(1-f)\,\lambda\,3.773\,N_2 + 16\,f\,H_2 + \\ 8\,f\,\lambda\,O_2 + 3.773\,\lambda\,8\,f\,N_2 \quad \rightarrow \quad aCO_2 + bH_2O + cO_2 + dN_2\end{aligned} \tag{G.1}$$

[1] This equates to a hydrogen energy fraction of approximately 11%

[2] It was later calculated that using the correct molar masses of 32.04 and 2.015 for methanol and hydrogen respectively resulted in differences in the calculated exhaust gas pollutant levels of less than 0.3%.

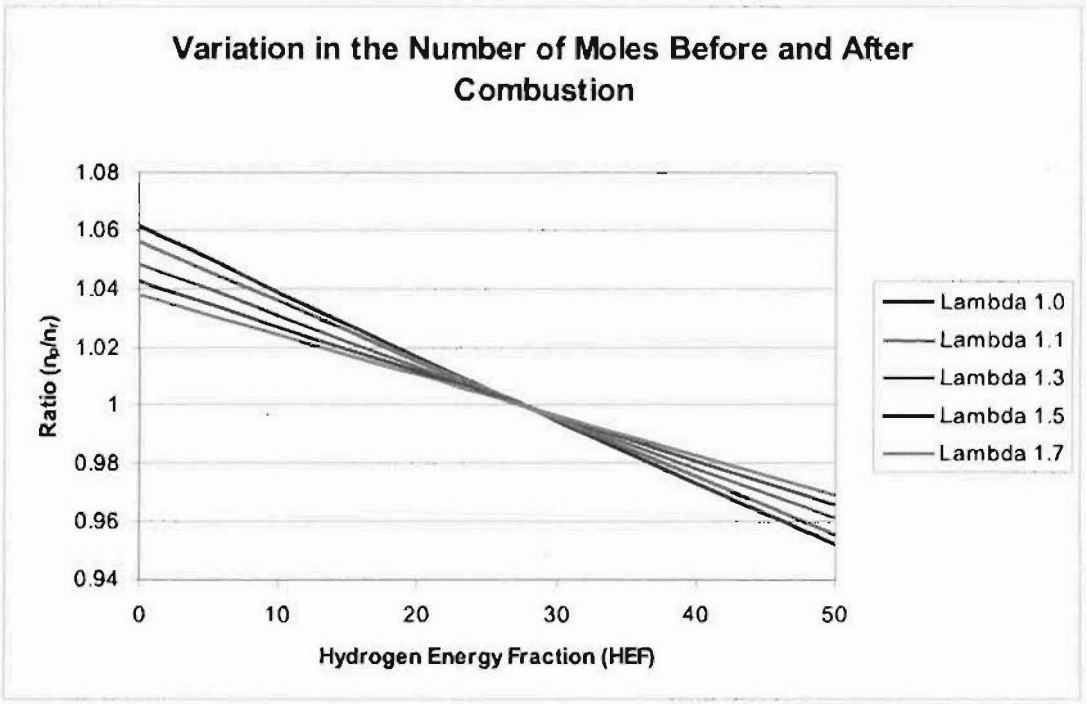

Figure G.1 Effect of Combustion on Number of Moles of Products

where f = hydrogen mass fraction
λ = relative air/fuel ratio
a = (1-f)
b = 2 + 14f
c = 6.5 f λ + 1.5 λ - 6.5 f - 1.5
d = 5.6595 λ + 24.5245 λ f

The hydrogen mass fraction and hydrogen energy fraction are related by:

$$f = \frac{1}{1 + \left[\left(\frac{1}{HEF} - 1\right)\frac{LCV_{H2}}{LCV_{MeOH}}\right]} \tag{G.2}$$

where HEF = hydrogen energy fraction
LCV_{H2} = lower calorific value of hydrogen
LCV_{MeOH} = lower calorific value of methanol

The stoichiometric combustion equation can be used to determine the change in the number of moles between reactants and products for various values of λ and HEF. The resultant plot is shown in Figure G.1.

The following key points are apparent from Figure G.1.

1. The combustion of methanol alone results in an increase in the number of moles

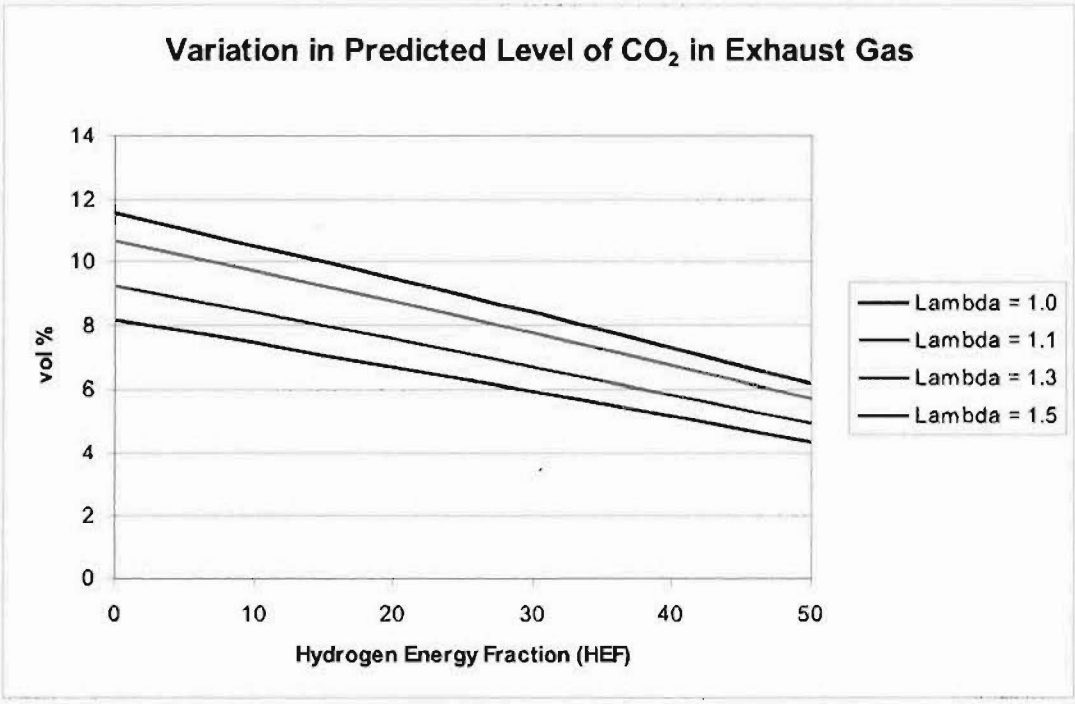

Figure G.2 Predicted Level of CO_2 Pollutant in Exhaust Gas

present for all air/fuel ratios with the richest mixtures showing the greatest increase.

2. As the HEF is increased for a given air/fuel ratio, the ratio n_p/n_r decreases.

3. The ratio n_p/n_r decreases at a greater rate with HEF for richer air/fuel ratios.

4. At HEF $\approx$ 27.5 for all air/fuel ratios, the number of moles before and after combustion are equal.

Equation G.2 can also be used to predict the level of exhaust gas pollutants that would be formed in the ideal combustion of a dual fuel mixture of methanol and hydrogen. Figures G.2 to G.4 show the predicted exhaust gas pollutant levels of CO_2, H_2O and O_2. CO emissions are not included as rich mixtures are not of interest. In practice however there will be some small emission of CO when using lean air/fuel ratios.

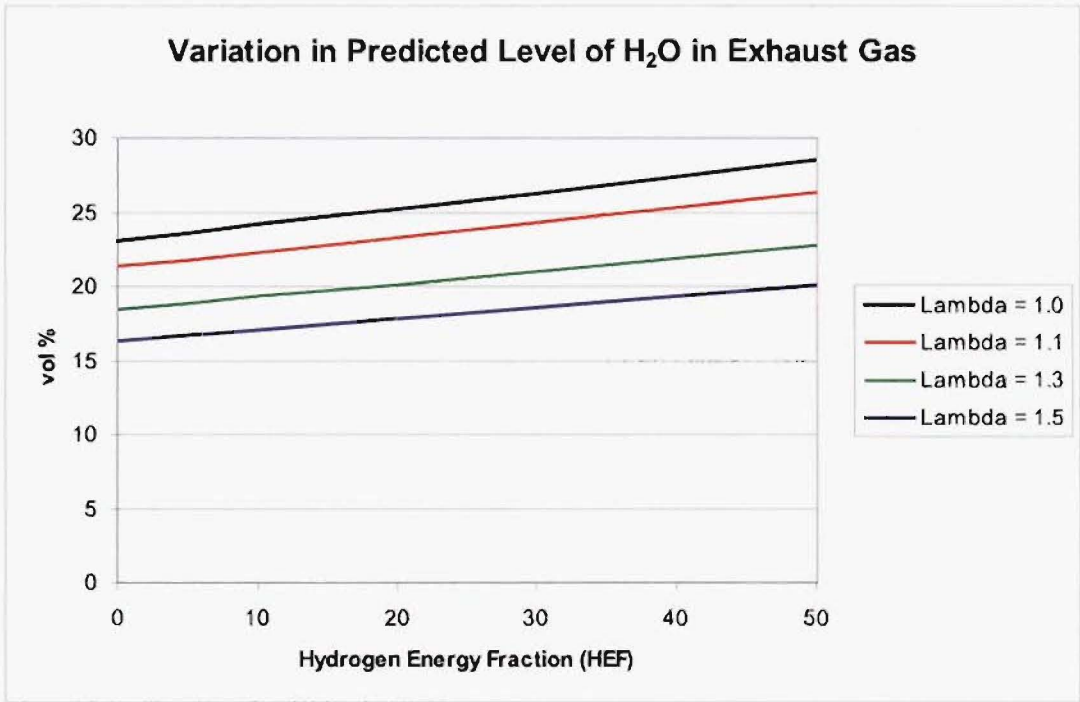

Figure G.3 Predicted Level of H_2O Pollutant in Exhaust Gas

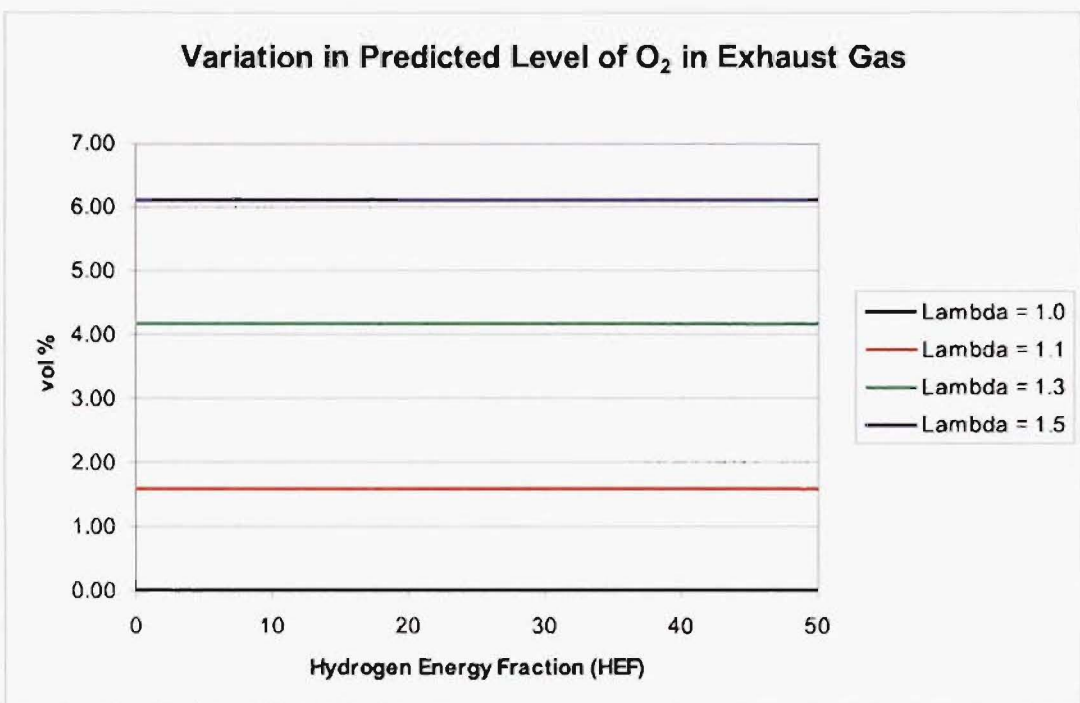

Figure G.4 Predicted Level of O_2 Pollutant in Exhaust Gas

References

AMANN, C. (1985), 'Cylinder-Pressure Measurement and its Use in Engine Research', *SAE 852067.*

ANNAND, W. (1983), 'The Estimation Of Flame Propogation Rates In Routine Computer Synthesis Of Spark Ignition Engine Combustion', In *International Conference on Combustion in Engineering Volume One*, I Mech E Conference Publications 1983-3, pp. 125 – 134.

APOSTOLESCU, N. AND CHIRAC, R. (1996), 'A Study Of Combustion Of Hydrogen-Enriched Gasoline In A Spark Ignition Engine', *SAE 960603.*

ATKINSON, C., TRAVER, M., TENNANT, C., ATKINSON, R. AND CLARK, N. (1995), 'Improving Combustion Stability In A Bi-Fuel Engine', *Automotive Engineering*, June, pp. 77–80.

BALL, J., RAINE, R. AND STONE, C. (1998a), 'Combustion Analysis And Cycle-By-Cycle Variations In Spark Ignition Engine Combustion. Part 1: An Evaluation Of Combustion Analysis Routines By Reference To Model Data', *Proc. Instn. Mech. Engrs.*, Vol. 212, No. Part D, pp. 381–399.

BALL, J., RAINE, R. AND STONE, C. (1998b), 'Combustion Analysis And Cycle-By-Cycle Variations In Spark Ignition Engine Combustion. Part 2: A New Parameter For Completeness Of Combustion And Its Use In Modelling Cycle-By-Cycle Variations In Combustion', *Proc. Instn. Mech. Engrs.*, Vol. 212, No. Part D, pp. 507–523.

BECKMAN (1980), *Beckman Model 951A NO/NO_x Analyzer Instruction Manual*, Beckman Instruments Inc., Fullerton, California, United States of America.

BECKMAN (1981), *Beckman Model 402 Hydrocarbon Analyzer Instruction Manual*, Beckman Instruments Inc., Fullerton, California, United States of America.

BELL, A., TAYLOR, A., MORAN, D., HODGSON, N., MYBURGH, I. AND BOTHA, J. (1996), 'Propyl Alcohols As Alternative And Supplementary Spark-Ignition Fuels - Part 2: Exhaust Emissions', In *Eleventh International Sysmposium on Alcohol Fuels*, pp. 774 – 785.

BERNHARDT, W. (1977), 'Future Fuels And Mixture Preparation Methods For Spark Ignition Automobile Engines', *Prog. Energy Combustion Sci.*, Vol. 3, pp. 139 – 150.

BINDER, K. AND WITHALM, G. (1980), 'Mixture Formation And Combustion In Interaction With The Hydrogen Storage Technology', In *3rd World Hydrogen Energy Conference*, pp. 1103 – 1117.

BOSCH, R. (1986), *Automotive Handbook*, Robert Bosch GmbH, Postfach 50, D-7000 Stuttgart 1, Germany, p. 331.

BRINKMAN, N. AND STEBAR, R. (1985), 'A Comparison Of Methanol And Dissociated Methanol Illustrating Effects Of Fuel Properties On Engine Efficiency - Experiments And Thermodynamic Analyses', *SAE 850217.*

BROWN, R. (2001), *Hydrogen Fueling of a Wankel Rotary Engine*, PhD thesis, (In Progress), Department of Mechanical Engineering, University of Canterbury, Christchurch, New Zealand.

BRUNT, M. AND EMTAGE, A. (1996), 'Evaluation Of IMEP Routines And Analysis Errors', *SAE 960609.*

BRUNT, M. AND EMTAGE, A. (1997), 'Evaluation Of Burn Rate Routines And Analysis Errors', *SAE 970037.*

BRUNT, M. AND POND, C. (1997), 'Evaluation Of Techniques For Absolute Cylinder Pressure Correction', *SAE 970036.*

CAE (1996), *Energy Efficiency - A Guide to Current and Emerging Technologies*, Vol. 1, Centre for Advanced Engineering, University of Canterbury, Christchurch, New Zealand.

CALVERT, I. (1994), *Prechamber Charge Stratification of an Internal Combustion Engine*, Master's thesis, Department of Mechanical Engineering, University of Canterbury, Christchurch, New Zealand.

CHEN, T. (1991), *Diesel Engine Operation on Alcohol Fuels Using a Computer Controlled Fumigation Process*, Master's thesis, Department of Mechanical Engineering, University of Canterbury, Christchurch, New Zealand.

CHENG, W., HAMRIN, D., HEYWOOD, J., HOCHGREB, S., MIN, K. AND NORRIS, M. (1993), 'An Overview Of Hydrocarbon Emission Mechanisms In Spark Ignition Engines', *SAE 932708.*

CHUN, K. AND HEYWOOD, J. (1987), 'Estimated Heat-Release And Mass-Of-Mixture Burned From Spark-Ignition Engine Pressure Data', *Combust. Sci. and Tech.*, Vol. 54, pp. 133–143.

COATES, S. AND LASSANSKE, G. (1990), 'Measurement And Analysis Of Gaseous Exhaust Emissions From Recreational And Small Marine Craft', *SAE 901597.*

COHN, D., RABINOVICH, A. AND TITUS, C. (1996), 'Onboard Plasmatron Generation Of Hydrogen For Extremely Low Emission Vehicles With Internal Combustion Engines', *Int. J. of Vehicle Design*, Vol. 17, No. 5/6 (Special Issue), pp. 550–561.

COLE, P., GREEN, R., RAINE, J., SMITH, N. AND WARING, P. (1986), 'Transport Fuels In New Zealand - A New Direction', In *Proceedings of World Energy Conference Regional Symposium, "Energy Towards 2000", Perth, Australia, 24-26 March*, pp. 553 – 577.

CREE, A. (1992), *Methanol Injection of a High Performance Two-Stroke Engine*, Bachelor of Engineering Project Report 28/92, Department of Mechanical Engineering, University of Canterbury, Christchurch, New Zealand.

DAMIANO, L. (1993), *The Effect of Charge Stratification on the Combustion of Lean Methane-Oxygen Mixtures Under Constant Volume Conditions.*, Master's thesis, Department of Mechanical Engineering, University of Canterbury, Christchurch, New Zealand.

DAS, L. (1990), 'Abnormal Combustion In Hydrogen Engines: Causes And Remedies', In *Proceedings of the Eighth World Hydrogen Energy Conference*, pp. 1379 – 1397.

DAS, L. AND MATHUR, R. (1993), 'Exhaust Gas Recirculation For NO_x Control In A Multicylinder Hydrogen-Supplemented S.I. Engine', *Int. J. Hydrogen Energy*, Vol. 18, No. 12, pp. 1013–1018.

DATE, T., YAGI, S., ISHIZUYA, A. AND FUJI, L. (1974), 'Research And Development Of The Honda CVCC Engine', *SAE 740605.*

DE GOEDE, S., ENGELBRECHT, W., VAN DER MERWE, L., BELL, A. AND TAYLOR, A. (1996), 'Aldehyde Emissions Quantification With Primary And Secondary Alcohols In Spark-Ignition Fuel Blends', In *Eleventh International Sysmposium on Alcohol Fuels*, pp. 796 – 808.

DELUCHI, M. (1989), 'Hydrogen Vehicles: An Evaluation Of Fuel Storage, Performance, Safety, Environmental Impacts, And Cost', *Int. J. Hydrogen Energy*, Vol. 14, No. 2, pp. 81–130.

EMA (1982), 'A Technical Assessment Of Alcohol Fuels', *SAE 820261.* Alternative Fuels Committee of the Engine Manufacturers Association.

FERGUSON, C. (1986), *Internal Combustion Engines - Applied Thermosciences*, John Wiley & Sons, Inc.

FINEGOLD, J. (1978), 'Hydrogen: Primary Or Supplementary Fuel For Automotive Engines', *International Journal of Hydrogen Energy*, Vol. 3, pp. 83 – 104.

FLAGAN, R. AND SEINFELD, J. (1988), *Fundamentals of Air Pollution Engineering*, Prentice Hall.

FURUHAMA, S. (1979), 'Two-Stroke Hydrogen Injection Engine', *International Journal of Hydrogen Energy*, Vol. 4, pp. 571 – 576.

FURUHAMA, S. AND KOBAYASHI, Y. (1982), 'Development Of A Hot-Surface-Ignition Hydrogen Injection Two-Stroke Engine', In *World Hydrogen Energy Conference IV*, pp. 1009 – 1020.

FURUHAMA, S. AND KOBAYASHI, Y. (1982a), 'A Liquid Hydrogen Car With A Two-Stroke Direct Injection Engine And LH_2 Pump', *International Journal of Hydrogen Energy*, Vol. 7, No. 10, pp. 809 – 820.

FURUHAMA, S., HIRUMA, M. AND ENOMOTO, Y. (1978), 'Development Of A Liquid Hydrogen Car', *International Journal of Hydrogen Energy*, Vol. 3, pp. 61 – 81.

FURUHAMA, S., HIRUMA, M., KOYANAGI, K., TOMISAWA, N. AND YAMAURA, K. (1991), 'The Power System Of A Computer Controlled Hydrogen Car - GH_2 Injection And Spark Ignition Engine With LH_2 Tank And Pump', In *Proceedings of the Institution of Mechanical Engineers - Computers in Engine Technology*, pp. 179 – 188. Paper no. C430/028.

GATOWSKI, J., BALLES, E., CHUN, K., NELSON, F., EKCHIAN, J. AND HEYWOOD, J. (1984), 'Heat Release Analysis Of Engine Pressure Data', *SAE 841359*.

GERMANE, G., WOOD, C. AND HESS, C. (1983), 'Lean Combustion In Spark-Ignited Internal Combustion Engines - A Review', *SAE 831694*.

GLASSON, N.D. (1992), *Hydrogen Fuelling of an Internal Combustion Engine*, PhD thesis, Department of Mechanical Engineering, University of Canterbury, Christchurch, New Zealand.

GLASSON, N., LUMSDEN, G., DINGLI, R. AND WATSON, H. (1996), 'Development Of The HAJI System For A Multi-Cylinder Spark Ignition Engine', *SAE 961104*.

GUSSAK, L. (1975), 'High Chemical Activity Of Incomplete Combustion Products And A Method Of Prechamber Torch Ignition For Avalanche Activation Of Combustion In Internal Combustion Engines', *SAE 750890*.

GUSSAK, L. (1976), 'LAG -Process Of Combustion And It's Application In Automobile Gasoline Engines', *IMechE C257/76*, pp. 137 – 145.

HAACK, L., LACOURSE, D. AND KORNISKI, T. (1986), 'Comparison Of Fourier Transform Infrared Spectrometry And 2,4-Dinitrophenylhydrazine Impinger Techniques For The Measurement Of Formaldehyde In Vehicle Exhaust', *Analytical Chemistry*, Vol. 58, pp. 68 – 72.

HASALETT, R., MONAGHAN, M. AND M^{c}FADDEN, J. (1976), 'Stratified Charge Engines', *SAE 760755.*

HATANO, K., IIDA, K., HIGASHI, H. AND MURATA, S. (1993), 'Development Of A New Multi-Mode Variable Valve Timing Engine', *SAE 930878.*

HEYWOOD, J. (1988), *Internal Combustion Engine Fundamentals*, McGraw-Hill International, Singapore.

HEYWOOD, J. (1991), 'Future Engine Technology: Lessons From The 1980's For The 1990's', *Journal of Engineering for Gas Turbines and Power*, Vol. 113, July, pp. 319–330.

HEYWOOD, J. (1997), 'Motor Vehicle Emissions Control: Past Achievements, Future Prospects', *IMechE 1997 George Stephenson Lecture.*

HEYWOOD, J. AND VILCHIS, F. (1984), 'Comparison Of Flame Development In A Spark Ignition Engine Fueled With Propane And Hydrogen', *Combustion Science and Technology*, Vol. 38, pp. 313–324.

HIRES, S., TABACZYNSKI, R. AND NOVAC, J. (1978), 'The Prediction Of Ignition Delay And Combustion Intervals For A Homogeneous Charge, Spark Ignition Engine', *SAE 780232.*

HIROTA, T., OHTA, T. AND MITSUMOTO, H. (1991), 'R&d Activities For Methanol S.I. Engines At Nissan', *9th International Symposium on Alcohol Fuels, Firenze*, pp. 587–592.

HOEKSTRA, R., COLLIER, K. AND MULLIGAN, N. (1994), 'Demonstration Of Hydrogen Mixed Gas Vehicles', In *Hydrogen Energy Progress X*, Proceedings of the 10^{th} Worth Hydrogen Energy Conference, Cocoa Beach, Florida, USA, 20-24 June, pp. 1781–1796.

HOEKSTRA, R., COLLIER, K., MULLIGAN, N. AND CHEW, L. (1995), 'Experimental Study Of A Clean Burning Vehicle Fuel', *Int. J. Hydrogen Energy*, Vol. 20, No. 9, pp. 737–745.

HOLDER, D. AND NORTH, R. (1963), *Schlieren Methods*, Notes on Applied Science No. 31, National Physical Laboratory, Longmans (Dorchester) Ltd., The Friary Press, Dorchester, Dorset.

HOMAN, H., DE BOER, P. AND M^{c}LEAN, W. (1983), 'The Effect Of Fuel Injection On NO_x Emissions And Undesirable Combustion For Hydrogen Fueled Piston Engines', *International Journal of Hydrogen Energy*, Vol. 8, No. 2, pp. 131 - 146.

HORIBA (1988), *Horiba MEXA-534GE Automotive Emission Analyzer Operation Manual*, Miyanohigashi, Kisshoin, Minami-ku, Kyoto, Japan.

HOUSEMAN, J. AND HOEHN, F. (1974), 'A Two-Charge Engine Concept: Hydrogen Enrichment', *SAE 741169*.

HOUSEMAN, J. AND VOECKS, G. (1980), 'Hydrogen Engines Based On Liquid Fuels, A Review', *3rd World Hydrogen Energy Conference*, pp. 949–968.

HUFF, S. AND HODGSON, J. (1993), 'Demonstration Of The Fuel Economy Potential Of A Vehicle Fueled With M85', *10th International Symposium on Alcohol Fuels*, p. 597.

HUNTSMAN, I. (2000), 'Lecturer In Fluid Mechanics, University Of Canterbury'. Private Communication.

IWAMOTO, Y., NOMA, K., NAKAYAMA, O., YAMAUCHI, T. AND ANDO, H. (1997), 'Development Of Gasoline Direct Injection Engine', *SAE 970541*.

JAMAL, Y. AND WYSZNSKI, M. (1994), 'On-Board Generation Of Hydrogen-Rich Gaseous Fuels - A Review', *Int. J. Hydrogen Energy*, Vol. 19, No. 7, pp. 557 – 572.

JONES, M. AND WYSZYNSKI, M. (1990), 'Thermodynamic Feasibility Studies Of The Exhaust - Gas Reforming Of Hydrocarbon Fuels', *IMechE C394/014*, pp. 71–77.

JONES, M. AND WYSZYNSKI, M. (1993a), 'Exhaust-Gas Reforming Of Hydrocarbon Fuels', *SAE 931096*.

JONES, M. AND WYSZYNSKI, M. (1993b), 'Onboard Generation Of Hydrogen-Based Gaseous Engine Fuels By Exhaust-Gas Reforming Of Liquid Hydrocarbons', In *Autotech '93, 15-19 November*.

JORACH, R. AND PRESCHER, K. (1994), 'Development Of A Low-NO_x Truck Hydrogen Engine With High Specific Power Output', In *10^{th} World Hydrogen Energy Conference*, pp. 1857 – 1865.

JORDAN, W. (1979), 'The Influence Of Hydrogen Addition To The Air-Fuel Mixture On Otto Engine Combustion', *SAE 790678*.

KARIM, G. AND WATSON, H. (1971), 'Experimental And Computational Considerations Of The Compression Ignition Of Homogeneous Fuel-Oxidant Mixtures', *SAE 710133*.

KARIM, G., WIERZBA, I. AND AL-ALOUSI, Y. (1996), 'Methane-Hydrogen Mixtures As Fuels', *Int. J. hydrogen Energy*, Vol. 21, No. 7, pp. 625–631.

KONIG, A., ELLINGER, K. AND KORBEL, K. (1985), 'Engine Operation On Partially Dissociated Methanol', *SAE 850573.*

KOYANAGI, K., HIRUMA, M., YAMANE, K. AND FURUHAMA, S. (1993), 'Effect Of Hydrogen Jet On Mixture Formation In A High-Pressure Injection Hydrogen Fueled Engine With Spark Ignition', *SAE 931811.*

KRIEGER, R. AND BORMAN, G. (1966), 'The Computation Of Apparent Heat Release For I.C. Engines', *ASME 66, WA/DGP-4.*

KUME, T., IWAMOTO, Y., IIDA, K., MURAKAMI, M., AKISHINO, K. AND ANDO, H. (1996), 'Combustion Control Technologies For Direct Injection SI Engine', *SAE 960600.*

KYAW, Z. (1989), *Performance of Unmodified Spark Ignition Engine Using Methanol with Hydrogen Pilot Fuel*, Technical Report, The Development Technologies Unit, Faculty of Engineering, University of Melbourne, Australia.

KYAW, Z. (1992), *Chemical Control of SI Engine Combustion*, PhD thesis, Department of Mechanical and Manufacturing Engineering, University of Melbourne, Melbourne, Australia.

KYAW, Z. AND WATSON, H. (1993), 'Application Of The HAJI System For Near NO_x Elimination In The SI Engine', In *Worldwide Engine Emission Standards And How to Meet Them*, Mechanical Engineering Publications, May, pp. 49–56.

LANCASTER, D.R., KRIEGER, R.B. AND LIENESCH, J. (1975), 'Measurement And Analysis Of Engine Pressure Data', *SAE 750026.*

LAWRENCE, J. (1999), *Hydrocarbon Emissions from a HAJI Equipped Ultra Lean Burn Engine*, PhD thesis, Department of Mechanical and Manufacturing Engineering, University of Melbourne, Melbourne, Australia.

LEWIS, B. AND VON ELBE, G. (1987), *Combustion, Flames and Explosions of Gases*, Academic Press, third ed.

LIPARI, F. AND COLDEN, F. (1987), 'Aldehyde And Unburned Fuel Emissions From Developmental Methanol-Fueled 2.5L Vehicles', *SAE 872051.*

LIPARI, F. AND SWARIN, S. (1982), 'Determination Of Formaldehyde And Other Aldehydes In Automobile Exhaust With An Improved 2,4-Dinitrophenylhydrazine Method', *Journal of Chromatography*, Vol. 247, pp. 297 – 306.

LIPMAN, T. AND DELUCCHI, M. (1996), 'Hydrogen-Fuelled Vehicles', *Int. J. of Vehicle Design*, Vol. 17, No. 5/6 (Special Issue), pp. 562 – 589.

LU, J., GUPTA, A., POURING, A. AND KEATING, E. (1994), 'A Preliminary Study Of Chemically Enhanced Autoignition In An Internal Combustion Engine', *SAE 940758.*

LUMSDEN, G. (1995), *The Phenomena of Hydrogen Assisted Jet Ignition*, PhD thesis, Department of Mechanical and Manufacturing Engineering, University of Melbourne, Melbourne, Australia.

MACCARLEY, C. AND VAN VORST, W. (1980), 'Electronic Fuel Injection Techniques For Hydrogen Powered I.C. Engines', *International Journal of Hydrogen Energy*, Vol. 5, No. 2, pp. 179 – 203.

MACDONALD, J. (1976), 'Evaluation Of The Hydrogen Supplemented Fuel Concept With An Experimental Multicylinder Engine', *SAE 760101.*

MASSEY, B. (1989), *Mechanics of Fluids*, Chapman & Hall, sixth ed., pp. 102 – 103.

MATEKUNAS, F. (1983), 'Modes And Measures Of Cyclic Combustion Variability', *SAE 830337.*

MAXSON, J., HENSINGER, D., HOM, K. AND OPPENHEIM, A. (1991), 'Performance Of Multiple Stream Pulsed Jet Combustion Systems', *SAE 910565.*

MAXWELL, T., JONES, J., JAYAKARAN, J., BOYCE, C. AND PARKER, H. (1993), 'Cold-Starting Methanol Fueled Engines With Decomposed Methanol', In *10th International Symposium of Alcohol Fuels*, pp. 1001 – 1009.

MCCARTY, R., HORD, J. AND RODER, H. (1981), *Selected Properties of Hydrogen (Engineering Design Data)*, National Bureau of Standards Monograph 168, United States Department of Commerce.

MEARNS, A. AND DUTKIEWICZ, R. (1993), 'Aldehyde Emissions From Alcohol Fuels In A CI Engine Using Cetane Improver', In *10th International Symposium on Alcohol Fuels.*

MENARD, W., MOYNIHAN, P. AND RUPE, J. (1976), 'New Potentials For Conventional Aircraft When Powered By Hydrogen-Enriched Gasoline', *SAE 760469.*

MENZIES, K. AND BELTIS, K. (1982), 'Comparison Of Aldehyde Methods', *SAE 820965.*

MINISTRY OF COMMERCE (1990), *Final Report of Activities*, Technical Report LF 6020, Liquid Fuels Trust Board.

MORI, T., TSURUGA, F., SASAKI, S., MAEDA, A., KACHI, H. AND NIWA, K. (1993), 'Measurement Method Of Formaldehyde From Methanol-Fueled Vehicles', In *10th International Symposium on Alcohol Fuels.*

NEWHALL, H. AND SHAHED, S. (1971), 'Kinetics Of Nitric Oxide Formation In High Pressure Flames', In *Thirteenth Symposium (International) on Combustion*, pp. 381–389.

NICHOLS, R. (1994), 'The Challenges Of Change In The Auto Industry: Why Alternative Fuels?', *Journal of Engineering for Gas Turbines and Power*, Vol. 116, No. October, pp. 727–732.

NICHOLS, R., CLINTON, E., KING, E., SMITH, C. AND WINELAND, R. (1988), 'A View Of Flexible Fuel Vehicle Aldehyde Emissions', *SAE 881200.*

NOWELL, G. (1999), *Looking Beyond the Internal Combustion Engine - The Promise of Methanol Fuel Cell Vehicles*, http://www.methanol.org, State University of New York at Albany.

OWENS, E., NAEGELI, D., MARBACH, H., RYAN, T. AND FRAME, E. (1982), 'Approaches To Controlling Wear In Alcohol-Fueled Engines', In *Proceedings of the Fifth International Alcohol Fuel Technology Symposium, Auckland, New Zealand.*

OZDOR, N., DULGER, M. AND SHER, E. (1994), 'Cyclic Variability In Spark Ignition Engines. A Literature Survey', *SAE 940987.*

OZDOR, N., DULGER, M. AND SHER, E. (1996), 'An Experimental Study Of The Cyclic Variability In Spark Ignition Engines', *SAE 960611.*

PESCHKA, W. AND ESCHER, W.J.D. (1993), 'Germany's Contribution To The Demonstrated Technical Feasibility Of The Liquid-Hydrogen Fueled Passenger Automobile', *SAE 931812.*

PETTERSSON, L. AND SJOSTROM, K. (1991a), 'Decomposed Methanol As A Fuel - A Review', *Combust. Sci. and Tech.*, Vol. 80, pp. 265–303.

PETTERSSON, L. AND SJOSTROM, K. (1991b), 'Onboard Hydrogen Generation By Methanol Decomposition For The Cold Start Of Neat Methanol Engines', *Int. J. Hydrogen Energy*, Vol. 16, No. 10, pp. 671–676.

PICHAINARONG, P., IWATA, T. AND FURAHAMA, S. (1990), 'Study Of Thermodynamic Analysis In Hydrogen Injection Engines', In *Proceedings of the 8th World Hydrogen Energy Conference*, pp. 1275 – 1284.

RAMAN, V., HANSEL, J., FULTON, J., LYNCH, F. AND BRUDERLY, D. (1994), 'Hythane - An Ultraclean Transportation Fuel', In *Hydrogen Energy Progress X*, Proceedings

of the 10^{th} Worth Hydrogen Energy Conference, Cocoa Beach, Florida, USA, 20-24 June, pp. 1797–1806.

RAUCKIS, M.J. AND MCLEAN, W. (1979), 'The Effect Of Hydrogen Addition On Ignition Delays And Flame Propagation In Spark Ignition Engines', *Combustion Science and Technology*, pp. 207–216.

ROACHE, K. (1998), *A Study of Premixed and Stratified Charge Combustion of $CH_4/H_2/AIR$ and H_2/AIR Mixtures Under Constant Volume Conditions*, Master's thesis, Department of Mechanical Engineering, University of Canterbury, Christchurch, New Zealand.

ROBINSON, J. (1995), *Mass Spectrometric Determination of Nitric Oxide Formation from the Combustion of Heterogeneous Hydrogen-Air Mixtures Under Constant Volume Conditions*, Master's thesis, Department of Mechanical Engineering, University of Canterbury, Christchurch, New Zealand.

ROGERS, G. AND MAYHEW, Y. (1988), *Thermodynamic and Transport Properties of Fluids, S.I. Units*, Basil Blackwell.

RYAN, T., NAEGELI, D., OWENS, E., MARBACH, H. AND BARBEE, J. (1981), 'The Mechanisms Leading To Increased Cylinder Bore And Ring Wear In Methanol-Fueled S.I. Engines', *SAE 811200.*

RYAN, T., BOND, T. AND SCHIEMAN, R. (1986), 'Understanding The Mechanism Of Cylinder Bore And Ring Wear In Methanol Fueled S.I. Engines', *SAE 861591.*

SAGA, K. AND FURUHAMA, S. (1976), 'Performance And Emission Control In Stratified Charge Hydrogen Fuelled Engines', *Institution of Mechanical Engineers*, pp. 29 – 36. Paper no. C244/76.

SCHAFER, F. (1981), 'An Investigation Of The Addition Of Hydrogen To Methanol On The Operation Of An Unthrottled Otto Engine', *SAE 810776.*

SCOTT, D. (1994), 'Liberty', *International Journal of Hydrogen Energy*, Vol. 19, No. 4, pp. 313 – 315.

SEIFRITZ, W. (1989), 'Methanol As The Energy Vector Of A New Climate-Neutral Energy System', *Int. J. Hydrogen Energy*, Vol. 14, No. 10, pp. 717–726.

SHAYLER, P., WISEMAN, M. AND MA, T. (1990), 'Improving The Determination Of Mass Fraction Burnt', *SAE 900351.*

SHER, E. AND HACOHEN, Y. (1987), 'On The Modeling Of A SI 4-Stroke Cycle Engine Fueled With Hydrogen-Enriched Gasoline', *Int. J. Hydrogen Energy*, Vol. 12, No. 11, pp. 773–781.

SHER, E. AND HACOHEN, Y. (1989), 'Ignition Delay And Combustion Duration In H2-Enriched Gasoline SI Engines', *Combust. Sci and Tech.*, Vol. 65, pp. 263–275.

SIERENS, R. AND ROSSEEL, E. (2000), 'Variable Composition Hydrogen/Natural Gas Mixtures For Increased Engine Efficiency And Decreased Emissions', *Transactions of the ASME, Journal of Engineering for Gas Turbines and Power*, Vol. 122, pp. 135–140.

SINOR, J. (1996), 'Volkswagen Reviews Potential Of Renewable Methanol For Road Transport', *The Clean Fuels and Electric Vehicles Report*, Vol. 8, No. 5, p. 120.

SJOSTROM, K., ERIKSSON, S. AND LANDQVIST, G. (1981), 'Onboard Hydrogen Generation For Hydrogen Injection Into Internal Combustion Engines', *SAE 810348.*

SMITH, D., KLEINDIENST, T. AND HUDGENS, E. (1989), 'Improved High-Performance Liquid Chromatographic Method For Artifact-Free Measurements Of Aldehydes In The Presence Of Ozone Using 2,4-Dinitrophenylhydrazine', *Journal of Chromatography*, Vol. 483, pp. 431 – 436.

STONE, C. AND BECKWITH, P. (1992), 'A Turbulent Combustion Model Used To Give Insights Into Cycle-By-Cycle Variations In Spark Ignition Engine Combustion', *IMechE C448/013*, pp. 47–55.

SUZUKI, K., UCHIYAMA, Y. AND HAMA, J. (1980), 'Research Of Hydrogen Fueled Spark Ignition Engines.', In *World Hydrogen Energy Conference III Proceedings*, pp. 1027 – 1039.

SWAIN, M., SWAIN, M., LEISZ, A. AND ADT, R. (1990), 'Hydrogen Peroxide Emissions From A Hydrogen Fueled Engine', *Int. J. Hydrogen Energy*, Vol. 15, No. 4, pp. 263 – 266.

SWAIN, M.R., YUSUF, M.J., DULGER, Z. AND SWAIN, M. (1993), 'The Effects Of Hydrogen Addition On Natural Gas Engine Operation', *SAE 932775.*

TABACZYNSKI, R., FERGUSON, C. AND RADHAKRISHAN, K. (1977), 'A Turbulent Entrainment Model For Spark-Ignition Engine Combustion', *SAE Trans.*, Vol. 86, pp. 2414 – 2433.

TABACZYNSKI, R., TRINKER, F. AND SHANNON, B. (1980), 'Further Refinement And Validation Of A Turbulent Flame Propogation Model For Spark-Ignition Engines', *Combustion and Flame*, Vol. 39, pp. 111 – 121.

TAKIGUCHI, M., FURUHAMA, S., SUZUKI, T. AND TSUJITA, M. (1987), 'Combustion Improvement Of Liquid Hydrogen Fuelled Engine For Medium-Duty Trucks', *SAE 870535.*

TEJADA, S. (1986), 'Evaluation Of Silica Gel Cartridges Coated In Situ With Acidified 2,4-Dinitrophenylhydrazine For Sampling Aldehydes And Ketones In Air', *Int. J. Environ. Anal. Chem.*, Vol. 26, pp. 167 – 185.

THOMAS, J.C., THURLEY, R.W.F., BELMONT, M.R., MORRIS, E.L., HOTCHKISS, A.J. AND HACOHEN, J. (1993), 'The Multi-Variate Classification Approach Applied To Lean Burn Combustion Analysis And Development In A Spark Ignition Engine', *IMechE C465/027*, pp. 305–319.

TROLOVE, H. (1991), *Calibration of Piezo-Electric Pressure Transducers*, Bachelor of Engineering Project Report 37/91, Department of Mechanical Engineering, University of Canterbury, Christchurch, New Zealand.

UNICH, A., BATA, R. AND LYONS, D. (1993), 'Natural Gas: A Promising Fuel For I.C. Engines', *SAE 930929.*

WALLACE, J. AND CATTELAN, A. (1994), 'Hythane And CNG Fuelled Engine Exhaust Emission Comparison', In *Hydrogen Energy Progress X*, Proceedings of the 10^{th} Worth Hydrogen Energy Conference, Cocoa Beach, Florida, USA, 20-24 June, pp. 1761–1770.

WATSON, H.C. (1995), 'Cyclic Variability, Lean Burn And Hydrogen Addition', In *Spark Ignition Engine Emissions Course, 18-20 September*, Advanced Centre for Manufacturing, University of Melbourne.

WATSON, H. AND MILKINS, E. (1978), 'Some Problems And Benefits From The Hydrogen Fuelled Spark Ignition Engine', In *Proceedings of the 13^{th} Intersociety Energy Conversion Engineering Conference*, pp. 1170 – 1177. Paper no. 789212.

WITHALM, G. AND GELSE, W. (1986), 'The Mercedes-Benz Hydrogen Engine For Application In A Fleet Vehicle', In *6^{th} World Hydrogen Energy Conference*, pp. 1185 – 1198.

WYSZYNSKI, M. AND WAGNER, T. (1995), 'Concept Of On-Board Fuel Reforming', In *2nd International Conference on Combustion and Emissions Control*, Institute of Energy, London, U.K.

YAGI, S., FUJII, I., AJIKI, Y. AND TSUDA, T. (1980), 'The Antiknock Quality In The Stratified Charge Engine With An Auxiliary Combustion Chamber', In *C395/80, Stratified Charge Automotive Engines*, I Mech E Conference Publications, pp. 49 – 54.

YOUNG, M.B. (1981), 'Cyclic Dispersion In The Homogeneous-Charge Spark Ignition Engine - A Literature Survey', *SAE 810020.*

ZAVIER, C. (1991), *Charge Stratification for an Internal Combustion Engine*, Master's thesis, Department of Mechanical Engineering, University of Canterbury, Christchurch, New Zealand.